THE UNIVERSITY OF
SYDNEY

The Role and Ultrastructure of the Liver Sinusoidal Endothelial Cell in Fasting, Hepatotoxicity, and Ageing

Jenn N. O'Reilly

A thesis submitted for the degree of Doctor of Philosophy

Centre for Education and Research on Ageing and the ANZAC Research Institute,

Faculty of Medicine, University of Sydney

2014

Declaration of the candidate

All of the results, analyses, and electron and light micrographs presented in this thesis are my own original work (unless otherwise acknowledged), accomplished under the supervision of Professor David Le Couteur and Dr Victoria Cogger.

Jennifer N. O'Reilly

Acknowledgements

I warmly thank and acknowledge Professor David Le Couteur for his support and wonderful guidance in his supervision. I also warmly thank and acknowledge Dr Victoria Cogger, my associate supervisor, for her support and invaluable help with lab work including microscopy, specimen preparation and animal surgery. I would like to thank Dr Alessandra Warren for sharing her passion for microscopy with me, and for answering many questions, particularly concerning microscopy and the use of Photoshop. I wish to thank and acknowledge Dr Sarah Hilmer for her support and guidance during the early part of my candidature.

I thank all the other past and present members of the Biogerontology lab at the ANZAC Research Institute (not mentioned above), particularly Aisling, Vicky, and Mimi, for their support and encouragement along the way. I acknowledge and thank the staff of the ANZAC Research Institute and animal house, and I acknowledge Dr Michael Muller for his help with cell isolation and culture.

Many thanks go to Dorothy Kouzios from the Diagnostic Pathology Unit at Concord RG Hospital for her assistance with the analysis of blood samples. I would also like to acknowledge the technical assistance and generosity of staff at the Anatomical Pathology Unit Concord RG Hospital (histology and electron microscopy departments). In particular I gratefully thank Paul Kirwan who has spent many hours teaching me diagnostic electron microscopy, adding a much greater depth of understanding to my PhD research. Many warm thanks to Susan Brammah for also teaching me diagnostic electron microscopy and for her invaluable advice and support with lab work regarding the transmission electron microscope. Many thanks to Karen

MacKenney for facilitating my work experience in diagnostic electron microscopy. Also, thankyou to Stephanie Sampedro for her help in the Anatomical Pathology lab.

I gratefully acknowledge funding support from the National Health and Medical Research Council (NHMRC) Biomedical Postgraduate Scholarship and the Ageing and Alzheimer's Research Foundation (AARF).

Thanks to the staff and students at the ANZAC Research Institute and Centre for Education and Research on Ageing (CERA) for providing such a welcoming space to conduct research.

Thankyou to my close friends and my partner Ben for their support, love, and encouragement, and to those dear to me that have passed away for continuing to give me strength.

Publications and Conference abstracts

Publications derived from the thesis

Jennifer N. O'Reilly, Victoria C. Cogger, Robin Fraser and David G. LeCouteur. *The effect of feeding and fasting on fenestrations in the liver sinusoidal endothelial cell*. Pathology. 2010 Apr; 42(3):255-8

Jennifer N. O'Reilly, Victoria C. Cogger and David G. Le Couteur. *Old age is associated with ultrastructural changes in isolated rat liver sinusoidal endothelial cells*. Journal of electron microscopy. 2010; 59:65-9

Publications related to the work in this thesis

Victoria C. Cogger, Dmitri Svistounov, Alessandra Warren, Svetlana Zykova, Richard G. Melvin, Samantha M. Solon-Biet, Jennifer N. O'Reilly, Aisling C. McMahon, J. William O. Ballard, Rafa De Cabo, David G. Le Couteur, and Michel Lebel. *Liver ageing and pseudocapillarization in a Werner Syndrome mouse model*. J Gerontol A Biol Sci Med Sci, 2013 Oct 22 [Epub ahead of print]

Laurent Massip, Chantal Garand, Eric R. Paquet, Victoria C. Cogger, **Jennifer N. O'Reilly**, Leslee Tworek, Avril Hatherell, Carla G. Taylor, Eric Thorin, Peter Zahradka, David G. Le Couteur, and Michel Lebel. *Vitamin C restores healthy aging in a mouse model for Werner syndrome*. The FASEB journal: official publication of the Federation of American Societies for Experimental Biology. 2010; 24:158-72

Tharani Sabaretnam, Leonard Kritharides, **Jennifer N. O'Reilly** and David G. Le Couteur. *The effect of aging on the response of isolated hepatocytes to hydrogen peroxide and tert-butyl hydroperoxide.* Toxicology in vitro: an international journal published in association with BIBRA. 2010; 24:123-8

Tharani Sabaretnam, **Jennifer N. O'Reilly**, Leonard Kritharides, and David G. Le Couteur. *The effect of old age on apolipoprotein E and its receptors in rat liver*. Age (Dordr). 2010 Mar;32(1):69-77

Other publications

Rajkumar Cheluvappa, Victoria C. Cogger, Sun Young Kwun, **Jennifer N. O'Reilly**, David G. Le Couteur, Sarah N. Hilmer. *Liver sinusoidal endothelial cells and acute non-oxidative hepatic injury induced by Pseudomonas aeruginosa pyocyanin*. International Journal of Experimental Pathology. 2008 Dec; 89(6):410-418

Kelly J. Skilbeck, **Jennifer N. O'Reilly**, Graham A.R. Johnston, Tina Hinton. *Antipsychotic drug administration differentially affects [3H]muscimol and [3H]flunitrazepam GABAA receptor binding sites.* Progress in Neuro-Psychopharmacology and Biological Psychiatry. 2008 Feb; 32(2):492-498

Rajkumar Cheluvappa, Sarah N. Hilmer, Sun Young Kwun, Hamish A. Jamieson, **Jennifer N. O'Reilly**, Michael Muller, Victoria C. Cogger, David G. Le Couteur. *The effect of old age on liver oxygenation and the hepatic expression of VEGF and VEGFR2*. Experimental Gerontology. 2007; 42:1012-1019.

Kelly J. Skilbeck, **Jennifer N. O'Reilly**, Graham A.R. Johnston, Tina Hinton. *The effects of antipsychotic drugs on $GABA_A$ receptor binding depend on period of drug treatment and binding site examined*. Schizophrenia Research. 2007; 90:76-80

Abstracts from conference presentations

J. N. O'Reilly, V. C. Cogger and D.G. Le Couteur: *Acetaminophen, P407 and the liver sinusoidal endothelial cell*. 16th Meeting of the International Society for Hepatic Sinusoid Research (ISHSR), September 2011, Florence (poster presentation).

J. N. O'Reilly, V. C. Cogger and D.G. Le Couteur: *Protective Effect of Co-Polymer on Liver in Paracetamol Overdose*. Joint meeting of ASCEPT and SEAWP-RMP, 2007 Adelaide (oral presentation).

J. N. O'Reilly, K. J. Skilbeck, G. A. R. Johnston, & T. Hinton: *The Effects of the Antipsychotic Drugs Haloperidol and Olanzapine on $GABA_A$ Receptor Binding in the Thalamus and Hippocampus*. Australian Neuroscience Society, 26th Annual meeting, Sydney Convention Centre, Darling Harbour, 31st of Jan-3rd of Feb, 2006 (poster presentation).

Summary

The microvasculature of the liver is specialised in that it facilitates a relatively unimpeded bi-directional exchange of substances between the blood and parenchyma. Liver sinusoidal endothelial cells (LSECs) line the liver sinusoids and are perforated with thousands of transcellular fenestrations (open pores of approximately 100 nm in diameter devoid of diaphragms) and are underlined by a very sparse extracellular matrix. Thus, a virtually unimpeded passage of substances smaller than fenestrations to and from hepatocytes (the primary liver parenchymal cells) is facilitated. Direct contact between hepatocytes and circulating leukocytes is also facilitated through fenestrations, having implications for immune tolerance or activation. The diameter and number of fenestrations in the LSEC cytoplasm is modulated by both endogenous and exogenous substances such as drugs, hormones, and toxins, also pathological states and ageing. Modulation of fenestrations can have serious implications for drug and lipid metabolism as the liver is main site of drug and lipid metabolism in the body. Xenobiotics and chylomicron remnants smaller than fenestrations pass from the sinusoid lumen to the perisinusoidal space and hepatocytes for metabolism. As the diameter and number of fenestrations change, alterations in drug and lipid uptake follow that may alter the clearance of a drug or contribute to hyperlipidemia.

Pathological states and oxidative stress in the sinusoids contribute to the capillarisation of LSECs. Capillarisation describes the alteration of LSEC phenotype to that of a defenestrated and thickened endothelial cell, similar to a typical capillary endothelial cell with underlying basement membrane. Capillarisation impedes the bi-directional exchange of substances and decreases hepatocyte oxygenation, having severe consequences for liver functioning and perpetuation of disease states including

fibrosis and cirrhosis. Pseudocapillarisation is a less severe form of capillarisation associated with ageing. During pseudocapillarisation, LSECs lose about 50 % of their fenestrations, experience mild thickening and an increase of perisinusoidal extra cellular matrix. Ageing is associated with alterations in drug metabolism, postprandial hyperlipidemia, atherosclerosis, and an increased incidence of immune-related disorders, all of which are linked to pseudocapillarisation and defenestration. As such, modulation of fenestrations and maintenance of the fenestrated LSEC phenotype are important therapeutic targets.

Chapter 3 of this thesis investigated the effect of fasting on the number and diameter of fenestrations in LSECs. In this study I found that fenestration diameter was significantly increased by approximately 10 % in fasted compared to ad libitum fed rats. However, a concomitant significant decrease in the number of fenestrations rendered the overall porosity of the LSECs unchanged. Increase in fenestration diameter during fasting has implications for the transfer of substrates and fluid between blood and hepatocytes, and allows increased passage of chylomicron remnants and nutrients through to the perisinusoidal space and hepatocytes. This is the first *in vivo* demonstration that fenestrations alter with physiological stimuli, in this case, the fasting or fed state. Increased fenestration diameter during fasting should therefore be considered in studies utilising fasted animals.

Drug induced liver injury (DILI) is a major cause of mortality and fulminant hepatic failure. Acetaminophen (APAP) toxicity is one of the leading causes of DILI and liver failure in humans. In APAP toxicity, early injury to the LSEC initiates a cascade of events that exacerbate and sometimes initiate hepatocyte necrosis. Studies have shown

that protection of the liver microvasculature during APAP toxicity markedly reduces liver injury however the process of LSEC injury in APAP toxicity is not fully understood. Some studies suggest that early injury to the LSEC may be repaired during the course of APAP toxicity although the mechanisms are unknown. In Chapter 4 a thorough ultrastructural investigation on the liver sinusoids after an overdose of APAP in fed and fasted rats was performed. The morphology of the LSEC was observed on both SEM and TEM soon after overdose at 6 hours and again after the progression of hepatocyte centrilobular necrosis at 24 hours. There was injury to the LSEC at 6 hours after APAP in the form of gap formation, defenestration, and swelling. Gaps enabled RBCs to pass through and accumulate in the perisinusoidal space, decreasing sinusoid lumen size and promoting congestion and hypoxia. At 24 hours, LSEC injury was variable. Some LSECs were dead however some were viable and fenestrated in areas of severe hepatocyte necrosis. There were more viable LSECs observed in fed than fasted rats. Viable LSECs in necrotic zones were tethered to HSCs with some basement membrane formation between the cells, and both LSECs and HSCs were attached to degenerate hepatocytes. Retaining the sinusoid wall structure in at least some areas of the liver with hepatocyte necrosis may be vital to the restoration of hepatic microvasculature and subsequent regeneration of parenchyma in APAP toxicity.

In Chapter 5 the therapeutic potential of a substance known to modulate fenestrations, poloxamer 407 (P407), was studied in the setting of APAP toxicity in fed and fasted rats. P407 has been shown in previous studies to defenestrate the LSEC by up to 80 % however the mechanism is unknown. In this study it was hypothesised that P407 micelles may coat the LSEC, offering some protection from toxic insult and oxidative

stress. Defenestration by P407 may also decrease the amount of drug available to hepatocytes thus reduce the metabolism of APAP and production of toxic metabolites. It may also prevent gap formation in LSECs and subsequent hemorrhage leading to hepatocyte hypoxia. Rats were pre-treated with P407 via an intraperitoneal injection 18 hours prior to an APAP overdose. Pre-treatment was not protective at 6 or 24 hours after APAP, and appeared to increase toxicity in some rats. This may have been due to an increase of inflammation stimulated by P407.

Another cohort of rats was given an intraperitoneal injection of P407 one hour after APAP overdose. P407 post-treatment appeared to have a protective effect on the fed APAP group. At 24 hours after APAP only one of the rats had some very mild centrilobular necrosis, and no necrosis was observed in the other rats. In the fasted P407 post-treated rats at 24 hours after APAP the effect of P407 was unclear as there was extreme variability of toxicity throughout the group. In addition, at 6 hours after APAP in fasted P407 post-treated rats, gap formation in LSECs was not prevented. The mechanism of protection of P407 post-treatment in the fed group is unclear. The LSECs in the fed P407 post-treated group displayed some degree of defenestration which may have reduced the amount of APAP delivered to hepatocytes, whereas in the fasted post-treated group there was less defenestration and more gap formation, increasing hepatocyte vulnerability to toxic insult.

In Chapter 6, LSEC isolation from old and young rats was performed to observe whether the pseudocapillarisation of LSECs associated with ageing is maintained *in vitro*. We found no change in the overall porosity in the isolated LSECs of young and old rats, however there was a significant decrease in the diameter of fenestrations

from 194 ± 1 nm in young to 185 ± 1 nm in old isolated LSECs. Thus LSECs from old livers maintained some, but not all, of their reported *in vivo* ultrastructural changes. The results of this study suggest that reduced fenestration diameter in old age is intrinsic to the LSEC.

The work in this thesis supports the vital role of the fenestrated LSEC phenotype in maintaining healthy functioning of the liver, and the integral role of the LSEC in liver injury and repair. In addition, fenestration modulation appears to be an important therapeutic target in ageing, disease, and toxicity.

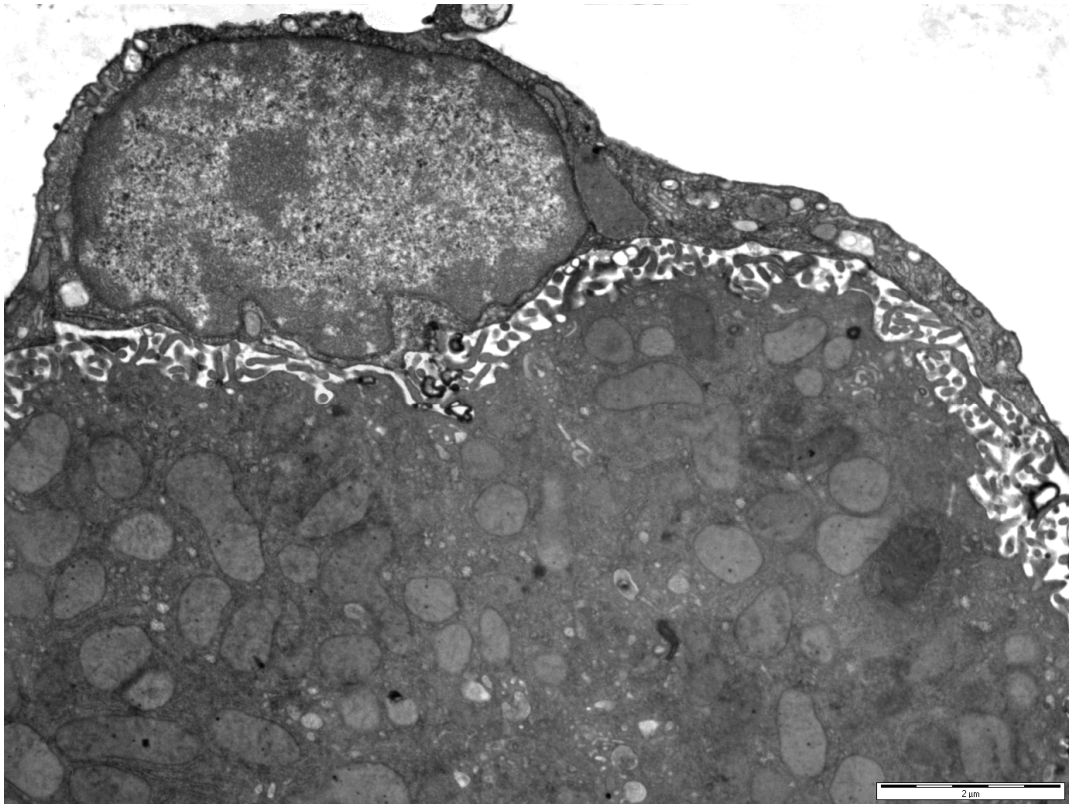

Cover Plate: The Liver Sinusoidal Endothelial Cell

Thesis Contents

Declaration of the Candidate	ii
Acknowledgements	iii
Publications and Conference Abstracts	v
Summary	vii
Cover Plate	xii
Table of Contents	xiv
List of Figures	xviii
List of Tables	xxii
List of Appendices	xxv
List of Abbreviations	xxvii

Table of Contents

CHAPTER 1:

INTRODUCTION AND LITERATURE REVIEW 1

1.1 THE LIVER 2

1.1.1 LIVER FUNCTION AND ANATOMY 2
1.1.2 LIVER ULTRASTRUCTURE 8
1.1.2.1 The sinusoids and hepatocyte cords 8
1.1.2.2 The perisinusoidal space of Disse 11

1.2 ULTRASTRUCTURE AND FUNCTION OF LIVER CELLS 13

1.2.1 LIVER SINUSOIDAL ENDOTHELIAL CELLS 13
1.2.1.1 Structure and function 13
1.2.1.2 The sieving function of LSECs 16
1.2.1.3 Fenestration structure 17
1.2.1.4 Fenestration formation 19
1.2.1.5 Fenestration modulation 21
1.2.1.6 Methods for the study of fenestration modulation 25
1.2.2 HEPATIC STELLATE CELLS 26
1.2.3 HEPATOCYTES 28
1.2.4 RESIDENT MACROPHAGES AND LYMPHOCYTIC CELLS OF THE LIVER 32
1.2.4.1 Kupffer cells 32
1.2.4.2 Pit cells 34
1.2.4.3 Dendritic cells and lymphocytes 34

1.3 THE EFFECT OF FASTING ON THE LIVER 36

1.3.1 FASTING AND XENOBIOTIC METABOLISM 38
1.3.2 FASTING AND THE LSEC 39

1.4 DRUG-INDUCED LIVER INJURY 39

1.4.1 DRUG-INDUCED LIVER INJURY AND THE HEPATIC MICROVASCULATURE 40
1.4.2 MORPHOLOGY OF THE INJURED LSEC 41
1.4.3 OXIDATIVE STRESS AND THE LSEC IN DRUG-INDUCED LIVER INJURY 42
1.4.4 CAPILLARISATION OF THE SINUSOIDAL ENDOTHELIUM 43
1.4.5 FIBROSIS AND CIRRHOSIS 44
1.4.6 DRUG INDUCED LIVER INJURY FOLLOWING DIRECT LSEC TOXICITY 45
1.4.6.1 Sinusoidal Obstruction Syndrome 45
1.4.6.2 Peliosis Hepatis 47

1.5 AGEING AND THE LIVER 50

1.5.1 IMPLICATIONS OF AGE-RELATED PSEUDOCAPILLARISATION OF THE LSEC 52

1.6 SCOPE AND AIMS OF THE THESIS 54

CHAPTER 2:

METHODOLOGY 57

2.1 FIXATION 58

2.2 LIGHT MICROSCOPY 58

2.2.1 HISTOLOGICAL FIXATION 58
2.2.2 EMBEDDING OF SPECIMENS 60
2.2.3 HISTOLOGICAL STAINING 60
2.2.3.1 Hematoxylin and eosin 60
2.2.3.2 Periodic acid-Schiff 61
2.2.3.3 Sirius red 61

2.2.4 VIEWING ON THE COMPOUND LIGHT MICROSCOPE 61

2.3 ELECTRON MICROSCOPY 62

2.3.1 THE ELECTRON MICROSCOPE 62
2.3.2 ULTRASTRUCTURAL FIXATIVES AND BUFFERS 62
2.3.3 METHODS OF PRIMARY ULTRASTRUCTURAL FIXATION 63
2.3.4 SECONDARY FIXATION AND CONTRAST ENHANCING OF SPECIMENS 67
2.3.4.1 Osmium 67
2.3.4.2 Tannic acid 67
2.3.4.3 Uranyl 68
2.3.5 DEHYDRATION, EMBEDDING, SECTIONING, AND STAINING FOR TEM ANALYSIS 70
2.3.6 REPROCESSING PARAFFIN EMBEDDED TISSUE FOR TEM ANALYSIS 71
2.3.7 DEHYDRATION AND SPECIMEN PREPARATION FOR THE SEM 72
2.3.8 INDICATORS OF POOR ULTRASTRUCTURAL FIXATION ON ELECTRON MICROGRAPHS 73

2.4 EXPERIMENTAL MATERIALS AND PROTOCOLS 74

2.4.1 ANIMALS 74
2.4.2 BLOOD ANALYSIS 75
2.4.3 PERFUSION FIXATION PROTOCOL 75
2.4.4 HISTOLOGICAL SPECIMEN PREPARATION 76
2.4.5 ELECTRON MICROSCOPY SPECIMEN PREPARATION 77
2.4.5.1 Scanning electron microscopy 77
2.4.5.2 Transmission electron microscopy 78
2.4.5.3 Reprocessing paraffin-embedded specimens for TEM analysis 79
2.4.5.4 SEM analysis of fenestration and gap diameter using Image J 79
2.4.5.5 SEM analysis of porosity and fenestration frequency 81

CHAPTER 3:

THE EFFECT OF FASTING ON FENESTRATIONS IN THE LIVER SINUSOIDAL ENDOTHELIAL CELL 82

3.1 INTRODUCTION 83

3.2 MATERIALS AND METHODS 85

3.2.1 ANIMALS 85
3.2.2 SURGERY AND SPECIMEN PREPARATION 85
3.2.3 SEM ANALYSIS 85
3.2.4 LIVER WEIGHTS AND BLOOD ANALYSIS 86
3.2.5 STATISTICAL ANALYSIS 86

3.3 RESULTS 87

3.4 DISCUSSION 91

CHAPTER 4:

ACETAMINOPHEN TOXICITY AND THE LIVER SINUSOIDS OF FED AND FASTED F344 RATS 95

4.1 INTRODUCTION 96

4.2 MATERIALS AND METHODS 102

4.2.1 ANIMALS AND APAP DOSAGE 102
4.2.2 SURGERY AND SPECIMEN PREPARATION FED GROUPS 103
4.2.3 SURGERY AND SPECIMEN PREPARATION FASTED GROUPS 103
4.2.4 HISTOLOGY FED AND FASTED GROUPS 104
4.2.5 ELECTRON MICROSCOPY FED AND FASTED GROUPS 105
4.2.5 STATISTICAL ANALYSIS 106

4.3 RESULTS: FED RATS AT 24 HOURS AFTER APAP 107

4.3.1 MACROSCOPIC OBSERVATIONS 107
4.3.2 BLOOD RESULTS 107
4.3.3 HISTOLOGY 108
4.3.4 ELECTRON MICROSCOPY 110

4.4 RESULTS: FASTED RATS AT 6 AND 24 HOURS AFTER APAP 118

4.4.1 MACROSCOPIC OBSERVATIONS 118
4.4.2 BLOOD RESULTS COMPARING 6 TO 24 HOURS AFTER APAP 118
4.4.3 BLOOD RESULTS COMPARING 24 HOURS AFTER APAP TO CONTROLS 118
4.4.4 HISTOLOGY 120
4.4.5 ELECTRON MICROSCOPY AT 6 HOURS AFTER APAP 125
4.4.6 ELECTRON MICROSCOPY AT 24 HOURS AFTER APAP 126
4.4.7 SUMMARY OF DIFFERENCES BETWEEN FED AND FASTED APAP-TREATED RATS 131

4.6 DISCUSSION 133

CHAPTER 5:

THERAPEUTIC EFFECT OF POLOXAMER 407 ON ACETAMINOPHEN TOXICITY IN THE F344 RAT LIVER 141

5.1 INTRODUCTION 142

5.2 MATERIALS AND METHODS 146

5.2.1 MATERIALS 146
5.2.2 METHODS 146

5.3 RESULTS: P407 PRE-TREATED RATS 149

5.3.1 MACROSCOPIC OBSERVATIONS 149
5.3.2 BLOOD ANALYSIS 149
5.3.2.1 Fed P407 pre-treated 24 hour group 149
5.3.2.2 Fasted P407 pre-treated 6 and 24 hour groups 149
5.3.3 HISTOLOGY 151
5.3.3.1 Fed P407 pre-treated 24 hour group 151
5.3.3.2 Fasted P407 pre-treated 6 hour group 153
5.3.3.3 Fasted P407 pre-treated 24 hour group 154
5.3.4 ELECTRON MICROSCOPY 158
5.3.4.1 Fasted P407 pre-treated 6 hour group 158
5.3.4.2 Fed and fasted P407 pre-treated 24 hour groups 160
5.3.5 SUMMARY OF P407 PRE-TREATED RATS 166

5.4 RESULTS: P407 POST-TREATED RATS 167

5.4.1 MACROSCOPIC OBSERVATIONS 167
5.4.2 BLOOD ANALYSIS 167
5.4.2.1 Fed P407 post-treated 24 hour group 167
5.4.2.2 Fasted P407 post-treated 6 and 24 hour groups 167
5.4.3 HISTOLOGY 168
5.4.3.1 Fed P407 post-treated 24 hour group 168
5.4.3.2 Fasted P407 post-treated 6 hour group 171
5.4.3.3 Fasted P407 post-treated 24 hour group 173
5.4.4 ELECTRON MICROSCOPY 178
5.4.4.1 Fed P407 post-treated 24 hour group 178
5.4.4.2 Fasted P407 post-treated 6 hour group 181
5.4.4.3 Fasted P407 post-treated 24 hour group 183
5.4.5 SUMMARY OF P407 POST-TREATED RATS 185
5.4.6 TABLE SUMMARY OF P407 PRE- AND POST-TREATED RAT DATA TRENDS 186

5.5 DISCUSSION 187

CHAPTER 6:

THE ULTRASTRUCTURE OF ISOLATED LIVER SINUSOIDAL ENDOTHELIAL CELLS FROM YOUNG AND OLD F344 RATS 198

6.1 INTRODUCTION 199

6.2 MATERIALS AND METHODS 201

6.2.1 ANIMALS AND GENERAL INFORMATION 201
6.2.2 SURGERY AND LSEC ISOLATION METHOD USING A 2-STEP PERCOLL GRADIENT 201
6.2.3 SPECIMEN PREPARATION FOR SCANNING EM 203
6.2.4 ANALYSIS 204

6.3 RESULTS 205

6.4 DISCUSSION 209

CHAPTER 7:

GENERAL DISCUSSION 213

REFERENCE LIST 219

APPENDICES 263

List of Figures

Chapter 1

1.1 A portal tract from the liver of an F344 rat

1.2 Light and electron micrographs of the central vein, portal tract, and liver sinusoids from an F344 rat

1.3 A diagrammatic representation of the classic lobule and liver acinus

1.4 A histological representation of the F344 rat liver lobule

1.5 A transmission electron micrograph displaying layers of the sinusoid wall from an F344 rat

1.6 A scanning electron micrograph from an F344 rat displaying the one cell thick hepatocyte plates that run between the sinusoids

1.7 A transmission electron micrograph showing the connection of the SoD to the portal interstitium and portal tract in an F344 rat

1.8 Micrographs of the LSEC perinuclear region and intercellular junction from an F344 rat

1.9 Electron micrographs from an F344 rat displaying transverse and obliquely sectioned views of fenestrations on TEM and a 3-dimensional view on SEM

1.10 Transmission electron micrograph of a hepatic stellate cell, F344 rat

1.11 Transmission electron micrograph of a hepatocyte nucleus and cell body

1.12 Transmission electron micrograph of a Kupffer cell from an F344 rat

1.13 Transmission electron micrograph of a KC, pit cell, and lymphocyte from an F344 rat

Chapter 2

2.1 Examples of good and poor histological fixation

2.2 Histological and electron micrographic representation of high perfusion pressure artefact in hepatocytes and liver sinusoids

2.3 Examples of good and poor ultrastructural fixation of liver sinusoids from F344 rats for SEM

2.4 Micrographs displaying the effect of uranyl acetate and tannic acid *en bloc* staining on TEM specimen contrast

2.5 Toluidine blue stained 0.5 μm thick sections

2.6 Examples of transmission electron micrographs from F344 rat specimens prepared after perfusion fixation and after reprocessing from a formaldehyde-fixed paraffin block

2.7 Examples of poor fixations of F344 livers and specimen artefacts on TEM

2.8 An example of an Image J analysis of the LSEC cytoplasm

Chapter 3

3.1 Scanning electron micrographs of sinusoids from livers of fed and fasted F344 rats

3.2 Liver weight of the whole liver and of four liver lobes relative to body weight in fed and fasted F344 rats

3.3 Frequency distribution of fenestration diameter between fed and fasted F344 rats

Chapter 4

4.1 Pathways of APAP metabolism

4.2 Experimental treatment groups

4.3 H&E, PAS, and Sirius Red stained sections from fed APAP-treated rats

4.4 Transmission electron micrographs of specimens reprocessed from paraffin from the fed APAP-treated rat with the most severe toxicity

4.5 Transmission electron micrographs from a fed APAP-treated rat with mid-range toxicity. Viable LSECs and HSCs are surrounded by necrotic hepatocytes

4.6 Transmission electron micrograph from a fed APAP-treated rat with mid-range toxicity. Tethering of a HSC, necrotic hepatocyte, and LSEC

4.7 Transmission electron micrographs of sinusoids in CL necrotic zones from fed APAP-treated rats with moderate toxicity

4.8 Micrographs of CL necrotic zones from fed APAP-treated rats

4.9 Electron micrographs of sinusoids of fed APAP-treated rats with low to moderate toxicity

4.10 Liver Histology from fasted APAP-treated rats: H&E and PAS stains

4.11 Sirius Red stained sections of liver from fasted APAP-treated rats

4.12 Electron micrographs from fasted rats 6 hrs after APAP

4.13 Electron micrographs from fasted rats 24 hrs after APAP

4.14 Electron micrographs from fasted rats 24 hrs after APAP

4.15 Electron micrographs from fasted rats 24 hrs after APAP

4.16 Electron micrographs from fasted rats 24 hrs after APAP

Chapter 5

5.1 Experimental treatment groups

5.2 Histological example of intralobular differences in P407 pre-treated rats

5.3 H&E, PAS, and Sirius Red stained sections from Fed P407 pre-treated APAP rats

5.4 Histology of fasted P407 pre-treated rats at 6 hrs after APAP: H&E, PAS, and Sirius Red

5.5 Histology of fasted P407 pre-treated rats 24 hrs after APAP: H&E, PAS, and Sirius Red

5.6 Micrographs of fasted P407 pre-treated rats 6 hrs after APAP

5.7 Micrographs of fed P407 pre-treated rats 24 hrs after APAP

5.8 Micrographs of necrotic LSECs from fasted P407 pre-treated rats in areas of CL hepatocyte necrosis

5.9 Transmission electron micrographs of fasted P407 pre-treated rat sinusoids in areas of moderate and low toxicity at 24 hrs after APAP including a necrotic LSEC

5.10 Renal histology and electron micrographs from a fasted P407 pre-treated rat with hematuria at 24 hrs after APAP

5.11 Histology of P407 post-treated fed rats: H&E, PAS, and Sirius Red

5.12 Histology of 6 hr fasted P407 post-treated APAP rats: H&E, PAS, and Sirius Red

5.13 Histology of P407 post-treated fasted rats 1, 2, and 3 (with mild toxicity) 24 hrs after APAP: H&E, PAS, and Sirius Red

5.14 Liver and kidney histology of the fasted 24 hr post-treated APAP rat with extreme hepatotoxicity: H&E, PAS, and Sirius Red

5.15 Electron micrographs from fed P407 post-treated rats 24 hrs after APAP

5.16 Transmission electron micrographs from reprocessed tissue from the fed P407 post-treated rat with mild toxicity showing areas of CL necrosis

5.17 Electron micrographs from P407 post-treated fasted rats 6 hrs after APAP

5.18 Electron micrographs of a fasted P407 post-treated rat with severe toxicity 24 hrs after APAP

Chapter 6

6.1 Frequency distribution graph of the fenestration diameter in LSECs isolated from young and old rats

6.2 Electron micrographs of isolated young and old LSECs

6.3 Scanning electron micrographs of unusual fenestration structures

List of Tables

Chapter 1

1.1 Modulation of fenestration diameter and number via particular substances, disease, and environmental factors

1.2 Symptoms of injury to the microvasculature during disease and toxicity

Chapter 3

3.1 Quantification of the fenestrations in LSECs of fasted and fed rats

3.2 The effects of fasting on liver weight and blood measures of hepatic and renal function

Chapter 4

4.1 Mean and individual serum aminotransferase levels, total bilirubin, and weight loss at 24 hrs after APAP in fed rats

4.2 Grade of necrosis, sinusoidal collagen, and glycogen distribution 24 hrs after APAP in fed rats

4.3 Serum aminotransferase and total bilirubin raw data and mean from fasted APAP-treated rats

4.4 Serum lipids and kidney function test raw data and mean from fasted APAP-treated rats

4.5 Hematocrit, liver weight, and weight loss raw data and mean from fasted APAP-treated rats. Mean ± SD of fasted APAP-control rats is included for comparison

4.6 6 hrs after APAP in fasted rats - graded necrosis and sinusoidal collagen with comparative ALT level and glycogen presence in each rat

4.7 24 hrs after APAP in fasted rats - graded necrosis and sinusoidal collagen with comparative ALT level and glycogen presence in each rat

4.8 Table of raw and mean ± S.D. data from ad libitum fed and fasted APAP treated rats culled 6 or 24 hrs after APAP, including necrosis and sinusoidal collagen scores

Chapter 5

5.1 Raw and mean ± S.D. data from ad libitum fed or fasted APAP treated rats culled 6 or 24 hrs after APAP and pre-treated with P407 18 hrs before APAP

5.2 Graded necrosis and sinusoidal collagen, glycogen distribution, and serum ALT value for comparison in the P407 pre-treated fed APAP rats 24 hrs after APAP

5.3 Graded necrosis and sinusoidal collagen, glycogen distribution, and serum ALT value for comparison in the P407 pre-treated fasted rats 6 hrs after APAP

5.4 P407 pre-treated fasted 24 hr group: individual graded centrilobular necrosis in four liver lobes, graded sinusoidal collagen, glycogen distribution, and ALT values for comparison in each rat

5.5 Histology summary and comparison table of necrosis, sinusoidal collagen deposition, and glycogen deposition in P407 pre-treated rats from fed and fasted groups

5.6 Raw and mean ± S.D. data from ad libitum fed or fasted APAP treated rats culled 6 or 24 hrs after APAP and post-treated with P407 1 hr after APAP

5.7 Graded necrosis and sinusoidal collagen, glycogen distribution, and serum ALT value for comparison in the P407 post-treated fed APAP rats 24 hrs after APAP

5.8 Graded necrosis and sinusoidal collagen, glycogen distribution, and serum ALT value for comparison in the P407 post-treated fasted rats 6 hrs after APAP

5.9 P407 post-treated fasted 24 hr group: individual graded centrilobular necrosis in four liver lobes, graded sinusoidal collagen, glycogen distribution, and ALT values for comparison in each rat

5.10 Histology summary and comparison table of necrosis, sinusoidal collagen deposition, and glycogen deposition in P407 post-treated rats from fed and fasted groups

5.11 Summary and trends in the blood, histological, and EM data comparing APAP controls to P407 treatment groups

List of Appendices

Appendix 1: Embedding protocols

A) Spurr's resin embedding protocol for TEM specimens

B) Paraffin embedding protocol for histological specimens

Appendix 2: Staining protocols for histology

A) Hematoxylin and Eosin

B) Periodic Acid Schiff

C) Sirius Red and Fast Green FCF

Appendix 3: Staining protocols for TEM

A) Toluidine blue stain

B) Staining of ultrathin sections for TEM

Appendix 4: Table of results from Chapters 4 and 5

Table 1: Summary of trends in the data from Chapters 4 and 5 comparing APAP controls to P407 pre- and post-treatment groups

Appendix 5: Micrographs not included in thesis chapters

A1: Portal tract (TEM)

A2: Eosinophil (TEM)

A3: Direct communication between cells of the hepatic sinusoids (TEM)

A4: H & E stained sections of old rats (from Chapter 6)

A5: Sirius red stained section of male 9 month old mouse with Werner's syndrome

A6: Sinusoids from mice with Werner's syndrome aged 7-9 months (TEM)

A7: A sinusoid showing pseudocapillarisation from a male mouse with Werner's syndrome aged 7 months

A8: A plasma cell (effector B-cell) in a sinusoid lumen of a Werner Syndrome mouse.

A9: Fibrin (TEM, from a reprocessed specimen, Chapter 4)

A10: Glomerular endothelial cells (a reprocessed TEM specimen from Chapter 5)

A11: Control F344 rat and APAP-treated F344 rat renal histology

List of abbreviations

ALT	Alanine transaminase
APAP	Acetaminophen (paracetamol)
AST	Aspartate transaminase
CL	Centrilobular
CV	Central vein/venule
DNA	Deoxyribonucleic acid
EM	Electron microscopy
ER	Endoplasmic reticulum
GSH	Glutathione
HSC	Hepatic stellate cell
IP	Intraperitoneal
IVC	Inferior vena cava
KC	Kupffer cell
LFT	Liver function test
LSEC	Liver sinusoidal endothelial cell
ML	Midlobular
Mt	Mitochondria
NAC	*N*-acetylcysteine
NAPQI	*N*-acetyl-*p*-benzoquinone imine
P407	Poloxamer 407
PAS	Periodic acid Schiff
PC	Pericentral
PP	Periportal
PT	Portal tract
PV	Portal vein/venule
RBC	Red blood cell
RNA	Ribonucleic acid
SEM	Scanning electron microscope/microscopy
SoD	Space of Disse
TEM	Transmission electron microscope/microscopy
VLDL	Very low density lipoprotein

Chapter 1:

Introduction and Literature Review

1.1 The liver

1.1.1 Liver function and anatomy

The liver is a complex organ with many vital functions (Cattley, 2002, Kmiec, 2001). It has a major role in drug and pathogen detoxification, immunity, lipoprotein synthesis and metabolism, bile formation and secretion, and nutrient storage and processing, and is considered the primary "metabolic clearing house" for both endogenous chemicals (steroid hormones, fatty acids, proteins, and cholesterol) and xenobiotics. The liver is located in the upper right quadrant of the abdominal cavity consisting of four main lobes (left, right, median or quadrate, and caudate) surrounded by a fibrous capsule of connective tissue (Glisson's capsule) and is the largest internal organ. The histological lobular architecture of the liver is similar in all species (Malarkey, 2005).

The liver is the first organ exposed to ingested pathogens and toxins, receiving blood directly from the gastrointestinal tract. As such it is the primary site of drug and toxin (xenobiotic) metabolism in the body (Neal, 1992). About 70 % of blood is supplied to the liver via the hepatic portal vein carrying blood from the abdominal organs via the mesenteric (intestines), gastric (stomach), splenic (spleen), and pancreatic (pancreas) veins. This deoxygenated blood delivers a mixture of micro and macro nutrients for processing and storage, and pathogens, drugs, and toxins for metabolism and/or elimination. The other 30 % of blood flow is supplied by the hepatic artery, branching from the celiac trunk and delivering oxygenated blood to the liver. These blood supplies enter the liver at a hilum, the *porta hepatis* (otherwise known as the portal tract or portal triad (fig 1.1)), mixing together as they empty into the liver sinusoids

(through terminal hepatic arterioles and terminal portal venules) such that the cells of the liver are never exposed to fully oxygenated blood. Blood leaves the sinusoids via the central venules (otherwise known as terminal hepatic venules or central veins (fig 1.2)) and empties into the hepatic veins before the inferior vena cava (Cattley, 2002, Malarkey, 2005). The length from each portal tract to central venule is approximately 250 μm in the rat (Oda, 2006).

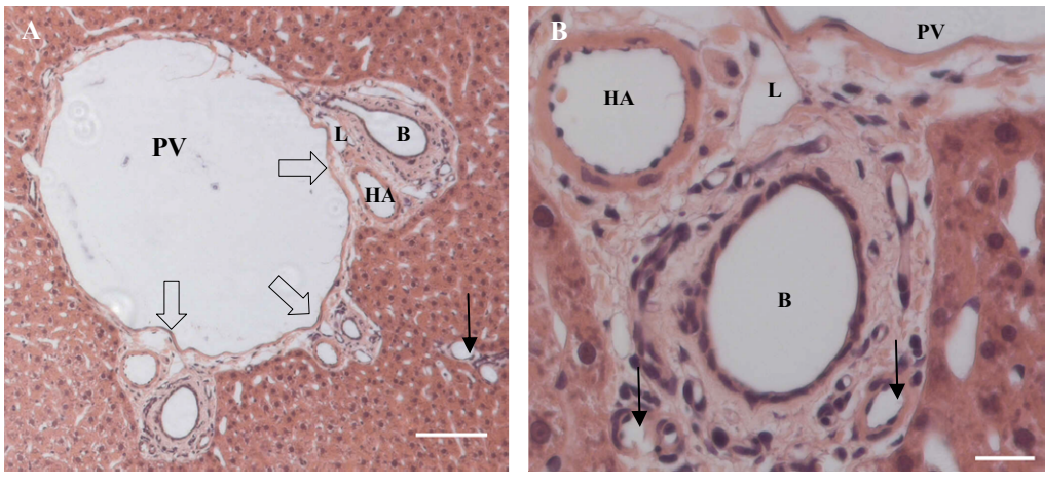

Figure 1.1 *A portal tract from the liver of an F344 rat*
A) A portal tract consisting of a portal vein (PV) and branches (open arrows) of the hepatic artery and arterioles (HA), bile ducts (B) and lymphatic vessels (L). The thin arrow points to a smaller branch of the portal venule, possibly a terminal venule. Bar = 100 μm.
B) Magnified view of a branch of vessels in the portal tract. Arrows point to smaller branches of hepatic arterioles. Bar = 20 μm

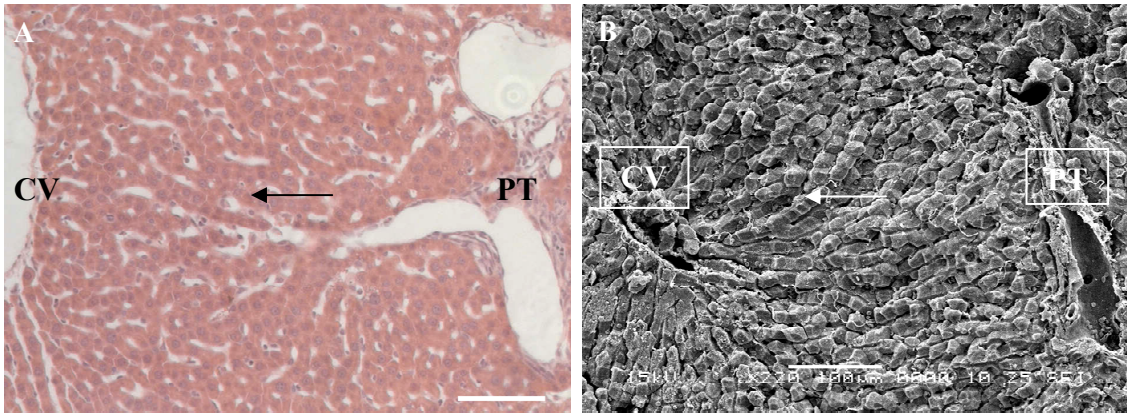

Figure 1.2 *Light and electron micrographs of the central vein, portal tract, and liver sinusoids from an F344 rat*
A) Histological and B) scanning electron micrographs of the portal tract (PT), central vein (CV), and sinusoids. Blood enters and exits the sinusoids in the direction of the arrow. The sinusoids are noticeably more tortuous around the portal tract, and run more parallel as they reach the central venule. Both bars = 100 μm.

Lymph and bile exit the liver through lymphatic vessels and bile ducts respectively which are part of the portal tracts, flowing in the opposite direction to the blood. Together with unmyelinated nerve endings (Oda, 2006), bile ducts and lymphatic vessels are adjoined with the portal venule and hepatic artery in a connective tissue matrix primarily made from type 1 collagen (MacSween, 2002, Ohtani, 2003) (fig 1.2).

The internal histological structure of the liver appears homogenous. It consists of a repetitive lobule, known as the "classic lobule" (Kiernan, 1833), that is roughly hexagonal in shape containing a central venule surrounded by repeating branches of portal tracts (figs 1.3 and 1.4). Within each lobule, the anatomical zones are classified as centrilobular (or central zone), containing the sinusoids and hepatocytes surrounding the central venules, periportal (or portal zone), containing the sinusoids and hepatocytes surrounding the portal tracts, and midzonal or midlobular, containing

the sinusoids and hepatocytes between these two (fig 1.3). Lobules are easily identified in the pig liver as each lobule is surrounded by connective tissue, and vascular septa (septal branches of portal veins and hepatic arterioles) are present in human and pig livers (fig 1.3), however these are not present in the rat (fig 1.4) (Teutsch, 1999).

Despite structural homogeneity, functional zones of the liver are heterogeneous within each lobule, across regions of each individual lobe, and between individual lobes. The metabolic zones or functional units of the liver, known as the acinus (first described in (Rappaport, 1954)), are defined according to the level of oxygenation and nutrient exposure of the cells (fig 1.3). Zone 1 contains the cells receiving the most oxygenated and nutrient rich blood lying closest to the portal venules and hepatic arterioles of the portal tracts and vascular septa. These cells are the first exposed to portal blood and are thus the first exposed to pathogens and toxins. Zones 2 and 3 respectively contain cells that are exposed to less oxygenated and less nutrient rich blood as they lie further and furthest away from the arteriolar blood. Rats lack the vascular septa present in humans and pigs (that more clearly outline the lobular pattern) and instead have a polyhedral portal unit that terminates in all branches of the central vein (Bhunchet, 1998). As such it has been suggested that the concept of the liver acinus may not be directly applied to the rat (Saxena, 1999, Teutsch, 1999). One method proposed to visualise a primary parenchymal functional unit in the rat is by immunohistochemical analysis of liver enzyme activity (Teutsch, 1992, Teutsch, 1999). Hepatocyte function (and enzyme activity) differs depending on cell location along the sinusoidal axis and the origin of the sinusoids (or sinusoidal blood). This serves to compartmentalise opposing metabolic functions. Using histochemical

analysis it is easy to visualise that the activity of the gluconeogenic enzyme glucose-6-phosphatase is highest in hepatocytes around portal tracts and has a decreasing gradient of activity along sinusoids towards the central venules (Teutsch, 1999). Whereas the activities of the glycolytic enzyme glucokinase (Teutsch, 1988) and the ketogenic enzyme 3-hydroxybutyrate dehydrogenase (Teutsch, 1992) are distributed reciprocally to glucose-6-phosphatase, being lowest in hepatocytes around the portal tracts and having a gradient of increasing activity along the sinusoids towards the central venules. Results from these studies suggest that the angioarchitecture and arrangement of hepatocytes into functional units in the rat are very similar to that described in the anatomical "classic" lobule (fig 1.3) in humans (Teutsch, 1988). Although the most widely accepted and used models are the (classic) lobule to describe the liver anatomical unit, and the acinus to describe the liver functional unit, many other alternative models of the functional and anatomical units of the liver have been proposed such as the "portal lobule" defined by the central venules with a portal tract at the centre, and the "primary lobule" combining function and anatomy (MacSween, 2002, Malarkey, 2005, Matsumoto, 1979, McCuskey, 2008, Teutsch, 1999).

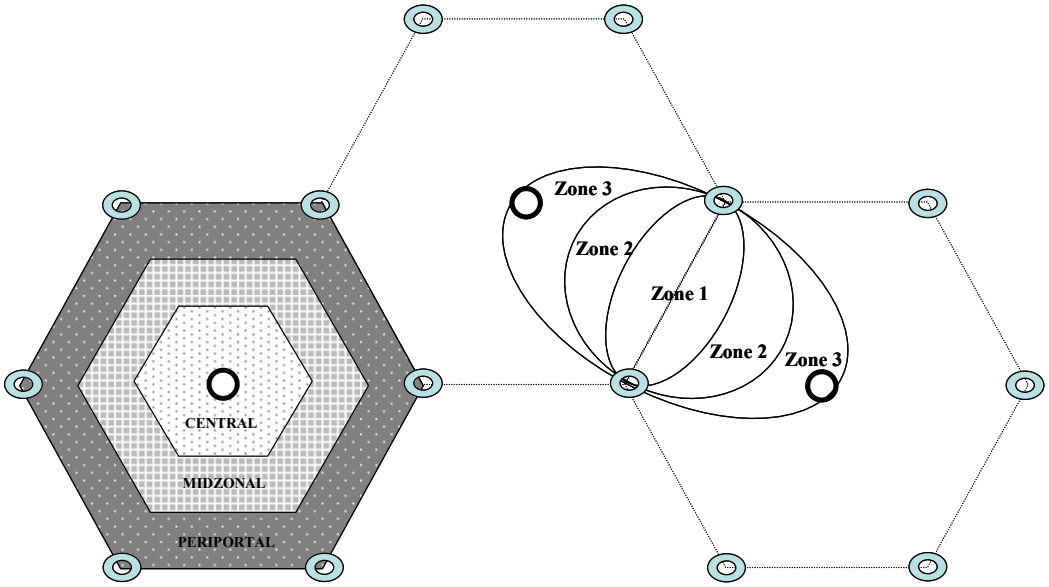

Figure 1.3 *A diagrammatic representation of the classic lobule and liver acinus*
The classic lobule is represented on the right, and the liver acinus (metabolic zones) to the left. Donuts at the corners of hexagons represent portal tracts and the circles at the centre represent central veins. The hexagons not only outline each lobule, but represent the path of vascular septa (adapted from (Cattley, 2002)).

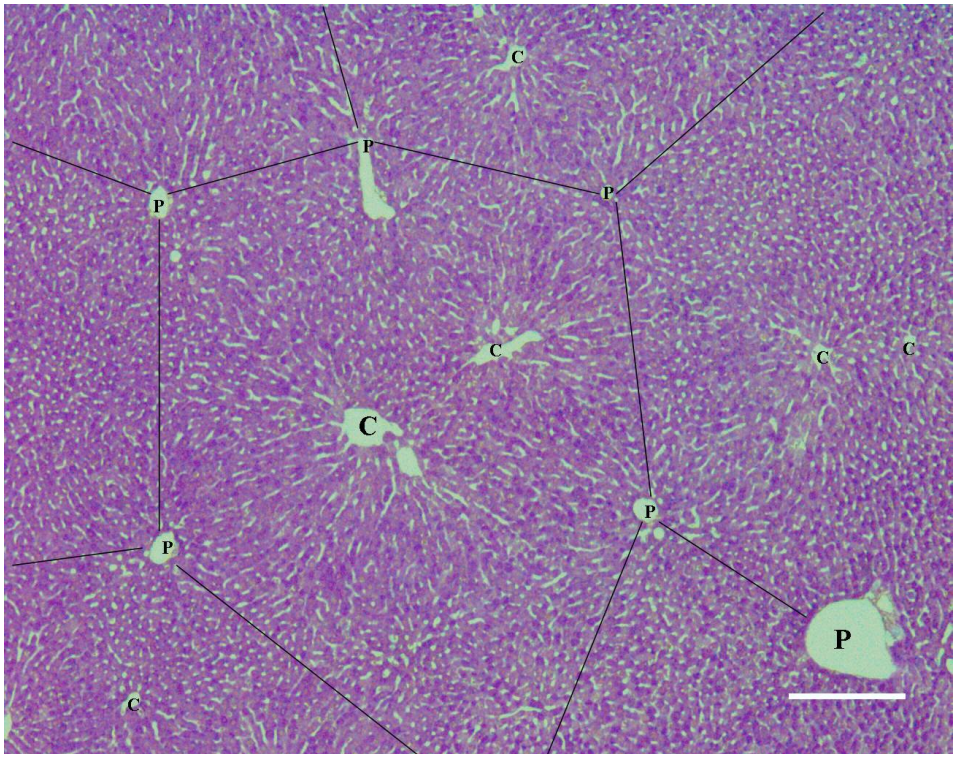

Figure 1.4 *A histological representation of the F344 rat liver lobule*
There is a repeating pattern of a central venule (C) surrounded by portal tracts (P) lacking connective tissue and vascular septa. Lines were added to roughly outline each lobule. The section was stained with Periodic acid Schiff (bar = 200 µm).

There is often variability in response to disease and toxicity within and across each liver lobe. Reasons for this are not well understood, however portal streamlining could influence variability (Malarkey, 2005). Blood flow to each lobe or lobule can be regulated by nerve stimulation or contraction of hepatic stellate cells (HSCs) (Reynaert, 2002), and the blood supply (branching of portal tracts) to each lobe varies. In addition there can be incomplete mixing of blood from the spleen and gastrointestinal tract, resulting in a variation of nutrients, toxins, and oxygen supply being delivered to each lobe. There are also differences in gene expression patterns across and between each liver lobe that could lead to variability in response to disease and toxins (Irwin, 2005).

1.1.2 Liver ultrastructure

1.1.2.1 The sinusoids and hepatocyte cords

The hepatic sinusoids, stretching between the portal tract and central venules (fig 1.2), are different to true capillary beds in that the endothelium lacks a proper basement membrane and is full of open transcellular pores (fenestrations) of approximately 0.1 - 0.2 μm in diameter that facilitate the unimpeded passage of blood plasma. Each sinusoid lumen is 7 - 15 μm in diameter, and is wider with smaller and more numerous fenestrations in Zone 3 than Zone 1 (Oda, 2006, Wisse, 1985).

The sinusoid wall can be classified into four concentric layers (Wake, 1999) (fig 1.5). The innermost luminal layer comprises the resident liver macrophages, Kupffer cells (KCs), and resident lymphocytic cells, pit cells and dendritic cells that travel the sinusoid lumens. The next layer contains the liver endothelial cells (LSECs) and the

third the hepatic stellate cells (HSCs), with a very underdeveloped basement membrane between the two. The outermost layer contains a small number of perisinusoidal sheaths of collagen (type 1 and 3 (Geerts, 1990)) fibrils for structural support, and occasional nerve fibres. The area between the LSEC and hepatocyte cell body (containing microvilli, stellate cells and ECM) is defined as the perisinusoidal space of Disse (SoD) (see section 1.4) (Wisse, 1985).

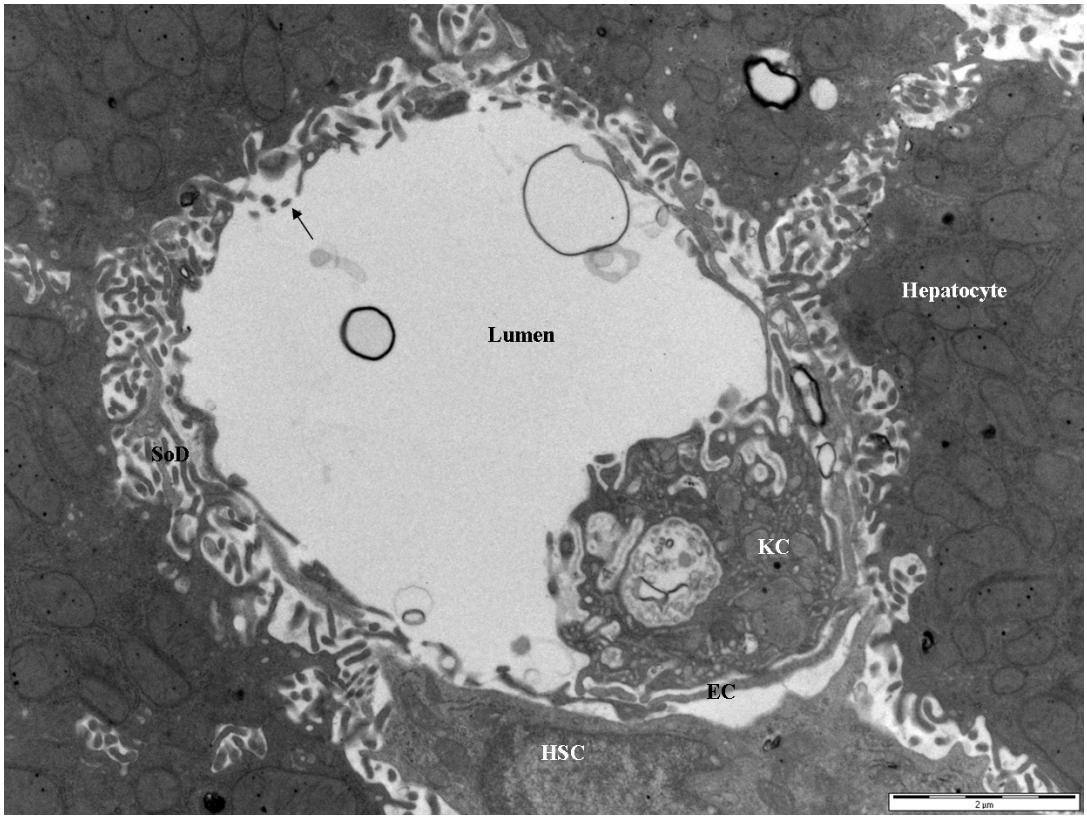

Figure 1.5 *A transmission electron micrograph displaying layers of the sinusoid wall from an F344 rat*
The space of Disse (SoD) contains the cytoplasmic processes of a hepatic stellate cell (HSC) and hepatocyte microvilli. The arrow points to fenestrations in a liver sinusoidal endothelial cell (EC) cytoplasm, and a Kupffer cell (KC) resides in the sinusoid lumen (bar = 2 µm).

Hepatocyte cords (otherwise known as sheets or plates) run between the sinusoids, joined together by desmosomes and tight junctions. Bile is produced by hepatocytes and secreted from their apical membrane. It flows through bile canaliculi (1 - 2 μm wide) made from the apical membranes of adjoined hepatocytes and sealed by tight junctions (fig 1.6). The bile then empties into the Canals of Hering and intrahepatic bile ductules that reside near the outer edges of each lobule, lined partially by cholangiocytes (epithelial cells of the bile ducts) and partially by a limiting plate of hepatocytes (fig 1.7). The bile then collects into the larger bile ducts of the portal tract before the hepatic duct (Saxena, 2004, Saxena, 1999, Strazzabosco, 2008).

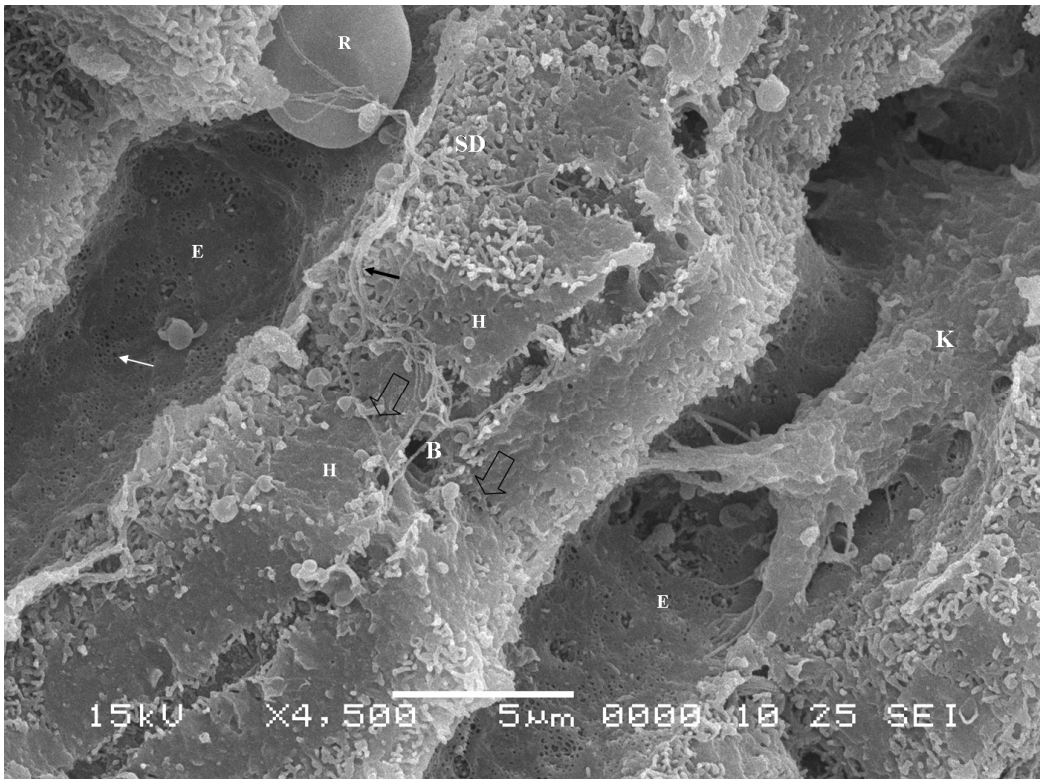

Figure 1.6 *A scanning electron micrograph from an F344 rat displaying the one cell thick hepatocyte plates that run between the sinusoids.* E = endothelium, R = RBC, H = hepatocyte, B = bile canaliculi, K = Kupffer cell, SD = space of Disse, the white arrow points to a fenestration, the black arrow indicates a collagen fibril, the open arrows indicate tight junctions between two hepatocytes (bar = 5 μm).

1.1.2.2 The perisinusoidal space of Disse

The perisinusoidal space of Disse (SoD), named after the German anatomist and histologist Joseph Disse (1852-1912), contains abundant hepatocyte microvilli, hepatic stellate cells, and extra cellular matrix (ECM), and marks the region between the hepatocyte cell body and LSEC. The flow of plasma and macromolecules in and out of the SoD via fenestrations is influenced by the passage of blood cells through the sinusoidal lumen and the composition of ECM. Blood cells (particularly white blood cells) are often larger than the diameter of the sinusoid and thus squeeze through the luminal space, sometimes modulating their shape to do so. This action promotes "forced sieving" of substances through fenestrations, and compression of the SoD by the movement of larger more rigid white blood cells along the lumens ("endothelial massage") promoting displacement of fluid in the SoD (McCuskey, 1979, Wisse, 1985). Movement of blood cells may also increase the uptake and exchange of substances by liver cells, and influence the flow and formation of lymph. Lymph (protein rich cell-free plasma) is believed to form in the SoD and be channelled through the collagen fibres (Ohtani, 2008) to the periportal tissue of Mall (or space of Mall), the area between the limiting plate of hepatocytes surrounding the portal tract and the portal tract interstitium (fig 1.7). It then drains through the portal interstitium to the portal lymphatic vessels before reaching the thoracic duct (Heath, 1998, MacSween, 2002, Ohtani, 2003, Saxena, 1999).

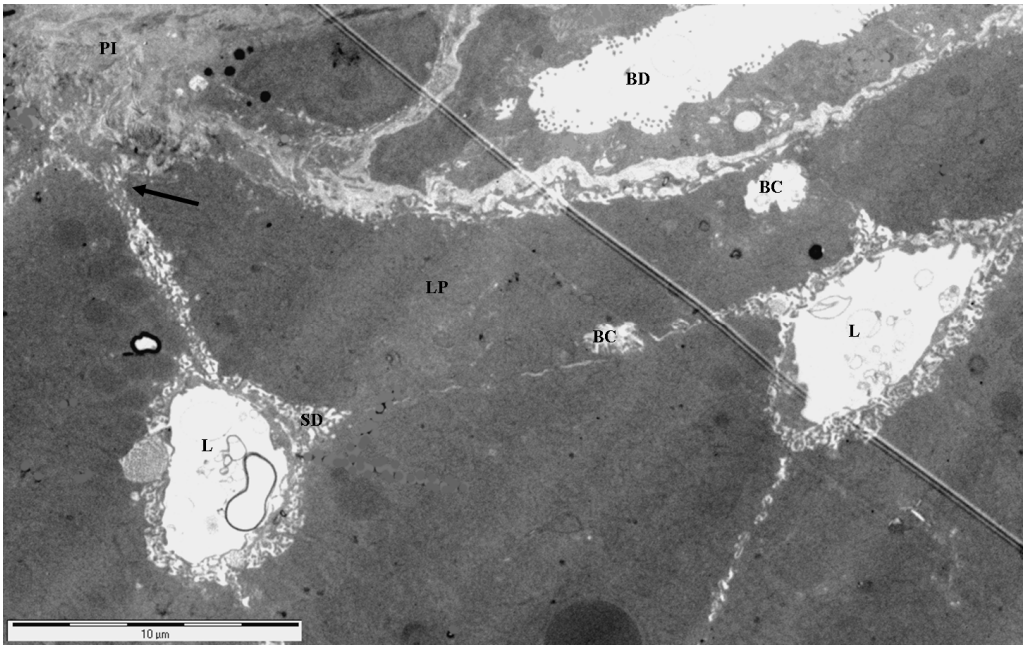

Figure 1.7 *A transmission electron micrograph showing the connection of the SoD to the portal interstitium and portal tract in an F344 rat.* An arrow points to the passage joining the SoD to the portal interstitium (PI) and lymphatic vessels in the portal tract. BD = bile duct, BC = bile canaliculi, L = sinusoid lumen, LP = limiting plate of hepatocytes (bar = 10 µm).

The ECM components in the SoD are primarily produced by HSCs and are very low density, allowing for mostly unimpeded transfer of substances through the fenestrations whilst providing some structural support for the parenchyma and LSECs (Yang, 2003). In the rat, ECM is made primarily of microfilamentous type VI collagen and minor amounts of other interstitial collagens (for example XIV and XVIII), few bundles of fibrillar collagen I and III (Benyon, 1998, Musso, 1998), and other macromolecules such as glycoproteins, proteoglycans, and adhesion proteins laminin and fibronectin (Kmiec, 2001, Reid, 1992). Alterations in the ECM modulate the phenotype and function of the surrounding cells including HSCs, hepatocytes, and LSECs (Benyon, 1998, McGuire, 1992, Reid, 1992). In fibrotic diseases of the liver the normal ECM is disrupted by the upregulation of enzymes such as matrix metalloproteinases and excess collagen (particularly fibril-forming types I and III) is

deposited (Musso, 1998). These changes interrupt the free passage of macromolecules and plasma through fenestrations and normal hepatocyte function (Neubauer, 2001, Yang, 2003).

1.2 Ultrastructure and function of liver cells

1.2.1 Liver sinusoidal endothelial cells

1.2.1.1 Structure and function

The liver sinusoidal endothelial cell (LSEC) was first distinguished as a unique cell type after the advent of high quality fixation and electron microscopy (Wisse, 1970, Wisse, 1972). As discussed in section 1.1.2.1, sinusoidal endothelial cells of the liver are distinct to those of other organs in that they are very thin and perforated with fenestrations of approximately devoid of diaphragms (Wisse, 1970) with very little underlying extra cellular matrix (Reid, 1992). This facilitates virtually unimpeded transfer of plasma and substances smaller than fenestrations between the sinusoid lumens and the SoD (Wisse, 1996). Maintenance and induction of this unique endothelial cell phenotype is regulated via paracrine secretion of vascular endothelial growth factor (VEGF) by neighbouring hepatocytes and HSCs, and autocrine production of nitric oxide by endogenous nitric oxide synthase (DeLeve, 2004). Each fenestration is supported by a cytoskeletal ring of actin and myosin, rendering them dynamic structures able to contract or dilate in response to various stimuli. Liver diseases, toxicity, and ageing are associated with loss of fenestrations and alterations of LSEC phenotype (as will be discussed further in sections 1.3 and 1.4).

LSECs form a continuous tubular lining of the vascular sinusoid lumens, sometimes extending cytoplasmic processes between hepatocytes ("tails") and into neighbouring sinusoids ("intersinusoidal bridges") (Wake, 1989). The LSEC perikaryon is found bulging into the sinusoid lumen or fitting snugly into a corner between hepatocytes, and contains the majority of cell organelles (fig 1.8). These include rough and smooth ER, Golgi apparatus, mitochondria, centrioles, and an abundance of lysosomes (dense bodies), clathrin-coated micropinocytotic vesicles, macropinocytotic vacuoles, and small uncoated vesicles important for scavenger functions (Blouin, 1977, Wisse, 1972). The remaining cytoplasm is much thinner, and contains sieve plates (fenestrated areas devoid of organelles) interspersed between cytoplasmic arms containing limited organelles, membrane rafts and caveolae (Braet, 2007, Svistounov, 2012, Wake, 1988, Wisse, 1972).

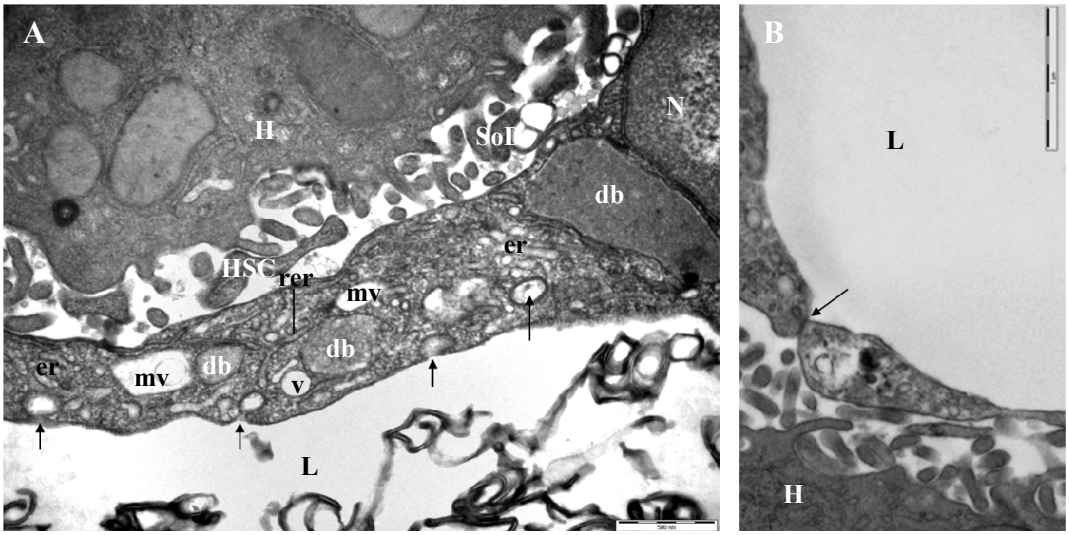

Figure 1.8 *Micrographs of the LSEC perinuclear region and intercellular junction from an F344 rat*
A) Arrows indicate different stages of receptor-mediated endocytosis via bristle- or clathrin-coated micropinocytotic vesicles. mv = macropinocytotic vacuoles, v = vacuole, db = dense bodies (lysosomes), rer = rough endoplasmic reticulum, N = nucleus, H = hepatocyte, HSC = hepatic stellate cell, L = sinusoid lumen, SoD = space of Disse (bar = 500 nm).
B) The arrow points to an intercellular junction between LSEC cytoplasmic processes. H = hepatocyte, L = sinusoid lumen (bar = 1 μm).

LSECs are professional pinocytes with specialised receptor-mediated endocytic scavenger functions, clearing the body of waste products such as acetylated and oxidised low density lipoproteins, advanced glycation end products, breakdown products of extra cellular matrix, and denatured plasma proteins (Parker, 2005, Smedsrod, 1990). Being in a prime position in the sinusoid with immediate exposure to sinusoidal blood, they work with KCs to form the reticuloendothelial system of the liver (DeLeve, 2007b, Smedsrod, 1997, Smedsrod, 1990) and possess high lysosomal enzyme activity similar or higher to that of KCs in order to efficiently degrade endocytosed macromolecules (Knook, 1980). By clearing the blood of foreign and physiological waste molecules, antigens, and viral particles, LSECs are important contributors to innate immunity (DeLeve, 2009, Sorensen, 2012). LSECs also contribute to adaptive immunity and have important immunomodulatory functions (Warren, 2006). They process and present antigens primarily to induce immune tolerance towards non-harmful antigens, and express cellular adhesion molecules (CAMs) for leukocyte adhesion and migration (DeLeve, 2007b, Parker, 2005). In addition, LSECs have a secretory role, synthesising substances that effect neighbouring and distant cells, such as endothelin, prostanoids, nitric oxide, and various other cytokines that activate and recruit leukocytes (Kmiec, 2001, Smedsrod, 1994). LSECs also secrete tissue specific growth factors, for example hepatocyte growth factor, that are vital for liver regeneration and hepatocyte proliferation during liver disease and toxicity (Kato, 2011). They also contribute to the production of ECM (Smedsrod, 1994) and express enzymes for xenobiotic metabolism (Steinberg, 1987).

1.2.1.2 The sieving function of LSECs

Fenestrations in the LSEC cytoplasm facilitate the size-dependent exchange of macromolecules and the free passage of vital nutrients and plasma proteins to and from the SoD, often described as the "liver sieve" (Fraser, 1995). This sieving function regulates the filtration of chylomicron remnants from the blood into the SoD and plays a critical role in lipid homeostasis. Chylomicron remnants deliver fat-soluble vitamins, dietary cholesterol, and other lipoproteins to HSCs and hepatocytes for processing. The diameter of fenestrations determines the size of remnants that are able to pass into the SoD, keeping the larger triglyceride-rich chylomicrons and remnants in circulation (Fraser, 1978). The "liver sieve" also enables lipoproteins such as very low density lipoproteins synthesised in hepatocytes (less than 90 nm in diameter) (Smedsrod, 1994) and retinoids released from hepatocytes and HSCs a passage to the blood, thereby influencing the fat and fat-soluble vitamin balance between the liver and other organs (Fraser, 1995, McCuskey, 2008). Reduction in size and/or number of fenestrations has been associated with hyperlipidemia (Cogger, 2006) and atherosclerosis (Fraser, 1995). Alterations or increases in the ECM of the SoD during disease states (such as cirrhosis) or toxicity alter lipid homeostasis by hindering the free passage of chylomicron remnants, as well as changing the LSEC phenotype to a less fenestrated form (Fraser, 1995, McGuire, 1992).

Fenestrations allow both drugs bound to albumin (or other serum proteins) and unbound drugs entry to the SoD. As unbound drug is taken up by the hepatocyte, the proportion of bound and unbound drug in the SoD re-equilibrates such that the fraction of drug cleared during one pass through the liver exceeds the unbound fraction, enhancing clearance and metabolism of drugs that are highly extracted

(DeLeve, 2009). Fenestrations also maximise oxygen delivery from the blood to hepatocytes. Sinusoidal blood is less oxygenated than blood from other tissues as it is a combination of arterial and venous blood. The thin cytoplasm of the LSEC that is devoid of a basal lamina and contains open fenestrations minimises the distance from the sinusoid to hepatocyte and maximises oxygen delivery (DeLeve, 2009). Defenestration and increased endothelial thickness has been associated with hepatocyte hypoxia (Le Couteur, 2001).

1.2.1.3 Fenestration structure

In the nineteenth century, free communication via small channels between the sinusoid lumens and SoD was observed using light microscopy and a technique of injecting dye (Fraser, 1895). However fenestrations, being smaller than the resolving power of a light microscope, could not be visualised before the advent of electron microscopy in the mid 20th century (Cogger, 2009, Fawcett, 1955). Wisse, using a high quality ultrastructural fixative and perfusion fixation, was first to document the structure and organisation of fenestrations (Wisse, 1970, Wisse, 1972). Fenestrations (fig 1.9) are grouped into sieve plates of 10 - 100 fenestrations that occupy about 5 - 10 % of the cell surface (Svistounov, 2012). The size of fenestrations are approximately 50 - 200 nm in diameter and differ slightly in different species (Braet, 2002). Actin microfilaments encircle each fenestration (fig 1.9 C) (Nagai, 2004), and a ring of F-actin supports each sieve plate, indicating the LSEC cytoskeleton influences the formation and modulation of fenestrations (Braet, 2007, Yokomori, 2006). The calcium-calmodulin-actomyosin complex is crucial to the regulation of fenestral diameter, and Rho A (a GTPase protein that regulates the actin cytoskeleton) is one of the key regulators of fenestration contractility (Yokomori, 2004a, Yokomori,

2004b). Enzymes associated with contraction and relaxation of the cytoskeleton, endothelial nitric oxide synthase (Yokomori, 2001) and calcium ATPase (Yokomori, 2004a), have been identified on the membranes of fenestrations.

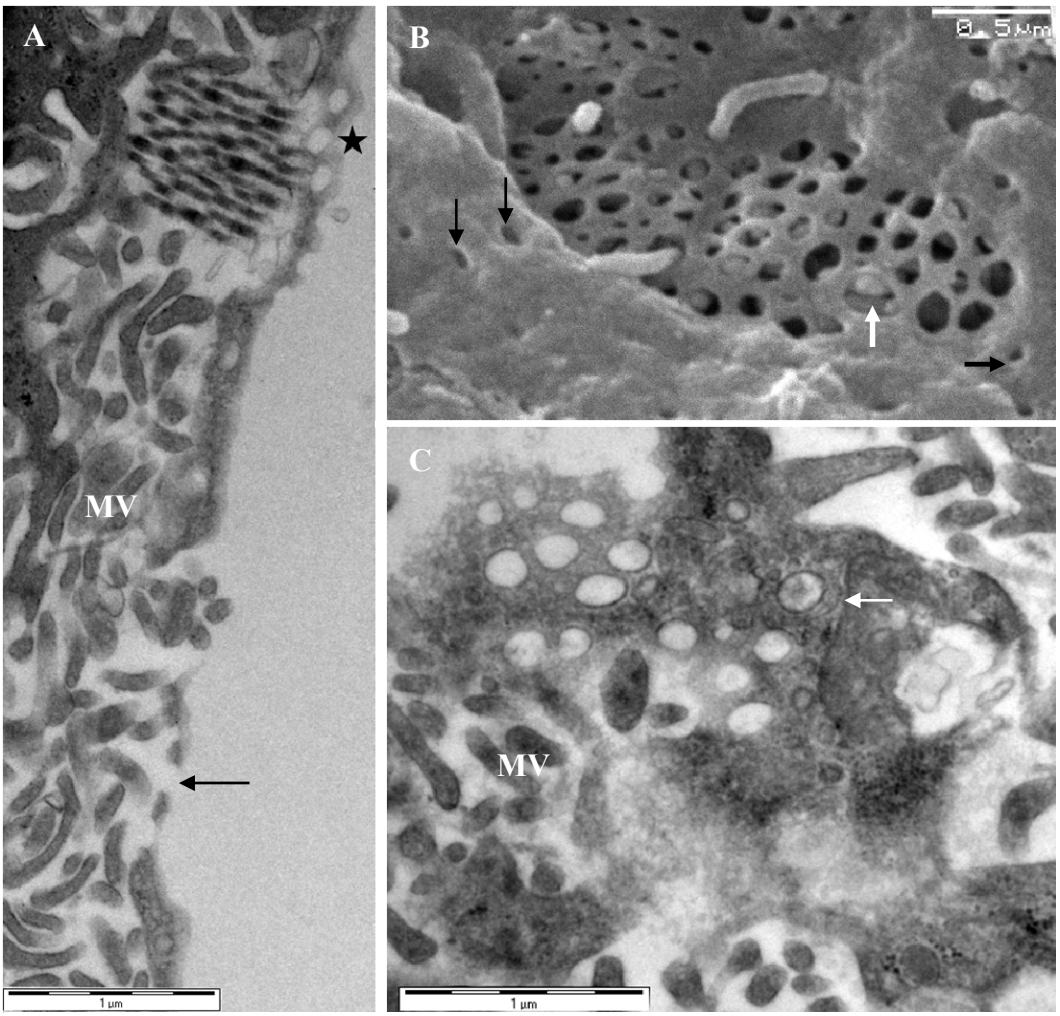

Figure 1.9 *Electron micrographs from an F344 rat displaying transverse and obliquely sectioned views of fenestrations on TEM and a 3-dimensional view on SEM*
A) TEM: Transverse section of the cytoplasmic extension of an LSEC containing transcellular fenestrations (arrow) and obliquely cut fenestrations (star). Hepatocyte microvilli (MV) fill the SoD interspersed with a collagen bundle (Co) (bar = 1 µm).
B) SEM: Three dimensional image of the LSEC cytoplasm showing a sieve plate interspersed between thicker regions containing organelles and "pits" or caveolae (black arrows). A white arrow indicates hepatocyte microvilli that are visible through a fenestration (bar = 0.5 µm).
C) TEM: An obliquely sectioned LSEC cytoplasm showing actin microfilaments that encircle fenestrations (arrow). MV = hepatocyte microvilli (bar = 1 µm).

Fenestrations are not always of the simple single-layered type, but are sometimes organised into labyrinthine structures of unknown function found mostly in the perinuclear region (Braet, 2009). These structures have previously been described as tortuous or meandering canaliculi (Ohata, 1984) and resemble vesiculo-vacuolar organelles (Dvorak, 2001). “Pored domes” (Ohata, 1984) or “loops” (Braet, 2007) are another frequently observed fenestration-associated structure of unknown function. With the appearance of a fenestrated vacuole, they are usually found over the nuclear area of the LSEC.

Gaps represent pores in the LSEC cytoplasm greater than approximately 300 nm. Gaps are thought to occur as a result of fusion of fenestrations, with the maximal size of a gap equalling that of a sieve plate (Wisse, 1985). Dumbell shaped fenestrations have occasionally been observed in the LSEC cytoplasm and may represent a stage in the fusion of fenestrations during the process of gap formation (Shin, 1997). It is not known whether gaps are present in normal physiological conditions as large chylomicrons, that would have otherwise traversed through the gaps, are not found in the SoD (Wisse, 1985), and gaps can form after inadequate fixation techniques and high-pressure perfusion of fixative (Braet, 2004, Fraser, 1980). However, gaps also form in LSECs as a result of cellular injury in disease states and toxicity (Ito, 2006).

1.2.1.4 Fenestration formation

The mechanism of fenestration formation and loss remains unclear, and no markers have been found that specifically label fenestrations. It has been postulated that fenestrations form from fusion between opposite sheets of plasma membrane that are depleted of intramembrane particles, or from coated-pits and caveolae that share a

similar size and position to fenestrations (Braet, 2007). Caveolae are invaginations of the plasma membrane abundant in several types of endothelial cells (Yokomori, 2012). Their functions include transcytosis, cytoplasmic calcium regulation, potocytosis, and signal transduction, and they are a specific type of membrane raft (Sowa, 2001). Caveolar formation is dependent on the presence of caveolin, a transmembrane scaffolding protein. Caveolin is sometimes found in the membranes around fenestrations (Yokomori, 2003b), however it has recently been shown that caveolin is not necessary for the formation of fenestrations as LSECs of caveolin-knockout mice are normally fenestrated (Warren, 2010).

It is now known that the regulation of membrane rafts (found in the thicker cytoplasmic regions between sieve plates) is influential to the formation of fenestrations. Membrane rafts are highly dynamic sterol and sphingolipid enriched lipid-ordered domains of the cell membrane that compartmentalise cellular signalling molecules. Rafts range from 10 - 200 nm in width and may aggregate into micrometer sized structures ("platforms") for signal transduction (Viola, 2007). They are tethered to the actin cytoskeleton, essential to the maintenance of their structure and integrity. Actin disruptors decrease the presence of membrane rafts and increase the number of sieve plates such that rafts and sieve plates may have an inverse relationship in the LSEC cytoplasm (Svistounov, 2012). Fenestrations have also been observed to form in non-raft lipid-disordered (fluid) regions once the stabilising effects of actin and rafts are depleted, and it is possible that fenestrations are created as a result of vesicles that spontaneously form in the cell membrane after it is destabilised (Svistounov, 2012). Agents that increase fenestration number (table 1.1) contract F-actin, therefore it is also possible that fenestrations spontaneously form in response to stretching and

thinning of the cytoplasm between the contracted ring of F-actin (Cogger, 2010) analogous to the manufacture of expanded film ultrafiltration membranes (Baker, 2004). Areas of cytoplasm containing fenestrations are about 50 nm, approximately half as thick as the cytoplasm surrounding the sieve plate (Cogger, 2010).

It is also possible to induce acute fenestration formation (within minutes) via actin-disrupting agents (table 1.1). Studies on acute fenestration formation have revealed a structure named the "fenestration forming centre" that may be involved in fenestration formation. It consists of thin filaments that fan out from the centre of sieve plates that may serve to guide newly formed fenestrations into position. A potential "defenestration centre" has also been proposed (Braet, 2002, Braet, 2007).

1.2.1.5 Fenestration modulation

A combination of human and animal clinical and experimental studies have shown that fenestration diameter and frequency can be modulated through acute and chronic exposure to a number of substances and conditions (table 1.1) including cytokines and hormones, inflammation, dietary fat load, ECM, ageing, toxicity, and disease states (Cogger, 2009). The exact mechanisms that govern how LSEC size is maintained *in vivo* is not fully understood. However it is known that fenestration diameter is regulated by the calcium-calmodulin-actinomyosin complex (the cytoskeleton ring shown in fig 1.9 C) around fenestrations, and thus contraction of fenestrations is associated with calcium influx (Braet, 2002). Intracellular calcium binds with calmodulin, activating myosin light chain kinase which phosphorylates the 20 kD subunit of myosin light chain initiating contraction of actin filaments. Calcium ionophores and substances that stimulate G-protein coupled receptor opening of

calcium channels (such as serotonin) induce contraction of fenestrations, whereas substances that chelate extracellular calcium, calcium channel blockers, and calmodulin antagonists suppress contraction (Gatmaitan, 1996). For example, prostaglandin E1 is a fenestration dilating agent as it enhances calcium ATPase pump activity on the membranes of fenestrations, leading to fenestration dilation (as cytoplasmic calcium is extruded) (Oda, 1997). On the other hand endothelin 1 is a fenestration contracting agent as it diminishes calcium ATPase pump activity, thereby increasing the concentration of intracellular calcium (Yokomori, 2003a).

How LSECs regulate their number of fenestrations *in vivo* is also not completely understood. It is known that actin disruptors (cytochalasins and latrunculins for example) induce profound changes in microfilament organisation in the LSEC, including depolymerisation and destabilisation of the actin cytoskeleton, and increase the number of fenestrations per cell (Braet, 1996). The actin cytoskeleton is bound to lipid rafts in order to tether and maintain lipid raft structure (Chichili, 2009, Viola, 2007), and recently it has been shown that disruption of both actin filaments and lipid rafts act via a similar or associated mechanism to increase fenestrations. 7-Ketocholesterol, a membrane disrupting lipid raft destabilising agent (Kahn, 2011), and cytochalasin D, an actin disruptor, similarly increased the number of fenestrations when applied to LSECs *in vitro* (Svistounov, 2012). In addition, substances that are associated with increasing lipid-ordered membrane and lipid raft formation, such as triton X-100 (Ingelmo-Torres, 2009), reduce the number of fenestrations when applied to LSECs *in vitro* (Svistounov, 2012).

Alterations to fenestrations influence many *in vivo* processes such as chylomicron trafficking (Fraser, 1978, Hilmer, 2005), drug clearance (Mitchell, 2010), oxygen supply to hepatocytes (Le Couteur, 2001), and immune function. T-lymphocytes in the sinusoid lumens project cytoplasmic extensions through fenestrations (see Appendix 5, A3) in order to interact with major histocompatibility complex/peptide complexes and intercellular adhesion molecules expressed on the hepatocyte perisinusoidal surface (Warren, 2006). These interactions are crucial to immune modulation and may be important for immune tolerance and activation of naïve T-lymphocytes. Table 1.1 lists a number of substances, environmental factors, and disease states that influence fenestration size and the number of fenestrations per LSEC.

Table 1.1 Modulation of fenestration diameter and number via particular substances, disease, and environmental factors, adapted from (Cogger, 2009) and (Braet, 2002).

Treatment	Diameter of fenestrations	Number of fenestrations per cell
Actin disruptors		
Cytochalasin B and D	↑↓	↑
Dihydrohalichondramide	↓	↑
Latrunculin A	↓	↑
Misakinolide	↓	↑
Swinholide A	↓	↑
Other		
Acetylcholine	↑	?
Adrenaline	↓	?
Bethanechol	↑	?
Calmodulin agonist W-7	↑	?
Carbon tetrachloride	↑	↓
Cocaine and ethanol	?	↓
Collagen IV	n.c.	↑
Diethyl nitrosamine	?	↓
Dimethyl nitrosamine	n.c.	↓
DOI (2,5-dimethoxy-4-iodoamphetamine) young mice (Furrer, 2011)	n.c.	n.c.
DOI (2,5-dimethoxy-4-iodoamphetamine) old mice (Furrer, 2011)	↑	↑
Endothelin 1	↓	↓
ET_A-R antagonist (BQ123)	↑	?
Ethanol acute dose	↑	↓
Ethanol chronic dose	↑↓	↓
Fatty liver	?	↓
Hypoxia	↑	?
Hepatectomy	↑	↓
Hepatitis C	↓	↓
Ionophore A23187	↓	?
Irradiation	↑	?
Isoproterenol	↑	?
Jasplakinolide	↓	↑
7-Ketocholesterol (Svistounov, 2012)	↑	↑
Laminin	n.c.	↓
Neuropeptide Y	↓	?
Noradrenaline	↓	?
Nicotine	↓	?
Pantethine	↑	↑
Phalloidin	↑	?
Phorbol myristate acetate	n.c.	↑↓
Pressure	↑	?
Prostaglandin E_1	↑	?
Serotonin	↓	?
Temperature 4 ºC	?	↓
Thioacetamide	↓	↓
Triton X-100 (Svistounov, 2012)	↓	n.c.
Tumour cells	↓	↓
TNF-α	?	↓
Vasoactive intestinal peptide	↑	?
Vascular Endothelial Growth Factor	↑	↑

Legend: ↑ = increase, ↓ = decrease, ↑↓ = conflicting reports, n.c. = no change, ? = unknown.

1.2.1.6 Methods for the study of fenestration modulation

The study and measurement of fenestrations is performed using a variety of methods (Braet, 2007, Cogger, 2009). Isolation of LSECs from rat livers has been the predominant method of studying fenestration biology and modulation in response to numerous stimuli, with subsequent viewing on electron or confocal microscopy (Cogger, 2009). A controlled dose of a chemical may be directly added to an *in vitro* culture of cells, and conditions may be altered such as temperature and oxygen tension, much more accurately than *in vivo*. However, there are issues associated with the *in vitro* method that must be taken into consideration on using this method for analysis. LSECs only remain viable for 1 – 2 days when cultured alone on collagen coated-wells (Sellaro, 2007), gradually changing from a fenestrated to a defenestrated phenotype (DeLeve, 2004). The fenestrated LSEC phenotype is maintained *in vivo* by a combination of paracrine and autocrine factors and a specific ECM. Thus, maintenance of fenestrations and increased cell survival in culture requires addition of paracrine factors to the culture media (such as VEGF) (DeLeve, 2004, Krause, 2000), using ECM of a similar nature to the sinusoids as a substrate (Sellaro, 2007), and maintaining the culture in an environment of physiological oxygenation (Martinez, 2008). The method of density gradient centrifugation and selective adherence has been thoroughly documented (Braet, 1994, Smedsrod, 1985) and produces high purity confluent LSEC cultures of a fenestrated phenotype, however this method is time consuming (DeLeve, 2009). Other simpler methods using immunomagnetic beads to sort LSECs from other liver cells are also currently used such as the anti-CD146 antibody immunomagnetic sorting method as CD146 is more expressed by LSECs than other liver cells (Tsuchiya, 2013). However as there are no known antigens specific to LSECs this method may yield mixed cell populations (DeLeve, 2009).

Anti-CD31 antibody separation was another immunomagnetic cell sorting method previously used to isolate LSECs, but was shown only to isolate LSECs of the defenestrated or capillarised phenotype and therefore results from this method were not reliable (DeLeve, 2006).

The formation of gaps as a result of non-specific cellular injury may occur *in vitro* and artefactually increase the average diameter of fenestrations during the analysis of fenestration diameter (Cogger, 2009). This occurs particularly when the mean diameter of fenestrations is taken before they are grouped into size-categories (for example from 0 – 300 nm, and greater than 300 nm). Porosity measurement may also be affected if gaps are not taken into consideration, as porosity is a measure of the perforated surface area of each cell (Wisse, 1983). Methods for fenestration diameter and porosity measurement are not standardised and thus subjectivity exists, however, thousands of fenestrations are measured in each study, increasing the confidence of results and providing important information on fenestration modulation.

1.2.2 Hepatic stellate cells

Hepatic stellate cells (HSCs) are also commonly known as fat-storing cells, vitamin A-storing cells, lipocytes, or Ito cells (as they were first described in detail by Ito and Nemoto in 1952) (Kmiec, 2001). They are perisinusoidal cells (residing in the SoD) with their nuclei commonly found wedged between hepatocytes (fig 1.10), and are more abundant in periportal regions of the liver (McCuskey, 2008, Senoo, 2004). HSCs have long, thin, and branching subendothelial processes that surround LSECs, and interhepatocellular (or intersinusoidal) processes that penetrate hepatocyte cell plates and extend processes along up to three adjacent sinusoids (Reynaert, 2002,

Zimmermann, 1999). These processes contain smooth muscle actin and desmin filaments, and can influence blood flow to sinusoids by constricting or relaxing in response to vasoactive substances (including contraction by endothelin-1, and vasopressin, and relaxation by nitric oxide) (Kawada, 1993, Reynaert, 2002).

HSCs regulate retinoid homeostasis (Senoo, 2007). In their quiescent state they store approximately 80 % of retinoids in the body as retinyl (vitamin A) palmitate in lipid droplets. They are the principle synthesisers of hepatic ECM, and also secrete ECM degrading components such as matrix metalloproteinases, cytokines, and growth factors, in order to regulate the SoD microenvironment (Arthur, 1995, Reynaert, 2002). In addition, HSCs are antigen presenting cells, eliciting T-cell responses as efficiently as dendritic cells (see section 1.2.4.3). Their location in the SoD gives them an optimal vantage point for detecting any pathogens that have crossed the endothelium to attack hepatocytes (Winau, 2007).

In their activated state (induced to aid in the repair of injury), HSCs adopt the phenotype of a myofibroblast, lose their lipid vitamin A droplets, express more smooth muscle actin (become more contractile), and alter their synthesis and degradation of ECM components (Senoo, 2007, Zimmermann, 1999). Chemotactic and autocrine stimulation as well as altered ECM composition stimulates proliferation of HSCs and their migration to areas of injury (Yang, 2003). Under chronic inflammatory and pathological conditions HSCs can promote and intensify the persistence of liver injury. Their continuing proliferation, release of proinflammatory cytokines, and increased ECM production can eventually lead to fibrosis and cirrhosis of the liver (Le Bail, 1990, Reynaert, 2002, Yang, 2003).

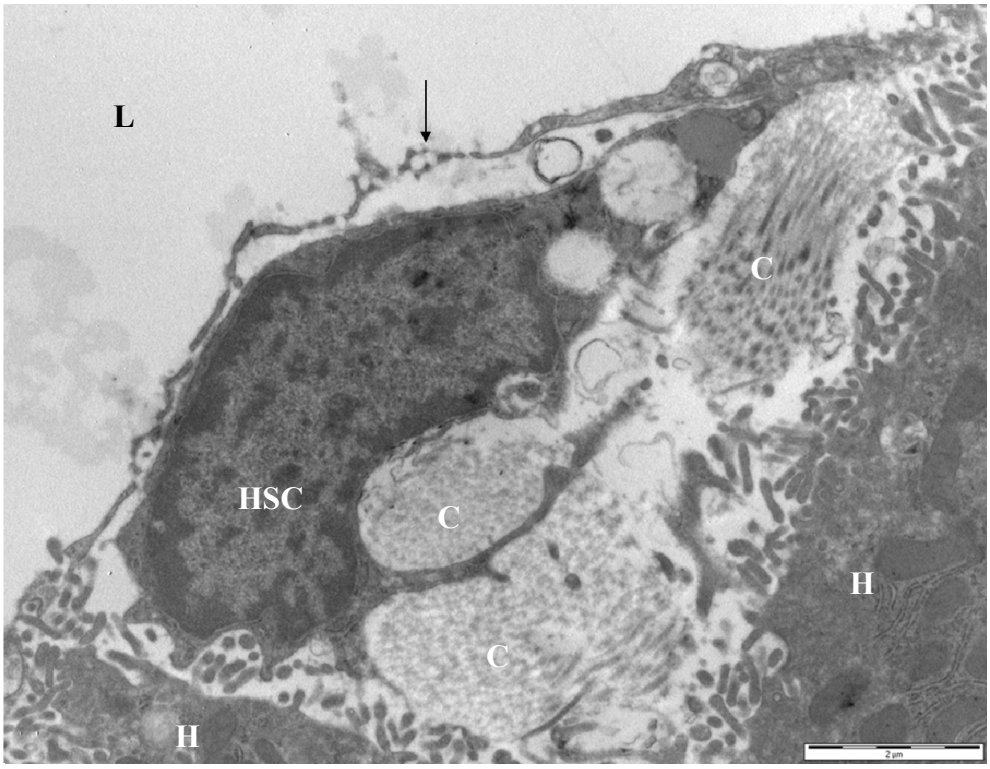

Figure 1.10 *Transmission electron micrograph of a hepatic stellate cell, F344 rat*
This micrograph shows the perikaryon of a HSC containing lipid droplets and producing fibrillar collagen (C). An arrow points to fenestrations in an LSEC cytoplasm. H = hepatocyte, L = sinusoid lumen (bar = 2 μm).

1.2.3 Hepatocytes

Hepatocytes comprise about 80 % of the total volume of the liver, forming the bulk of the parenchyma but representing only about half of the number of total cells (Kmiec, 2001). They have a role in almost all of the primary liver functions such as carbohydrate, lipid, and amino acid metabolism and storage, blood glucose regulation, and bile, cholesterol, and plasma protein (for example albumin) synthesis. They are also the main site of xenobiotic metabolism and transamination reactions in the body (Steinberg, 1987) and have the capacity for antigen presentation and T-cell activation (Crispe, 2011, Warren, 2006). The first thorough ultrastructural analysis of the hepatocyte was by Fawcett (Fawcett, 1955).

Hepatocytes are a polarised multifaceted polyhedral cell. They are mostly organised into plates of single cells (hepatocyte cords) supported by a fine reticular fibre (collagen III) framework, and surrounded by vascular sinusoids maximising their exposure to the blood (fig 1.6) (Cattley, 2002). The sinusoidal (basolateral) surfaces of the hepatocyte are abundant in microvilli that increase the area for hepatocyte substance uptake and exchange by six-fold and often protrude into the lumen through fenestrations (Wisse, 1985). The canalicular (apical) surfaces of the hepatocyte are its secretory poles where bile is released and are positioned between the lateral surfaces that face adjacent hepatocytes (figs 1.6, 1.7 and 1.12). These contain the zonula occludens (or tight junctions) that seal the bile canaliculi, and the adhering junctions (including intermediate junctions and desmosomes) that link neighbouring hepatocytes and express gap junctions facilitating intercellular communication and exchange (Kuntz, 2008).

Hepatocytes contain a high density of cytoplasmic organelles (fig 1.11) including over 1500 mitochondria that take up 20 - 30 % of the cell volume, and are abundant in smooth and rough ER, free ribosomes, Golgi apparatus, lysosomes, and peroxisomes (Blouin, 1977, Kmiec, 2001, Kuntz, 2008). They also possess great regenerative capacity, being able to proliferate rapidly in order to replace lost or damaged cells after partial hepatectomy and during disease and toxicity (Fausto, 2003). Hepatocytes have different functions and enzymatic expression depending on what zone of the acinus they reside in. Those hepatocytes closest to the portal tract (Zone 1) receive a blood supply richer in oxygen and nutrients than hepatocytes in Zones 2 and 3, such that their capacity for oxidative energy metabolism, glucose output, urea and bile synthesis, and antioxidant ability (with more glutathione storage and ability for

replenishment) is greater. Hepatocytes closest to the central vein have the highest capacity for glucose uptake, glutamine formation, and xenobiotic metabolism (Jungermann, 2000) which is a particularly important function of hepatocytes. Biotransformation of xenobiotics is generally classified into two phases (Gonzalez, 2006). Phase I metabolising enzymes (known as "oxygenases") include the large family of cytochrome P450 (CYP) enzymes located in the endoplasmic reticulum. Phase I enzymes carry out oxidative, reductive, or hydrolytic reactions to inactivate drugs, however are also able to activate pro-drugs such as cyclophosphamide into active metabolites, and activate pro-toxic substances and drugs such as carbon tetrachloride and acetaminophen into highly reactive radicals (Cattley, 2002, Kuntz, 2008). Phase II metabolism (Jancova, 2010) involves conjugation by specific transferases (such as glucuronidation and sulfation) that inactivate and increase the hydrophilicity of drugs for elimination via the bile canaliculi (sometimes termed as the phase III pathway) or via the blood stream to the kidneys, and detoxify substances including those metabolites of atoxic drugs that were transformed into toxic metabolites during phase I reactions. An abundant supply of the antioxidant glutathione in hepatocytes is often necessary for phase II detoxification of toxic metabolites (Lauterburg, 2002). If the presence of a toxic metabolite is too great such as during overdose or poisoning, glutathione stores may deplete, resulting in cellular injury by oxidative damage and conjugation of toxic metabolites with important cellular proteins (Jaeschke, 2012a). Zone 3 or centrilobular hepatocytes are particularly vulnerable to such injury (Cattley, 2002) as they express the highest level of CYP450s, combined with the lowest glutathione stores and the lowest capacity to replenish these stores after depletion.

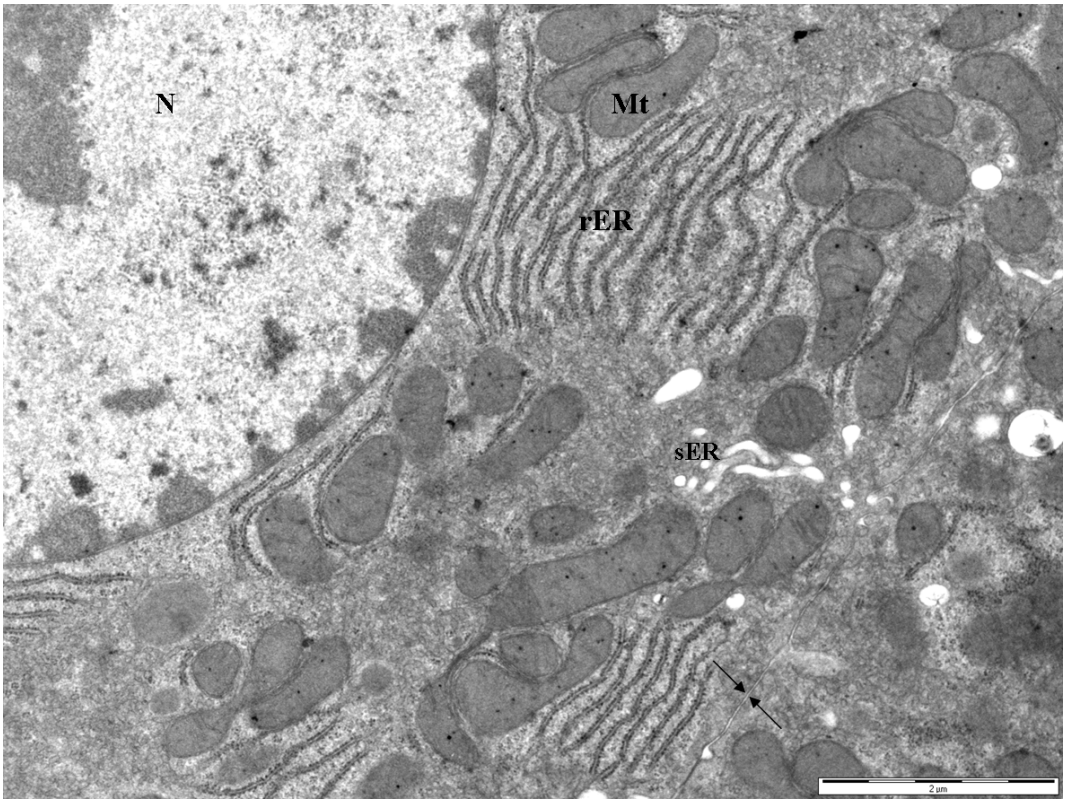

Fig 1.11: ***Transmission electron micrograph of a hepatocyte nucleus and cell body*** showing a typical abundance of rough ER, mitochondria, and some smooth ER. The arrows point to the outer membranes of two adjacent hepatocytes (bar = 2 μm).

1.2.4 Resident macrophages and lymphocytic cells of the liver

Being the first organ exposed to gut and intestinal blood and the body's first line of defence against pathogens, the liver contains a dense supply of specialised resident macrophages (Kupffer cells) and is constantly surveyed by lymphocytes (Lalor, 2002) and dendritic cells.

1.2.4.1 Kupffer cells

Kupffer cells (KCs) are a long lived resident macrophage population of the liver and are of monocyte origin (McCuskey, 1990, Naito, 2004, Smedsrod, 1994). They were discovered by von Kupffer in 1876, although were not distinguished as a distinct cell type from the LSEC until the early 1970s (Wisse, 1972). KCs form the frontline of host defence, being the first macrophage population exposed to freshly ingested pathogens and toxins from the gut. They have an important role in the phagocytosis and destruction of bacteria and bacterial endotoxin, viruses, fungi, and parasites. They also help to clear the sinusoids of cellular debris and of cells that are foreign or old and damaged such as effete RBCs and dead leukocytes, and are more numerous with greater endocytotic ability in the periportal regions where the portal blood first enters (Kmiec, 2001, Parker, 2005). KCs act synergistically with pit cells (see section 1.2.4.2) in the killing of tumour cells (Wisse, 1997) and are antigen-presenting cells (Bouwens, 1992). They have an important role in immunomodulation through secretion of various cytokines (interleukins, prostanoids, TNF-alpha, nitric oxide) and reactive oxygen species, and as such their persistent activation and proliferation can contribute to the pathogenesis of liver disease and drug toxicity (Bilzer, 2006).

KC cytoplasms contain well developed ER and Golgi apparatus as well as many digestive organelles such as lysosomes (dense bodies), clear vacuoles, and fuzzy coated vacuoles, along with vermiform processes (worm-like bodies) and bristle coated micropinocytotic vesicles (fig 1.12) involved in their phagocytic and cytotoxic action (McCuskey, 2008). They are irregularly shaped cells with many cytoplasmic projections (including microvilli, pseudopodia, lamellopodia, filopodia) that increase upon their activation (Bilzer, 2006) and are involved in their phagocytotic functions, migration, and anchoring. KCs travel through the sinusoids adherent to the luminal membrane of LSECs, projecting their cytoplasmic processes through fenestrations for further anchorage and to contact HSCs and hepatocytes. They are occasionally observed in direct contact with hepatocytes interdigitated between LSECs (McCuskey, 2008).

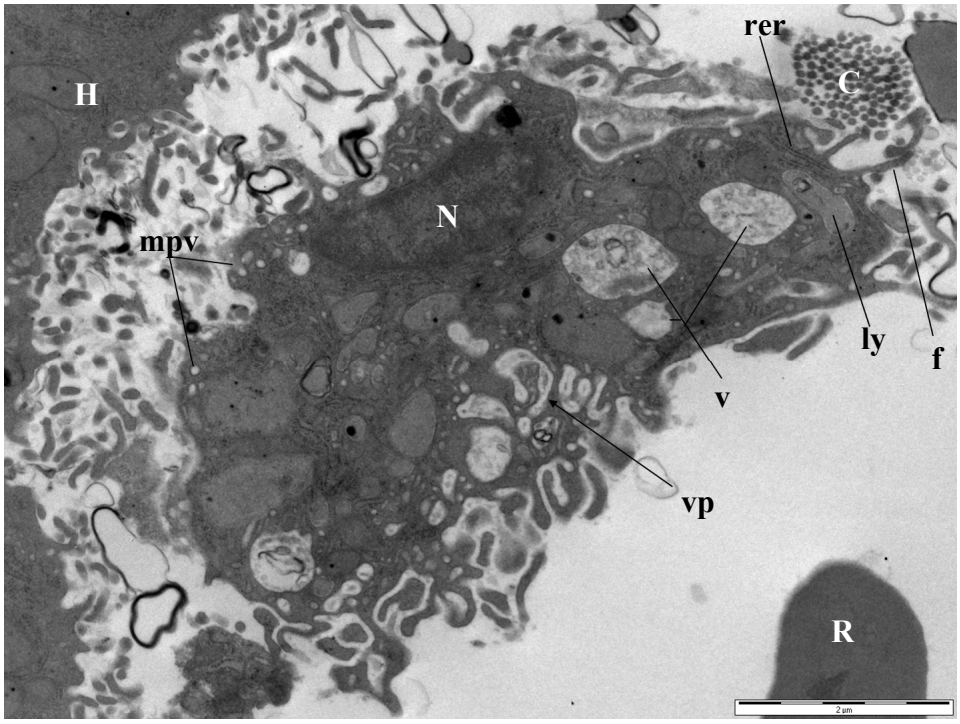

Figure 1.12 *Transmission electron micrograph of a Kupffer cell from an F344 rat*
N = nucleus, mpv = micropinocytotic vesicles, vp = vermiform process, ly = lysosomes, v = endocytic vacuoles, f = filopodia, rer = rough endoplasmic reticulum, H = hepatocyte, R = RBC, C = collagen (bar = 2 µm).

1.2.4.2 Pit cells

Pit cells, so named due to their characteristic dense spherical cytoplasmic granules or 'pits', are large granular lymphocytes exclusive to the liver and first described in 1976 (Wisse, 1976). They are a type of natural killer (NK) cell that are differentiated from precursor blood NK cells into liver specific NK cells (pit cells) on reaching the liver. Pit cells are found in the sinusoid lumens (fig 1.13) often in contact with KCs, adherent to LSECs (Nakatani, 2004), and project their long pseudopodia through fenestrations to contact hepatocytes (Luo, 2000). The pit cell cytoplasm is polarised with a kidney-shaped nucleus on one side and an array of organelles on the other. They are not easily morphologically distinguished from peripheral NK cells, however, pit cells generally contain numerous small sized granules whereas blood NK cells have larger and fewer granules and less rod-cored vesicles (Luo, 2000). Pit cells, similar to NK cells, possess cytotoxic activity and are able to kill tumour and virus-infected cells without prior sensitisation by releasing their granules containing lysosomal enzymes. They are more cytotoxic than other natural killer cell lineages (Bouwens, 1992, Luo, 2000) and are able to induce apoptosis of target cells, release cytokines that influence activity of other immune cells, and participate in resistance to microbial pathogens. The discovery and recognition of the pit cell and its function in the liver helped to establish the liver's early role in the defence against tumour and microbial targets, and the liver as an immunological organ (Nakatani, 2004).

1.2.4.3 Dendritic cells and lymphocytes

Dendritic cells are bone marrow-derived professional antigen presenting cells that travel the liver sinusoids (typically located near central veins and portal tracts), capturing and processing antigens before translocating to the portal interstitium and

lymphatic vessels (Ohtani, 2003). Eventually they accumulate in lymph nodes where they present the antigens to T- and B-cells in order to initiate immune response or tolerance (Matsuno, 2000). Dendritic cells have characteristic veils (long, thin membrane extensions) and sometimes bundles of microvilli on their surface, important for their interaction with T-cells (Fisher, 2008, Setum, 1993). Along with LSECs, HSCs, and KCs, and hepatocytes, dendritic cells present antigens to lymphocytes (fig 1.13) scattered throughout the liver sinusoids and portal tracts from the innate (NK and NK T-cells) and adaptive (T- and B-cells) immune systems (Crispe, 2009, Racanelli, 2006, Winau, 2007).

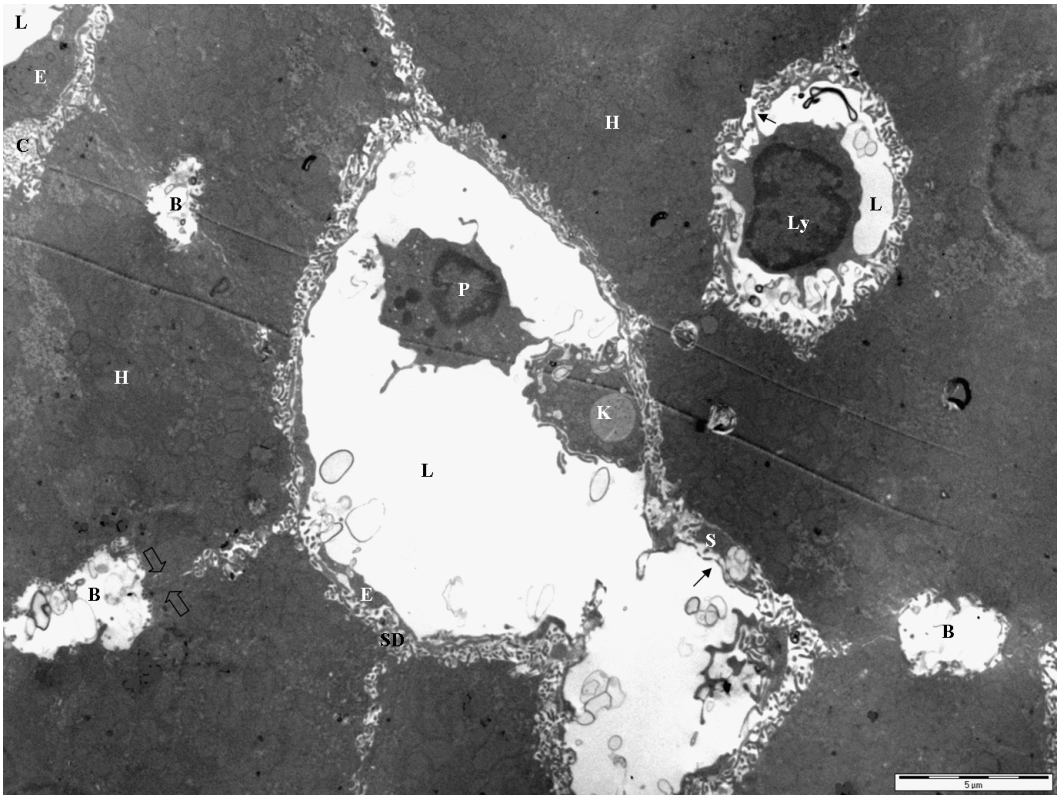

Figure 1.13 *Transmission electron micrograph of a KC, pit cell, and lymphocyte from an F344 rat. The lymphocyte is extending processes through fenestrations.*
P = Pit cell, K = Kupffer cell, Ly = lymphocyte, L = sinusoid lumen, S = stellate cell, C = collagen bundle, SD = space of Disse, E = endothelium, arrows point to fenestrations, H = hepatocyte, B = bile canaliculi, open arrows indicate a tight junction between hepatocytes (bar = 5 µm).

1.3 The effect of fasting on the liver

During fasting the body adapts in order to survive long periods of starvation. The liver plays a crucial role in energy metabolism and is therefore significantly affected. An overnight fast reduces the weight of the liver by about 30 % in rats, primarily due to a loss of water that is bound to glycogen and protein (Rothacker, 1988). Liver weight loss correlates to a decrease of liver cell size rather than a loss of cells (as non-essential cellular components are broken down to liberate nutrients) (Sokolovic, 2008). Glycogen stores are depleted in order to liberate glucose, and falling insulin levels induce hepatocyte autophagy releasing a substantial amount of amino acids for gluconeogenesis (Ezaki, 2011). Enzymes associated with amino acid metabolism such as those from the urea cycle, tricarboxylic acid cycle, malate aspartate shuttle, in addition to genes for ammonia detoxification, aspartate transferase and proteins from the electron transport chain, are all upregulated throughout fasting (Sokolovic, 2008).

Despite liver weight loss, liver structure and metabolic zonation are maintained during fasting (that is fasting does not change the lobular distribution of enzymes) (Sokolovic, 2008). Zonal differences in gene expression of the antagonistic enzymes of glucose metabolism, glucokinase (predominant in the central zone) and glucose-6-phosphatase (predominant in the portal zone), compartmentalise storage and production of glucose, enabling net glucose output from the periportal hepatocytes and net glucose uptake from the centrilobular hepatocytes in the fed state (Jungermann, 1982). During fasting, the expression of glucokinase and glucose-6-phosphatase are regulated to enable more glucose production and output than glucose uptake and storage (Jonges, 1992, Jungermann, 1982, Sokolovic, 2008). In addition, the expression of phosphoenolpyruvate carboxykinase, a key enzyme in

gluconeogenesis, is upregulated across the lobule in the fasted state to favour glucose production, remaining distributed in the same lobular pattern as during feeding (most strongly expressed in the periportal hepatocytes, with a decreasing gradient to the centrilobular hepatocytes) (Giffin, 1993).

Glycogen is steadily lost during fasting (to liberate glucose). As glucose storage is a dominant function of centrilobular cells these are the last to be depleted of glycogen. Thus a centrilobular glycogen pattern persists later into the fast where periportal cells are glycogen deplete (Giffin, 1993). During a prolonged fast (after 1 - 2 days of fasting in rats) centrilobular glycogen begins to be replenished (from the 3rd to 5th day of fasting in rats) after its initial depletion exclusively in centrilobular hepatocytes (Minassian, 1994). This is probably due to an increase in the glyconeogenic substrate glucose-6-phosphate and the very low expression of glucose-6-phosphatase in centrilobular hepatocytes, although the mechanism is not fully understood (Sokolovic, 2008).

There is an increase in intrahepatic lipid during fasting in both humans (Moller, 2008) and murine animals (Trotter, 1967). The hormonal profile of low insulin, and high glucagon, glucocorticoid, and noradrenaline/adrenaline serum concentrations in fasting liberates fat from adipose tissue, increasing the concentration of serum free fatty acids (FFAs) available for uptake by hepatocytes. This accommodates the increased requirement for hepatic fatty acid oxidation essential for glucose and ketone production (Kalderon, 2000, Kersten, 1999). Some of the FFAs taken up by hepatocytes are re-esterified into triacylglycerol for very low density lipoprotein (VLDL) formation. Cholesterol trafficking genes are upregulated in the liver probably

due to an increased need for VLDL secretion as not many chylomicrons are being produced (Sokolovic, 2010). VLDL secretion contributes to the maintenance of normal blood cholesterol and triglyceride levels.

1.3.1 Fasting and xenobiotic metabolism

Fasting prior to the exposure of xenobiotics metabolised by the cytochrome P450 pathway increases hepatotoxicity, primarily because of a reduced availability of glutathione (GSH) (Pessayre, 1979, Strubelt, 1981). GSH is a molecule used in important cellular processes such as DNA repair and gene expression, and is essential to detoxifying electrophilic metabolites that would otherwise irreversibly bind to cellular proteins, damaging the cell (Lauterburg, 2002). During fasting, GSH (made from cysteine, glutamate, and glycine) stores cannot be replenished from dietary amino acids and are reduced by about 50 % after a 24 hour fast in mice (Strubelt, 1981). Even more GSH than usual is broken down during fasting to liberate its amino acid components for energy and protein synthesis (Cho, 1981, Tateishi, 1977). During xenobiotic metabolism via the cytochrome P450 pathway, toxic metabolites are produced that are inactivated via conjugation with GSH. As GSH stores are depleted by fasting there is less GSH available to deactivate these metabolites. Thus a fasted animal is more vulnerable to hepatotoxicity at a lower dosage of a drug metabolised by cytochrome P450s than a fed animal.

Fasting is also associated with increased inflammatory cell recruitment in drug induced liver injury (Antoine, 2010). Inflammation is associated with free radical production and an increase in inflammation may exacerbate drug induced hepatotoxicity.

1.3.2 Fasting and the LSEC

Most of the studies on fasting and the liver have investigated hepatocytes therefore little is currently understood about changes to the LSEC during fasting. A study on isolated LSECs from 24 hour fasted rats reported an increased amount of mannose/*N*-acetylglucosamine receptors (a type of scavenger receptor also involved in the innate immune response) on LSECs, and a significant decrease in the activity of the mitochondrial enzyme succinate dehydrogenase (an enzyme of the electron transport chain) (Summerfield, 1982). Currently there are no ultrastructural studies on the effects of fasting on the LSEC.

1.4 Drug-induced liver injury

The liver is particularly vulnerable to drug induced liver injury (DILI) because of its extensive role in drug metabolism (Russmann, 2009). DILI can occur after acute or chronic use of xenobiotics (including synthetic drugs, alcohol, herbal medications (Teschke, 2011) and dietary supplements) and is a significant cause of liver failure and mortality. The process of DILI involves direct liver injury by a drug and/or its metabolites and a subsequent inflammatory reaction (Russmann, 2009). Diagnosis and management is often difficult as DILI can mimic any form of acute and chronic hepatobiliary disease (such as acute hepatitis and cholestatic liver disease), has a highly variable clinical presentation (Au, 2011), and on some occasions renal toxicity is associated (Mazer, 2008). In many cases of DILI there is currently no effective treatment other than stopping the drug and providing supportive care. Fulminant liver failure may occur as a result of severe DILI (Gotthardt, 2007) often requiring liver transplantation (Fontana, 2008).

Certain people (and animals) are more vulnerable to DILI than others because of genetic polymorphisms in metabolic and drug-transporter enzymes (Au, 2011, Heinloth, 2004) and idiosyncratic adverse drug reactions are not uncommon (Boelsterli, 2007, Fontana, 2008). Nutritional status and fasting (Pessayre, 1979), gender, age (Le Couteur, 1998), co-infections (such as HIV), alcohol and recreational drug consumption (Trigueiro de Araujo, 1993), environmental exposure to other toxins, and co-administration of drugs (Neal, 1992), all influence the toxicity of a drug (Au, 2011).

1.4.1 Drug-induced liver injury and the hepatic microvasculature

The liver microvasculature plays a key role in the course of DILI (during both acute and chronic toxicity) (DeLeve, 2007a) and the ability of the liver to repair and regenerate after an insult (Donahower, 2010, Furrer, 2011, Kato, 2011). Endothelial dysfunction is often an early event in the process of liver injury (DeLeve, 2007a, Iwakiri, 2012, Iwakiri, 2007). LSECs in particular are susceptible to DILI as they are directly exposed to portal blood, express CYP450 enzymes for drug metabolism, have a low storage capacity for glutathione (GSH, an antioxidant detoxifying molecule), and are directly exposed to toxins released from hepatocytes that become concentrated in the SoD (DeLeve, 2007b). In particular, damage to the LSEC (and other hepatic cells) occurs as toxic metabolites covalently bind and form adducts with important cellular proteins and mitochondria damaging their function. After an overwhelming amount of oxidative stress, onset of mitochondrial permeability transition (MPT) occurs. This stops ATP production in those mitochondria affected and leads to cellular necrosis, apoptosis, and more free radical production (Hinson, 2004, Jaeschke, 2002, Kim, 2003). With increasing oxidative stress and production of toxic metabolites,

cellular stress and inflammation perpetuates causing severe microvascular dysfunction (Au, 2011, Jaeschke, 2006, Jaeschke, 2012a, Roth, 2009).

1.4.2 Morphology of the injured LSEC

Some common morphological changes to LSECs during the process of DILI injury are (Le Bail, 1990):

1) An increase or decrease in fenestration number and size, altering the crucial substance exchange process between the SoD and blood (sieving function).

2) Gap formation in the LSEC cytoplasm facilitating hemorrhage of RBCs and direct exposure of blood contents to hepatocytes.

3) Overload of dense bodies and/or lipid vacuoles in the cytoplasm, resulting in LSEC swelling and reduction of sinusoid lumen diameter.

4) LSEC hyperactivity or activation, resulting in an increased number of organelles (such as ER, Golgi apparatus, and pinocytotic vesicles) and thickening of cell processes, thereby decreasing oxygen availability to hepatocytes and HSCs.

These LSEC changes accompany alterations to the microenvironment of the SoD, such as SoD dilation, increased ECM, decreased hepatocyte microvilli, and HSC activation (Sanchez-Valle, 2012). In addition, LSEC injury stimulates platelets to aggregate and release additional mediators that further stimulate HSC activation and promote vascular stasis (Burt, 1993, Zarbock, 2007). After overwhelming injury, necrotic or dying LSECs often appear as “bubbling cells” with the cell membrane exhibiting focal interruptions, detachments, and projections into the sinusoid lumen, with hydropic swelling of the cytoplasm. Mitochondria swell, ER dilates, organelles

are frequently damaged and often expelled (therefore reduced in number), and most of the pinocytotic vesicles and glycogen disappear (Le Bail, 1990).

1.4.3 Oxidative stress and the LSEC in drug-induced liver injury

Oxidative stress is a major cause of LSEC dysfunction during DILI (Jaeschke, 2002). LSECs (in addition to HSCs and KCs) have a much lower capacity to store GSH than hepatocytes, rendering them more vulnerable to oxidative injury (Cogger, 2004, DeLeve, 1998, Sanchez-Valle, 2012). In DILI, oxidative stress is induced early from inadequate detoxification of highly reactive drug metabolites as GSH stores deplete. In addition, reactive oxygen and nitrogen species (such as superoxide, hydrogen peroxide, and hydroxyl radicals) are released during the inflammatory reaction to injury and as a result of mitochondrial stress (Sanchez-Valle, 2012). Peroxynitrite, a highly potent oxidant that damages cell DNA, mitochondria, and other important cellular functions, is also subsequently produced on reaction of superoxide and nitric oxide (NO) (Hinson, 2004). Peroxynitrite is normally detoxified by GSH however GSH is sparingly available as DILI progresses.

In physiological conditions, cellular endogenous nitric oxide synthase (eNOS) in LSECs produces a small amount of NO. This is required to maintain perfusion of the microcirculation and appropriate vascular tone (Iwakiri, 2012), inhibit neutrophil adhesion and migration, inhibit platelet aggregation (Clemens, 1999), and maintain a fenestrated LSEC phenotype (Iwakiri, 2007). However, in conditions of oxidative stress, eNOS activity is lowered and superoxide reacts with NO to form peroxynitrite, thus increasing oxidative stress, causing LSEC dysfunction, and having prothrombotic effects (Iwakiri, 2012).

As DILI progresses, there is upregulation of inducible NOS (iNOS) in all types of liver sinusoidal cells and hepatocytes in response to increasing injury and inflammation (Clemens, 1999). In comparison to eNOS, iNOS produces large quantities of NO, having both a vasodilatory and inflammatory cell chemotactic effect (Jaeschke, 2002). Such a massive release of NO under these conditions also increases production of peroxynitrite as superoxide is readily produced and released by damaged mitochondria and inflammatory cells (including KCs and neutrophils) (Hinson, 2004, Knight, 2004).

1.4.4 Capillarisation of the sinusoidal endothelium

Hepatic sinusoidal capillarisation is a sign of LSEC toxicity and can arise as a result of chronic disease, oxidative damage, and drug toxicity (see table 1.2) (DeLeve, 2009, Sanchez-Valle, 2012). During capillarisation, the LSEC phenotype changes from fenestrated, to thickened and defenestrated, resembling the phenotype of a vascular capillary endothelial cell. LSEC capillarisation is generally accompanied by increasing subendothelial ECM (DeLeve, 2009) and formation of a continuous basement membrane (Le Bail, 1990). Capillarisation (and loss of the liver sieve) significantly affects liver function. It contributes to hepatocyte hypoxia (DeLeve, 2009, Le Couteur, 2005), reduced drug clearance (DeLeve, 2007a, Le Couteur, 2005), hindered hepatocyte-blood substance exchange (causing reduced chylomicron remnant clearance and promotion of atherosclerosis) (Fraser, 1978, Fraser, 1995), vasoconstriction and portal hypertension (Iwakiri, 2007), and altered immune function such as decreased T-cell tolerance (Iwakiri, 2012, Warren, 2007) stimulating even more inflammation and oxidative stress.

1.4.5 Fibrosis and Cirrhosis

Sinusoidal fibrosis is initiated as part of the liver's tissue repair response to hepatocyte and LSEC injury, and is preceded by LSEC capillarisation (DeLeve, 2007a, DeLeve, 2009). The capillarised LSEC becomes "hypoactive" (Iwakiri, 2007) and loses the ability to revert activated (myofibroblastic) HSCs to a quiescent phenotype (DeLeve, 2008, Xie, 2012). HSCs subsequently produce large quantities of ECM, particularly fibrillar collagens type I and III (Bataller, 2009, Bedossa, 1990, Benyon, 1998, Burt, 1993, Reeves, 2002, Sanchez-Valle, 2012). Production of NO and other vasodilators in hypoactive capillarised LSECs decreases, enhancing sinusoidal vasoconstriction (Iwakiri, 2012).

Fibrosis is often associated with chronic hepatic diseases (Boyer, 2012, Burt, 1993, Le Bail, 1990, Sanchez-Valle, 2012) and drug toxicity (Cederbaum, 2006, Dasarathy, 2007, Iwakiri, 2007, Trigueiro de Araujo, 1993) (see table 1.2). In cases of chronic liver injury, a continuous wound-healing (fibrotic) process is activated that progresses to hepatic cirrhosis in a large number of diseases and drug induced toxicity (see table 1.2) (Govindarajan, 2009, Le Bail, 1990). During cirrhosis, liver function is severely affected as capillarisation of sinusoids, vasoconstriction, and anatomical remodelling, lead to a blockage of blood flow that contributes to portal hypertension and venous thrombosis (Iwakiri, 2012). Progressive accumulation of ECM results in areas of permanent fibrous scar tissue replacing those areas once filled with hepatocytes and sinusoids, a feature characteristic of cirrhosis (Bosch, 2007, Sanchez-Valle, 2012).

1.4.6 Drug induced liver injury following direct LSEC toxicity

When DILI is initiated by a substance directly toxic to LSECs rather than hepatocytes, hepatic injury commonly manifests with some or all of the features of sinusoidal obstruction syndrome and peliosis hepatis (DeLeve, 2007a).

1.4.6.1 Sinusoidal Obstruction Syndrome

Sinusoidal obstruction syndrome (SOS) begins with LSEC injury, initiating a cascade of events including severe microvascular disruption, followed by hepatocyte necrosis and liver failure (DeLeve, 2003a). SOS is often associated with the myoablative conditioning regimes used prior to hematopoietic stem cell transplantation, including chemotherapy, radiation therapy, and immuno-suppressant drugs (for a comprehensive list of drugs refer to (DeLeve, 2011)). An animal model that accurately resembles the clinical and histological symptoms of human SOS is produced by treatment with monocrotaline or other pyrrolizidine alkaloids (DeLeve, 1999). These alkaloids were first discovered to induce SOS after accidental dietary ingestion by humans and cattle (DeLeve, 2007a).

LSEC injury first occurs after profound GSH depletion, resulting in an inability to neutralise the toxic metabolites of a drug or toxin. Covalent binding (adduct formation) of the toxic metabolites to the LSEC cytoskeleton causes F-actin to depolymerise, resulting in “rounding up” of LSECs and gap formation between and within LSEC cytoplasm. This stimulates production and increased activity of matrix metalloproteinase (MMP) -2 and MMP-9, both degrading the supportive ECM (thus loosening the tethering of LSECs to the sinusoid wall) and further inducing gap formation and defenestration. As the LSECs swell and the SoD enlarges (as a result of

loosened LSEC tethering), sinusoid lumens decrease in size, so much that the SoD becomes the path of least resistance for blood flow. Gaps between and within LSEC cytoplasms allow infiltration of RBCs into the SoD. Such hemorrhage increases the size of the SoD even more and consequently LSECs completely detach, together with the other cells of the sinusoid wall, the Kupffer and hepatic stellate cells. Aggregates of these cells embolise downstream, and along with monocytes that adhere to denuded sections of the sinusoid, obstruct sinusoidal flow. This process eventually leads to occlusion and fibrosis of the central vein, ischemia, and centrilobular necrosis (DeLeve, 2009, DeLeve, 2003a, DeLeve, 2002). In the animal model of SOS, LSEC injury is preventable by early administration of *N*-acetylcysteine (a glutathione precursor) and metalloproteinase inhibitors (DeLeve, 2003b).

Histological, ultrastructural, and biochemical features of early SOS resemble the early features of acetaminophen (APAP) poisoning. However, in APAP poisoning, the congestion and hemorrhage resolve relatively early in the course of toxicity, and injury does not progress to sinusoidal fibrosis or fibrotic occlusion of central veins (DeLeve, 2007a, DeLeve, 2009). Reasons why the microvasculature is able to rapidly repair during APAP toxicity and not during SOS are unknown. It has been suggested that as the LSECs remain more strongly tethered to the sinusoid wall during APAP toxicity, the general structure of the sinusoid wall is maintained, allowing for rapid repair of the microvasculature (Walker, 1983).

1.4.6.2 Peliosis Hepatis

Peliosis has the gross appearance of multiple cyst-like blood filled cavities measuring less than 1 mm to several centimetres, and may occur within any parenchymatous organ (DeLeve, 2007a, Tsokos, 2005). Peliosis hepatis (liver) is associated with toxicity from a wide variety of drugs such as immunosuppressant medications (for example steroids), oral contraceptives, intravenous drug use, and chronic alcoholism (Tsokos, 2005). Peliosis has been directly linked to drugs known to directly damage the LSEC (for example azathioprine, 6-thioguanine, oxaliplatin, urethane) and is often initiated after LSEC injury (DeLeve, 2009, DeLeve, 2011).

There are different types of peliotic lesions. "Parenchymal peliosis" describes irregular blood-filled cavities between atrophic, degenerating cords of hepatocytes lined neither by cells nor fibrous tissue. "Phlebectatic peliosis" describes blood-filled cavities that appear spherical and lined by one or multiple layers of littoral cells (for example LSECs, HSCs, or KCs) and/or a fibrin network and fibrous tissue (Tsokos, 2005, Zafrani, 1984a). Peliosis generally involves a combination of these cavity types (DeLeve, 2007a, DeLeve, 2009, DeLeve, 2011) and its clinical presentation varies according to the underlying disease process or toxicity (Zafrani, 1984b).

In peliotic lesions that are initiated subsequent to direct LSEC injury (during LSEC infection or drug toxicity for example) the first signs of microvascular damage are similar to sinusoidal capillarisation - LSEC gaps and defenestration, cytoplasmic swelling, formation of a basement membrane, and altered ECM composition (Zafrani, 1984a). The sinusoid lumen size decreases and RBCs enter the SoD through gaps in and between LSECs, such that the SoD becomes markedly dilated and eventually

denuded. Subsequently hepatocytes have no protective barrier from the blood and become increasingly subjected to hypoxic conditions. This leads to hepatocyte atrophy and degeneration, and the formation of “blood lakes” after disintegration of hepatocyte cords and sinusoid structure (Lee, 1983). Hepatocellular necrosis in conjunction with elevated intrahepatic vascular pressure results in severe congestion and sinusoid dilation, as well as dilation of portal veins (Tsokos, 2005). Rupture of a peliotic lesion can be fatal, resulting in intraperitoneal hemorrhage or hepatic hematoma. However peliosis may resolve with amelioration of the precipitating toxicity, disease, or infection (DeLeve, 2011).

Table 1.2 Symptoms of injury to the microvasculature during disease and toxicity

Disease process	Microvasculature symptom	References
Alcoholic hepatitis	Capillarisation Fibrosis Cirrhosis	(McCuskey, 2004) (Karsan, 2012)
Autoimmune hepatitis	Capillarisation Cirrhosis	(Fallatah, 2012) (Warren, 2007)
Budd-Chiari syndrome (hepatic vein obstruction)	Sinusoid dilation, Congestion, Fibrosis, Cirrhosis	(Ferral, 2012) (Tsokos, 2005)
Chronic alcoholism	Cirrhosis Peliosis	(Horn, 1987) (Tsokos, 2005) (Bataller, 2009) (Dasarathy, 2007) (Rehm, 2010)
Chronic drug use	Fibrosis	(Trigueiro de Araujo, 1993)
Chronic hypervitaminosis A	Peliosis	(Zafrani, 1984a)
Drug Induced Liver Injury	Capillarisation, Fibrosis, Cirrhosis, SOS, Peliosis	(DeLeve, 2009) (Au, 2011) (Russmann, 2009) (Wanless, 1996)
Diabetic microangiopathy	Capillarisation Fibrosis	(Tooke, 1995) (Harrison, 2006) (Hudacko, 2009) (Latry, 1987)
Extrahepatic cholestasis (bile duct obstruction)	Capillarisation	(Gulubova, 1996)
Hepatic amyloidosis	Fibrosis	(Sarsik, 2012)
Hepatocellular carcinoma	Capillarisation Cirrhosis	(Duffy, 2013) (Gomaa, 2008) (Yang, 2008)
Hepatic hemochromatosis	Fibrosis Cirrhosis	(Bacon, 2011) (Bataller, 2009)
Infection of LSEC in AIDS by Bartonella bacilli	Peliosis	(DeLeve, 2007a) (DeLeve, 2009) (Tsokos, 2005)
Non Alcoholic Fatty Liver Disease (NAFLD)	Capillarisation Fibrosis	(Fontana, 2013) (Farrell, 2008)
Steatohepatitis	Fibrosis	(McCuskey, 2004)
Toxic (acute) hepatitis	Capillarisation	(Bardadin, 1984) (Ramachandran, 2009)
Viral Hepatitis	Fibrosis Cirrhosis	(Protzer, 2012) (Schroeder, 2009) (Bardadin, 1984) (Bataller, 2009)
Wilsons disease	Fibrosis	(Reeves, 2002) (Bataller, 2009)

1.5 Ageing and the liver

Liver function is well maintained in ageing however there are some distinct structural and functional changes that occur. “Brown atrophy” is a distinct feature of the ageing liver whereby the liver reduces in size, and accumulates lipofuscin (pigmented lipid residues of lysosomal digestion) in hepatocytes giving it a distinct brown colour (Jansen, 2002, Le Couteur, 1998, Popper, 1986). Changes in hepatic microcirculation also accompany ageing. There is a substantial decrease in blood flow to the liver by about 40 % likely due to a reduction in splanchic blood flow that reduces the input of blood into the portal vein (Le Couteur, 1998). There is also a reduction in liver perfusion (the blood flow per mass of liver) due to ageing changes in the microvasculature (Jansen, 2002). In old people and animals, LSECs become thicker and HSCs accumulate more fat, narrowing the sinusoids and impairing sinusoidal perfusion (Ito, 2007). In addition, a chronic low grade activation of the immune system in ageing (Licastro, 2005) increases the number of macrophages and leukocytes accumulating in sinusoids (See Appendix A4), also contributing to impaired blood flow (Ito, 2007). Kupffer cells are morphologically unchanged by ageing, although are reported to have a decreased phagocytic capacity, prolonging the circulation of harmful substances in the blood such as endotoxin (Brouwer, 1986).

Apart from increased number of cytoplasmic lysosomes and dense bodies (Popper, 1986), hepatocytes have a similar ultrastructure in young and old age (Schmucker, 1978). Other reported hepatocyte ageing changes such as decreased SER, increased nuclear polyploidy and binucleation, and changes in hepatocyte size, have not been consistently confirmed (Schmucker, 1998). An age-related reduction in the phase I (CYP450) metabolism of certain drugs by hepatocytes has been reported in murine

studies however this has not been confirmed in primate or human studies (Schmucker, 2005, Woodhouse, 1990).

Impairment of drug clearance and a subsequent increase of adverse drug effects in ageing has been widely reported (Le Couteur, 1998). It is unlikely that this is due to an age-related deficiency in hepatocyte drug metabolism or an impaired detoxification of electrophilic metabolites (Woodhouse, 1992, Woodhouse, 1984). Changes to hepatic drug metabolism during ageing are primarily a result of reduced blood flow, decreased liver size (Woodhouse, 1988, Wynne, 1990), and age-related changes of the hepatic microvasculature (see section 1.5.1) (Le Couteur, 2008, McLean, 2003).

Alterations to the function and morphology of the LSEC during ageing with significant implications for age-related diseases and drug metabolism include:

1) A reduction in LSEC endocytosis and scavenger function (Brouwer, 1985, Le Couteur, 2008, Simon-Santamaria, 2010, Smedsrod, 1990, Yannariello-Brown, 1995).
2) A reduction in activity of some LSEC enzymes involved in the utilisation of energy (for example glucose-6-phosphatase, Mg-ATPase, and glucagon-stimulated adenyl cyclase) (De Leeuw, 1990).
3) An accumulation of iron ferritin both in dense bodies and free in the cytosol (De Leeuw, 1990).
4) Decreased expression of caveolin-1 (Jamieson, 2007).
5) Increased expression of von Willebrand factor and ICAM-1, a sign of endothelial injury and inflammation (Le Couteur, 2001, McLean, 2003).
6) Pseudocapillarisation (Le Couteur, 2001) (see section 1.5.1).

1.5.1 Implications of age-related pseudocapillarisation of the LSEC

The incidence of liver disease and DILI increases with age (Junaidi, 2007, Lee, 1983, Schmucker, 2005). As cells are the basic components of tissues and organs, cell deterioration and stress have a significant impact on the ageing of an entire organism. It is uncertain how or why degenerative cell changes occur during ageing, however they may be due to a combination of genetic programming, randomly occurring errors during DNA/RNA replication, repeated exposure to ingested toxins, free radicals, and radiation (De Leeuw, 1990, Knook, 1982), increased cell sensitivity to oxidative stress (Schmucker, 2005), and/or an age-related overactive immune system (Licastro, 2005).

Pseudocapillarisation (first described by (Le Couteur, 2001)) of the liver sinusoids occurs as a result of ageing. It is an incomplete form of endothelial capillarisation that involves thickening of the LSEC (by approximately 50 %), decrease in fenestration number (by 30 - 50 %), a mild increase of collagen fibrils and sporadic formation of basal lamina, and a high number of non-activated lipid-engorged HSCs. Pseudocapillarisation has been observed in a number of species including rats (Le Couteur, 2001), baboons (*Papio hamadryas*) (Cogger, 2003), mice (Furrer, 2011, Ito, 2007, Stacchiotti, 2008, Warren, 2005) and humans (McLean, 2003). Age-related pseudocapillarisation is not a disease process in itself, although it has serious implications for the alteration of liver function, drug metabolism (Le Couteur, 1998), and the increased incidences of toxicity, disease, and dyslipidemia in ageing (Le Couteur, 2008), and may be regarded as a therapeutic target for prevention and treatment of age-related diseases.

Some of the functional implications of pseudocapillarisation in ageing include: decreased oxygen availability of hepatocytes (Le Couteur, 2001); impaired transfer of lipoproteins between the blood and SoD (Hilmer, 2005, Le Couteur, 2002, Le Couteur, 2005) leading to post-prandial hyperlipidemia and increasing risk of atherosclerosis (Cogger, 2006, Krasinski, 1990); decreased drug clearance and metabolism increasing the potential for adverse drug reactions and overdose (Le Couteur, 1998, Mitchell, 2011); vulnerability to hemostasis and inflammation (see Appendix 5 A4) with increased expression of von Willebrand factor and ICAM-1; vasoconstriction as a result of LSEC thickening; and increased vulnerability to autoimmune disease because of defenestration (Warren, 2006).

Werner's syndrome, a genetic disease that resembles premature ageing, is also associated with LSEC pseudocapillarisation, hyperlipidemia (see Appendix 5 A5, A6, and A7) (Murata, 1985), and significantly raised levels of serum hyaluronan indicative of decreased LSEC endocytotic capability (Tanabe, 2001). Pseudocapillarisation was ameliorated with antioxidant (vitamin C) treatment in an animal model of Werner's syndrome (Massip, 2010), highlighting the significance of the impact of oxidative stress. Reduction of oxidative stress in ageing such as during caloric restriction (decreasing oxidant dietary load) and antioxidant administration have been found to ameliorate pseudocapillarisation and slow the ageing process in animal models (Jamieson, 2007), reinforcing the importance of healthy LSEC functioning as a therapeutic target for ageing, toxicity, and disease.

1.6 Scope and aims of the thesis

The hepatic microvasculature plays a major role in the initiation, progression, and amelioration of multiple disease states, toxicity, and ageing, and plays a major part in the maintenance of homeostasis during health. Yet much of the focus has been on the role of the hepatocyte. This thesis endeavours to broaden the knowledge of the role of the liver sinusoids in health and toxicity, focusing on the LSEC, with the following specific aims and hypotheses:

In Chapter 3 we aim to study the impact of fasting on fenestration modulation to determine if this biological state alters porosity and fenestration size. We hypothesise that fenestration size and LSEC porosity will be increased in order to adapt to the decreased amount of circulating macronutrients in the fasted state, enabling more efficient uptake of nutrients into the hepatocytes improving homeostasis. Fenestration diameter and porosity analysis of fed and fasted rats will be done using scanning electron microscopy, and blood serum analysis will be performed to measure lipids and markers of liver injury.

Acetaminophen (APAP) is a commonly used over the counter medication to relieve pain and fever. High doses of APAP are hepatotoxic and accidental or deliberate overdose of APAP is a leading cause of drug induced liver injury. A toxic dose of APAP may result in severe liver injury with substantial hepatocyte death that can lead to fulminant liver failure. However in many cases the liver is able to regenerate without pharmaceutical intervention. The role of the LSEC both in APAP toxicity and subsequent hepatocyte regeneration after APAP toxicity is not completely understood. In Chapter 4 using electron microscopy we will observe whether LSECs thrive in

areas of severe hepatocyte necrosis during APAP toxicity in order to provide a scaffold and blood supply by which hepatocytes can regenerate, and investigate the ultrastructure of LSECs in areas of low and high hepatocyte injury to observe whether LSECs are injured to the same degree as hepatocytes. Histological and blood analysis will be performed to determine the degree of centrilobular hemorrhage and hepatocyte necrosis in each rat. We hypothesise that alterations to LSEC ultrastructure during APAP toxicity will play a role in both the progression of hepatocyte injury, and later in hepatocyte regeneration. We will also compare the sinusoids of rats fed and fasted before overdose, as fasting has been found to increase APAP toxicity. We hypothesise LSECs will sustain more injury in fasted rats due to decreased availability of energy and reduced antioxidant capacity. If increased numbers of necrotic LSECs are observed in fasted rats it may be linked to an increase in the severity of hepatocyte injury and poorer survival outcomes previously reported in APAP overdose after fasting.

In Chapter 5 we will investigate the therapeutic potential of P407 on hepatotoxicity and LSEC injury during APAP overdose in fed and fasted rats. P407 is a non-toxic substance already used in human pharmaceutical preparations, and is known to defenestrate LSECs. Our hypothesis is that administration of P407 before or after APAP overdose will protect the livers of fed and fasted rats from APAP toxicity. It may do this by defenestrating the LSECs thus decreasing the amount of APAP that will traverse from the sinusoid lumen to the hepatocytes, and by coating and forming a protective layer over the LSECs, preventing gap formation and hemorrhage. Histology and serum analysis will be conducted primarily to observe whether P407 treatment protected against hemorrhage and centrilobular necrosis, and an

ultrastructural (TEM and SEM) analysis will be conducted to observe whether P407 protected LSECs early and late in the course of toxicity.

Studies on LSEC ultrastructure are often performed *in vitro* rather than *in vivo,* as it is a good method of testing the direct effect of a variety of pharmacological agents on a particular isolated cell and without the challenge of getting a substance into an animal. No studies have previously been performed to assess isolated LSECs from old F344 rats, a breed that is commonly used in the study of ageing. In Chapter 6, scanning electron microscopy will be used to observe the ultrastructure of LSECs isolated from ageing rats in order to determine whether changes to the LSEC observed *in vivo* also occur *in vitro*. We hypothesise that LSECs isolated from old rats will reflect changes observed *in vivo* such as reduced fenestration size and porosity. If *in vivo* and *in vitro* studies prove to be congruent, isolation of LSECs from old rats may be useful in testing substances that could potentially modulate ageing changes, such as pseudocapillarisation, *in vivo*.

Chapter 2:

Methodology

A variety of methods were used to study morphology and ultrastructure in livers including histological and electron microscopic analysis as discussed below.

2.1 Fixation

Chemical fixation involves a reaction between the fixative and chemical groups in living tissue to preserve and freeze the structure of the tissue, thereby creating an *in vivo* "snapshot" for subsequent analysis on light and electron microscopes. Inter and intra molecular cross-linking of molecules by the fixative enables the cellular substructures within the tissue to survive further processing including dehydration and exposure to a vacuum and electron beam during electron microscopy (Hayat, 2000). Fixation must occur immediately after biopsy to arrest metabolic processes and subsequent autolysis of the cells that can occur within seconds or minutes (Wisse, 2010). The liver in particular is very susceptible to autolysis because it contains a dense concentration of metabolic enzymes. Chemical fixation also prevents attack by bacteria during processing and storage (Hopwood, 1969). Fixation quality is affected by the method of applying the fixative, fixative osmolarity, pH, temperature, ionic strength and composition, length of fixation, and specimen size (Hayat, 1981).

2.2 Light microscopy

2.2.1 Histological fixation

Immersion fixation using formaldehyde is a suitable method for histological analysis. The specimens should not be thicker than 0.5 cm, and the fixative volume at least ten times that of the specimen for optimal and rapid fixation. Cross-linking of proteins occurs slowly, thus specimens should be incubated overnight to allow proper fixation

(fig 2.1). Proteins in blood or bodily fluids will inactivate the fixative and washing in saline or exsanguination before fixation is essential (Bancroft, 2008).

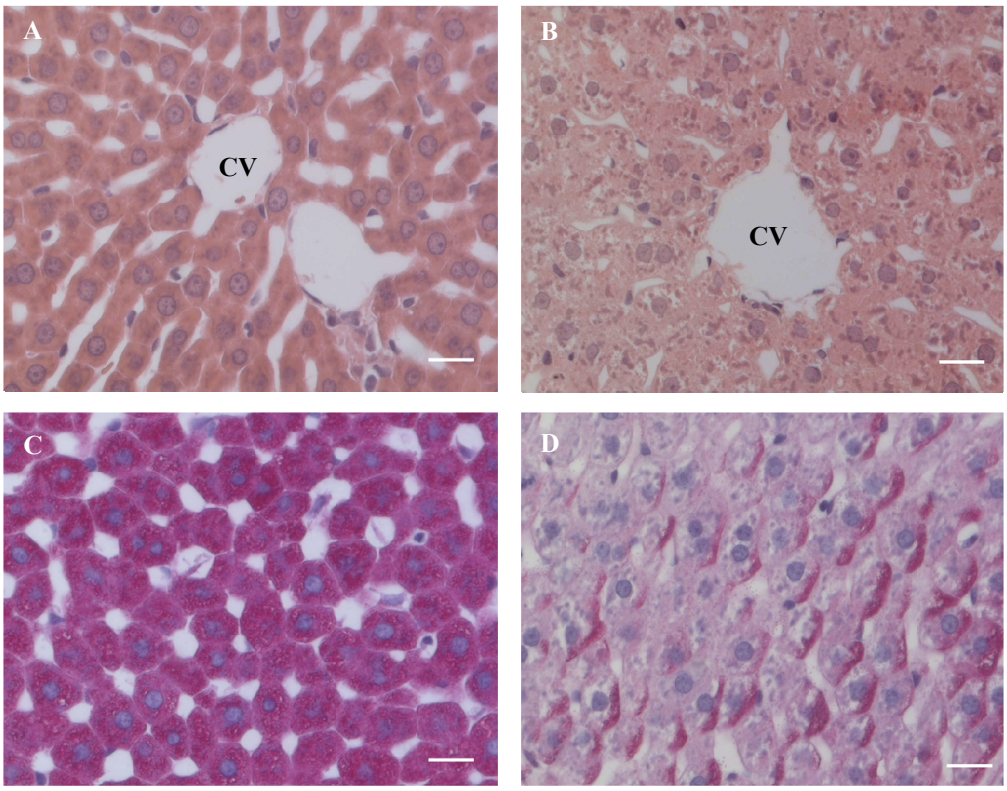

Figure 2.1 *Examples of good and poor histological fixation*
A) H&E stained specimen, good fixation. The specimen was fixed overnight in formaldehyde after exsanguination. Cells are intact and sinusoids are open. CV= central venule.
B) H&E stained specimen, poor fixation. The specimen was fixed in formaldehyde for an insufficient time. Many of the sinusoids are collapsed and the hepatocytes are not well preserved.
C) PAS stained specimen from an ad libitum fed rat, good fixation. The specimen was fixed overnight in formaldehyde after exsanguination. Glycogen (coloured magenta) is evenly distributed throughout the hepatocytes.
D) PAS stained specimen from an ad libitum fed rat, poor fixation. The specimen was fixed in formaldehyde for an insufficient time. There is pooling of glycogen at the edge of hepatocytes and leakage of glycogen from the cells.

All bars = 20 µm.

2.2.2 Embedding of specimens

After fixation, water must be removed from biological specimens to allow infiltration of an appropriate embedding media. This enables mechanical support during thin sectioning of the specimens for microscopy and gives protection during long-term storage. Ethanol is used as the dehydrating agent as it ensures complete dehydration of biological specimens and also enhances the fixation as it is a coagulant fixative. However ethanol is not miscible with paraffin wax, the usual embedding medium for histological sectioning. Thus after dehydration the specimens are incubated in xylene, a clearing agent, that removes all traces of ethanol enabling subsequent infiltration of paraffin wax into the specimen (Bancroft, 2008).

2.2.3 Histological staining

After specimens are embedded in paraffin and sections cut, the sections are stained for analysis and viewing under the microscope (see Appendix 2 for protocols). Sections must first be re-hydrated to allow affinity for the dyes. After staining they are again dehydrated and cleared with xylene so that they may be coverslipped using a permanent mounting media, analysed with the microscope, and stored safely for long periods of time. The following 3 stains were used in our experiments.

2.2.3.1 Hematoxylin and eosin

Hematoxylin and eosin (H & E) is a stain routinely used to view the general pathology of the specimen. Hematoxylin stains cell nuclei (chromatin) blue, and eosin stains the cytoplasm and connective tissues different shades of pink, orange, and red, and red blood cells intensely red (fig 2.1 A).

2.2.3.2 Periodic acid-Schiff

The periodic acid-Schiff (PAS) stain is used to visualise glycogen, basement membranes, and neutral mucosubstances. Oxidation with periodic acid exposes the aldehyde groups in sugars that subsequently react with the chromophores in Schiff's reagent, producing a bright pink colour. A basic stain such as Harris' Hematoxylin is used as a counterstain to stain the cells blue (fig 2.1 C).

2.2.3.3 Sirius red

The Sirius red stain is an extremely hydrophilic dye that stains collagen, reticulin fibres, basement membranes, and mucins red, and is used to evaluate liver fibrosis. Fast Green FCF is a dye that primarily stains proteins and is useful as a counterstain for Sirius red.

2.2.4 Viewing on the compound light microscope

After staining and coverslipping, sections are viewed on a compound light microscope using bright field illumination. Light is focused through a condenser lens and passed through the specimen. The light is then collected by an objective lens and eyepieces that magnify and focus the specimen image. Contrast comes from the absorption of light by the specimen. The image can also be captured by a light-sensitive camera. Maximum resolving power of a compound microscope is 0.2 μm.

2.3 Electron microscopy

2.3.1 The electron microscope

Electron microscopes were developed due to the limitations in resolving power on the light microscope. The transmission electron microscope (developed in the 1930s) has a resolving power of 0.2 nm or less, and can thus reveal the ultrastructure of individual cells (Bancroft, 2008). A focused electron beam is fired upon an ultrathin section of a prepared specimen under a vacuum. An image is formed as some electrons are reflected off the tissue (or scattered), and other electrons pass through the specimen where there is no tissue. The scanning electron microscope (developed in the mid 20th century) has a resolving power of 2.5 nm and provides a three dimensional surface image of a specimen such as a cell or block of hepatic tissue. A focused electron beam is scanned across the surface of a prepared specimen under a vacuum. Morphological detail is collected as the electrons hit the specimen surface causing secondary electrons to be released from the specimen (inelastic collisions) and collected by a detector. An image of the specimen is created according to the secondary electrons' energy, number, and angle of their path. The image is then sent to a television screen for viewing (Slayter, 1992).

2.3.2 Ultrastructural fixatives and buffers

Glutaraldehyde is the most effective aldehyde fixative for preserving ultrastructure, stabilising microtubules and microfilaments better than any other fixative. It has an aldehyde group on both ends of the molecule facilitating more extensive, rapid, and irreversible cross-linking of proteins. Glutaraldehyde and its oligomers are larger than formaldehyde and penetrate the tissue much slower (Bancroft, 2008). Thus, a fixative

including a mixture of glutaraldehyde and formaldehyde is optimal for ultrastructural fixation. Formaldehyde penetrates quickly, initiating structural stabilisation before thorough and rapid cross-linking of proteins by glutaraldehyde. Osmolarity of the fixative is crucial to maintaining appropriate osmotic pressure during fixation, preventing extraction of cellular materials and swelling or shrinking of cells. Osmolarity can be altered by addition of electrolytes (such as calcium) to the fixative buffer that have additional membrane stabilising properties, and non-electrolytes (such as sucrose) that act as osmotic stabilisers due to their slow rate of penetration through cell membranes. Sodium cacodylate buffer is commonly used for electron microscopy because it does not precipitate calcium ions and resists bacterial contamination during storage. The pH of the fixative must remain close to that of the tissue (ideally between pH 7.2 - 7.4) to avoid alterations to the structure and behaviour of tissue proteins that are responsible for cell shape.

2.3.3 Methods of primary ultrastructural fixation

The two main methods of ultrastructural fixation are perfusion and immersion fixation. Perfusion fixation is primarily used in animal experiments and fixative is perfused through the blood vessels. It is the most superior method of chemical fixation (Dariush Fahimi, 1967, Wisse, 2010) particularly for the liver. The portal vein is cannulated and fixative is perfused through the sinusoids enabling fast and direct contact of the fixative with the cells, and good consistency of fixation quality. Brief exsanguination (via perfusion with heparinised saline for example) before the fixative prevents thrombosis and improves the subsequent perfusion of the fixative (Dariush Fahimi, 1967). It is also important that the perfusion pressure be kept low (at about 5 - 10 ml per 100 g animal per minute), and the IVC cut at the diaphragm

immediately before perfusion, as damage to the hepatocytes, sinusoids and LSEC fenestrations occurs if the pressure is too high (Fraser, 1980, Wisse, 1970) (fig 2.2).

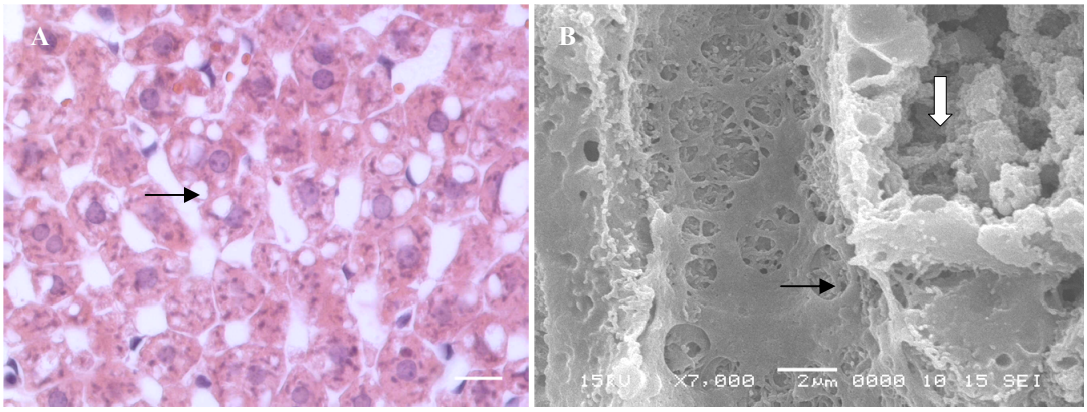

Figure 2.2 *Histological and electron micrographic representation of high perfusion pressure artefact in hepatocytes and liver sinusoids*
A) H & E stained histological section after high perfusion pressure. Hepatocytes contain vacuoles (arrow). Bar = 20 µm.
B) Scanning electron micrograph after high perfusion pressure. The LSEC fenestrations are disrupted and large gaps appear in the cytoplasm (arrow). The hepatocytes are vacuolated and damaged (white arrow). Bar = 2 µm.

Incubation in a fixative volume of at least ten times that of the tissue blocks overnight after the initial perfusion ensures adequate penetration of the fixative and increases the cross-linking of proteins as fixation proceeds slowly (fig 2.3 A). This is carried out at 4 ºC to decrease extraction of cellular constituents and minimise post-mortem change (Bancroft, 2008). Specimens can be left in fixative for more extended periods of time. After incubation in fixative for 7 days at 4 ºC the tissue appeared well fixed and had not deteriorated when assessed with SEM analysis (fig 2.3 B).

Needle fixation is a variant of this process that involves injection of the fixative directly into biopsied tissue. The aim is for fixative to be flushed through the blood vessels in order to exsanguinate them and directly and quickly expose the cells inside

the tissue block to fixative. In needle fixation of the liver, care must be taken to keep the injecting pressure low to avoid destroying the sinusoids (Wisse, 2010). Although this method is not as fast or consistent as perfusion fixation, it is a far superior alternative to immersion fixation and can be used on human biopsies.

In the process of immersion fixation, blocks of tissue are removed during surgery, minced into small blocks whilst in fixative, and incubated in fresh fixative for 1 - 4 hours at room temperature, or overnight at 4 ºC. This method is the least ideal for ultrastructural analysis because of the slow penetration of fixative through the tissue resulting in autolytic changes at the centre of the blocks and poor consistency of fixation (Dariush Fahimi, 1967, Hayat, 2000, Wisse, 1970) (fig 2.3 E and F). There is also the potential for mechanical damage during the mincing process as the tissue (and particularly the centre of the tissue because of the slow penetration of fixative) has often not yet hardened sufficiently from its brief exposure to fixative (fig 2.3 D).

Different levels of fixation quality can be visually recognised early in the fixation process and inadequately fixed tissue may be discarded before processing. Whilst immersed in the primary fixative, well-fixed tissue appears a yellow-brown colour and is transparent and firm, whereas poorly fixed areas appear pale-brown or red-brown and soft. On washing of the tissue blocks after fixation in sodium cacodylate buffer then distilled water, unfixed areas change from brown to white, whereas the well-fixed areas remain hard and yellow brown (Dariush Fahimi, 1967).

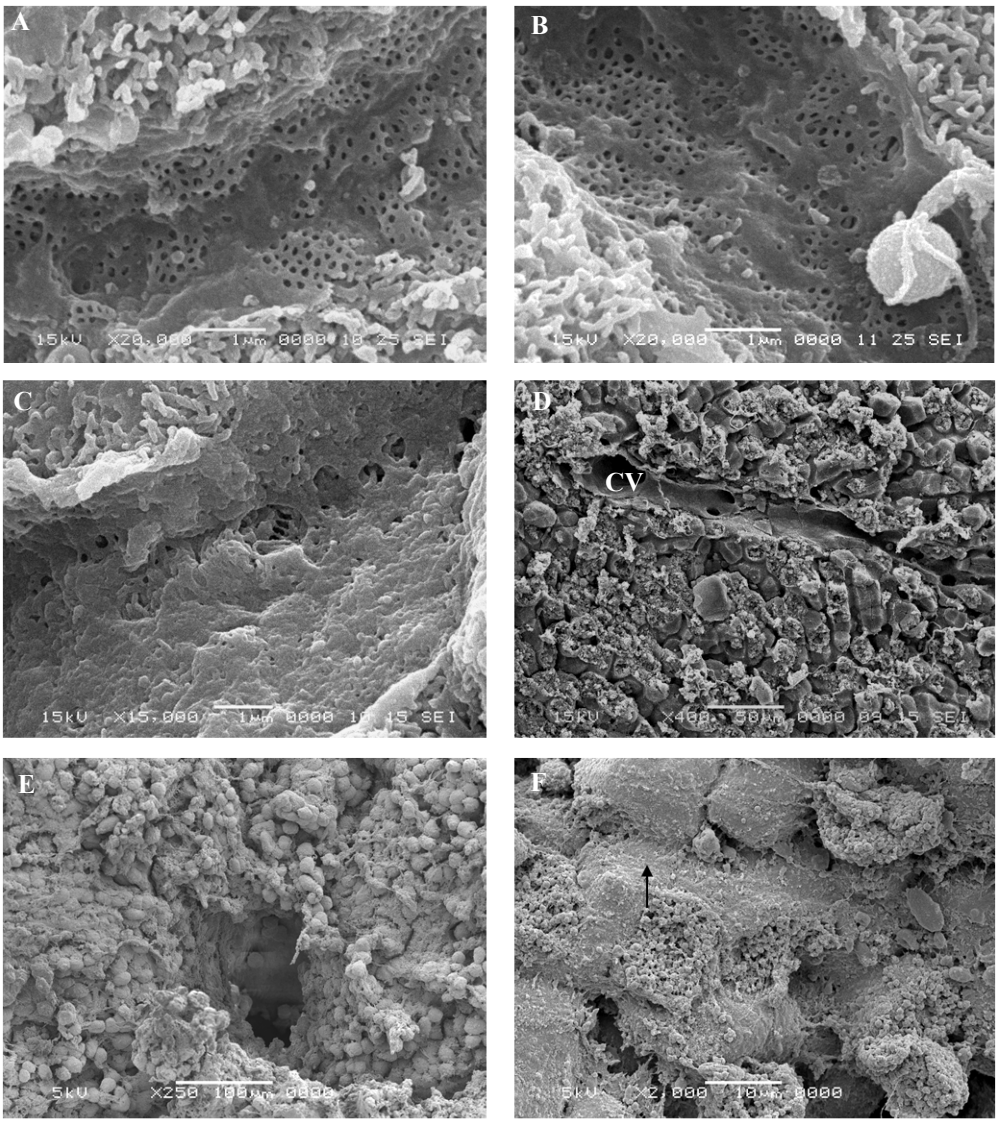

Figure 2.3 *Examples of good and poor ultrastructural fixation of liver sinusoids from F344 rats for SEM*
A) Good fixation with a combined glutaraldehyde-formaldehyde fixative. Perfusion fixation followed by incubation in fixative overnight. Fenestrations, and hepatocyte microvilli are well defined (bar = 1 µm).
B) Good fixation with a combined glutaraldehyde-formaldehyde fixative. Perfusion fixation followed by incubation for 7 days in fixative (bar = 1 µm).
C) A poorly fixed sinusoid, LSEC cytoplasm is defenestrated with gaps (bar = 1 µm).
D) Mechanical damage to the hepatocytes during mincing before the tissue has sufficiently hardened. CV = central venule (bar = 50 µm).
E) and F) This specimen was immersion fixed in 2.5 % glutaraldehyde without formaldehyde overnight at 4 ºC. Fixation quality is very poor. CV = central vein in (E) and an arrow points to an LSEC in (F). In (E) the scale bar = 100 µm, and in (F) the magnification is higher, bar = 10 µm.

2.3.4 Secondary fixation and contrast enhancing of specimens

Secondary-fixatives are applied to specimens after the primary (aldehyde) fixation step. Specimens are immersed in secondary fixatives to strengthen and enhance the initial fixation, and increase contrast of the specimen for viewing on the electron microscope. These are discussed below.

2.3.4.1 Osmium

Osmium tetroxide is routinely used as a secondary fixative (Griffith, 1974, Hayat, 2000). It fixes and cross-links unsaturated lipids by reacting with their double bonds, and incorporates into cell membranes by binding with phospholipids. Osmium is a heavy metal oxide that has a high electron density. Thus incorporation of osmium into the specimen increases the scattering of the electron beam and greatly improves specimen contrast (fig 2.4). Osmium only penetrates tissue to about 1 mm deep and so specimen blocks should ideally be 1 - 2 mm^3 (Bancroft, 2008). The primary aldehyde fixative must be thoroughly washed out of the specimen before incubation in osmium to avoid precipitation of osmium ("peppering") throughout the specimen caused by its cross-reaction with free aldehyde groups.

2.3.4.2 Tannic acid

Tannic acid is a contrast-enhancer and supplemental fixative that may be applied to the specimens after primary fixation. It has mordant properties and forms complexes with heavy metals such as osmium, lead, and uranium, increasing their uptake into the tissue and improving contrast of fine cellular structures (fig 2.4 D). Tannic acid is a large molecule with many active groups and can interact with a diverse array of

cellular components and increase their electron density even without the aid of osmium (Hayat, 1993). It is more routinely used in specimen preparation for SEM than TEM.

2.3.4.3 Uranyl

Uranyl acetate is the acetate salt of uranium (an electron dense heavy metal), and is commonly used as an *en bloc* stain (of the whole specimen rather than a section) after osmication in TEM specimen preparation to improve the contrast of membranes (fig 2.4 B and C). It also has some fixation properties (Hayat, 2000). Uranyl can bind with tannic acid and further increase the electron density and contrast of a specimen (Dykstra, 1992) (fig 2.4 D). It is also a mordant for lead staining that is performed after sectioning, resulting in a much more intense stain. The use of *en bloc* uranyl acetate staining in liver specimens is often omitted as it causes leaking of hepatocyte glycogen.

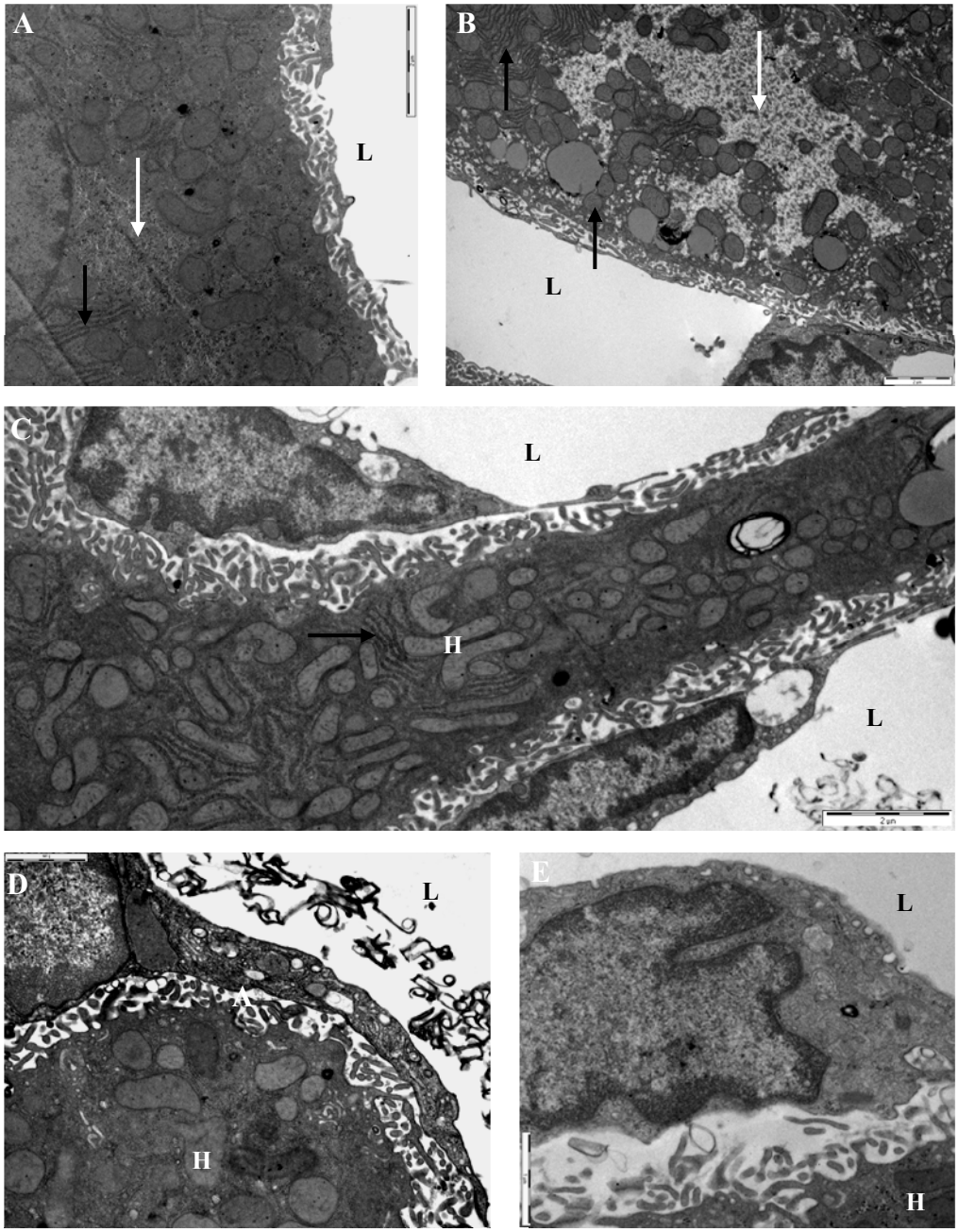

Figure 2.4 *Micrographs displaying the effect of uranyl acetate and tannic acid en bloc staining on TEM specimen contrast. All specimens (from F344 rats) were perfusion fixed with formaldehyde-glutaraldehyde, secondary fixed with osmium, and stained after sectioning with uranyl acetate and lead citrate. L = sinusoid lumen.*
A) Hepatocyte and sinusoid from an ad libitum fed F344 rat without *en bloc* uranyl or tannic acid treatment (bar = 2 μm).
B) Micrograph from an ad libitum fed rat and C) from a fasted rat (with low glycogen stores) *en bloc* stained with uranyl acetate (bar = 2 μm). There is increased membrane staining and contrast in (B) and (C) compared to (A). Patches of glycogen are marked with white arrows and mitochondria and ER are marked with black arrows. Areas of glycogen are less dense in (B) than (A), as some glycogen has leaked out of the hepatocytes (marked H) during the uranyl *en bloc* incubation (bar = 2 μm).

D) and E) show micrographs of the perikaryon of LSECs. In (D) the specimen was incubated with tannic acid before osmication and *en bloc* stained with uranyl acetate. The cell and organelle membranes show much stronger contrast than in micrograph (E) where there was no tannic acid or uranyl *en bloc* treatment (bar = 1 µm).

2.3.5 Dehydration, embedding, sectioning, and staining for TEM analysis

Dehydration of specimens after secondary fixation with a series of ethanols and acetone is performed to remove water so that specimens can be infiltrated with embedding media (resin). Resins provide stability for the specimen during sectioning and under the electron beam. Prior to ultrathin sectioning, semithin sections are cut at 0.5 µm and stained with toluidine blue. Subsequent viewing of toluidine blue stained sections under the light microscope provides information about the quality of fixation and location of the block within the liver (fig 2.5).

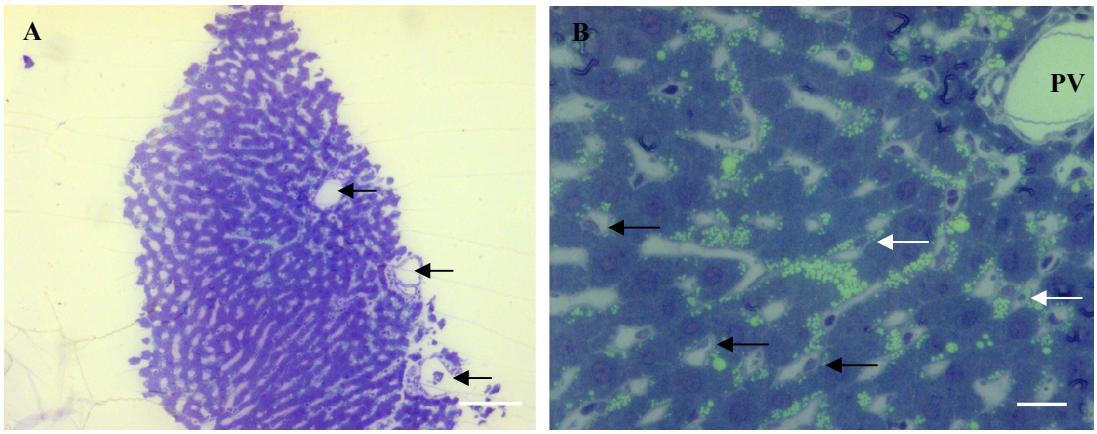

Figure 2.5 *Toluidine blue stained 0.5 µm thick sections showing that the specimen has good fixation and that the region is a periportal zone (arrows point to portal tracts). Lipid vacuoles are clearly seen in the hepatocytes, as are LSEC (black arrows) and HSC (white arrows) nuclei, and KCs/leukocytes in the sinusoids. PV = portal venule.* (A) Bar = 100 µm, (B) Bar = 20 µm.

Ultrathin sections are then cut at 80 nm with a diamond knife, mounted on grids and stained first with uranyl (acetate) then lead (citrate) before viewing on the TEM. As described in section 2.3.4.3, uranyl adds electron density to the specimens by binding

with proteins, phospholipids and nucleic acids, and is a mordant for lead staining. Lead enhances the stains effected by other metals such as osmium and uranyl primarily by binding to them, and this scatters electrons very effectively (Dykstra, 1992, Hayat, 1993). Uranyl acetate solutions are saturated and care must be taken not to draw solution from the bottom of the bottle where precipitate is found otherwise angular uranyl acetate crystals will be found on the specimens. Artefactual lead stain (globular) deposits can also form as lead will precipitate to highly insoluble lead carbonate crystals on reaction with carbon dioxide and oxygen in the air. These can present as very fine or large globular deposits (fig 2.7 A).

2.3.6 Reprocessing paraffin embedded tissue for TEM analysis

Tissue fixed in formaldehyde and embedded in paraffin can be reprocessed for transmission electron microscopy when extra specimens are required for ultrastructural analysis (Lighezan, 2009). Mincing of glutaraldehyde-formaldehyde perfusion fixed tissue into 1 mm^3 blocks and preparing them for EM immediately after surgery is a somewhat random and blinded process, and as such, critical areas for analysis may not be sampled. It is much easier to select samples for EM analysis from a specific region of a paraffin block after histological sections have been viewed on a light microscope, however the quality of fixation is comparatively poor (Wang, 1987). Formaldehyde (as discussed earlier) is less effective for preserving ultrastructural components of cells. Poorly preserved structures commonly include the loose components of the cells such as lipid, glucose, and ribosomes (Nasr, 2007). In addition, the reprocessing includes an extra dehydration step before the initial paraffin embedding thus there is increased tissue dehydration, resulting in greater extraction of lipids, proteins and subsequent shrinkage of cells and subcellular components (fig 2.6

B). However, reprocessed formaldehyde-fixed specimens can still provide important diagnostic information.

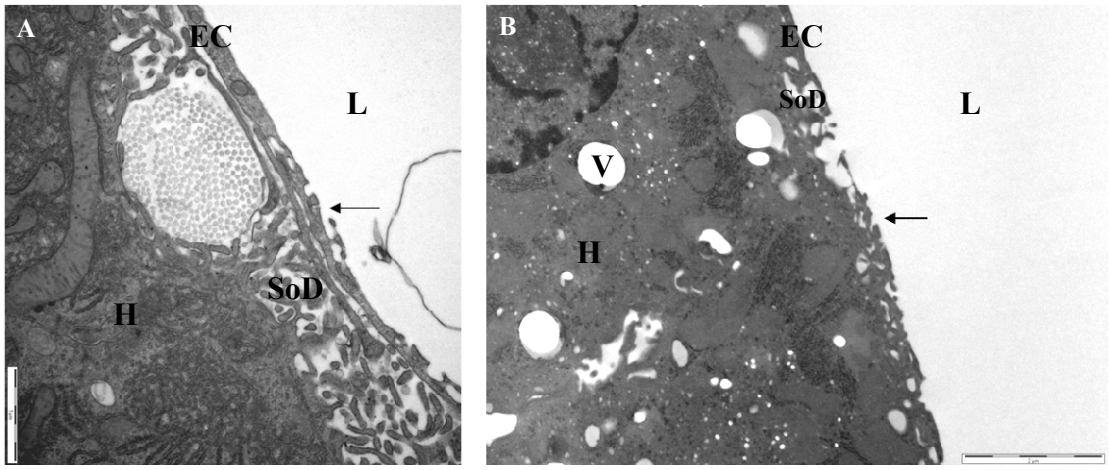

Figure 2.6 *Examples of transmission electron micrographs from F344 rat specimens prepared after perfusion fixation and after reprocessing from a formaldehyde-fixed paraffin block*
A) A sinusoid and hepatocyte from a formaldehyde-glutaraldehyde fixed specimen. EC = LSEC, H = hepatocyte, SoD = space of Disse, L = sinusoid lumen (bar = 1 μm).
B) A sinusoid and hepatocyte from a reprocessed formaldehyde-fixed specimen. H = hepatocyte, V = a vacuole in the hepatocyte cytoplasm, EC = LSEC, SoD = space of Disse, L = sinusoid lumen (bar = 2 μm).
The clarity and definition of the LSEC cytoplasm and fenestrations are much higher in (A) than (B) (arrows), although it is still possible to see fenestrations in (B). Some lipid and cell components have been extracted from the hepatocytes in (B), and the LSEC cytoplasm is much thinner probably also due to cell component extraction. Both specimens were *en bloc* stained with uranyl acetate.

2.3.7 Dehydration and specimen preparation for the SEM

After secondary fixation, specimens must be dehydrated and dried to remove all water from the sections as the SEM specimen chamber is at high vacuum. Dehydration is carried out in a gradient series of ethanols to absolute ethanol. Hexamethyldisilazane, a drying agent, is then added to the specimens, removed and evaporated, before the specimens are mounted onto aluminium stubs with double sided conductive tape (Dykstra, 1992). Next the specimens are coated in metal. Biological materials are

good insulators and if the net specimen current is not grounded the specimen will build up negative charge, repel the electron beam, and result in image distortion. Coating with a conductive material helps to alleviate this problem. Sputter coaters are used to produce a cloud of metal atoms (usually gold or platinum) to finely and evenly coat specimens. Colloidal carbon paint is also applied to reduce charge by being painted down one side of the specimen to the tape (Dykstra, 1992). Specimens are then ready to be placed in the specimen chamber of the SEM and viewed.

2.3.8 Indicators of poor ultrastructural fixation on electron micrographs

Two of the most sensitive indicators of poor fixation quality include swollen mitochondria and endoplasmic reticulum (Bancroft, 2008) (fig 2.7 B). The absence of fenestrations in LSECs or the appearance of large gaps can also indicate poor fixation (fig 2.3 C) or inadequate perfusion pressure (fig 2.2 B) (Wisse, 2010). Collapsing of sinusoids and accumulation of RBCs within them are commonly signs of poor perfusion of the fixative (fig 2.7).

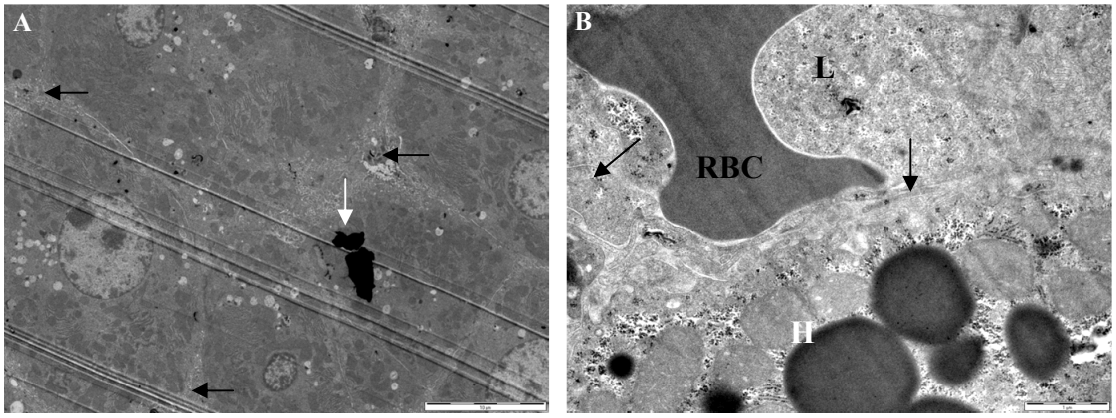

Figure 2.7 *Examples of poor fixations of F344 livers and specimen artefacts on TEM*
A) Poor perfusion of sinusoids has resulted in poor LSEC fixation and collapsed lumens (arrows). There is an artefactual lead stain deposit on the specimen (white arrow). The long parallel stripes through the section are knife marks, a result of nicks and debris on the diamond knife edge scarring the section (bar = 10 μm).
B) Closer view of a poorly perfused poorly fixed sinusoid. The hepatocyte appears swollen and the LSEC is not clearly defined (arrows). This section also displays chatter artefact, parallel lines through the section caused by vibration during sectioning. Chatter occurs perpendicularly to knife marks. L = lumen (bar = 1 μm).

Some experience is required to distinguish between artefact and real structures in a diseased specimen. If the fixation process is carried out carefully and thoroughly and poorly fixed areas of tissue are discarded, the presence of artefacts will be minimal, and an accurate diagnosis of the tissue is possible.

2.4 Experimental materials and protocols

2.4.1 Animals

Male Fischer F344 rats were obtained from the Animal Resources Centre (ARC), Perth, Western Australia. Rats were housed in cages of 2 or 3 at 25 ˚C, fed with standard rat chow and allowed access to water at all times. Ethical approval for

experiments was given by the Sydney South Western Area Health Service Animal Welfare Committee.

2.4.2 Blood analysis

The rats were weighed then deeply anaesthetised by an intraperitoneal injection of 2 ml/kg ketamine (60 mg/ml) and xylazil (6 mg/ml), a laparotomy was performed and the intestines pushed aside to reveal the portal vein. Approximately 3 ml blood was taken from the inferior vena cava (IVC) and transferred into an EDTA tube. Blood was spun at 1500 rpm for 10 min at 25 ˚C. Using a ruler, the packed RBC layer and the total volume including plasma was measured in centimetres. The hematocrit was then calculated by dividing packed RBC layer height by the total volume height then multiplying by 100. The plasma was removed and stored at -20 ˚C before analysis (of blood biochemistry and liver function tests) by the Biochemistry Department, Diagnostic Pathology Unit, Concord RG Hospital, using the automated Roche Diagnostics Modular Analytics Serum Work Area (F. Hoffman-La Roche Ltd). Lipoclear (Lomb Scientific, product number: LC40), a non-ionic solution used to remove lipoproteins, was added to grossly lipemic samples to yield clear samples suitable for analysis.

2.4.3 Perfusion fixation protocol

Following from the procedure described in section 2.4.2, the portal vein was cannulated using an 18 gauge intravenous cannula. Care was taken to prevent air bubbles from entering the portal vein during perfusion. The liver was exsanguinated with approximately 5 - 10 ml heparinised phosphate buffered saline (PBS; 1 PBS

tablet dissolved in 100 ml dH_2O, heparin 1000 I.U. per ml, pH 7.4). The perfusion flow was set at 5 - 10 ml per minute using a gravity-mediated system. Perfusion of PBS was only continued until the liver became a tan colour indicating the removal of blood from the sinusoids. Both the abdominal and thoracic IVC were cut immediately at the commencement of perfusion to reduce any pressure build up in the sinusoids and to allow perfusate to freely flow out. Fixative was then perfused through the liver until the tissue became hard (approximately 20 ml) indicating adequate fixation. The liver was removed and prepared for both histology and electron microscopy analysis as described below.

2.4.4 Histological specimen preparation

The fixative used for histology was 4 % formaldehyde (freshly prepared from paraformaldehyde) in PBS with 1 % sucrose, pH 7.4. Fixative pH was adjusted with concentrated sodium hydroxide and hydrochloric acid. Liver lobes were sectioned into pieces with a scalpel, placed in fixative (4 % formaldehyde, 1 % sucrose in PBS, pH 7.4), and left overnight in the fridge (at 4 ˚C). The fixative was then removed and the pieces washed in buffer (PBS with 1 % sucrose, pH 7.4) three times. Liver pieces were placed in cassettes and using a Leica® Microsystems (North Ryde, Australia) TP 1020 automatic tissue processor, dehydrated through a graded series of ethanol before clearing with xylene and infiltration by paraffin wax (see Appendix 1B). Liver pieces were placed into moulds and set in paraffin wax on a cold plate, ready for sectioning. Sections were cut on a microtome at 4 μm, and firmly stuck on Superfrost Plus® glass slides by heating in the oven at 60 ˚C for 10 min before rehydration and staining with hematoxylin and eosin, PAS, or Sirius red (see Appendix 2 for protocols). After staining, sections were dehydrated with ethanol and cleared with

xylene, coverslipped with mountant and coverglass, and observed on a compound light microscope. Micrographs were taken using a Zeiss AxioCam MRc camera.

2.4.5 Electron microscopy specimen preparation

The fixative used for electron microscopy was 2.5 % glutaraldehyde (EM grade) /2 % formaldehyde (prepared fresh from paraformaldehyde) in sodium cacodylate buffer (0.1 M sodium cacodylate, 10 mM $CaCl_2$, 1 % sucrose, pH 7.4, 440 mOsmol). Fixative pH was adjusted with concentrated sodium hydroxide and hydrochloric acid. Immediately after perfusion fixation and removal of liver, sections of liver were immersed in EM fixative and cut into small blocks of approximately 1 mm^3. The blocks were placed in tubes containing EM fixative, designated for scanning or transmission electron microscopy, left overnight in the fridge (4 ˚C), then processed as described below.

2.4.5.1 Scanning electron microscopy

Approximately 10 blocks per liver were washed 3 times (1st wash 10 min, 2nd wash overnight, 3rd wash 10 min) in 0.1 M sodium cacodylate buffer to remove any trace of fixative before incubation in 1 % tannic acid (in 0.15 M sodium cacodylate buffer with 1 % sucrose) for 1 hour. Blocks were then washed 3 × in sodium cacodylate buffer before secondary fixation in 1 % osmium in 0.1 M sodium cacodylate buffer pH 7.4 with 1 % sucrose for 1 hour. After osmication, specimens were washed 3 × 10 min each in sodium cacodylate buffer then dehydrated in a series of ethanols: 3 × 50 % (5 min each wash), 4 × 70 % (5 min each), 3 × 90 % (10 min each), 3 × 95 % (10 min each), 4 × 100 % (10 min each) ethanol. Specimens were immersed in

hexamethyldisilazane for 10 min. After the hexamethyldisilazane was removed the specimens were left in the fume hood for 10 min so that any remaining hexamethyldisilazane could evaporate, and placed in a dessicator overnight. Specimen blocks were mounted onto stubs using double sided carbon tape and carbon paint, and gold coated in a sputter coater under argon (45 secs at 40 mV). They were viewed and micrographs taken using a JEOL JSM-6380 scanning electron microscope. Pictures were taken at an acceleration voltage of 15 kV and specimens stored in a dessicator.

2.4.5.2 Transmission electron microscopy

Approximately 5 blocks per liver were processed in a Lynx™ Electron Microscopy Tissue Processor where they were washed in 0.1 M sodium cacodylate buffer, secondary fixed in 2 % osmium, again rinsed in buffer, and dehydrated in a series of ethanols and acetone before being infiltrated with Spurr's resin (see Appendix 1A for full protocol). Blocks were placed at the bottom of BEEM® capsules (moulds) that were filled with Spurr's resin. They were left to set overnight in an oven at 75 ˚C. Semithin sections were then cut on an ultratome with a glass knife at 0.5 µm and stained with toluidine blue (see Appendix 3A) to observe the orientation of sections on a light microscope and to ensure good fixation. Once this was achieved, ultrathin 80 nm sections were taken using a diamond knife and stuck on formvar-coated nickel slot grids (ProSciTech-Australia) to be viewed on the Philips CM10 transmission electron microscope fitted with a Megaview III camera and Analysis® software (Olympus).

2.4.5.3 Reprocessing paraffin-embedded specimens for TEM analysis

There are different methods of reprocessing as described (Hayat, 2000, Lighezan, 2009). All are based on a generalised protocol of deparaffinisation, rehydration, osmication, dehydration, and embedding of the specimen in resin. The method we applied is as follows. A 4 μm histological section was cut from a paraffin-embedded formaldehyde-fixed specimen and stained with Hematoxylin and Eosin. After viewing on the light microscope, the areas of interest that contained examples of a particular pathological process were selected from the section, and referred to the face of the tissue in the paraffin block that contained the adjacent layer of tissue to the section. Four 1 - 2 mm^3 blocks were cut from these selected areas of the paraffin block using a scalpel blade. Blocks were deparaffinised by incubation in xylene (occasionally agitating) for 2 hours and rehydrated by being immersed for 15 min each in a solution of 50:50 xylene/100 % ethanol, then a series of ethanols (100 %, 95 %, 90 %, 70 %, 50 %), and washed in distilled water then sodium cacodylate buffer for 15 min each. The blocks were subsequently processed for transmission electron microscopy exactly as described in section 2.4.5.2 including osmication, dehydration, and embedding of the specimen in resin. In addition, after osmication the specimens were *en bloc* stained with uranyl acetate (see Appendix 1A for protocol) in order to increase the contrast and improve specimen preservation (Bancroft, 2008). Specimens were viewed and pictures taken as described in section 2.4.5.2.

2.4.5.4 SEM analysis of fenestration and gap diameter using Image J

Micrographs of LSEC cytoplasm from each rat were opened using Image J software. The scale bar from each micrograph was used to calibrate the measurements. A line was drawn through each fenestration and gap in the LSEC cytoplasm by selecting the

longest straight line from one side of the fenestration to the other (fig 2.8). This was defined as the diameter. Selecting the longest line increases the measurement accuracy as fenestrations are sometimes on an angle and appear oval, and keeps the measuring process consistent.

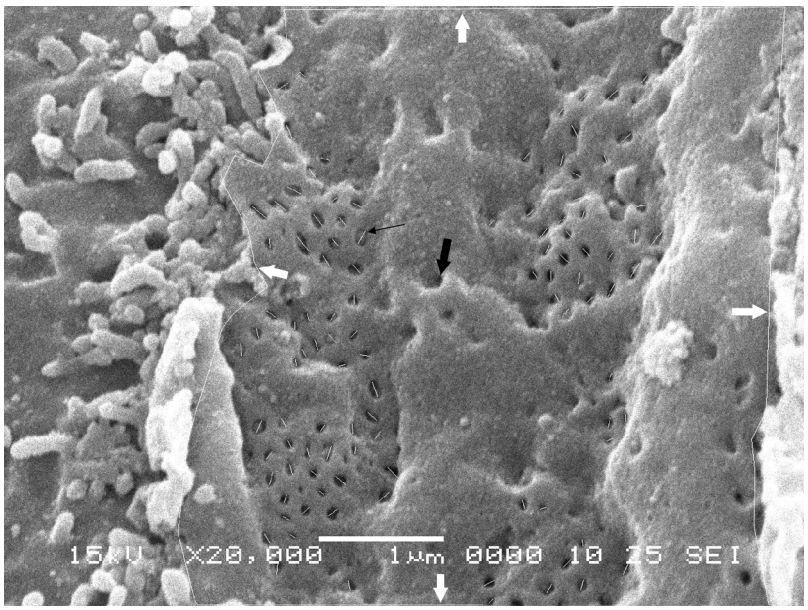

Figure 2.8 *An example of an Image J analysis of the LSEC cytoplasm*. A line was drawn through each fenestration (black arrow) to calculate fenestration diameter. Pits on the LSEC cytoplasmic arms (bold black arrow) that look similar to fenestrations were not measured. A line was drawn around the LSEC cytoplasm (indicated by the bold white arrows) to calculate the area of the cell surface for porosity and fenestration frequency measurements.

The length of the diameter of each fenestration was calculated using Image J (fig 2.8). The average fenestration diameter was recorded from the total number of fenestrations from each animal. SigmaPlot 11.0 was used for statistical analysis. Standard deviation of averages from each rat was calculated. A Student's *t*-test was also performed to calculate any significant difference (defined by a p value of < 0.05) between groups.

2.4.5.5 SEM analysis of porosity and fenestration frequency

Porosity is a measurement of how porous the cell surface is and is calculated with the formula:

Porosity (%) = (sum of fenestration areas/sum of cell surface areas) × 100, where fenestration area = $(\pi(\text{fenestration diameter}/2))^2$.

Fenestration frequency is a measure of how many fenestrations there are per area of cell and is calculated by the formula:

Fenestration frequency = total number of fenestrations/total cell surface area.

Total cell surface area was defined as the total area of LSEC cytoplasm in the micrograph excluding any areas covered in debris on the LSEC that obscured fenestrations from view.

Chapter 3:

The Effect of Fasting on Fenestrations in the Liver Sinusoidal Endothelial Cell

3.1 Introduction

To maintain homeostasis of energy metabolism when the dietary nutrient supply is stopped, significant changes occur in hepatocyte metabolism and gene expression (Sokolovic, 2008). In order to sustain adequate blood glucose levels, glycogen stores are depleted, gluconeogenic pathways are upregulated, and there is increased oxidation of fatty acids and amino acids (for glucose and energy production). The role of the LSEC in metabolic homeostasis during fasting has not been studied. However as LSECs form a fenestrated and dynamic barrier between the blood and hepatocytes they may play an important role in regulating nutrient supply to and from hepatocytes in the fasted state.

The regulation and normal function of LSEC fenestrations, and their changes in disease and aging, suggest that fenestrations have important implications for hepatic metabolism and subsequent systemic exposure to many substrates and toxins (Arias, 1990, Cogger, 2009, Fraser, 1995). The effects of a variety of pathological states on the LSEC and its fenestrations have been widely reported. In general, acute and toxic injury causes large gaps to form in the LSEC while chronic disease states and aging are associated with reductions in the diameter and/or frequency of fenestrations (Clark, 1988, Cogger, 2009, Cogger, 2004, DeLeve, 1999, Le Couteur, 2008, McCuskey, 2006, Warren, 2007).

Because of technical difficulties associated with the study of fenestrations in LSECs, physiological regulation of fenestrations is less clear (Cogger, 2009). Studies where livers or isolated LSECs have been treated acutely with external agents have shown that vascular endothelial growth factor (VEGF) increases the diameter and frequency

of fenestrations (Funyu, 2001) while endothelin 1, calcium, noradrenaline and serotonin reduce the diameter of fenestrations (Cogger, 2009, Gatmaitan, 1996, Kamegaya, 2002, Wisse, 1980). Although it has been proposed that fenestrations are dynamic structures that respond to physiological stimuli (Arias, 1990, Wisse, 1985), it is as yet unknown whether fenestrations do change in response to such stimuli *in vivo*.

Nutritional state influences the levels of VEGF (Dandona, 2003, Wang, 2003), noradrenaline (Blum, 1992, Young, 1977), serotonin (Blum, 1992), and endothelin 1 (Ferri, 1995), and has effects on endothelial cells in many tissues (Alipour, 2007). Furthermore, if fenestrations are involved in the transfer of nutrients between hepatocytes and blood, it is plausible that fenestrations might respond to feeding and fasting. For these reasons, it was hypothesized that nutritional status influences fenestrations and in this study the effects of fasting on fenestrations were investigated.

3.2 Materials and Methods

3.2.1 Animals

Male F344 rats (as described in section 2.4.1), 3 months old, weighing 290 - 330 g were used. Eight animals were housed in cages of 2. Four rats received ad libitum access to rat chow and water until time of surgery, and 4 received only water for 48 hours prior to surgery. The study was approved by the Sydney Southwest Area Health Service Animal Ethics Committee.

3.2.2 Surgery and specimen preparation

All surgery was performed in the afternoon between 2 and 4 pm. Rats were anesthetised as described in section 2.4.2 and surgery and perfusion fixation were performed as described in section 2.4.3. Liver specimens from each rat were processed for scanning electron microscopy and viewed on a Jeol JSM 6380 scanning electron microscope as described in sections 2.4.5 and 2.4.5.1.

3.2.3 SEM analysis

Scanning electron micrographs of ten sinusoids that appeared flat from regions midway between the portal and central vein were taken for each liver at 25000 × magnification for analysis of fenestration diameter, porosity (percentage of the LSEC surface area perforated with fenestrations), and frequency (number of fenestrations per area of cell) using Image J (1.41 NIH, USA) as described in section 2.4.5.4 and 2.4.5.5. In addition, fenestrations were grouped into size categories to observe the

frequency (number) of fenestrations of a particular size in each group. This data was displayed as a frequency distribution graph. All evaluations were blinded.

3.2.4 Liver weights and blood analysis

Livers were weighed, then separated into four main lobes (caudate, median, left, right) and each lobe weighed individually. The right kidney was also weighed as a reference. Blood was removed from the inferior vena cava during surgery and processed and analysed as described in section 2.4.2. Hematocrit was measured after centrifugation of the samples and the plasma was tested for alanine transaminase (ALT), aspartate transaminase (AST), cholesterol, triglyceride, urea, and creatinine concentrations (Department of Pathology, Concord RG Hospital, NSW).

3.2.5 Statistical analysis

Statistical differences between means were determined using Student's *t*-test and χ^2.

A p-value of < 0.05 was considered to be statistically significant. Data is presented as means ± standard deviation (SD). The fenestration frequency distribution graph data was tested for significant difference by a non-parametric *t*-test comparing the medians of each fenestration size category from the fed group with the medians of each fenestration size category from the fasted group.

3.3 Results

Figure 3.1 shows representative scanning electron micrographs of LSECs from a fed and a fasted rat. Results of the quantification of the fenestrations are shown in Table 3.1. There was a significant difference between mean fenestration diameters ($p = 0.003$) and the frequency of fenestrations ($p < 0.05$). In the fasted state, the fenestrations were approximately 10 % larger than in the fed state. Porosity was not significantly influenced by fasting state because of a concomitant decrease in the frequency of the fenestrations.

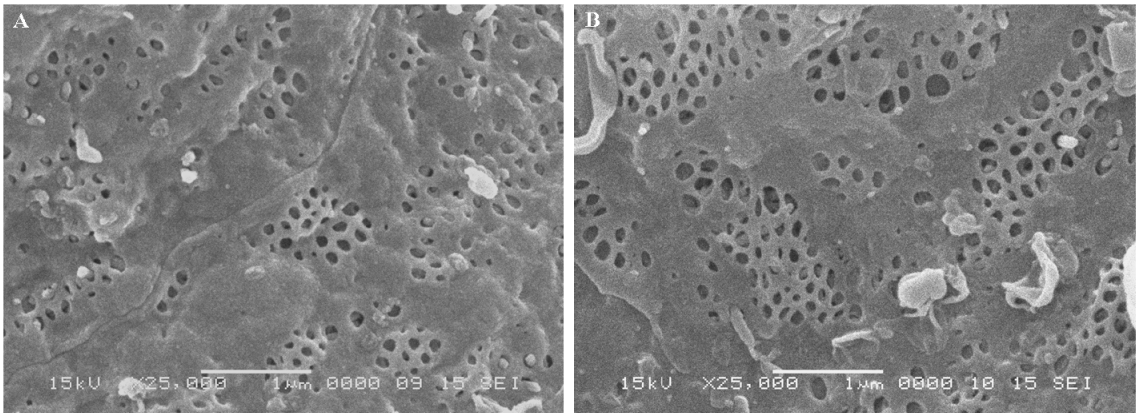

Figure 3.1 *Scanning electron micrographs of sinusoids from livers of (A) fed and (B) fasted F344 rats. Fenestrations are clustered into sieve plates and there is a significantly increased fenestration size in the fasted rat LSEC (bar = 1 µm).*

Table 3.1 *Quantification of the fenestrations in LSECs of fasted and fed rats*.
There was an increase in the diameter of the fenestrations in the fasted state associated with an increased in fenestration frequency. Data is presented as mean ± SD.

F344 rats	Fed rats	Fasted rats
Fenestration diameter (nm)	90.7 ± 11.7	99.0 ± 12.11*
Frequency of fenestrations per μm^2	8.45 ± 2.43	7.39 ± 2.28**
Porosity (%)	5.93 ± 2.05	6.07 ± 1.96
No of animals	4	4
No of fenestrations counted	5142	4551
Surface area analysed (μm^2)	607	617

*$p < 0.005$, **$p = 0.05$.

Table 3.2 shows the effects of feeding and fasting on weights and blood measurements of renal and hepatic function. With fasting, AST was significantly increased (71 ± 9 vs 54 ± 2 U/L, $p < 0.05$) while there was a decrease in triglycerides (0.4 ± 0.1 vs 1.7 ± 0.4 μmol/L, $p < 0.01$), urea (4.6 ± 0.3 vs 8.0 ± 0.3 mmol/L, $p < 0.001$) and liver weight. Such changes are well recognized with fasting and reflect altered utilization of energy sources during starvation (Moriyama, 2008). Liver weight loss during fasting was fairly evenly distributed across the lobes, although the largest lobes lost a greater amount of weight than the smaller lobes (fig 3.2). Figure 3.3 shows the frequency distribution graph of fenestration diameter. There was an overall shift to the right for fenestration size distribution in the fasted group compared to the fed ($p < 0.001$).

Table 3.2 *The effects of fasting on liver weight and blood measures of hepatic and renal function.*

F344 Rats	Fed rats	Fasted rats
Body weight at time of surgery (g)	321 ± 13	290 ± 15*
% Body weight loss after fast	-	5.8 ± 0.7
Liver wet weight (% body weight)	3.1 ± 0.22	2.4 ± 0.14***
Right kidney wet weight (% body weight)	0.33 ± 0.03	0.34 ± 0.02
ALT (U/L)	38 ± 2	40 ± 4
AST (U/L)	54 ± 2	71 ± 9*
Bilirubin (µmol/L)	1	1
Total cholesterol (µmol/L)	1.4 ± 0.1	1.5 ± 0.1
Triglycerides (µmol/L)	1.7 ± 0.4	0.4 ± 0.1**
Creatinine (µmol/L)	25 ± 2	24 ± 2
Urea (mmol/L)	8.0 ± 0.3	4.6 ± 0.3***

*$p < 0.05$, **$p < 0.01$, ***$p < 0.001$

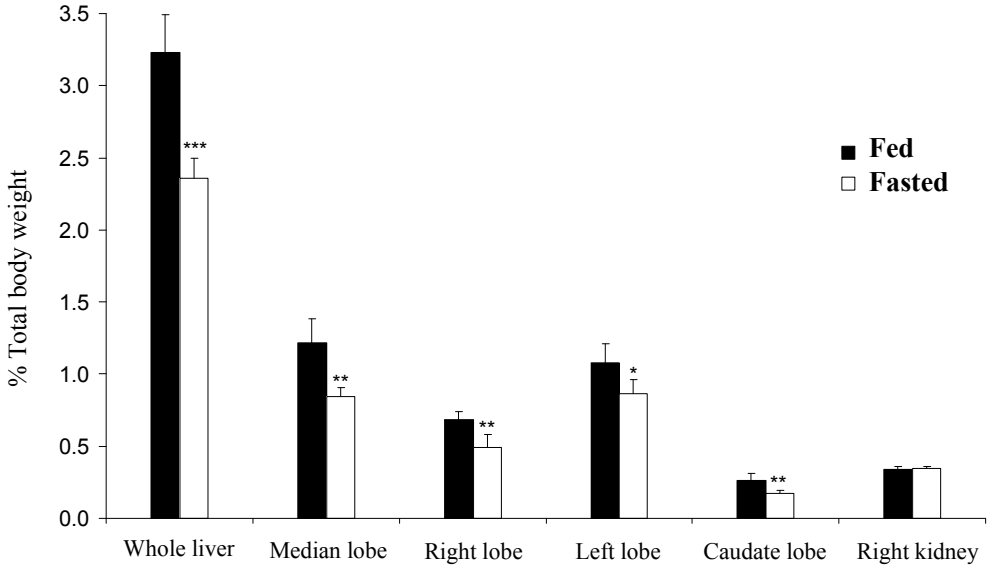

Figure 3.2 *Liver weight of the whole liver and of four liver lobes relative to body weight in fed and fasted F344 rats. Kidney weight relative to body weight remained consistent in fed and fasted groups (*p < 0.05, **p < 0.01, ***p < 0.001).*

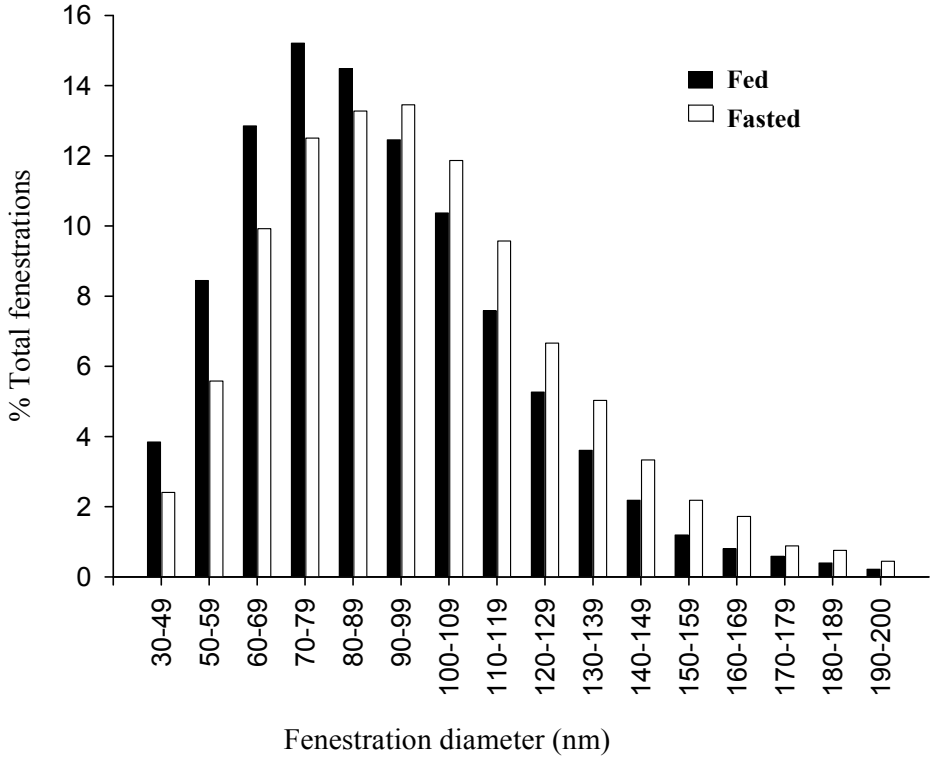

Figure 3.3 *Frequency distribution of fenestration diameter between fed and fasted F344 rats. There is a shift to the left indicating larger fenestrations in the fasted state.*

3.4 Discussion

Fenestrations are dynamic structures that can alter their frequency and diameter in response to a wide variety of stimuli (Cogger, 2009, Fraser, 1995, Wisse, 1985). This has been investigated widely for disease states, toxic injuries and aging. However whether fenestrations change in response to physiological stimuli *in vivo* has not previously been established. In this study, fasting was associated with an increase in fenestration diameter of approximately 10 % with a reduction in fenestration frequency of a similar magnitude. The result is the first *in vivo* demonstration that fenestrations alter with physiological stimuli, in this case, the fasting or fed state. There are several possible mechanisms and mediators for this response. A number of cytokines and vasoactive agents have been reported to influence fenestrations. Fenestration diameter is increased by VEGF (Funyu, 2001). Endothelin 1, calcium, noradrenaline and serotonin reduce the diameter of fenestrations (Cogger, 2009, Gatmaitan, 1996, Kamegaya, 2002, Wisse, 1980). Whether these have any effect on overall porosity is less clear. Porosity depends upon both diameter and frequency of fenestrations, and frequency is technically more difficult to assess especially in isolated LSECs (Cogger, 2009). Even so, it is known that fasting influences the levels of these agents, in a direction that would tend to increase fenestration diameter. For example, VEGF has been reported to be suppressed by insulin which is released in the fed state (Dandona, 2003), whereas fasting is associated with decreased levels of noradrenaline (Blum, 1992, Young, 1977), serotonin (Blum, 1992), calcium (Karkkainen, 1997), and endothelin 1 (Ferri, 1995). It is of note that Kupffer cells become inactivated after 2 days of fasting in rats (Sankary, 1995). The responses of fenestrations to many other parameters that change with feeding (such as insulin, glucose, leptin, ghrelin, shear stress) have not been reported.

A change in fenestration size during fasting will have implications for the transfer of substrates and plasma between blood in the lumen and hepatocytes. The fenestrated LSEC is somewhat analogous to an ultrafiltration system because it is a low pressure system with pores approximately 100 nm in diameter. The structure of the liver sieve is comparable to the typical structure of anisotropic (asymmetrical) membranes (Baker, 2004). These have a thin surface layer (the permselective layer), analogous to the LSEC layer, supported by a thicker porous substructure, analogous to the HSC layer. In anisotropic membranes, filtration rate is determined only by the surface layer of the membrane, with the substructure functioning as mechanical support and having virtually no separating function.

The transfer of fluid, and subsequently substrates in fluid smaller than the filtration pores, across an ultrafiltration system is estimated by the Hagen Poiseuille equation for ultrafiltration (Cherkasov, 1990) :

$$J = (fR^2\Delta P)/(8\eta l)$$

Where J = the volume flux of fluid, f = the porosity of the membrane, R = the diameter of the pores, ΔP = the pressure gradient across the membrane, η = viscosity, and l = thickness of the membrane. Thus the flux of fluid per unit area is proportional to the membrane porosity and the diameter of the pores. The hydraulic pressure driving filtration through LSEC fenestrations is a very low and fairly constant sinusoidal pressure of only a few centimetres of water (Le Couteur, 1992). Thus the influence of changes to porosity of the LSEC and diameter of fenestrations could have a significant effect on flux of plasma and substrates from the lumen to the SoD. In the current study an increase in fenestration diameter without a change in porosity during

fasting would therefore be associated with an increase in the flux of plasma through fenestrations compared to the fed state (assuming there is no change in the pressure gradient, LSEC thickness, or blood viscosity with nutritional status). This could have implications for increasing the efficiency of nutrient delivery to hepatocytes for gluconeogenesis (such as free fatty acids and amino acids), and increasing delivery of newly formed glucose and VLDL to the lumen to maintain blood glucose, triglyceride, and cholesterol levels.

In addition, the diameter of the fenestrations will determine the permselectivity, that is, the size of the particles or solutes that are retained in the blood. The sieving relationship provides an estimate of the ratio of the concentrations of the solute on either side of the ultrafiltration membrane. This is determined from the size of the solute and the diameter of the pores (Baker, 2004, Cherkasov, 1990). When applied to the LSEC, it is apparent that lipoproteins with diameters of 20 - 100 nm are most likely to be influenced by changes in fenestration diameter (such as chylomicrons, chylomicron remnants and VLDL remnants) (Warren, 2005). Thus, the reduction in fenestration diameter with feeding might contribute to the postprandial increase in circulating lipoproteins such as chylomicron remnants (Yu, 2001). Fasting for 24 hours in mice leads to an improvement in the clearance of chylomicron remnants (Martins, 2002). A possible mechanism is the increase in fenestration diameter associated with fasting seen in this study. Also there is increased production and secretion of VLDLs in fasting probably in response to the near cessation of chylomicron production (Sokolovic, 2010). An increase in fenestration diameter could facilitate the increased secretion of VLDL to the blood.

Results of our study also showed that liver weight loss was fairly evenly distributed across all the lobes of the liver and was not restricted to any one lobe in particular. Consistent with previous findings (Rothacker, 1988), kidney weight relative to body weight remained constant in both the fed and fasted rats, whereas liver weight decreased relative to body weight after the fast. Liver weight loss in fasting is mainly due to a combination of carbohydrate (glycogen) and water loss from the liver during fasting, and a less prominent loss of protein content. The carbohydrate loss results in a metabolic shift from glycogen and free fatty acids to protein and free fatty acids as a source of energy (Rothacker, 1988). Such a metabolic shift could explain the significant decrease in serum triglycerides we observed in the fasted rats.

In conclusion, nutritional state influences the diameter and frequency of fenestrations in the LSEC. This confirms that fenestrations are indeed dynamic structures that are influenced by physiological factors. Furthermore, the observation provides an additional mechanism for the effects of nutritional state on circulating large lipoproteins.

Chapter 4:

Acetaminophen Toxicity and the Liver Sinusoids of Fed and Fasted F344 Rats

4.1 Introduction

Paracetamol (also known as acetaminophen, N-acetyl-p-aminophenol, or APAP) is the most widely used over the counter drug in the world. It is involved in many accidental and deliberate self-poisonings that require hospitalisation, and is the leading cause of acute fulminant liver failure in the western world (Jaeschke, 2012b). At therapeutic doses, APAP is primarily metabolised via the sulfation and glucuronidation pathways to non-toxic metabolites. A small percentage of APAP is metabolised via the CYP450 pathway (mainly CYP2E1) (Hinson, 2010) to the very reactive electrophile and oxidant *N*-acetyl-*p*-benzoquinone imine (NAPQI), that is then detoxified by glutathione (γ-L-glutamyl-L-cysteinylglycine or GSH; fig 4.1). After larger doses of APAP, the non-toxic metabolic pathways become overwhelmed, and more APAP is converted to NAPQI. As hepatic GSH stores deplete and NAPQI continues to be produced it can no longer be detoxified. It begins to react with cellular components and form protein adducts, a process that can eventually lead to confluent hemorrhagic hepatic necrosis, and progress to fulminant liver failure (Jaeschke, 2012a).

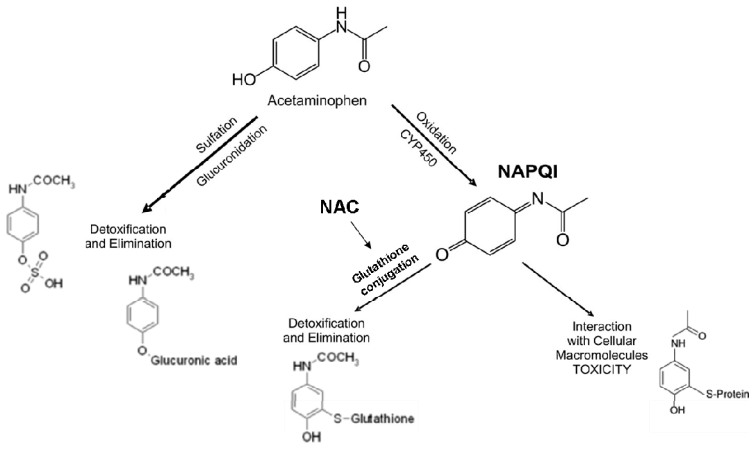

Figure 4.1 *Pathways of APAP metabolism. NAPQI = N-acetyl-p-benzoquinone imine, NAC = N-acetylcysteine.*

Toxicity from APAP metabolism is exacerbated if GSH stores and anti-oxidant capacity are reduced before dosage, such as during fasting (Pessayre, 1979, Pessayre, 1980, Price, 1987, Walker, 1982, Whitcomb, 1994). Covalent binding of APAP metabolites to liver proteins is greater and develops more rapidly in fasted animals because the amount of GSH in hepatocytes is about 50 % lower than the fed state. Fasting does not change CYP450 content or microsomal monooxygenase activity thus increased toxicity is primarily a result of the reduced ability of the fasted liver to deactivate toxic metabolites of APAP rather than a greater production of these metabolites (Walker, 1982). There is also a decreased capacity for non toxic glucuronidation pathways in fasting (approximately 60 % of that of fed animals) at least partially due to the reduced availability of glucose for conversion to glucuronic acid (Price, 1987). In addition, more lipid peroxidation occurs in fasted animals in conjunction with increased protein binding of toxic APAP metabolites (Wendel, 1979). Fasting may also potentiate APAP toxicity through the actions of glucagon which activates receptors coupled to cyclic AMP causing a positive sensitivity modulation to calcium (Saville, 1988). GSH depletion in APAP toxicity is linked with increased cytosolic calcium levels as calcium is released from intracellular compartments such as ER and mitochondria as the cell becomes increasingly damaged by toxic metabolites. Increased cytosolic calcium concentration alters cell function to promote toxicity by activating enzymes such as phospholipases (that damage membranes), proteases (that break down proteins), endonucleases (responsible for DNA and chromatin fragmentation), and ATPases (that hasten the depletion of ATP) (Kumar, 2009). Increased calcium sensitivity in the cells of fasted animals during APAP toxicity further increases the activation of these enzymes, promoting even more cellular damage than in fed animals (Saville, 1988). An increase in intracellular

calcium is also associated with fenestration contraction and could be a contributing factor to LSEC defenestration in APAP toxicity. Hemorrhage and congestion of RBCs in the liver, a sign of endothelial injury, is also increased in fasted animals resulting in enlargement of livers to a greater extent than in fed animals (Walker, 1982). This suggests that LSECs sustain greater levels of injury in animals fasted prior to APAP overdose.

The main current therapeutic drug for APAP toxicity is *N*-acetylcysteine (NAC) which is a cysteine prodrug that can stimulate GSH synthesis (refer to fig 4.1), and has antioxidant properties (Cacciatore, 2010). It also has antithrombotic properties primarily via limiting platelet aggregation (Chen, 2011). If administered early enough after overdose, NAC can reverse some of the liver damage preventing liver failure and death. However, in some less severe cases the patient survives the initial insult (which usually lasts for 3 or 4 days after the overdose in humans and 1 or 2 days in rats and mice) regeneration of the liver begins and the necrosis and congestion resolve naturally (Rowden, 2005). In addition to hepatotoxicity, nephrotoxicity and tubular necrosis may occur in about 1 - 2 % of human patients presenting after APAP overdose, although rats may be more susceptible (Mazer, 2008, McMurtry, 1978, Newton, 1982).

The earliest histopathologic changes found in APAP toxicity prior to any signs of necrosis are hydropic vacuolisation of hepatocytes along the sinusoidal margins in centrilobular zones, followed by a mild steatosis of centrilobular hepatocytes and centrilobular congestion (Walker, 1980). As oxidative stress increases, alterations in calcium homeostasis disrupt mitochondria stopping the production of ATP and

promoting hepatocyte degeneration and necrosis (Hinson, 2010). Centrilobular hepatocytes are most vulnerable to APAP toxicity because they contain much higher levels of CYP2E1 (and CYP450s) than periportal hepatocytes and thus produce much more NAPQI (Gooding, 1978). In addition, hepatocytes in centrilobular zones contain much less GSH than periportal hepatocytes, lowering their ability to detoxify NAPQI (Smith, 1979). Oncotic necrosis is the primary mechanism of hepatocyte death in APAP toxicity, with relatively mild amounts of apoptosis occurring (Gujral, 2002, Jaeschke, 2002). Eventually necrosis becomes confluent in centrilobular zones and is accompanied by an inflammatory response. In severe cases the necrosis spreads to midzonal cells, and periportal hepatocytes develop hydropic vacuoles (Dixon, 1971). The pattern of toxicity and necrosis in APAP overdose is variable across the liver and not every central zone is equally affected (Walker, 1985).

The severity of toxicity in mice can be greatly decreased by pre-treatment with heparin suggesting that congestion has an important role in increasing hepatotoxicity, and that damage to the liver can be significantly reduced without reducing APAP bioactivation to NAPQI (Ganey, 2007). Studies at an ultrastructural (Lim, 1995, Walker, 1983) and in vivo microscopic level (Ito, 2003, McCuskey, 2006) reveal that there is microvascular injury before any histopathological changes or rise in serum aminotransaminase levels that are indicative of hepatocyte injury (Hessel, 1996), however the exact mechanism by which APAP is toxic to the endothelium is still not clear. Initial signs of injury to LSECs in APAP overdose in mice can occur as early as 30 minutes into toxicity and include swelling of the LSEC cytoplasm and reduced endocytosis mediated by the scavenger receptor (Ito, 2003). Also development of gaps (0.5 - 3 μm in diameter) in the LSEC cytoplasm early on facilitate the movement

RBCs into the SoD resulting in congestion by collapsing the sinusoid lumen and reducing blood flow (McCuskey, 2008, Walker, 1983). The congestion becomes increasingly aggravated as platelets enter the SoD and fibrin is deposited, resulting in secondary ischemic damage (Walker, 1985). Dilation of sinusoids in centrilobular regions becomes prominent by 8 hours after APAP overdose in rats, and is thought to be contributed to increased pressure in the sinusoids that are directly adjacent to congested sinusoids affected by hemostasis and congestion (Lim, 1995).

Free radicals released as a result of oxidative stress (such as superoxide and nitric oxide) are injurious to LSEC (Deaciuc, 1999) and mitochondrial dysfunction and peroxynitrite formation in LSECs may be a critical factor for microvascular injury in APAP overdose (Knight, 2004). In vitro studies have shown that APAP is directly more toxic to LSECs than hepatocytes, and also that LSECs are capable of metabolising APAP and may produce small amounts of NAPQI (DeLeve, 1997, Steinberg, 1987). Additionally, LSECs are directly exposed to NAPQI released from both viable and necrotic or lysed hepatocytes and concentrated in the SoD (DeLeve, 2007b). LSECs contain GSH stores, but these are much less concentrated than hepatocytes and thus may render LSECs more vulnerable to APAP toxicity (DeLeve, 1998).

Although there is microvascular damage and hemorrhage in APAP toxicity, ultrastructural studies (by Walker et al) in the 1980s found that the main sinusoid structure appears mostly to be conserved throughout the course of toxicity. Intercellular junctions between LSECs remain intact, and LSECs are anchored to hepatocyte and Ito cell processes in areas of SoD enlargement and sinusoid lumen

collapse (Walker, 1983). At least some LSECs are preserved in areas of hepatocyte necrosis as they were observed in a fenestrated phenotype overlying necrotic hepatocytes on scanning electron microscopy (Walker, 1983). It is possible that initial injury to LSECs in APAP-induced hepatotoxicity is repaired during the process of toxicity (DeLeve, 2007a) and that preservation of LSECs and their place in the sinusoid by attachments to Ito cells and degenerate hepatocytes is pivotal in enabling recovery from congestion and reducing ischemic insult later in toxicity (Walker, 1983). Recent studies have found that the ability of the liver parenchyma to regenerate and recover from APAP-induced toxicity is highly dependent on the ability of the liver to first repair its microvasculature and to attenuate LSEC dysfunction (Donahower, 2010, Kato, 2011, Papastefanou, 2007). Damage to endothelium (assessed by measuring serum hyaluronic acid levels) in human patients with severe hepatotoxicity from APAP overdose is greater in those that do not recover than the survivors (Williams, 2003) suggesting the extent of damage to LSEC in APAP toxicity influences prognosis.

The purpose of this chapter was to observe the various features of APAP toxicity, comparing the hepatotoxicity in rats fed to rats fasted prior to APAP dosage. We focused on observing morphological changes to LSECs during the course of hepatotoxicity to determine their viability in both necrotic and non-necrotic areas. We particularly aimed to provide further information on what happens to the LSEC at an ultrastructural level in necrotic zones as there is currently little information available.

4.2 Materials and Methods

4.2.1 Animals and APAP dosage

The rats used in experiments were male Fisher 344 rats, approximately 3 months old weighing 300 - 400 g. Rats were housed in groups of 3 on a 12 hour light and dark cycle, temperature at 25 ºC. APAP was dissolved in warm distilled water, and administered to rats via gavage at a dose of 1000 mg/kg.

Six rats were allowed free access to standard chow and water until food was removed at the time of APAP gavage in order to maximise toxicity by preventing replenishment of GSH stores as APAP was being metabolised (fig 4.2). Ten rats were fasted from 24 hours prior to APAP gavage (1000 mg/kg) to increase toxicity by depleting GSH stores prior to APAP dose (fig 4.2). All rats were allowed free access to water at all times. An additional 8 rats used as controls (the same rats as used for the study in Chapter 3) were ad libitum fed or fasted but were not given APAP, and were analysed in the same way as rats administered APAP (fig 4.2). A more extensive blood and histological analysis was carried out on the fasted rats than the fed.

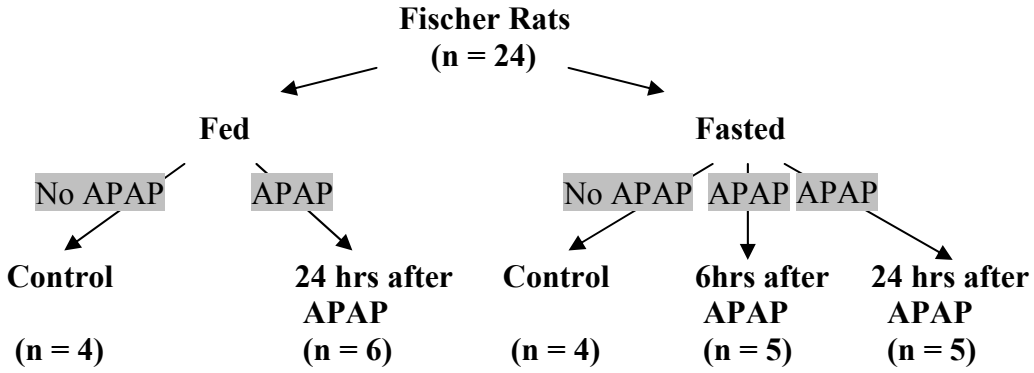

Figure 4.2 *Experimental treatment groups: Rats were fed or fasted until APAP gavage, then culled at either 6 or 24 hrs after APAP. Controls were not given APAP.*

4.2.2 Surgery and specimen preparation fed groups

Twenty-four hours after APAP gavage, rats were placed under general anaesthesia and a laparotomy and perfusion performed as described in Chapter 2 (general methods). Briefly, blood was taken from the IVC for liver function tests measuring serum alanine aminotransferase (ALT), aspartate aminotransferase (AST), and total bilirubin. The liver was then briefly perfused with PBS to exsanguinate the sinusoids. The right inferior lobe was tied off with a suture, cut out, and immersed in fixative for histology before the remainder of the liver was perfused with fixative for electron microscopy. After the liver sufficiently hardened it was removed and prepared for scanning and transmission electron microscopy as described in Chapter 2.

4.2.3 Surgery and specimen preparation fasted groups

Five rats were placed under general anaesthesia 6 hours after APAP (6 hour rats), and 5 rats at 24 hours after APAP gavage (24 hour rats), and 4 control rats were fasted for 48 hours before surgery but not administered APAP. Twenty four hours was chosen because this is a time reported in studies at which aminotransferase levels and

necrosis is high in rats (Papastefanou et al., 2007), and the 6 hour time point was chosen to examine LSEC before hepatocyte necrosis was expected to occur. Body weights were recorded at the beginning of the fast and after anaesthesia. Surgery and perfusion were carried out as previously described in Chapter 2. Briefly, a laparotomy was performed and approximately 3 ml of blood was taken from the IVC to be analysed for ALT, AST, total bilirubin, total cholesterol, triglycerides, creatinine, urea, and hematocrit. The portal vein was cannulated, and 10 ml of PBS was perfused to exsanguinate the liver. Immediately after, approximately 40 ml of 4 % paraformaldehyde in PBS pH 7.4 was perfused through the liver. When the perfusion ended, the liver was removed and weighed. A sample from each lobe was prepared for histological analysis, and another sample was placed in EM fixative where it was sectioned into approximately 10 to 20 blocks (approx 1 mm^3) with a scalpel and prepared for scanning and transmission electron microscopy analysis as previously described in Chapter 2. The left kidney in the fasted groups was also removed immediately after surgery and incubated in 4 % paraformaldehyde (with 1 % sucrose in PBS) overnight then processed for histology (in the same way as described for liver processing).

4.2.4 Histology fed and fasted groups

Livers were prepared and sectioned for histology as described in Chapter 2. Sections from the right lobe were stained with Hematoxylin and Eosin (see Appendix 2A for protocol) to observe any necrosis, hemorrhage, and congestion. In addition, sections were taken from four liver lobes (median, right superior, left lateral, caudate) and stained with Hematoxylin and Eosin to observe any intra and inter lobular variability in toxicity in the 6 and 24 hour fasted groups. Sections were graded on the average

amount of necrosis across the section. 0 = no necrosis or focal necrosis of only a few single cells, + = minor levels of centrilobular confluent necrosis, ++ = major levels of centrilobular confluent necrosis with spreading of necrosis to midzonal cells, +++ = severe levels of centrilobular confluent necrosis with prominent bridging necrosis across midzones and occasionally some necrotic periportal cells.

A section was cut and stained with Periodic Acid Schiff's (PAS, see Appendix 2B for protocol) to observe glycogen distribution, and another section cut and stained with Sirius Red (see Appendix 2C for protocol) to observe any increase in sinusoidal collagen or fibrosis. Sections at a magnification of 100 × were graded blinded for degrees of collagen in sinusoids. 0 = no increase compared to controls, + = mild increase, ++ = moderate increase, +++ = severe increase. Sections from the kidney were also cut at 4 μm and stained with Hematoxylin and Eosin, PAS, and Sirius Red (staining protocols are described in Appendix 2) to observe for any pathology such as tubular necrosis.

4.2.5 Electron microscopy fed and fasted groups

Approximately 20 pieces sampled from all liver lobes were cut into blocks 1 mm^3, incubated in EM fixative, and processed for scanning and transmission electron microscopy as described in Chapter 2. If not enough blocks were adequately fixed from the necrotic zones of a particular rat (as the fixative did not always penetrate well enough through congested and necrotic areas of the liver during perfusion), extra blocks were cut from paraffin embedded livers from specific areas targeted after observing H & E stained sections and reprocessed for viewing on TEM (as described in Chapter 2). At least 5 blocks per liver on SEM, and 2 - 3 blocks on TEM were

observed to analyse the liver cells at an ultrastructural level, particularly looking at LSEC morphology in areas of low to severe toxicity. Measurements were taken using Image J of control and APAP rats to estimate the size of the sinusoid lumen, SoD, fenestrations, gaps, and LSEC cytoplasm in different areas of the liver. The intralobular toxicity was variable, thus average fenestration diameter and porosity could not be analysed to accurately determine whether there were any statistically significant differences between control and APAP-treated rats.

4.2.5 Statistical analysis

Data from blood analysis comparing control and APAP rats was analysed using Microsoft Excel. An F-test was performed between control and APAP groups to measure the variance. The student's t-test was then used (according to whether the groups displayed equal variance or not) to determine any significant differences. A statistically significant difference was defined as $p < 0.05$.

4.3 Results: Fed rats at 24 hours after APAP

4.3.1 Macroscopic Observations

Twenty-four hours after APAP gavage rats were observed to be quiet and sleepy. During laparotomy particularly in the severely damaged livers, there was obvious variability in each lobe as to the extent of damage sustained.

4.3.2 Blood results

Total bilirubin levels were significantly raised in APAP rats. Serum aminotransferase data was quite variable in the APAP rats and as such there were no statistically significant differences, however, there was a trend towards increased ALT and AST (table 4.1). Only 1 rat out of 5 had a sharp increase in serum ALT with 2 other rats mildly increased (from 1.3 to 19 × higher than normal), and 4 out of 5 rats had increased AST from mild to severe (from 1.5 to 9 × the normal average). These results suggest some form of hepatocellular injury occurred in at least 4 of 5 APAP-treated rats. We did not obtain blood from one rat that was expected to have high range LFTs (as histology showed severe hepatotoxicity).

Table 4.1 *Mean and individual serum aminotransferase levels, total bilirubin, and weight loss at 24 hrs after APAP in fed rats. Mean fed control values are displayed for comparison.*

Rat	ALT (U/L)	AST (U/L)	TBil (µmol/L)	% Weight loss
1	48	96	3	4.9
2	38	86	6	4.4
3	52	104	4	3.8
4	16	32	1	4.8
5	702	459	3	4.9
6	no data	no data	no data	no data
Mean±SD	**171.2±297**	**155.4±172**	**3.4±1.8***	**4.6±0.5**
Mean±SD ctrls	**36.8±3**	**52.4±4**	**1±0**	**-**

* = significant difference to control rats, p=0.0001

4.3.3 Histology

Four of 6 APAP treated rats showed only some mild levels of damage to the liver 24 hours after APAP gavage. There were vacuoles in centrilobular hepatocytes and presence of inflammatory cells particularly in centrilobular zones, with some focal necrosis of centrilobular hepatocytes (fig 4.3 A). These rats had LFTs in the lower range, corresponding to a lower degree of hepatic damage. The remaining 2 of 6 rats (one with high range LFTs, and the other where no blood sample was collected) had more severe hepatotoxicity displaying confluent hemorrhagic necrosis of centrilobular zones (and midzones) with increased numbers of inflammatory cells in these areas (fig 4.3 B). Sinusoids that lay adjacent to necrotic regions were dilated and hepatocytes were affected by vacuolar and fatty degeneration.

PAS staining revealed glycogen was mostly depleted in 4 of the 6 APAP rats, but was present in the periportal zones in 2 of 6 rats (one with severe centrilobular necrosis and one without) (fig 4.3 C). Two out of 6 rats had increased collagen in the central venules of necrotic areas (fig 4.3 D and also refer to the electron micrograph fig 4.6 A), and displayed a mild increase in sinusoidal collagen in necrotic zones. Some of the increased collagen staining around necrotic hepatocytes may have also been related to the reticular framework collapsing (fig 4.4 D-F).

Table 4.2 *Grade of necrosis, sinusoidal collagen, and glycogen distribution 24 hrs after APAP in fed rats.*

Rat	Necrosis	Sinusoidal Collagen	Glycogen
1	0	0	Deplete
2	0	0	Deplete
3	0	0	Deplete
4	0	0	PP
5	++	+	PP
6	+++	+	Deplete

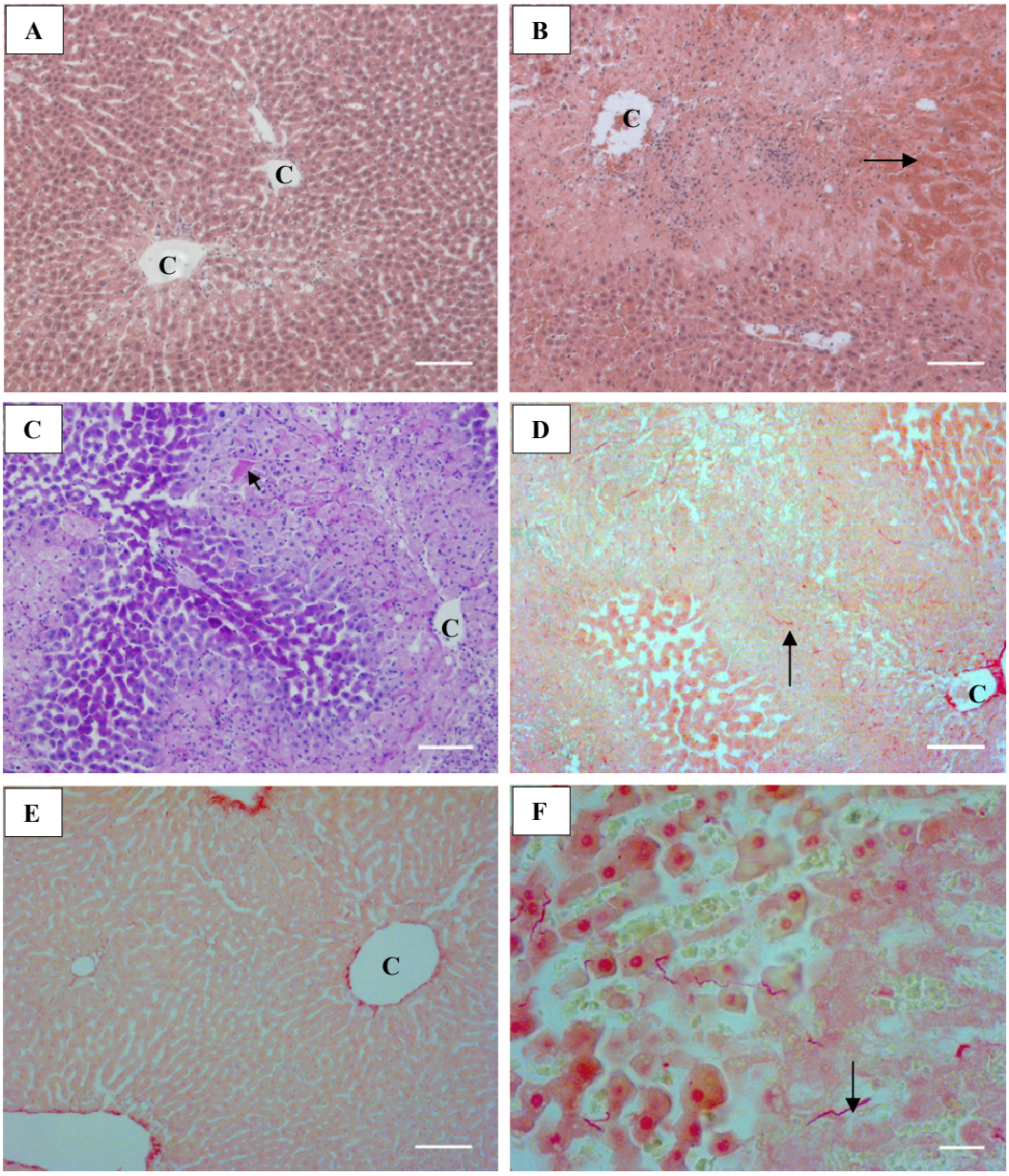

Figure 4.3 *H&E, PAS, and Sirius Red stained sections from fed APAP-treated rats*
A) H&E stain of an area of mild toxicity. There is vacuolisation of CL hepatocytes, the PP area is histologically normal. C = central venule, bar = 100 µm.
B) H&E stain of an area of severe toxicity. There is a zonal pattern of damage with necrosis, congestion, and hemorrhage (arrow) primarily in CL and ML zones. Adjacent PP zones are mildly affected with toxicity including sinusoidal dilation and vacuolisation of hepatocytes. P = portal venule, bar = 100 µm.
C) PAS stain of an area of CL necrosis with glycogen present in PP hepatocytes. The collapsed reticular fibre network around necrotic/degenerate hepatocytes stained pink (indicated by arrow). Bar = 100 µm.
D) Sirius Red stain of an area of CL necrosis with some thick collagen fibres (see arrow). Bar = 100 µm.
E) Sirius Red stain of an area not affected by necrosis in a low toxicity rat. There is no increase in sinusoidal collagen. Bar = 100 µm. F) Sirius Red stain on the border of a necrotic and viable zone. There are some thick collagen fibres (see arrow) and congested RBCs stained brown. Bar = 20 µm.

4.3.4 Electron microscopy

In the rat with the most severe hepatotoxicity, LSECs were often dead and surrounded by fibrin in the worst affected centrilobular zones (fig 4.4 B). As observed in histology, large areas of coagulative hepatocyte necrosis were present with major congestion of sinusoids and leakage of RBCs into the SoD through gaps in the injured LSEC cytoplasm (fig 4.4 A). In periportal zones LSECs were viable although many platelets were observed in the sinusoid lumens.

In the rat with less severe centrilobular hemorrhagic necrosis, no dead LSECs were observed in areas of hepatocyte necrosis in the specimens analysed. The LSECs were closely associated with HSCs, and there was increased extracellular matrix deposition between these cell types (fig 4.5 B) particularly where the once underlying hepatocytes had died or retracted from the sinusoidal cells. It also appeared that there were increased numbers of HSCs that may have migrated to or proliferated in the necrotic regions (fig 4.5 C). HSC processes seemed to increase their surface area so that they were maximally in contact with the LSECs, often completely covering LSEC cytoplasms or nuclear regions in places where there were no underlying hepatocytes (fig 4.5 - 4.7). Both LSECs and HSCs formed attachments to necrotic and degenerating hepatocytes, tethering the sinusoids and parenchyma together and maintaining some organisation of the cells. Sinusoid lumens were significantly reduced in size (by at least 50 % compared to controls) or completely collapsed, although LSEC cytoplasms still contained some fenestrations (fig 4.5 - 4.7). Again, there was hemorrhage of RBCs into the SoD although fibrin deposition in necrotic areas and platelets (in sinusoid lumens and the SoD) were less common. Inflammatory cells were most concentrated in necrotic areas (fig 4.8).

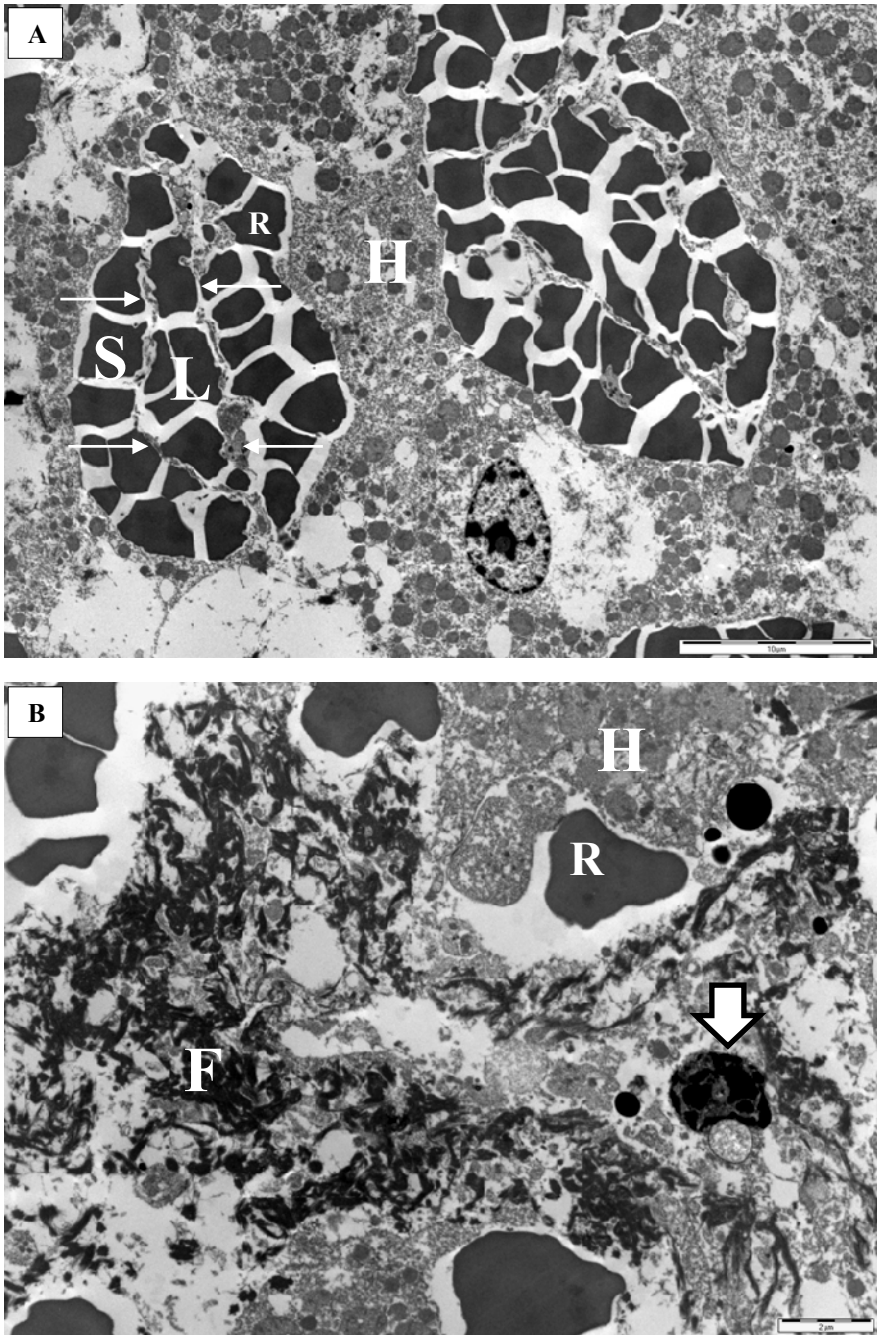

Figure 4.4 *Transmission electron micrographs of specimens reprocessed from paraffin from the fed APAP-treated rat with the most severe toxicity*
A) Two congested sinusoids with collapsing lumens (L) and hemorrhage of RBCs into the SoD (S). Arrows point to the outline of a degenerating LSEC, marking the border of the lumen and SoD. The hepatocytes (H) are affected by oncosis. The RBC marked R is in the SoD Bar = 10 μm.
B) A dead LSEC (arrow points to the nucleus) is surrounded by a dense network of fibrin (F; dark fibrous material) and RBCs (R). The surrounding hepatocytes (H) are dead (bar = 2 μm).

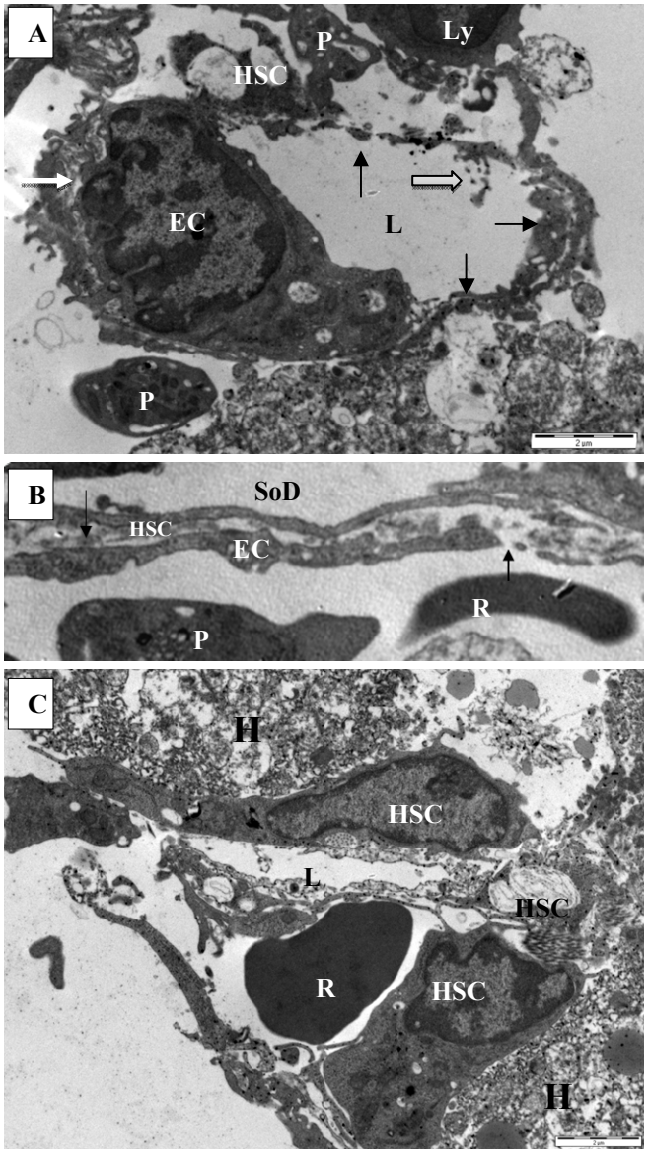

Figure 4.5 *Transmission electron micrographs from a fed APAP-treated rat with mid-range toxicity. Viable LSECs and HSCs are surrounded by necrotic hepatocytes.*
A) In this micrograph, a viable LSEC (EC marks the nucleus and black arrows mark the cytoplasm) is strongly tethered to a HSC surrounded by, and attached to, necrotic hepatocytes. A platelet (P) and lymphocyte (Ly) are in the SoD and the sinusoid lumen (L) is collapsing. A white arrow points to increased ECM between the LSEC and HSC, and a bold arrow indicates what may be an obliquely sectioned sieve plate in the LSEC cytoplasm (bar = 2 μm).
B) A section of LSEC cytoplasm in a CL necrotic zone. The long arrow points to basement membrane deposition between LSEC and HSC processes. The small arrow points to fenestrations. A RBC (R) and platelet (P) are in the sinusoid lumen.
C) In general there appears to be increased numbers of HSCs in necrotic zones and in this micrograph there are two HSC nuclei adjacent to the LSEC cytoplasm, and other processes possibly projecting from additional HSCs to the LSEC. An RBC (R) is outside of the collapsed sinusoid lumen (L). H = necrotic hepatocyte. Bar = 2 μm. The small black dots on the surface of cells and other structures in the micrograph are an artefact, probably of lead staining where globular precipitates form on reaction with carbon dioxide.

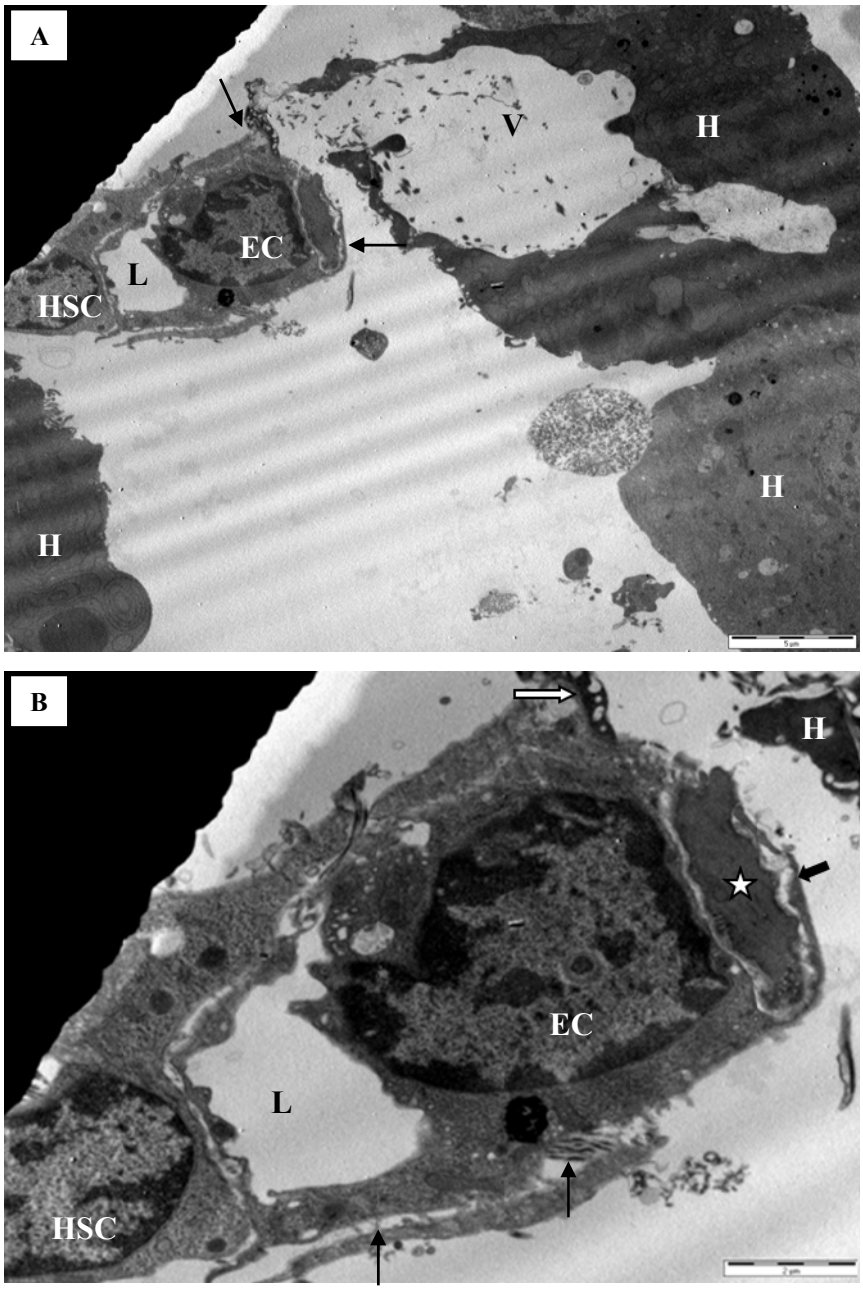

Figure 4.6 *Transmission electron micrograph from a fed APAP-treated rat with mid-range toxicity. Tethering of a HSC, necrotic hepatocyte, and LSEC.*
A) The sinusoid in this micrograph is made of a tightly associated LSEC (EC) and HSC complex with a severely shrunken lumen. It is almost floating free of a degenerating hepatocyte (H) that contains a giant vacuole (V), however there are some points of attachment (marked by arrows). Bar = 5 μm.
B) A close up of the sinusoid in 'A' shows an increased deposition of collagen holding the LSEC and HSC together (arrows) and an LSEC process (bold black arrow) is wrapped around what appears to be part of a degenerating hepatocyte, or else another HSC (star). There is also an area where the hepatocyte appears to be directly joined to the HSC (white arrow). The sinusoid lumen (L) is severely decreased in size. Bar = 2 μm.

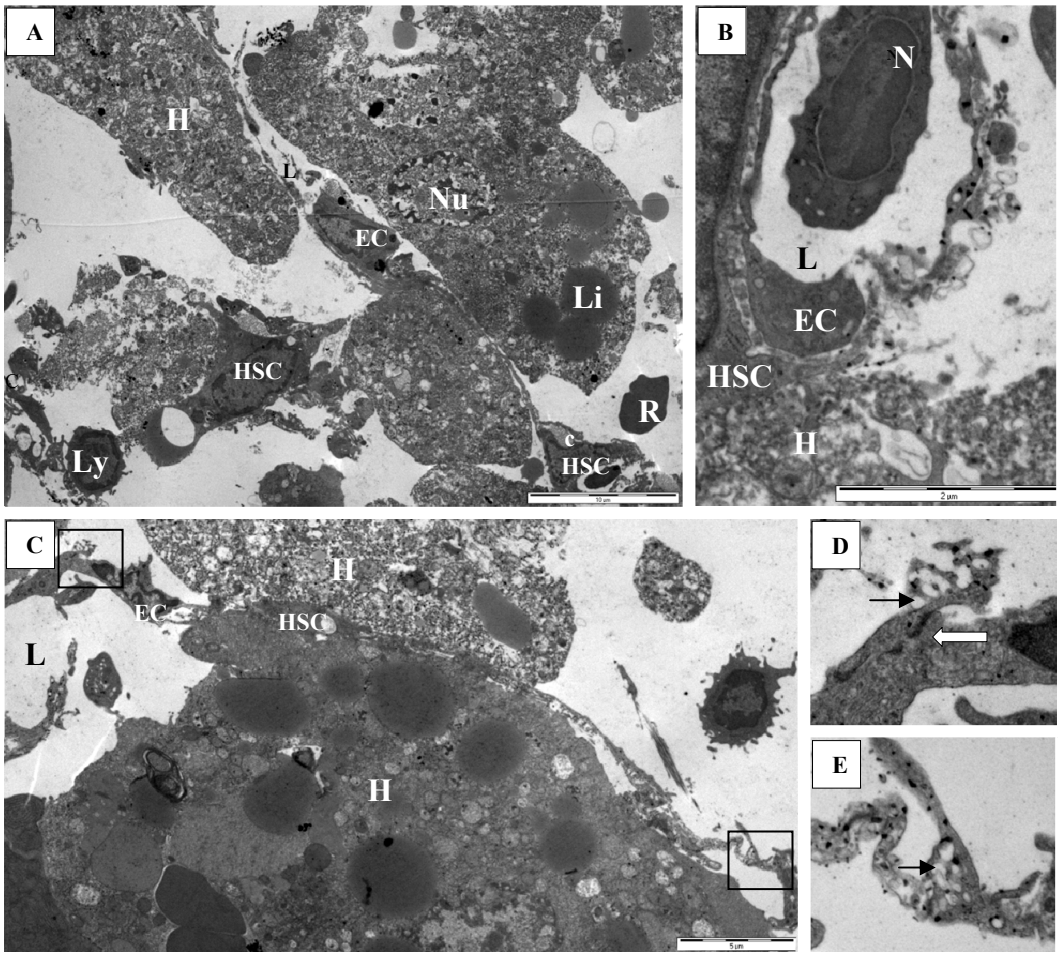

Figure 4.7 *Transmission electron micrographs of sinusoids in CL necrotic zones from fed APAP-treated rats with moderate toxicity. As in figure 4.5 the small black particles in these micrographs are an artefact of staining.*
A) Viable LSECs (EC) and HSCs amongst necrotic hepatocytes with karyolytic nuclei (Nu) and fatty degeneration (Li = lipid). A sinusoid lumen (L) is squashed between degenerating hepatocytes. A collagen bundle (c) is associated with a HSC (bottom left corner), and a lymphocyte (Ly) and RBC (R) are in the spaces between hepatocytes. The boxed area is shown enlarged in (B) (bar = 5 μm).
B) There is basement membrane between the LSEC (arrow) and HSC, and the HSC is adhered to a necrotic hepatocyte. There is a neutrophil (N) in the collapsing sinusoid lumen (L; bar = 2 μm).
C) On the edge of a necrotic zone LSEC and HSC processes stretch between a dead hepatocyte and another with fatty degeneration and RBCs (R) in its cytoplasm. The LSECs display an unusual morphology with wrinkled cytoplasms, as is seen more clearly in the enlarged micrographs of the boxed areas in (D) and (E) (bar = 5 μm).
D) Two LSEC are adhered together via intercellular junctions (bold arrow), one LSEC process contains a sieve plate obliquely sectioned (top arrow).
E) Another obliquely sectioned sieve plate on an LSEC cytoplasm (arrow).

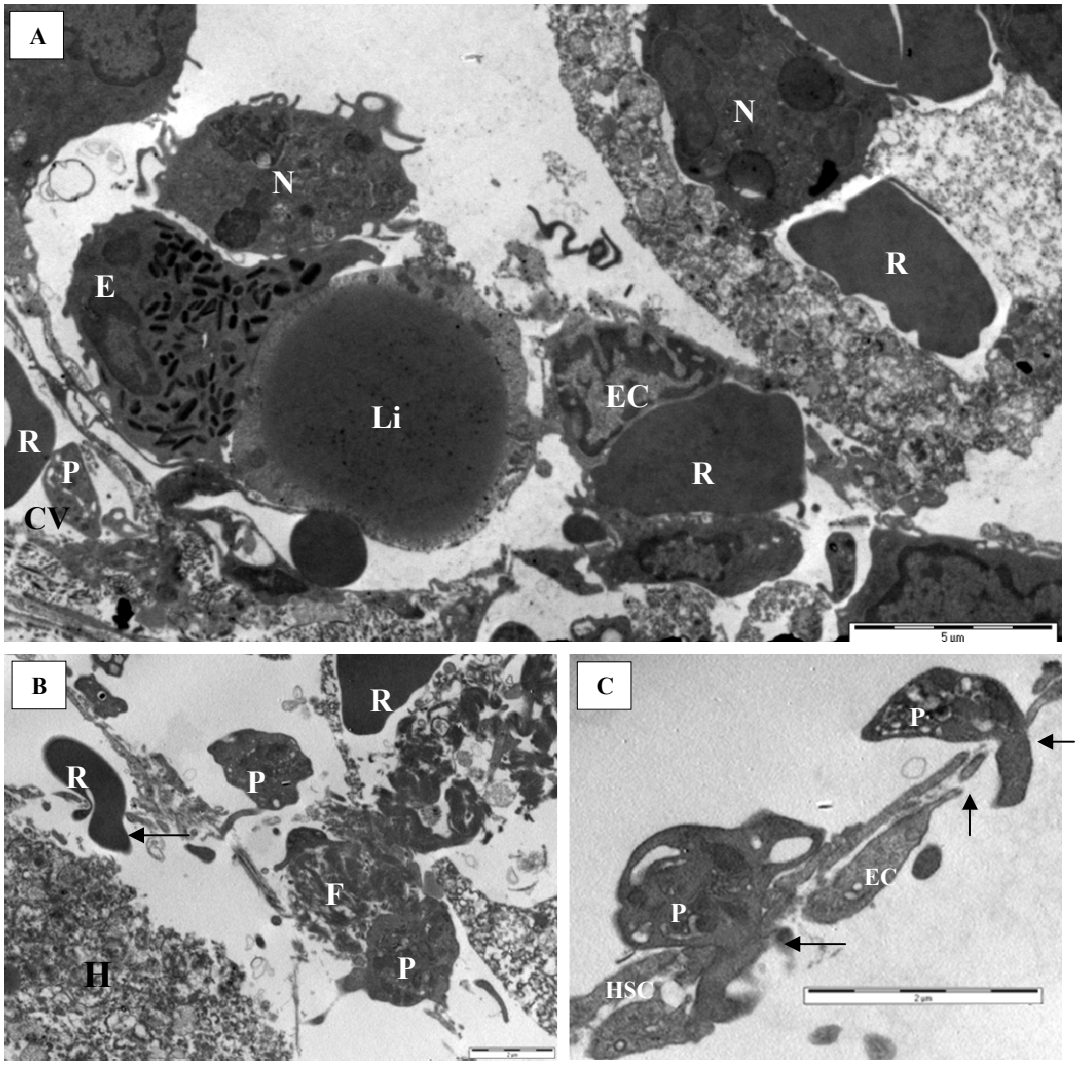

Figure 4.8 *Micrographs of CL necrotic zones from fed APAP-treated rats*
A) A micrograph of a CL necrotic area. There is increased collagen deposition around the central venule (CV), part of which lies in the bottom left hand corner. Adjacent to the central venule there is an eosinophil (E) next to an unknown cell-type that has endocytosed a large amount of lipid (Li), or is possibly a dying hepatocyte with fatty degeneration. A neutrophil and RBCs (R) are in a necrotic hepatocyte (H) in the top right hand corner. There appears to be a viable LSEC (EC) perikaryon in between the degenerate hepatocytes (bar = 5 μm).
B) This micrograph displays a region of necrotic hepatocytes associated with fibrin (F) and platelets (P). The sinusoid structure is still somewhat intact and a RBC is crossing through a gap in an LSEC (arrow) (bar = 2 μm).
C) In this micrograph, two platelets are travelling to the SoD through fenestrations (arrows) in an LSEC (EC) and spaces between HSC processes (bar = 2 μm).

In areas on the border of necrotic zones, hepatocytes were atrophied and mostly devoid of microvilli resulting in enlargement of the SoD and spaces between hepatocytes (sinusoid dilation) (fig 4.9 A). LSECs and HSCs stayed closely associated but were often separate from hepatocytes apart from small areas of contact between the cells (fig 4.9 B-D). Sinusoid lumens were mildly reduced in size. There were some gaps in LSECs that ranged up to approximately 3 μm in diameter and there were RBCs in the hepatocytes, providing evidence of hemorrhage in these areas which likely contributed to the sinusoid dilation.

Often centrilobular zones of rats with low serum aminotransferase levels did not appear to be damaged. LSEC were normal and fenestrated without any gaps, and hepatocytes normal with abundant microvilli (fig 4.9 E). In areas of the liver with mild toxicity where hepatocytes contained vacuoles and were mildly steatotic, some LSECs were defenestrated (fig 4.9 F), some LSECs contained gaps, some LSECs were activated with some swollen areas containing lysosomes and many pinocytic vesicles (fig 4.9 G), and some LSECs displayed a combination of all these traits. Intercellular junctions between LSECs were always preserved and there were no gaps between cells. The SoD (approx 0.3 – 1 μm) and sinusoid lumen (approx 7 – 10 μm) were of a similar size to that measured in controls.

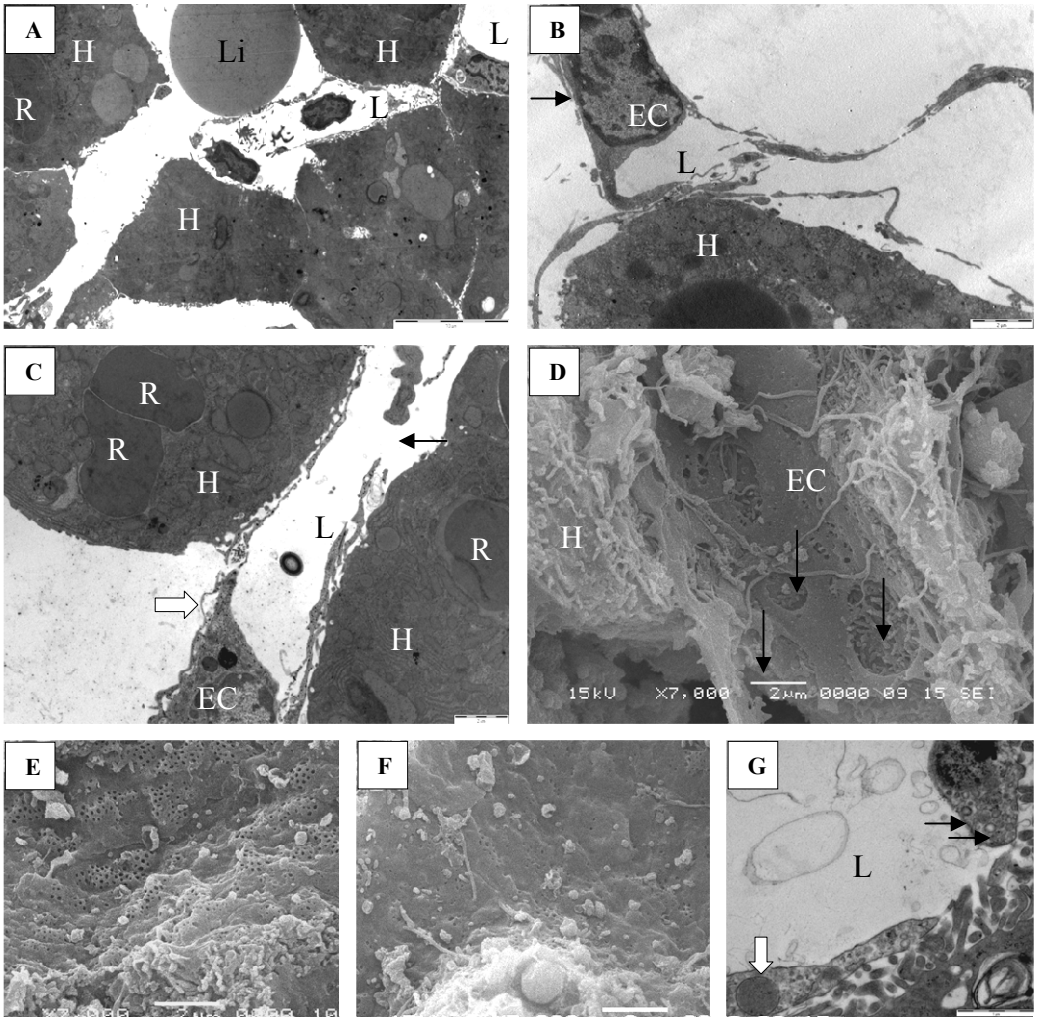

Figure 4.9 *Electron micrographs of sinusoids of fed APAP-treated rats with low to moderate toxicity*
A) This micrograph shows an area of sinusoid dilation on the edge of a CL necrotic zone. The hepatocytes are degenerating and atrophied with only some microvilli remaining. The sinusoid lumen (L) is decreased in size. A large lipid droplet (Li) lies in the space between the hepatocytes (H) (bar = 10 µm).
B) A close view of an LSEC nucleus and cytoplasm where surrounding hepatocytes are degenerating. The LSEC cytoplasm is thin and contains fenestrations however the sinusoid lumen (L) is squashed and misshapen. HSC processes (arrow) surround the LSEC (bar = 2 µm).
C) TEM and D) SEM representation of an area of hepatocyte (H) degeneration and sinusoid dilation. A HSC process (fig C bold arrow) wraps around the LSEC where there is no underlying hepatocyte. There are gaps in the LSECs (arrows) and RBCs (R) in hepatocyte vacuoles can be seen in micrograph (C) (bar = 2 µm).
E) SEM of a normally fenestrated LSEC from a fed APAP-treated rat (bar = 2 µm).
F) SEM of a defenestrated LSEC from a fed APAP-treated rat (bar = 2 µm).
G) TEM of an LSEC swollen with lysosomes (bold arrow) and pinocytic vesicles (arrows) in an area of mild toxicity. Microvilli are still present in the underlying hepatocyte (bar = 1 µm).

4.4 Results: Fasted rats at 6 and 24 hours after APAP

4.4.1 Macroscopic Observations

At 6 and 24 hours after APAP gavage rats were quiet and sleepy. On observation of the liver during laparotomy there was inter and intra lobular variability in hepatotoxicity.

4.4.2 Blood Results comparing 6 to 24 hours after APAP

Total bilirubin increased significantly from normal levels at 6 hours to elevated levels at 24 hours suggesting liver function was deteriorating during this time. There was a trend towards an increase in ALT ($p = 0.055$) and AST ($p = 0.066$) from 6 to 24 hours post APAP, indicating that damage to the parenchyma was increasing (see table 4.3). Total cholesterol significantly decreased from 6 to 24 hours after APAP, however, triglyceride serum levels did not change. Creatinine and urea significantly increased from normal at 6 hours to mildly elevated by 24 hours (see table 4.4). Average liver weight increased significantly from 6 to 24 hours. Hematocrit did not significantly change from 6 to 24 hours, but the average was higher at 24 hours (see table 4.5).

4.4.3 Blood results comparing 24 hours after APAP to controls

At 24 hours after APAP, total bilirubin was significantly raised above normal, suggestive of reduced liver function. There was a trend towards an increase in ALT ($p = 0.0549$) and AST ($p = 0.0657$). Even though all of the rats had elevated ALT and AST the result was not significant, probably due to variability (see table 4.3). Total cholesterol was significantly lower than normal, although triglyceride levels were

similar. Creatinine and urea were raised, but only by a very mild amount (see table 4.4). Hematocrit was significantly higher in APAP-treated rats, and the average weight of the liver had increased approximately 40 % in size by 24 hours after APAP (see table 4.5).

Table 4.3 *Serum aminotransferase and total bilirubin raw data and mean from fasted APAP-treated rats. Mean ± SD fasted APAP-control rat data is included for comparison.*

Rat	ALT (U/L)		AST (U/L)		TBil (µmol/L)	
	6 hr	24 hr	6 hr	24 hr	6 hr	24 hr
1	46	1129	80	1124	1	2
2	50	124	100	143	1	2
3	33	220	60	209	1	1
4	45	4690	72	7053	1	3
5	51	4550	95	6513	1	2
Mean±SD	**45±7.2**	**2143±2296**	**81.4±16.4**	**3008±3473**	**1±0**	**2±0.7**[*†]
Mean±SD ctrls	**-**	**40±3.6**	**-**	**70.7±9.1**	**-**	**1±0**

*p<0.05 compared to 6 hour rats.
[†]p<0.05 compared to control rats.

Table 4.4 *Serum lipids and kidney function test raw data and mean from fasted APAP-treated rats. Mean ± SD of fasted APAP- control rats is included for comparison.*

Rat	Total cholesterol (µmol/L)		Triglycerides (µmol/L)		Urea (mmol/L)		Creatinine (µmol/L)	
	6 hr	24 hr	6 hr	24 hr	6 hr	24 hr	6 hr	24 hr
1	1.3	1.3	0.5	1.5	-	7.4	-	50
2	1.5	1.2	0.8	0.9	3.8	-	13	-
3	1.3	1.1	1.1	0.6	5.1	6.5	22	27
4	1.2	1.1	0.7	0.2	6.3	6.2	28	27
5	1.3	0.8	0.9	0.5	1.4	10.8	-	43
Mean ±SD	**1.3±0.1**	**1.1±0.2**[*†]	**0.8±0.2**	**0.7±0.5**	**4.2±2.1**	**7.7±2.1**[*†]	**21±7.5**	**36.8±11.6**[*†]
Mean ±SD ctrls	**-**	**1.5±0.1**	**-**	**0.4±0.1**	**-**	**4.6±0.3**	**-**	**24.3±1.5**

*p<0.05 compared to 6 hr rats.
[†]p<0.05 compared to control rats.

Table 4.5 *Hematocrit, liver weight, and weight loss raw data and mean from fasted APAP-treated rats. Mean ± SD of fasted APAP-control rats is included for comparison.*

Rat	Hematocrit %		Liver wet weight % body weight		% Weight loss from time of fast	
	6 hr	24 hr	6 hr	24 hr	6 hr	24 hr
1	58	73	2.9	4.9	10.4	13.7
2	59	63	3.4	4.9	5.9	15.6
3	63	65	3.3	3.4	8.3	12.4
4	56	61	4.5	4.0	5.6	11.8
5	62	50	2.7	4.1	7.4	11.3
Mean±SD	**59.5±2.7**	**62±8†**	**3.3±0.7**	**4.3±0.6*†**	**7.5±1.9**	**13±1.7*†**
Mean±SD ctrls	**-**	**52.7±2.1**	**-**	**2.5±0.2**	**-**	**7±1.6**

*p<0.05 compared to 6 hr rats.
†p<0.05 compared to control rats.

4.4.4 Histology

Six hours after APAP gavage, the liver appeared mostly to be histologically normal (fig 4.10 A). Infrequently there was centrilobular hydropic vacuolisation of hepatocytes and mild amounts of centrilobular congestion and infiltrate. Renal histology was normal in all rats. By 24 hours after APAP, all rats had sustained some degree of centrilobular necrosis, and necrotic regions contained infiltrate even if the amount of necrosis was very mild (fig 4.10 C). Necrosis and hepatotoxicity was most severe in rats with the highest serum aminotransferase levels. Areas of significant sinusoid dilation were often observed either at the border of necrotic zones or surrounding central venules (fig 4.10 E). Interlobular and intralobular variability of toxicity was present in all rats at both 6 and 24 hours, with more extremely contrasting degrees of toxicity across the livers of rats with the most severe hepatotoxicity. Renal histology was normal in all rats at 24 hours after APAP (see Appendix 5 A11).

Sinusoidal collagen was increased at both 6 (fig 4.11 B) and 24 (fig 4.11 C) hours after APAP in both periportal and centrilobular zones, but mainly in centrilobular zones. There was increased collagen in central venules particularly in necrotic zones indicative of the increasing hepatotoxicity. In areas of sinusoidal dilation, collagen appeared to help tether LSEC and HSC processes (that mainly were located in the centre of the expanding sinusoids) to the degenerating hepatocytes (fig 4.11 D). Collagen deposition tended to be more diffuse at 6 hours than at 24 hours when collagen bundles appeared to be longer and more linear particularly in rats with higher toxicity. At least some of the collagen fibres around necrotic/degenerating hepatocytes could have been a part of the collapsing reticular fibre framework. The amount of sinusoidal collagen was variable in each rat, consistent with variable toxicity across the liver.

At 6 hours after APAP hepatocytes were mostly devoid of glycogen (fig 4.10 B) however by 24 hours after APAP some of the glycogen was replenished in the periportal zones of 4 out of 5 rats (fig 4.10 D). Consistent with the intralobular variability of toxicity, the amount of glycogen was variable across the livers and some periportal zones were glycogen deplete. This was significantly different to control rats where glycogen was either depleted across the section, or mild amounts of glycogen were present in centrilobular zones.

Table 4.6 *6 hrs after APAP in fasted rats- graded necrosis and sinusoidal collagen with comparative ALT level and glycogen presence in each rat*

Rat	ALT (U/L)	Grade of necrosis per lobe				Collagen	Glycogen
		Median	Right	Left	Caudate		
1	46	0	0	0	0	++	Deplete
2	50	0	0	0	0	++	Deplete
3	33	0	0	0	0	++	Deplete
4	45	0	0	0	0	++	Deplete
5	51	0	0	0	0	++	Deplete

Table 4.7 *24 hrs after APAP in fasted rats- graded necrosis and sinusoidal collagen with comparative ALT level and glycogen presence in each rat*

Rat	ALT (U/L)	Grade of necrosis per lobe				Collagen	Glycogen
		Median	Right	Left	Caudate		
1	1129	++	++	++	++	+	Deplete
2	124	0	+	+	0	++	PP
3	220	+	+	+	0	++	PP
4	4690	+++	+++	++	+	+	PP
5	4550	+++	+++	+++	+	+	PP

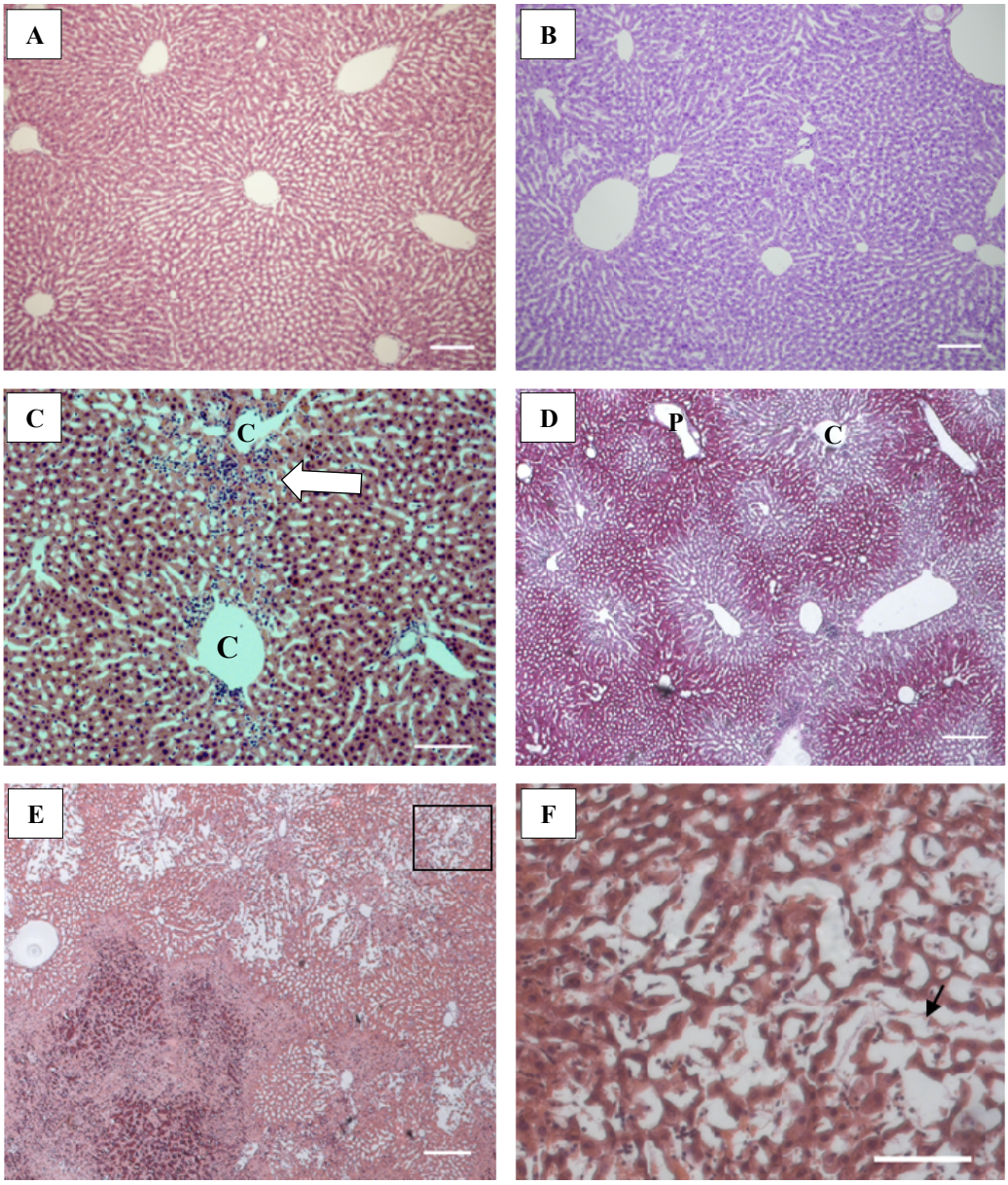

Figure 4.10 *Liver Histology from fasted APAP-treated rats: H&E and PAS stains*
A) H&E. Normal histology at 6 hours after APAP. Bar = 200 µm.
B) PAS. A glycogen depleted area at 6 hours after APAP. Bar = 200 µm.
C) H&E. Grade 1 (+) necrosis at 24 hours after APAP, there is mild necrosis with increased infiltrate in CL areas (arrow). C = central venule. Bar = 100 µm.
D) PAS. In this section at 24 hours after APAP, PP hepatocytes contain glycogen however CL hepatocytes are depleted. C = central venule, P = portal venule. Bar = 200 µm.
E) Grade 3 (+++) CL hemorrhagic necrosis in a fasted rat 24 hours after APAP. There is intralobular variability of toxicity. The bottom left of the micrograph shows a region of CL hemorrhagic necrosis, and in the top half there is less necrosis however the CL sinusoids are dilated. Bar = 200 µm.
F) A magnified image of the boxed area in fig (E) showing an area of sinusoid dilation with the LSEC and HSCs at the centre (arrow) and mostly detached from hepatocyte contact. Bar = 100 µm.

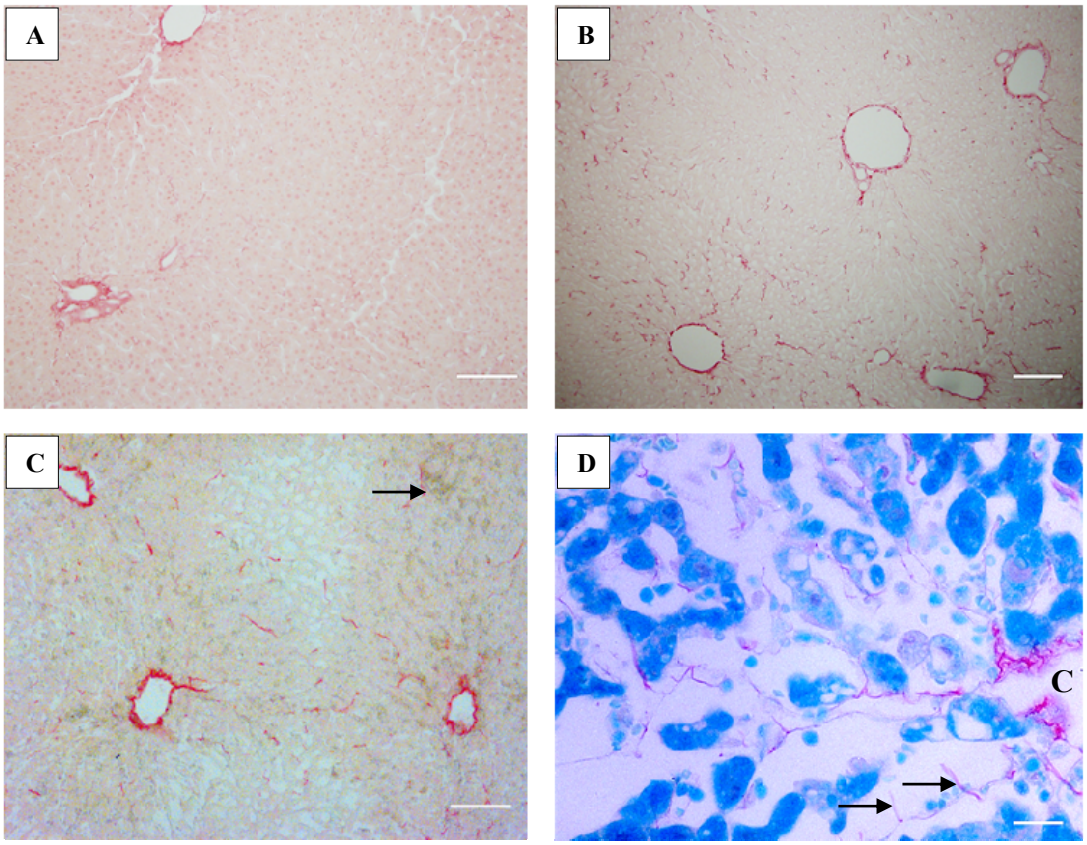

Figure 4.11 *Sirius Red stained sections of liver from fasted APAP-treated rats showing increased liver collagen*
A) Control liver from a fasted rat with very little collagen in the sinusoids. Bar = 100 µm.
B) Increased sinusoidal collagen at 6 hours after APAP. Bar = 200 µm.
C) A necrotic region with increased collagen around central venules and in the necrotic areas at 24 hours after APAP. An arrow points to an area of hemorrhage. Bar = 100 µm.
D) A micrograph counterstained with Fast Green FCF. Collagen fibres (red) are running through dilated sinusoids in a central zone 24 hours after APAP. The fibres (arrows) appear to be helping to connect degenerating hepatocytes with LSECs/HSCs. C = central venule. Bar = 20 µm.

4.4.5 Electron microscopy at 6 hours after APAP

LSEC cytoplasms contained gaps ranging up to 3 μm in diameter (fig 4.12 A), although intercellular junctions were maintained. Some LSECs had mildly swollen cytoplasms that contained vacuoles, dense bodies, and pinocytotic vesicles. Where hepatocytes were degenerating in more severely damaged centrilobular zones, processes from hepatocytes were found extending through the enlarged SoD to the LSECs appearing to tether LSECs and hepatocytes together (fig 4.12 B). Platelets were occasionally observed in the sinusoids.

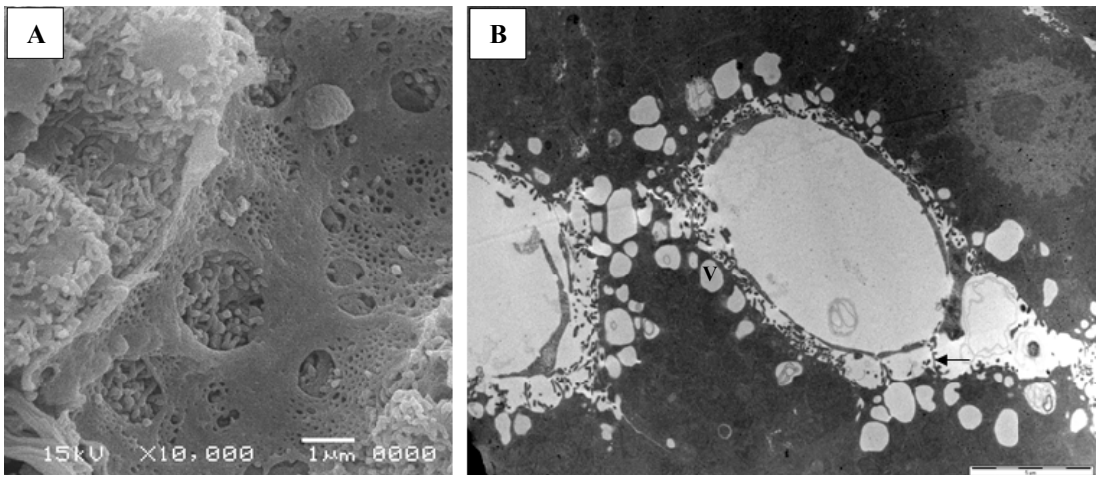

Figure 4.12 *Electron micrographs from fasted rats 6 hrs after APAP*
A) SEM: An LSEC containing gaps (bar = 1 μm).
B) TEM: hydropic vacuoles in hepatocytes at the sinusoid edge (V). There are hepatocyte processes that extend to LSECs where the SoD is expanding (black arrow) (bar = 5 μm).

4.4.6 Electron microscopy at 24 hours after APAP

In areas of hemorrhagic necrosis most LSECs were viable (fig 4.13 A), although some dead LSECs with pyknotic nuclei were observed (fig 4.13 B). Sinusoid lumens were often decreased in size presumably because of hemorrhage and swelling of hepatocytes undergoing oncotic necrosis. Fibrin and platelets were present particularly in the SoD and adjacent to or around necrotic cells (fig 4.14 A and B). There was increased infiltrate including monocytes, Pit cells, neutrophils, and some eosinophils. Hepatocytes undergoing ballooning degeneration (with dilated ER, nuclear shrinkage, and loss of microvilli) were sometimes found on the edge of necrotic zones (fig 4.16 A), appearing to force the sinusoids between them to decrease in diameter.

In areas affected by sinusoid dilation, LSECs maintained their fenestrated phenotype and were of a normal thickness (fig 4.15 A). Occasionally gaps were observed up to 2 μm in diameter. LSECs and HSCs were tightly associated with each other, and maintained some attachments to the degenerating hepatocytes (fig 4.15 A and B). Sinusoid lumens were sometimes moderately collapsed but often remained at a normal size. In contrast the SoD expanded significantly (ranging up to 30 μm in length, instead of normally measuring 0.3 - 1 μm) as the hepatocytes atrophied and lost their microvilli (fig 4.15 A). Large activated KCs were found mainly in the periportal sinusoids containing huge vacuoles of cellular debris (fig 4.16 B). In periportal zones and other areas of the liver not affected by necrosis, the sinusoids appeared mostly normal apart from occasional vacuolar and fatty degeneration of hepatocytes, and some mild defenestration and gaps in LSECs.

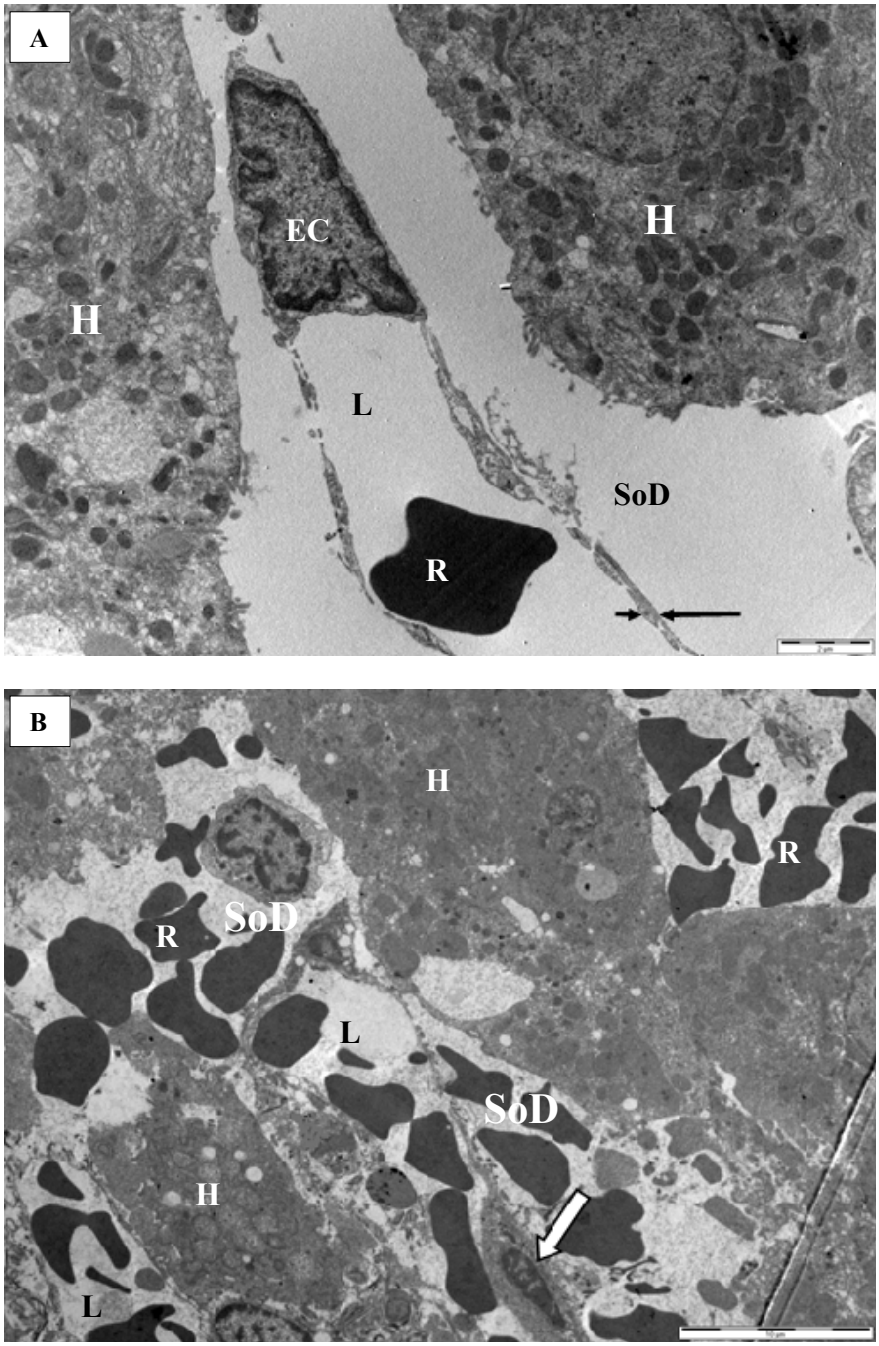

Figure 4.13 *Electron micrographs from fasted rats 24 hrs after APAP*
A) TEM: A viable LSEC surrounded by hepatocytes that are dead or succumbing oncotic necrosis. An arrow points to LSEC (EC) cytoplasm, and a longer arrow points to a HSC process which remains closely associated to the LSEC. H = hepatocyte, R = RBC, L = lumen. Bar = 2 μm.
B) TEM: A dead LSEC in a necrotic and hemorrhagic zone with a nucleus containing condensed chromatin (white arrow). Bar = 10 μm.

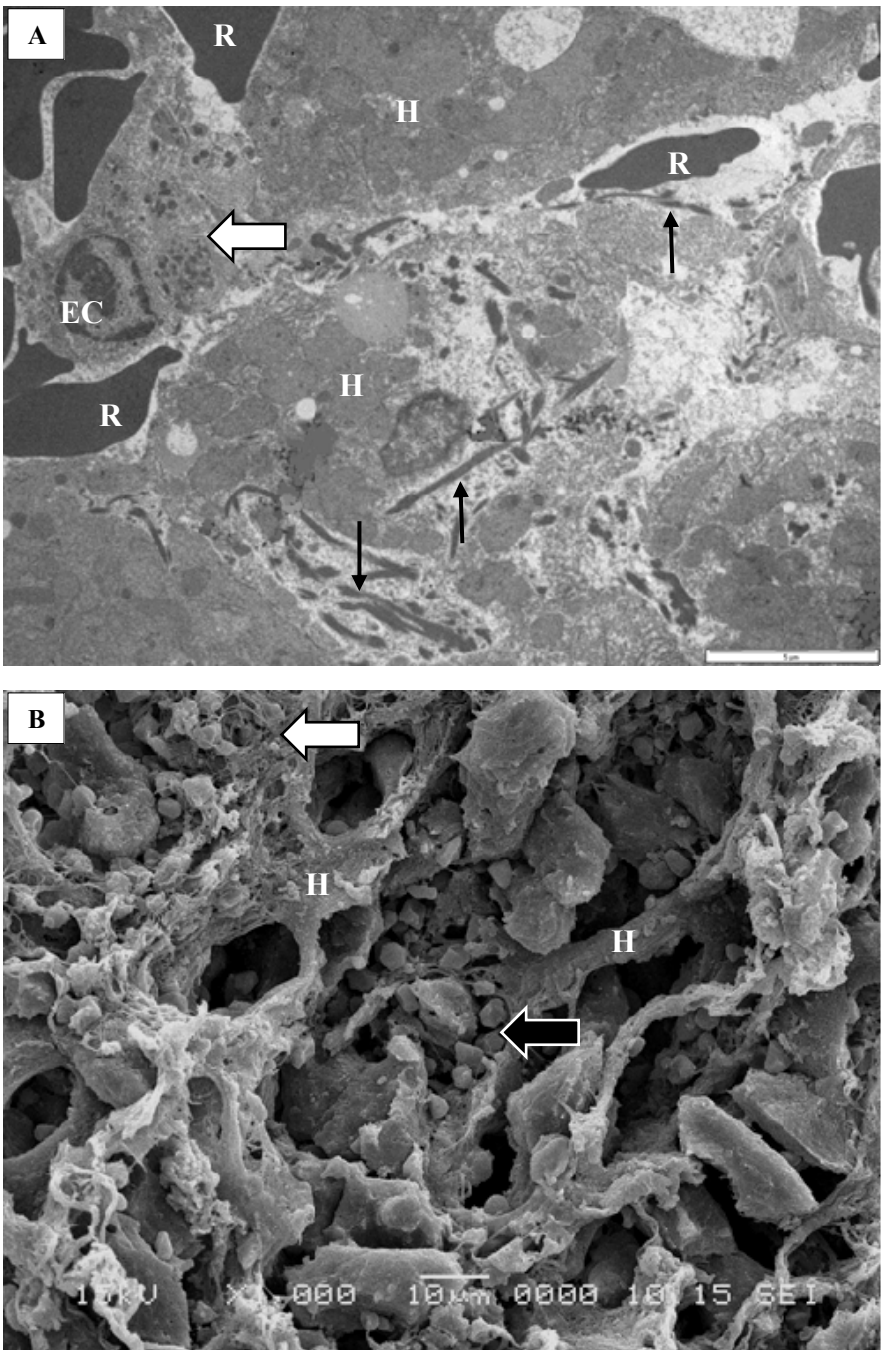

Figure 4.14 *Electron micrographs from fasted rats 24 hrs after APAP*
A) TEM: Fibrin deposition (black arrows) in amongst necrotic hepatocytes and associated with RBCs (R) that are no longer in the sinusoid lumens. A platelet clot (white arrow) lies next to what may be an LSEC (EC). Bar = 10 μm.
B) SEM: An area of sinusoid dilation showing atrophied hepatocytes (H) that appear as thin cords, and RBCs in the SoD (black arrow), some of which are trapped in fibrin clots (white arrow) (bar = 10 μm).

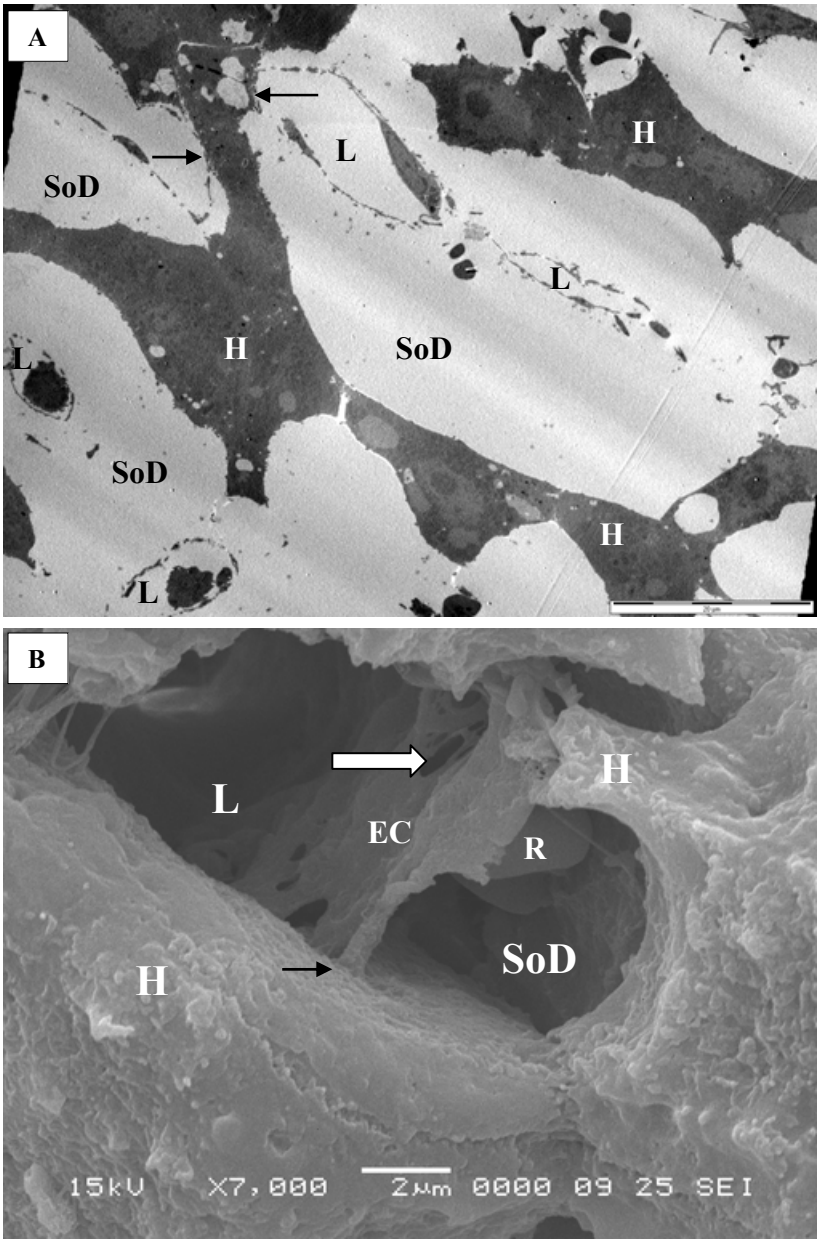

Figure 4.15 *Electron micrographs from fasted rats 24 hrs after APAP*
A) TEM: A 2-dimensional view of a sinusoid dilated area. The SoD is greatly expanded and LSECs and HSCs are mostly floating free from hepatocytes although maintain some attachments (arrows). L = lumen, SD = SoD, H = hepatocyte. Bar = 20 µm. Also refer to fig 4.10 E for a histological comparison.
B) SEM: 3-dimensional view of a sinusoid dilated area. The LSEC contains gaps (white arrow) and has attachments (arrow) to a degenerating hepatocyte (H). An RBC (R) is in the SoD, L = lumen (bar = 2 µm).

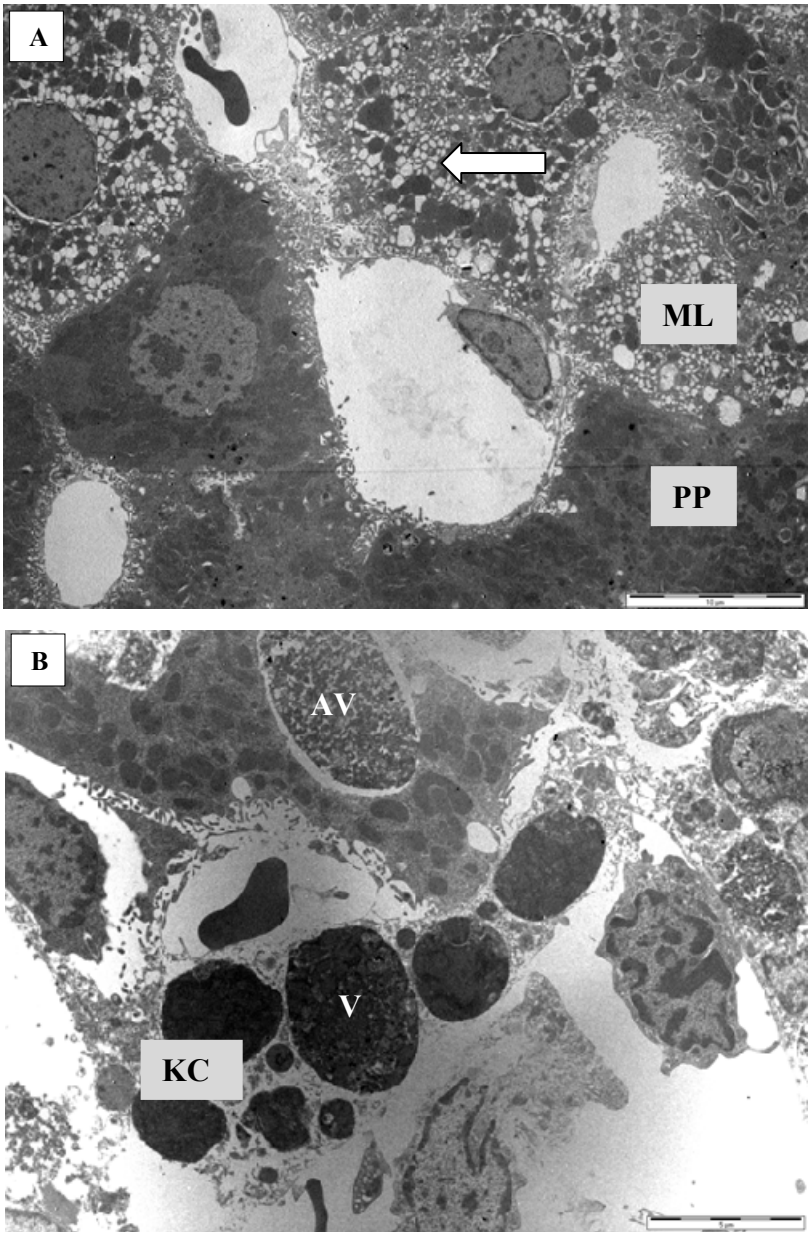

Figure 4.16 *Electron micrographs from fasted rats 24 hrs after APAP*
A) TEM: A section of hepatocytes probably from the midlobular zone (ML) undergoing balloon degeneration (arrow) that are adjacent to viable hepatocytes probably from the periportal (PP) zone. The lumens are smaller in where they are surrounded by ballooning hepatocytes (bar = 10 μm).
B) TEM: A KC in the sinusoid contains large vacuoles/lysosomes (V) full of cellular debris. There is an autophagic vacuole (AV) in the hepatocyte (bar = 5 μm).

4.4.7 Summary of differences between fed and fasted APAP-treated rats

Overall there was less hepatotoxicity in the fed than the fasted APAP-treated rats (see table 4.8). On average at 24 hours after APAP fed rats had lower serum aminotransferase levels, less centrilobular hemorrhagic necrosis, less infiltrate in areas of mild toxicity, and greater resilience of LSECs in areas of centrilobular necrosis. Fasted rats also displayed greater amounts of sinusoid dilation with more severe dilation, and more collagen deposition in the sinusoids and around venules than the fed rats suggestive of increased oxidative damage. Refer to Appendix 4, table 1 for a table of means ± S.D. of APAP-treated and F344 untreated rats.

Table 4.8 *Table of raw and mean ± S.D. data from ad libitum fed and fasted APAP treated rats culled 6 or 24 hours after APAP. Scores for centrilobular necrosis and sinusoidal collagen are the sum of the '+'s in each group divided by the number of rats*

		Rat						
APAP treated rats	**Group**	**1**	**2**	**3**	**4**	**5**	**6**	**Mean ± SD**
ALT (U/L)	**6 hr fast**	46	50	33	45	51		**45±7.2**
	24 hr fast	1129	124	220	4690	4550		**2143±2296**
	24 hr fed	48	38	52	16	702	no data	**171.2±297**
AST (U/L)	**6 hr fast**	80	100	60	72	95		**81.4±16.4**
	24 hr fast	1124	143	209	7053	6513		**3008±3473**
	24 hr fed	96	86	104	32	459	no data	**155.4±172**
Total Bilirubin (U/L)	**6 hr fast**	1	1	1	1	1		**1±0**
	24 hr fast	2	2	1	3	2		**2±0.7*†**
	24 hr fed	3	6	4	1	3	no data	**3.4±1.8***
% Weight loss from time of fast	**6 hr fast**	10.4	5.9	8.3	5.6	7.4		**7.5±1.9**
	24 hr fast	13.7	15.6	12.4	11.8	11.3		**13±1.7*†**
% Weight loss	**24 hr fed**	4.9	4.4	3.8	4.8	4.9	no data	**4.6±0.5**
Total cholesterol (µmol/L)	**6 hr fast**	1.3	1.5	1.3	1.2	1.3		**1.3±0.1**
	24 hr fast	1.3	1.2	1.1	1.1	0.8		**1.1±0.2*†**
Triglycerides (µmol/L)	**6 hr fast**	0.5	0.8	1.1	0.7	0.9		**0.8±0.2**
	24 hr fast	1.5	0.9	0.6	0.2	0.5		**0.7±0.5**
Urea	**6 hr fast**	no data	3.8	5.1	6.3	1.4		**4.2±2.1**
	24 hr fast	7.4	no data	6.5	6.2	10.8		**7.7±2.1*†**
Creatinine	**6 hr fast**	no data	13	22	28	no data		**21±7.5**
	24 hr fast	50	no data	27	27	43		**36.8±11.6*†**
Hematocrit (%)	**6 hr fast**	58	59	63	56	62		**59.5±2.7**
	24 hr fast	73	63	65	61	50		**62±8†**
Liver wet weight % body weight	**6 hr fast**	2.9	3.4	3.3	4.5	2.7		**3.3±0.7**
	24 hr fast	4.9	4.9	3.4	4	4.1		**4.3±0.6*†**
Centrilobular Necrosis	**6 hr fast**	0	0	0	0	0		**0**
	24 hr fast	++	+	+	+++	+++		**32/25 = 1.28**
	24 hr fed	0	0	0	0	++	+++	**5/6 = 0.83**
Sinusoidal Collagen	**6 hr fast**	++	++	++	++	++		**10/5 = 2**
	24 hr fast	+	++	++	+	+		**7/5 = 1.4**
	24 hr fed	0	0	0	0	+	+	**2/6 = 0.33**
Glycogen Deposition	**6 hr fast**	0	0	0	0	0		**0**
	24 hr fast	0	PP	PP	PP	PP		**PP**
	24 hr fed	0	0	0	PP	PP	0	**0 - PP**

*$p<0.05$ compared to 6 hr rats.

†$p<0.05$ compared to control rats.

Note: The score for necrosis in the APAP 24 hr fasted group was calculated by the sum of all the scores for each lobe (see table 4.7) divided by the number of lobes analysed.

4.6 Discussion

APAP overdose resulted in a pattern of centrilobular toxicity that sometimes developed into severe centrilobular hemorrhagic necrosis although periportal hepatocytes remained viable, sustaining only mild damage. Injury to the microvasculature and LSECs was apparent before hepatocyte necrosis, however as parenchymal injury increased, damage to the LSECs appeared to ameliorate until the hepatotoxicity became too severe for the LSECs in the worst affected centrilobular zones to survive.

In instances of mid-range hepatotoxicity, LSECs surrounded by necrotic hepatocytes appeared to be very resilient to toxicity and were in their fenestrated phenotype. Although there was disorganisation of cells and squashed sinusoids in areas of significant necrosis and hemorrhage, LSECs and HSCs remained together with increased extracellular matrix between them and tethered to necrotic hepatocytes. Initial injury to LSECs could have improved and LSEC viability maintained as vascular endothelial growth factor A (VEGF) production and expression of VEGF receptors increase throughout the course of APAP toxicity (Papastefanou, 2007). VEGF is a cytokine important in angiogenesis and is a specific mitogen for endothelial cells. LSEC fenestration is normally maintained by paracrine secretion of VEGF by hepatocytes and HSCs (Xie, 2012) and VEGF has been shown to protect LSEC viability and maintain their fenestrated phenotype in vitro (Esser, 1998).

In addition, LSEC viability is strengthened in hypoxic environments (Martinez, 2008), and stimulation of VEGF production and its release by HSCs occurs in response to liver injury and hypoxia (Ankoma-Sey, 2000, Zhao, 2012). LSECs contain VEGF

receptors that when stimulated are not only protective to LSECs, but activate the production of hepatocyte growth factor (HGF) and other paracrine factors that are essential for liver regeneration after massive necrosis (LeCouter, 2003). Endogenous VEGF is essential for hepatocyte regeneration in the later recovery stages of APAP toxicity (Donahower, 2006, Donahower, 2010, Kato, 2011, Papastefanou, 2007) providing strong evidence to suggest that hepatoprotective effects of VEGF in APAP toxicity are secondary to amelioration of LSEC injury and regeneration of the microvasculature. It is possible that there would have been a decreased survival rate in the rats with high numbers of dead LSECs in areas of confluent hepatocyte necrosis.

Increased extracellular matrix production between LSECs and HSCs has been described in various disease states (Le Bail, 1990) and in ageing (Le Couteur, 2002), however has not been previously described in APAP toxicity. It is likely that the production of basement membrane increased the tethering of LSECs and HSCs, was essential to the maintenance of the sinusoid structure in disorganised necrotic areas (critical to the later process of liver regeneration), and helped to prevent LSECs from denuding and occluding sinusoids (as occurs in sinusoidal obstructive syndrome (DeLeve, 2007a)). The decreased lumen size where there was sinusoid dilation and necrosis could have been due to increased pressure in the SoD because of RBC accumulation, and contraction of HSC processes in order to regulate blood flow in the liver (Friedman, 2008, Thimgan, 1999, Vollmar, 2009) and decrease flow to areas of hemorrhage.

LSEC injury was apparent by 6 hours after APAP and prior to parenchymal necrosis. Injury consisted of gaps that replaced some of the fenestrations and sieve plates in the

cytoplasm, and mild swelling in parts of the cytoplasm containing many pinocytotic vesicles, vacuoles, and dense bodies. Generally the surrounding hepatocytes had developed signs of degeneration including hydropic vacuoles at the sinusoid border and loss of microvilli. It is possible that LSEC injury occurred prior to the hepatocytes as described in other studies (Ito, 2003) however the 6 hour time-point in our study was too late to observe the very first signs of LSEC injury. Analysis at 6 hours after APAP confirmed that microvasculature disruption, such as congestion and the appearance of platelets in centrilobular zones occurred prior to necrosis (Walker, 1985), and gaps in the LSECs and defenestration sometimes occurred where the underlying hepatocytes appeared to be morphologically sound.

Also at 6 hours after APAP, long processes from hepatocytes that were losing microvilli projected across the SoD to the LSECs. This appeared tether the sinusoids and degenerating parenchyma together, and is consistent with that described by a previous study (Walker, 1983). Both injury to LSECs (Xie, 2012) and hepatocytes (Svegliati Baroni, 1998) can stimulate HSC activation and collagen production. Increased production of collagen was observed mainly in the central zones at 6 hours after APAP implicative of oxidative damage to the liver, and has been previously found to occur early in APAP toxicity as a result of decreasing GSH levels (Morsy, 2010, Toklu, 2006).

Consistent with previous studies, glycogen stores were depleted or at very low levels at 6 hours after APAP (Jepson, 1987, Price, 1987). Glycogenolysis can be stimulated by hypoxic conditions and ionic changes in cells (such as increased intracellular Ca^{2+}) that can occur early in APAP toxicity (Hinson, 1983). At 24 hours both fed and fasted

rats displayed replenishments of periportal glycogen whilst centrilobular hepatocytes remained depleted. Glycogen phosphorylase activation in centrilobular hepatocytes occurs after glutathione levels are depleted and prior to loss of membrane integrity, and thus may be a sensitive indicator of early cell damage (Corcoran, 1988, Jepson, 1987). There is also a reciprocal and concurrent increase of glycogen levels in periportal hepatocytes (synthesised from gluconeogenic precursors rather than glucose) indicating heterogeneity of the centrilobular and periportal hepatocytes in response to toxicity from APAP overdose (Jepson, 1987). The degree of glycogen phosphorylase activation in centrilobular hepatocytes and glycogen formation in periportal hepatocytes is dose dependent, and increase with higher doses of APAP and as more severe histological damage is apparent. Changes in glycogen metabolism may therefore be linked to the cytotoxic effects of APAP metabolism, and be observed as a marker of hepatotoxicity (Jepson, 1987). APAP depletes GSH and glycogen by similar percentages at each dose, and if NAC is administered with APAP it prevents both the early APAP-induced glycogen depletion and toxicity. This suggests that glycogen depletion is somehow related to the formation of NAPQI (Hinson, 1983). The presence of glycogen may also play a minor role in protection from toxicity (Hinson, 1983).

By 24 hours after APAP, confluent hepatocyte necrosis had developed in centrilobular zones of most rats and serum aminotransferase levels rose in correlation with the severity of necrosis as previously reported (Hessel, 1996). Total serum bilirubin also significantly increased from normal in both fed and fasted APAP-treated groups. Bilirubin (the breakdown product of heme) is metabolised to a water-soluble molecule by glucuronidation (Wang, 2006) and thus would be expected to increase in APAP

toxicity as it is in competition with APAP for glucuronidation. Excretion of conjugated bilirubin into the bile is also inhibited in APAP toxicity (Davis, 1975).

As was expected, at 24 hours after APAP hepatotoxicity was more prominent in fasted rats than fed rats. Fasting is known to increase APAP toxicity in humans (Whitcomb, 1994) and rats fasted for 24 hours before dosage (Pessayre, 1979). Fasting significantly decreases GSH stores in the liver, reducing its anti-oxidant capacity and the ability for the toxic metabolite NAPQI to be detoxified (Walker, 1982). In addition, fasting increases the half-life of APAP by depressing the rates of glucuronidation and sulfation (the non-toxic elimination pathways for APAP), thereby increasing the proportion of APAP metabolised by the toxic CYP450 pathway (Price, 1988, Price, 1987). There was decreased survival of LSECs in areas of parenchymal necrosis 24 hours after APAP in fasted rats compared to rats ad libitum fed prior to APAP. The decreased resilience of LSECs may have been due to reduction of GSH stores during fasting thereby lowering the anti-oxidant and detoxifying capacity of the LSECs to NAPQI and other toxins produced during APAP toxicity. In addition, as fasting prior to APAP increases the half life of APAP and NAPQI production, the insult is further increased on cells that are already more vulnerable to damage. This decreased resilience of the LSECs to necrosis may have augmented the amount of hepatocyte necrosis in the fasted rats by affecting the viability of the microvasculature, enhancing the congestion, hemorrhage, and ischemic damage to hepatocytes. It is also possible that HSCs were more vulnerable to damage in fasted rats and were not able to release enough VEGF to maintain LSEC viability.

In addition to the more severe parenchymal and LSEC toxicity, there was additional collagen deposition in fasted APAP-treated rats at 24 hours probably in response to the decreased anti-oxidant capacity of the liver (Sener, 2005). Also there was a greater presence of infiltrate in the fasted rats in reaction to the increased necrosis. Whether inflammatory cells in APAP toxicity promote or abate further damage is still under discussion (Ishida, 2006, Jaeschke, 2012b). KCs also appeared to be more activated in fasted rats, however KC activation is important for clearing away cellular debris and is thought to be protective in APAP-toxicity (Holt, 2010).

The severity and amount of sinusoid dilation in fasted rats at 24 hours after APAP was much greater than in the fed rats with severe hepatotoxicity. The cause of the more extreme dilation appeared to be due to severe congestion and hemorrhage that increased pressure in the sinusoids (as suggested by (Lim, 1995)) combined with hepatocyte atrophy. Cells have the ability to atrophy to accommodate changes in oxygen and nutrient availability, such as in ischemic environments with decreased blood supply, and can decrease their size in response to this (Robbins, 2007). Autophagy can accompany this process and large autophagic vacuoles in some of the hepatocytes were observed particularly in the fasted group. Autophagy is a protective mechanism in APAP overdose, removing damaged mitochondria, stopping unessential cell processes, and freeing up nutrients such as sugars, fatty acids and amino acids (Igusa, 2012, Ni, 2012) for gluconeogenesis (Ezaki, 2011). Thus, more severe sinusoidal dilation in fasted rats was probably due to a combination of lower nutrient and antioxidant stores prior to APAP dosage, and increased amounts of congestion and hemorrhage which also led to a significant increase the liver weight of fasted rats at 24 hours after APAP. Hepatomegaly during the initial stages of APAP

toxicity is primarily a result of plasma accumulation, congestion and hemorrhage (thus increased blood volume), and increased numbers of inflammatory cells in the liver (Walker, 1985).

Regardless of the differences in severity of hepatotoxicity between fed and fasted rats, both groups displayed a wide range of response to APAP overdose. Twenty-four hours after an equivalent dose of APAP, some rats had developed massive necrosis whereas others sustained only mild damage consistent with the extremely variable range differences in serum aminotransferases. At 6 hours there was a less noticeable range of variability as the hepatotoxicity was not as intense and was still in the process of developing. The level of APAP toxicity from a particular dose is known to be extremely variable amongst subjects including humans (Whitcomb, 1994) and laboratory animals (Foley, 2006, McLean, 1975), however the reasons for this are unclear.

Another common feature of APAP toxicity observed in our study was inter and intra lobular variability of hepatotoxicity (McLean, 1975). Histological examination of four lobes of the liver revealed the amount of hemorrhage and necrosis in each lobe and each centrilobular zone of a particular liver could vary from none to severe. Reasons for this variability are not understood but could at least partially be due to differences in gene expression throughout the liver (Foley, 2006, Irwin, 2005). Consistent with the variations in toxicity, the density and zonal distribution of collagen and glycogen were variable throughout the liver.

In conclusion this study was the first to perform an ultrastructural analysis of LSECs using scanning and transmission electron microscopy after extensive centrilobular necrosis had occurred in APAP-treated rats, confirming that LSECs are able to remain viable and fenestrated in areas of confluent hepatocyte necrosis and ischemia. We also observed that HSCs appear to play a major role in physically protecting LSECs in areas of hepatocyte necrosis, and that there was extensive formation of extracellular matrix between the cells that helped to preserve sinusoid structure where the surrounding hepatocytes were dead.

Chapter 5:

Therapeutic Effect of Poloxamer 407 on Acetaminophen toxicity in the F344 Rat Liver

5.1 Introduction

Therapeutic substances that could aid in ameliorating APAP hepatotoxicity are still being investigated. LSEC injury, gap formation, and subsequent disruption of the microvasculature plays a major role in the severity of hepatotoxicity after APAP overdose, occurring prior to hepatocyte necrosis (see Chapter 4). Studies have shown that protection of the LSEC and hepatic microcirculation significantly decreases liver injury (Ganey, 2007, Ito, 2005, McCuskey, 2006) however the exact mechanism of LSEC injury during APAP toxicity remains unclear.

P407 (Pluronic® F-127 or P407) is an LSEC defenestrating agent (Cogger, 2006) that may be protective in APAP toxicity by preventing or delaying structural LSEC injury, such as the development of gaps that lead to hemorrhage, sinusoid lumen collapse, and congestion, and by reducing the amount of APAP and toxic substances from the blood reaching the hepatocytes. In addition, it may be capable of interacting with and restoring activity of damaged cell membranes (Frey, 2007). Thus P407 might ameliorate or prevent microvasculature dysfunction if it were to prevent endothelial injury and gap formation after APAP overdose. P407 is a triblock copolymer composed of repeating polyoxyethylene and polyoxypropylene units and has thermoreversible properties (Dumortier, 2006, Johnston, 2004). At approximately 4 - 5 °C and below, P407 is a low-viscosity solution, and as the temperature increases P407 molecules aggregate into micelles and form a semisolid gel (Zhang, 2002). P407 is regarded as a non-toxic substance and is already used in pharmaceutical preparations (Dumortier, 2006, Li, 1996).

P407 has been used in murine studies as an agent that effectively induces pronounced hyperlipidemia and hypercholesterolemia without any inherent toxicity (Palmer, 1997). In fact P407 can be administered chronically to induce atherogenic lesions without any other apparent adverse effects for the study of atherosclerosis (Palmer, 1997). P407 is also safely used to induce hyperlipidemia for the study of pharmacokinetics of various drugs during hyperlipidemia (Lee, 2011, Lee, 2012, Shayeganpour, 2008). Some of these studies showed that P407 reduces the expression of CYP450 enzymes (in particular those of the CYP3A family (Lee, 2011, Shayeganpour, 2008) involved in APAP metabolism (Kostrubsky, 1997, Thummel, 1993) which could be beneficial in APAP overdose by reducing the production of toxic metabolites.

It was previously thought that P407 primarily induces hypertriglyceridemia via a dose-dependent inhibition of lipoprotein lipase, and hypercholesterolemia by indirect effects on hepatic 3-hydroxy-3-methylglutaryl coenzyme A (HMG-CoA) reductase activity (Johnston, 2004), and by affecting the activities of various other lipid metabolising enzymes (Wasan, 2003). However, it is now known that defenestration of the LSEC by P407 also promotes hyperlipidemia by impairing the passage of chylomicrons to hepatocytes (Cogger, 2006). The mechanism of P407-induced LSEC defenestration *in vitro* and *in vivo* is not currently understood. It has recently been reported that fenestrations are regulated by lipid rafts in the cell membrane and that defenestration can be induced by removal of the non-raft membranes with detergents such as Triton X-100 (Svistounov, 2012). P407 has similar properties to Triton X-100 so might also cause defenestration by the same mechanism. Poloxamers have the ability to form tiny pores in membranes that can enable the flux of various cations

such as calcium and potassium (Krylova, 2004, Sutachan, 2006) thus the mechanism could be related to an effect of P407 on cytoplasmic ion concentrations that could increase contraction or dilation of actin filaments around fenestrations. When P407 is added to LSECs *in vitro* it induces profound and acute defenestration of the LSEC cytoplasm, and does this by a direct mechanism without influence from other cells (Cogger, 2006). *In vivo*, after intraperitoneal injection, P407 is avidly taken up into the liver (Li, 1996). Analysis of porosity using the scanning electron microscope showed that P407 significantly defenestrates LSECs (reducing fenestrations by up to 80 %) from 12 - 36 hours after injection in mice in accordance with a 10 fold increase in plasma lipids (Cogger, 2006). P407 does not affect mitochondria or ATP production but may work by direct interaction with the cell membrane (Cogger, 2006). Transmission electron microscopy analysis of murine livers one day after P407 injection showed that LSECs developed large vacuoles full of lipids and/or P407 micelles in conjunction with LSEC defenestration and swelling observed on scanning electron microscopy, probably in an effort to remove excess lipid and P407 from the blood (Warren, 2011).

In addition to LSECs, other liver cells are affected by P407. KCs, become engorged with vacuoles full of lipid and/or P407, and are occasionally so swollen they appear to completely occlude the sinusoid lumen (Warren, 2011). Hepatocytes, although involved in the endocytosis of P407, do not develop steatosis despite the hyperlipidemia (Millar, 2005, Warren, 2011), and the morphology of HSCs does not change. This could be because LSEC defenestration reduces the access of serum lipoproteins to the SoD (and thus the hepatocytes and HSCs).

P407 micelles are 20 - 80 nm in diameter being the perfect fit for plugging fenestrations that are on average 50 - 150 nm wide in a process equivalent to so-called 'fouling' of ultrafiltration membranes. A fenestration-plugging and/or defenestration action by P407 may be beneficial in reducing toxic metabolite production in APAP overdose by reducing APAP availability to hepatocytes. One study has shown that the passing of APAP from the lumen to the SoD (in the rat) is impeded by a pre-injection of P407 (Mitchell, 2010). P407 micelles have been observed throughout the SoD, adsorbed to LSECs and between fenestrations on transmission electron microscopy (Warren, 2011).

This study aimed to test whether P407, a non-toxic substance already used in pharmaceutical preparations that directly targets LSECs, had an ameliorative effect on hepatotoxicity during APAP overdose on fed rats, and on fasted rats with more severe hepatotoxicity. We pre-treated some rats with P407 to coincide LSEC defenestration with APAP administration, and post-treated some rats with P407 after APAP administration to observe whether P407 had any potential as a therapeutic substance by restoring the activity of damaged cell membranes and ameliorating LSEC injury and hepatic microcirculation.

5.2 Materials and Methods

5.2.1 Materials

0.5 g/ml of P407 (donated by BASF chemicals) in normal saline was prepared by mixing gently at 4 °C and kept in liquid form in the fridge or over ice. Animals and other chemicals used are identical to those described in section 4.2.

5.2.2 Methods

For P407 pre-treated rats, an intraperitoneal injection of P407 (1 g/kg rat) was administered 18 hours before a gavage of APAP (1000 mg/kg rat) which is the dose required to defenestrate the LSEC by the time of APAP gavage according to a previous study (Cogger, 2006). For P407 post-treated rats, an intraperitoneal injection of P407 (1 g/kg rat) was administered 1 hour after a gavage of APAP (1000 mg/kg rat). It was determined whether P407 successfully entered the blood by observing and testing whether the blood was lipemic (Wout, 1992). Apart from the P407 injection, the procedure for surgery, specimen preparation, and analysis used for these experiments were identical to those described in section 4.2.

Rats were divided into groups as follows (see fig 5.1). In the ad libitum fed groups (fed P407 pre-treated and post-treated groups) 12 rats were ad libitum fed until food was removed when 1 g/kg APAP was given. In the fasted rat groups (fasted P407 pre-treated and post-treated groups) 20 rats were fasted from 24 hours before APAP gavage until time of surgery. Ten of those rats were culled at 6 hours after APAP gavage (5 from each of the fasted P407 pre- and post-treated groups), and 10 were culled at 24 hours after APAP gavage (5 from each of the fasted P407 pre- and post-

treated groups). One rat was excluded from the 24 hour fasted P407 post-treated group after blood analysis because it was not hyperlipidemic and thus may not have properly received the dose of P407 (Wout, 1992), leaving this group with n = 4 rats for analysis. Control rats for this experiment were the fed and fasted APAP-treated rats from Chapter 4 (labelled in this chapter as APAP controls).

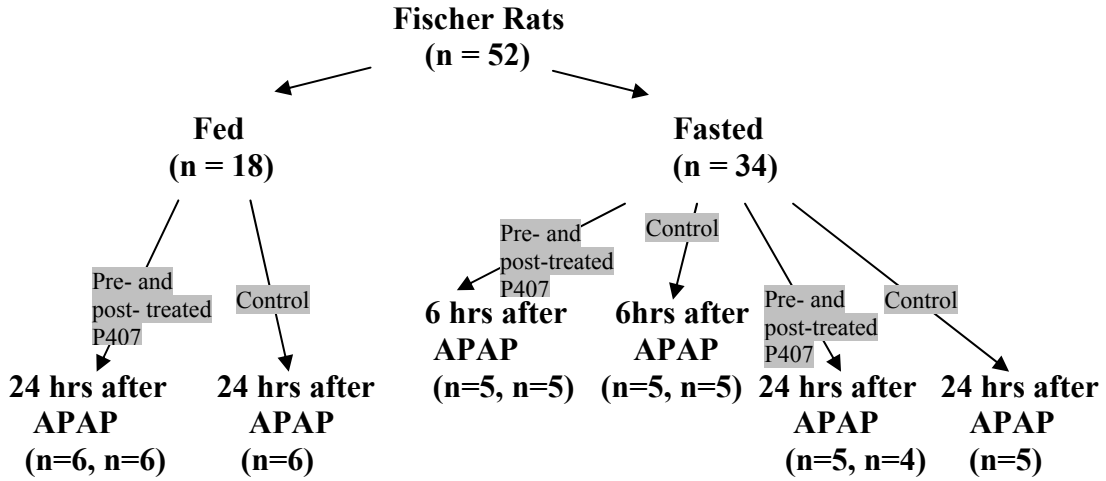

Figure 5.1 *Experimental treatment groups: P407 was injected 18 hours before or 1 hour after APAP gavage. APAP control rats received APAP and no P407. Surgery occurred either 6 or 24 hours after APAP.*

Apart from the P407 injection, the procedure for surgery and perfusion fixation, specimen preparation, and analysis used for these experiments were identical to those described in section 4.2. Briefly, after perfusion fixation specimens were collected for histology and electron microscopy analysis. Again, average porosity and fenestration diameter of LSECs were unable to be measured due to intralobular variability of toxicity (fig 5.2). Measurements were taken using Image J of control and P407 rats to estimate and compare the size of the sinusoid lumen, SoD, fenestrations, gaps, and LSEC cytoplasm in different areas of the liver. Blood samples were also collected.

Renal tissue from one rat was reprocessed from paraffin for transmission electron microscopy (as by the procedure described in Chapter 2) as an unknown substance was found in the tubules during histological analysis.

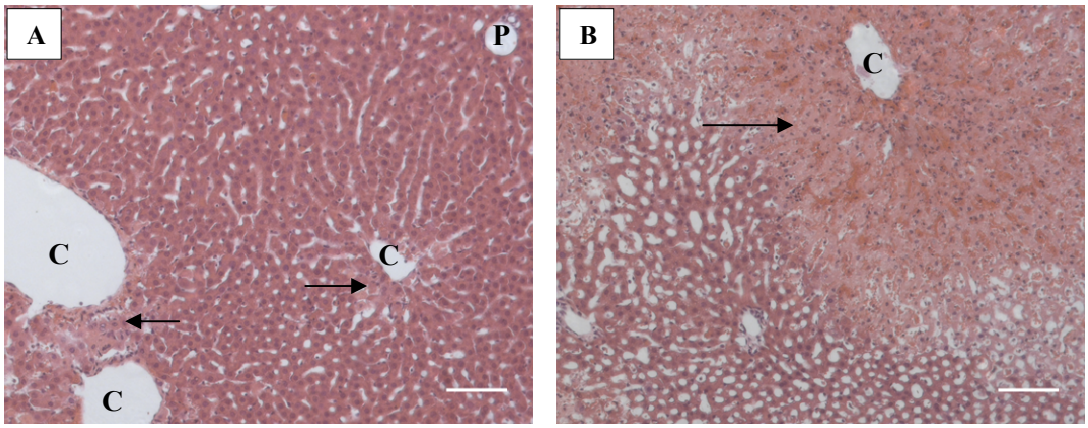

Figure 5.2 *Example of intralobular differences in P407 pre-treated rats*
A) and B) are micrographs taken from different areas of the same section of a P407 pre-treated rat liver at 24 hours after APAP showing severe differences in toxicity across the lobe. In A) there is only very mild centrilobular necrosis (arrows) however in B) there is severe hemorrhagic centrilobular necrosis (arrow) and sinusoidal dilation in midlobular and periportal zones. C = central venule, P = portal venule. Bars = 100 μm.

5.3 Results: P407 pre-treated rats

5.3.1 Macroscopic observations

At 6 and 24 hours after APAP rats mostly appeared quiet and sedated. Two 24 hour rats from the fasted group (with very high serum aminotransferase levels) had gross hematuria.

5.3.2 Blood analysis

5.3.2.1 Fed P407 pre-treated 24 hour group

In the 24 hour fed P407 pre-treated group, serum aminotransferases tended to be increased however were not significantly different as the data was highly variable (table 5.1). Total bilirubin was significantly lower in the P407 pre-treated 24 hour fed group, and weight loss was significantly higher than control (table 5.1).

5.3.2.2 Fasted P407 pre-treated 6 and 24 hour groups

At 6 hours after APAP the P407 pre-treated rats had significantly lower serum ALT and bilirubin than the APAP control rats however the difference was minor (table 5.1). In the 24 hour fasted P407 pre-treated group, average ALT and AST were increased, although not significantly due to variability in the data (table 5.1). There were significant increases in serum cholesterol and triglycerides at both 6 and 24 hours in the P407 pre-treated rats, and significant decreases in hematocrit (table 5.1).

Table 5.1 *Raw and mean ± S.D. data from ad libitum fed or fasted APAP treated rats culled 6 or 24 hrs after APAP and pre-treated with P407 18 hrs before APAP*

		Rats raw data							
P407 pre-treated rats	**Group**	**1**	**2**	**3**	**4**	**5**	**6**	**Mean ± SD**	**APAP control**
ALT (U/L)	**6 hr fast**	36	20.4	30	31.2	26.6		**29±6***	**45±7.2**
	24 hr fast	2210	14850	11370	29	185		**5729±6903**	**2143±2296**
	24 hr fed	164.4	64.8	76.8	153.6	1549	no blood	**402±643**	**171.2±297**
AST (U/L)	**6 hr fast**	70.8	76.8	76.8	54	60.2		**68±10**	**81.4±16.4**
	24 hr fast	3044	23830	20360	51	277		**9512±11612**	**3008±3473**
	24 hr fed	218.4	54	70.8	190.8	3378	no blood	**782±1453**	**155.4±172**
Total Bilirubin (U/L)	**6 hr fast**	0	0	0	0	1.4		**0.3±0.6***	**1±0**
	24 hr fast	1	5	4	0	0		**2±2.3**	**2±0.7**
	24 hr fed	0	0	0	0	0	no blood	**0***	**3.4±1.8**
% Weight loss from time of fast	**6 hr fast**	7	6.9	7.9	6.1	5.2		**6.6±1**	**7.5±1.9**
	24 hr fast	10.6	9.2	9.9	10.1	9.6		**10±0.5**	**13±1.7**
% Weight loss	**24 hr fed**	7.4	no data	no data	8.1	4.6	6.6	**6.7±1.5***	**4.6±0.5**
Total cholesterol (µmol/L)	**6 hr fast**	9.6	8.6	12.2	12.9	10.4		**10.7±1.8***	**1.3±0.1**
	24 hr fast	4.6	9.4	14.5	8	15.1		**10.3±4.5***	**1.1±0.2**
Triglycerides (µmol/L)	**6 hr fast**	44.7	31.9	61	67	60		**53±14.3***	**0.8±0.2**
	24 hr fast	11.3	28.5	64	27.7	69.6		**40±25.3***	**0.7±0.5**
Hematocrit (%)	**6 hr fast**	44	46	47	47	47		**46±1***	**59.5±2.7**
	24 hr fast	49	36	39	47	43		**43±5***	**62±8**
Liver wet weight % body weight	**6 hr fast**	3.5	3.3	3.6	3.7	2.9		**3.4±0.3**	**3.3±0.7**
	24 hr fast	4.1	5.6	4.8	4	3.7		**4.4±0.8**	**4.3±0.6**

*p<0.05 compared to APAP control

5.3.3 Histology

5.3.3.1 Fed P407 pre-treated 24 hour group

As was observed in APAP-control rats, toxicity was variable within the P407 pre-treated fed group (table 5.2). In contrast to APAP-controls, the hepatocytes often contained larger sized vacuoles and there was increased inflammation particularly in necrotic areas (fig 5.3 A and C). P407 was sometimes observed in the portal venules adjacent to both viable and necrotic centrilobular zones (fig 5.3 B). Glycogen was present in periportal zones of 3 out of the 6 rats, similar to the APAP controls (fig 5.3 C), and sinusoidal collagen was mildly increased compared to APAP controls (fig 5.3 D).

Table 5.2 *Graded necrosis and sinusoidal collagen, glycogen distribution, and serum ALT value for comparison in the P407 pre-treated fed APAP rats 24 hrs after APAP*

Rat	ALT (U/L)	Necrosis	Collagen	Glycogen
1	164.4	+	+	0
2	*no blood*	0	+	0
3	64.8	+	+	PP
4	76.8	0	++	0
5	153.6	0	0	PP
6	1549.2	+++	+	PP

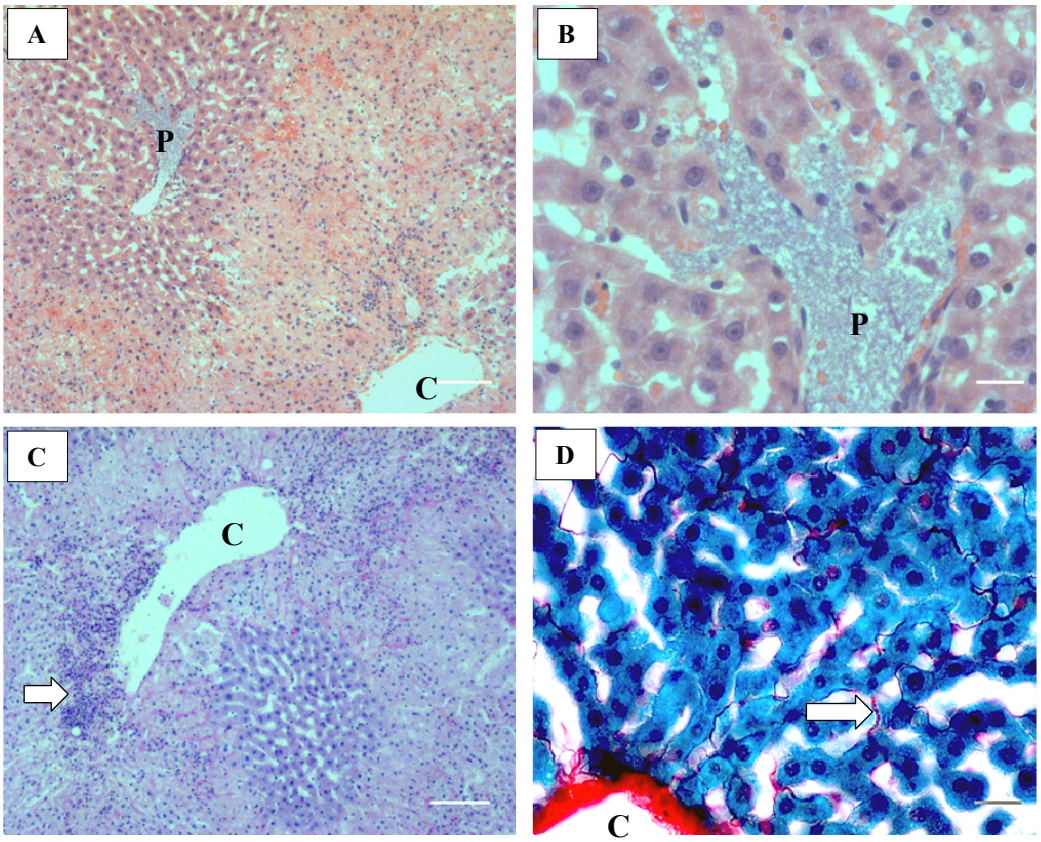

Figure 5.3 *H&E, PAS, and Sirius Red stained sections from Fed P407 pre-treated APAP rats*
A) H&E of an area of high toxicity showing CL hemorrhagic necrosis and a high amount of infiltrate. There is P407 in the portal venule (P) visible as a grey substance and shown magnified in (B). C = central vein. Bar = 100 µm.
B) Magnified view of the portal venule in (A) showing the P407 entering the sinusoids. Bar = 20 µm.
C) PAS. An area of CL necrosis that is glycogen depleted. There is dense infiltrate (arrow) around the central venule and the collapsed reticulin framework around necrotic hepatocytes is stained pink. Bar = 100 µm.
D) Sirius Red counterstained with Fast Green. This section is from a rat with mild hepatotoxicity and increased sinusoidal collagen (arrow). Bar = 20 µm.

5.3.3.2 Fasted P407 pre-treated 6 hour group

At 6 hours after APAP histology was mostly normal apart from some patchy inflammation and mild amounts of vacuolisation of hepatocytes in centrilobular zones (fig 5.4 A). One P407 pre-treated rat displayed mild centrilobular necrosis and severe congestion with sinusoidal dilation and large vacuoles in centrilobular hepatocytes (fig 5.4 B and table 5.3), a level of damage more severe than found in APAP controls at 6 hours. Glycogen was present mainly in a centrilobular and midzonal pattern (fig 5.4 C and table 5.3) which was in contrast to APAP control rats where glycogen was mostly depleted. Sinusoidal collagen increased by a similar amount to APAP controls (fig 5.4 D and table 5.3).

Table 5.3 *Graded necrosis and sinusoidal collagen, glycogen distribution, and serum ALT value for comparison in the P407 pre-treated fasted rats 6 hrs after APAP*

Rat	ALT (U/L)	Necrosis	Collagen	Glycogen
1	36	+	++	PP
2	20.4	0	++	CL and ML
3	30	0	++	CL and ML
4	31.2	0	++	Diffuse
5	26.6	0	++	CL

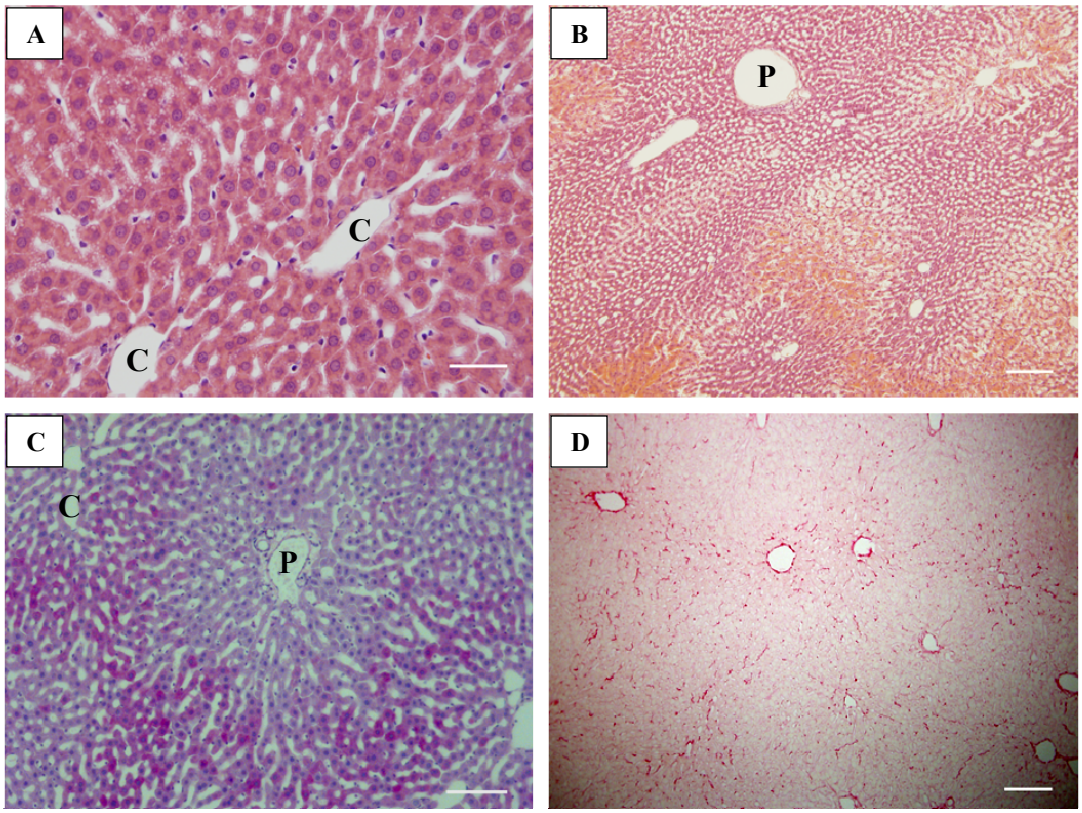

Figure 5.4 *Histology of fasted P407 pre-treated rats at 6 hrs after APAP: H&E, PAS, and Sirius Red*
A) H&E. There is vacuolisation of CL hepatocytes and what appears to be a KC (arrow) full of vacuoles filling the sinusoid lumen. C = central venule. Bar = 50 µm.
B) H&E. There is CL congestion and mild sinusoid dilation. P = portal venule. Bar = 200 µm.
C) PAS. Glycogen is in a CL pattern and PP hepatocytes are depleted. Bar = 100 µm.
D) Sirius Red. Sinusoidal collagen is increased. Bar = 200 µm.

5.3.3.3 Fasted P407 pre-treated 24 hour group

At 24 hours after APAP, P407 pre-treated rats displayed the same type of histological damage to the liver as the APAP control rats (centrilobular hemorrhagic necrosis, congestion, sinusoid dilation, vacuolisation of centrilobular hepatocytes; fig 5.5 A and B) with similar inter and intra lobular variability (table 5.4) although in 3 rats the hepatotoxicity was more severe than APAP controls. There were also larger vacuoles

in hepatocytes, and a greater presence of inflammatory cells particularly in necrotic areas (fig 5.5 C) than the APAP controls. Similar to APAP controls there was also variability in toxicity within the group (table 5.4). In two of the P407 pre-treated rats, the necrosis and congestion was more extreme than the controls. Both of these rats displayed macroscopic hematuria, and on examination of renal histology an unknown substance was observed in the tubules that may have consisted of P407 (see fig 5.10). In contrast, one rat displayed a milder degree of damage than the APAP controls (with histology relatively normal apart from some mild congestion and vacuolisation of centrilobular hepatocytes) and had normal range LFTs. ALT levels ranged from approximately 1 to 370 times the normal average (whereas control APAP rats ranged from 3 to 117 times). Similar to APAP controls, glycogen was present in the periportal zones of 3 out of the 5 rats (fig 5.5 C, table 5.4). Collagen was increased from normal with similar patterns to APAP controls, in the most severely necrotic areas there was mild bridging fibrosis (fig 5.5 D, table 5.4).

Table 5.4 *P407 pre-treated fasted 24 hr group: individual graded centrilobular necrosis in four liver lobes, graded sinusoidal collagen, glycogen distribution, and ALT values for comparison in each rat*

Rat	ALT (U/L)	Grade of Necrosis Per Lobe				Collagen	Glycogen
		Median	Right	Left	Caudate		
1	2210	++	+++	+++	++	+	PP
2	14850	+++	+++	+++	+++	+	N
3	11370	++	+++	++	+++	+	N
4	29	0	0	0	0	+	PP
5	184.8	+	++	+	+	++	PP

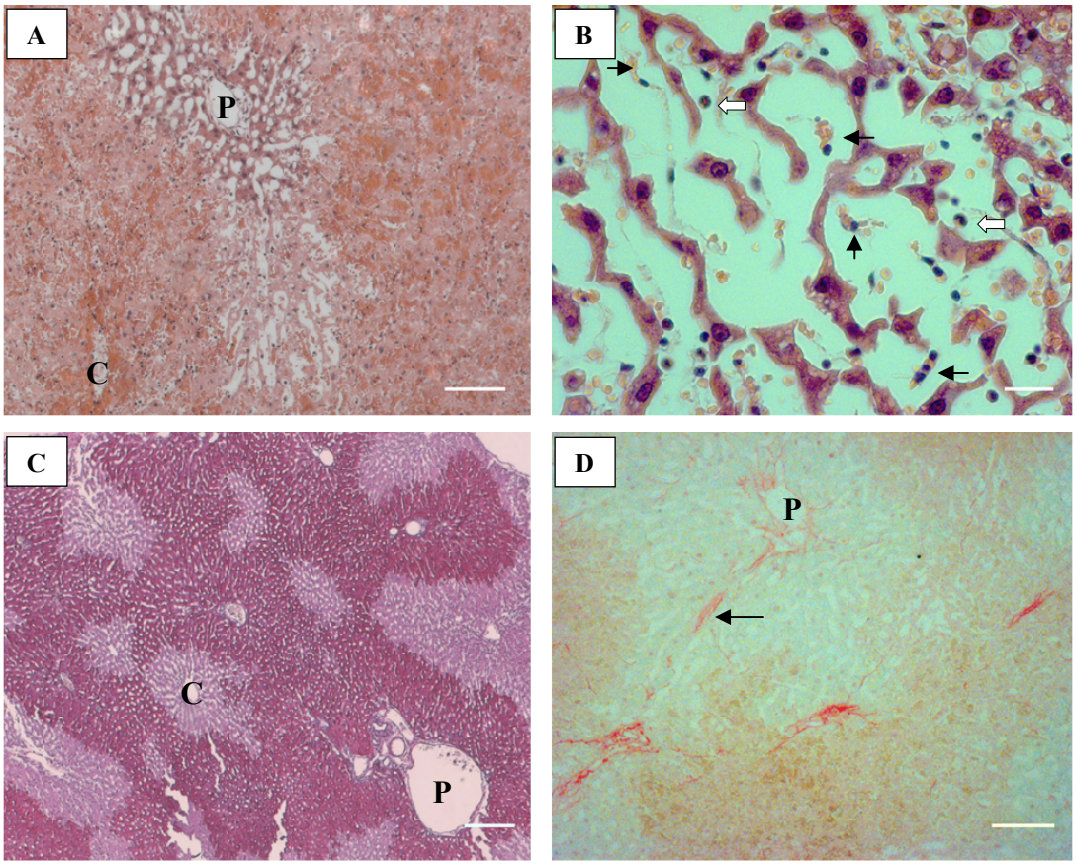

Figure 5.5 *Histology of fasted P407 pre-treated rats 24 hrs after APAP: H&E, PAS, and Sirius Red*
A) H&E. This micrograph shows an area of severe CL hemorrhagic necrosis and sinusoid dilation in a P407 pre-treated APAP rat. The PP zone contains heavily vacuolated hepatocytes (C = central venule, P = portal venule). Bar = 100 µm.
B) H&E. A magnified area of sinusoid dilation is displayed in this micrograph of a P407 pre-treated APAP rat. Arrows point to intact, collapsing sinusoid lumens containing RBCs and leukocytes. LSEC and HSC nuclei are visible in the middle of the grossly enlarged SoD with some attachments to cords of atrophied hepatocytes. Open arrows point to a neutrophil with a multi lobed nucleus (upper arrow) and a monocyte. Bar = 20 µm.
C) PAS. This micrograph taken from a P407 pre-treated APAP rat with moderate hepatotoxicity shows glycogen in a distinct PP pattern with CL hepatocytes glycogen deplete. Bar = 200 µm.
D) Sirius Red. This micrograph shows an area of CL necrosis from a P407 pre-treated APAP rat with high hepatotoxicity. Thick collagen bundles appear to be almost bridging portal tracts (arrow). Bar = 100 µm.

Table 5.5 is a summary of the histological results for centrilobular necrosis, collagen, and glycogen in each group. At 6 hours, P407 pre-treatment mildly increased sinusoidal collagen however did not change the level of histological necrosis from APAP controls. There was glycogen deposition at 6 hours after APAP whereas control APAP rats were depleted of glycogen. At 24 hours after APAP, P407 pre-treatment increased centrilobular necrosis in the fasted rats, whereas it had no effect in the fed rats. There was less sinusoidal collagen in the fasted pre-treated rats than APAP controls however there was increased sinusdoidal collagen in the fed pre-treated rats. Glycogen deposition was unaffected by P407 pre-treatment.

Table 5.5 *Histology summary and comparison table of necrosis, sinusoidal collagen deposition, and glycogen deposition in P407 pre-treated rats from fed and fasted groups*

		Rats raw data							
P407 pre-treated rats	**Group**	**1**	**2**	**3**	**4**	**5**	**6**	**Score**	**APAP control score**
Centrilobular Necrosis	**6 hr fast**	+	0	0	0	0		1/5 = **0.2**	0/6 = **0**
	24 hr fast	+++	+++	+++	0	+		37/25 = **1.4**	32/25 = **1.28**
	24 hr fed	+	0	+	0	0	+++	5/6 = **0.83**	5/6 = **0.83**
Sinusoidal Collagen	**6 hr fast**	++	++	++	++	++		10/5 = **2**	10/5 = **2**
	24 hr fast	+	+	+	+	++		6/5 = **1.2**	7/5 = **1.4**
	24 hr fed	+	+	+	++	0	+	6/6 = **1**	2/6 = **0.33**
Glycogen Deposition	**6 hr fast**	PP	CL&ML	CL&ML	Diffuse	CL		**CL - PP**	**0**
	24 hr fast	PP	0	0	PP	PP		**PP**	**PP**
	24 hr fed	0	0	PP	0	PP	PP	**PP**	**PP**

Note: The score from the 24 hr fasted group is the sum of all '+'s from each lobe (table 5.4) divided by the number of lobes analysed. The data shown for rats 1 - 5 in the 24 hr fasted group is an average estimate (from the four lobes) of the degree of necrosis overall in each rat.

5.3.4 Electron microscopy

5.3.4.1 Fasted P407 pre-treated 6 hour group

There were gaps in LSECs ranging from approximately 0.5 – 2.5 μm in diameter (fig 5.6 A) that were larger and more frequent in the rats with the most histological damage. Parts of LSEC cytoplasms were swollen (on average from 1 – 2 μm) containing large vacuoles and dense bodies and P407 was sometimes observed in the SoD (fig 5.6 B). Inflammatory cells such as neutrophils and monocytes were present throughout the sinusoids (fig 5.6 C).

One rat displayed greater toxicity than any APAP control rat with congestion and mild centrilobular necrosis, although the amount of necrosis was not severe enough to raise serum ALT or AST levels (fig 5.6 D-F). There were platelets and RBCs in the SoD in areas of sinusoid dilation and hepatocyte atrophy. LSECs and HSCs remained tightly associated even though sinusoid lumens were sometimes compressed and oddly shaped (fig 5.6 F).

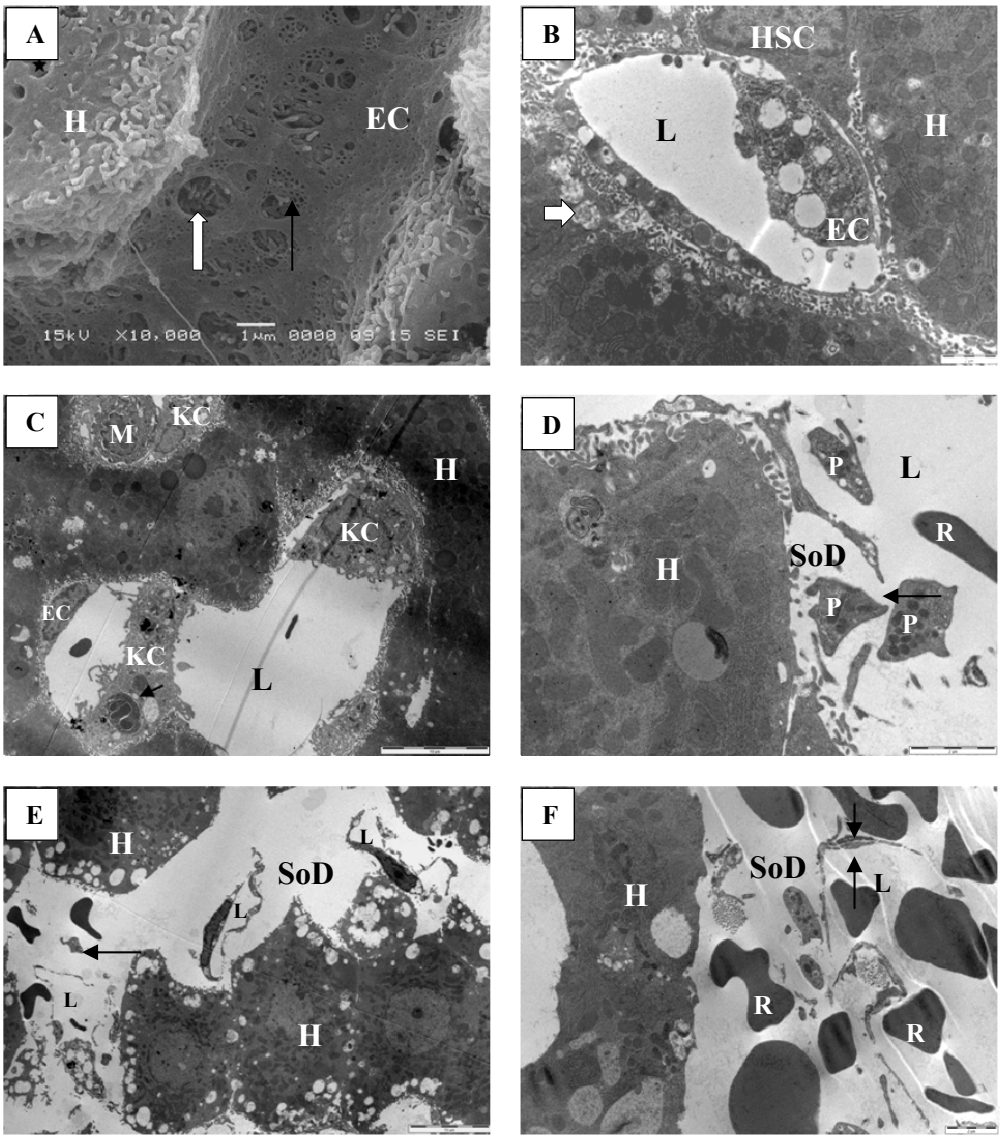

Figure 5.6 *Micrographs of fasted P407 pre-treated rats 6 hrs after APAP*
A) SEM. The LSEC contains gaps (bold arrow) that are replacing the fenestrations in sieve plates (arrow). The hepatocytes contain vacuoles (star; bar = 1 µm).
B) TEM. An activated LSEC (EC) containing many vacuoles and dense bodies is shown in this micrograph. P407 is present in the SoD (arrow) and moving into hepatocyte vacuoles. Bar = 2 µm.
C) TEM. This micrograph shows activated KCs and a monocyte (M) in the sinusoids. A dead neutrophil (arrow) has been phagocytosed by a KC (bar = 10 µm).
D) TEM. In this micrograph, platelets (P) are crossing through a gap in the LSEC cytoplasm (arrow) from the lumen (L) to the SoD. The hepatocyte is losing microvilli (bar = 2 µm).
E) TEM. This micrograph shows sinusoid dilation in a rat with high toxicity. The SoD is enlarged and contains RBCs and platelets (arrow). Sinusoid lumens (L) are collapsing, and the hepatocytes atrophied with many vacuoles (bar = 10 µm).
F) TEM. A close view of an area similar to (E), highlighting the association of LSEC and HSC processes (arrows) where the SoD has expanded and there is total loss of hepatocyte microvilli (bar = 2 µm).

5.3.4.2 Fed and fasted P407 pre-treated 24 hour groups

LSEC viability was decreased in comparison to APAP control rats. There was higher toxicity and LSEC injury in the fasted group than the fed, consistent with APAP control data. There were dead LSECs in areas of moderate toxicity where all or some of the surrounding hepatocytes were not dead (fig 5.9 A and 5.8 D). Necrotic LSECs were associated with masses of fibrin in the areas of highest toxicity (figs 5.7 A and 5.8 A-C). In both fed and fasted groups, sinusoid lumens were significantly decreased in size in necrotic zones and areas of sinusoidal dilation (fig 5.9 B), and often the lumen shape was distorted. The amount of fibrin clots, platelets, and inflammatory cells (including neutrophils, lymphocytes, monocytes, and eosinophils) appeared to be increased compared to APAP controls consistent with the heightened hepatotoxicity in the P407 groups (figs 5.7 A-C and 5.8 A-C) .

In periportal zones and other zones with low toxicity, LSECs were viable and less swollen at 24 hours after APAP compared to 6 hours, with swollen areas ranging up to 4.5 μm and averaging at 1 μm. There were gaps in LSEC cytoplasms ranging from approximately 0.5 - 2 μm (fig 5.7 E), similar to APAP control rats. Overall there was more defenestration in rats at 24 hours than at 6 hours after APAP particularly in the fed group (fig 5.7 D). However the amount of defenestration was similar to control APAP rats and was variable across the liver consistent with the intralobular variability of toxicity. Highly activated KCs were found in periportal sinusoids containing large amounts of cellular debris and full of vacuoles (fig 5.9 C), sometimes occluding sinusoid lumens in the fed group (fig 5.7 F). P407 was present in the SoD and in endocytotic vacuoles of LSECs, KCs, and hepatocytes (figs 5.7 E and 5.9 D).

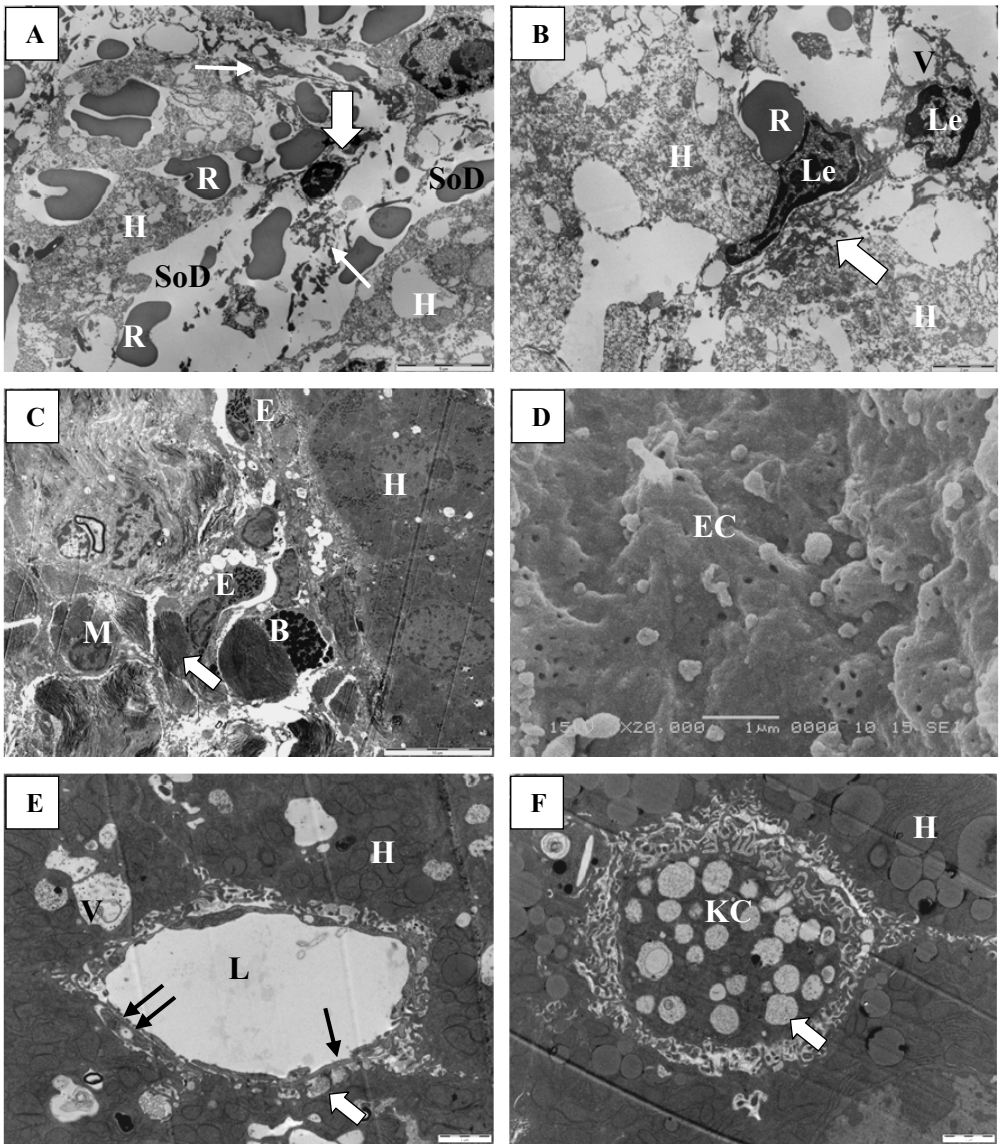

Figure 5.7 *Micrographs of fed P407 pre-treated rats 24 hrs after APAP*
A) TEM reprocessed from paraffin. An area of high toxicity showing a dead LSEC (white arrow) associated with fibrin (arrows). There is hemorrhage of RBCs and the hepatocytes (H) are dead (bar = 5 µm).
B) TEM reprocessed from paraffin. Two cells that appear to be leukocytes (Le), that could have been granulocytes as they contain empty vacuoles (V), are amongst necrotic hepatocytes. One appears to be squeezing through the hepatocytes and adjacent to fibrin (arrow). Bar = 2 µm.
C) TEM. A portal tract with increased interstitium (open arrow points to an example of a collagen bundle) and both granular and agranular leukocytes are making their way to the sinusoids. Monocyte = M, eosinophil = E, basophil = B (bar = 10 µm).
D) SEM. The LSEC (EC) contains less fenestrations than normal (bar = 1 µm).
E) TEM. An area of mild toxicity. There is P407 in the SoD (bold arrow) and hepatocyte vacuoles (V). The double arrows point to a sieve plate in an LSEC and the single arrow a gap in the LSEC exposing the underlying HSC process (bar = 2 µm).
F) TEM. A large activated KC filling a sinusoid lumen containing vacuoles (bold arrow) that may include P407. The hepatocytes (H) are mildly steatotic (bar = 2 µm).

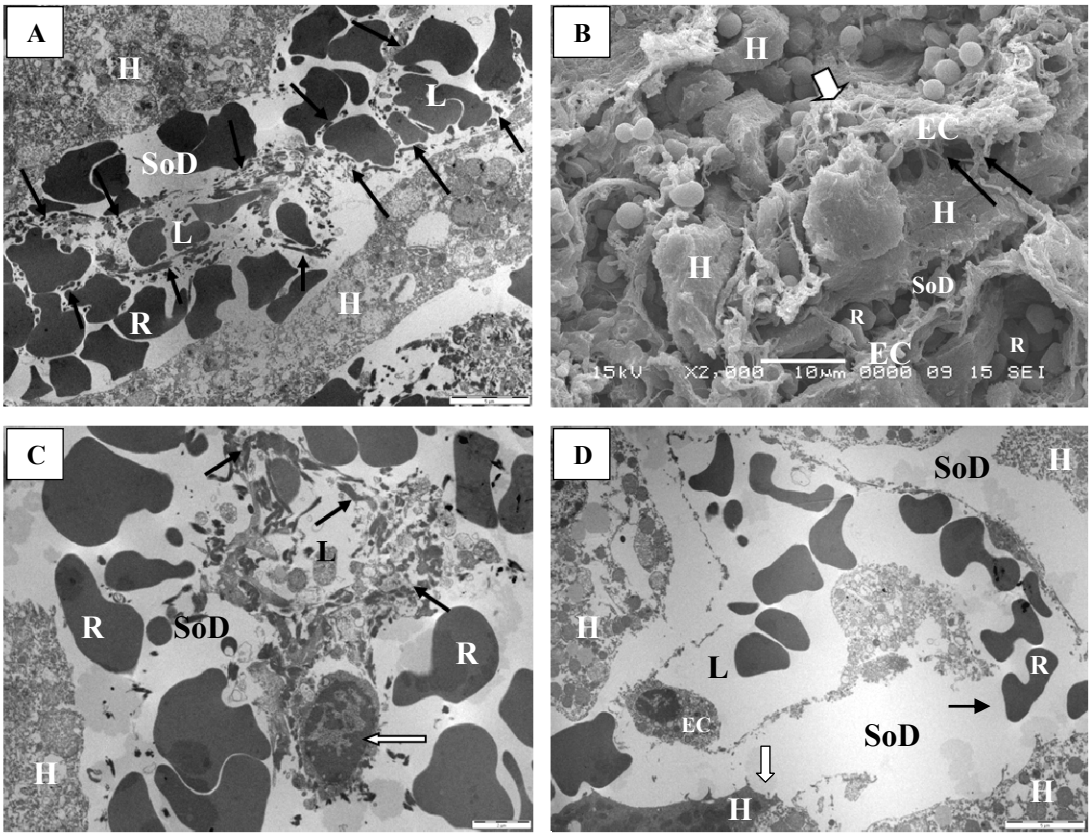

Figure 5.8 *Micrographs of necrotic LSECs from fasted P407 pre-treated rats in areas of CL hepatocyte necrosis*
A) TEM. In this micrograph, fibrin is associated with a necrotic LSEC (arrows). The sinusoid lumen (L) is collapsed, RBCs have hemorrhaged, and the surrounding hepatocytes (H) are necrotic (bar = 5 µm).
B) SEM. A 3-dimensional representation of the micrograph "A". The white arrow points to a fibrin clot associated with a dead LSEC (EC). There are RBCs (R) in the SoD and there appear to be processes (arrows) through the SoD from atrophied hepatocytes (H) to the degenerate LSECs (EC) (bar = 10 µm).
C) TEM. Fibrin (arrows) is associated with a dying LSEC with condensing chromatin (white arrow) in a CL zone of hepatocyte necrosis. There is severe hemorrhage and the sinusoid lumen is collapsed (bar = 2 µm).
D) RBCs are flowing to the SoD through a gap in a damaged LSEC cytoplasm (arrow). The LSEC and surrounding hepatocytes (H) are pale and necrotic, apart from the hepatocyte that is in a process of degeneration marked by a white arrow (bar = 5 µm).

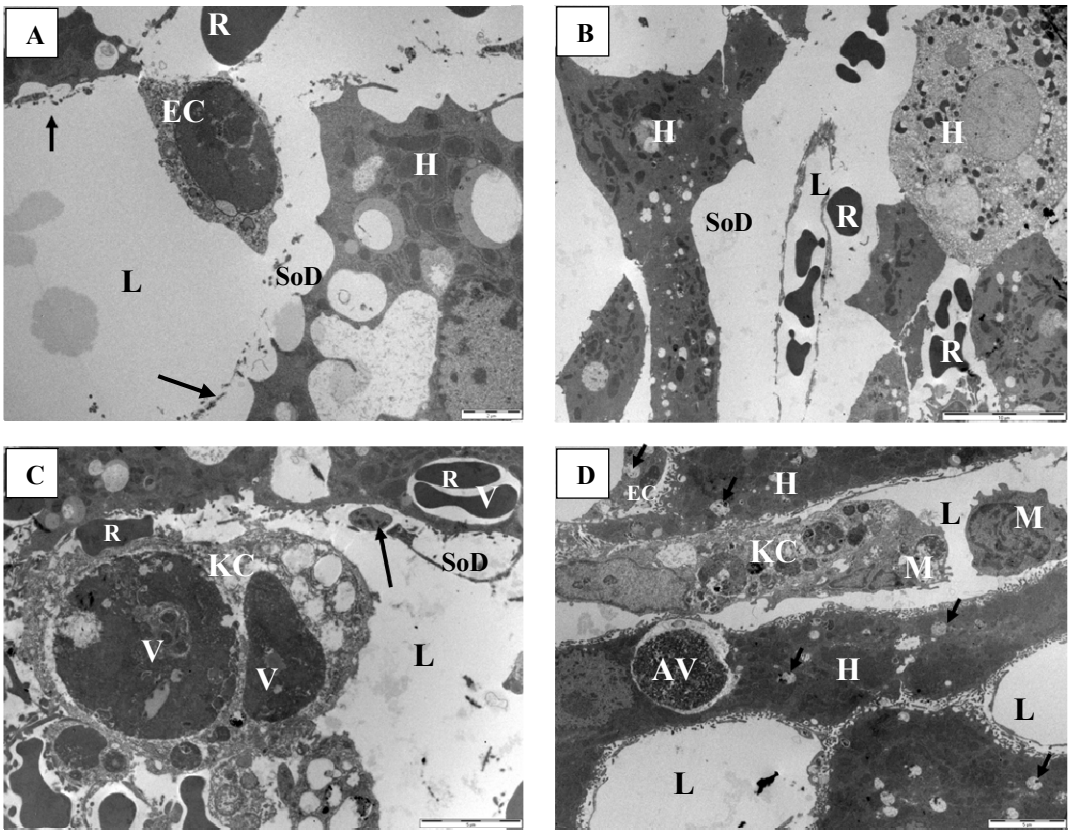

Figure 5.9 *Transmission electron micrographs of fasted P407 pre-treated rat sinusoids in areas of moderate and low toxicity at 24 hrs after APAP including a necrotic LSEC*

A) A dead LSEC with condensed chromatin (arrow) in a CL zone where hepatocytes (H) are degenerating but not yet necrotic. Arrows point to the remnants of the LSEC cytoplasm. L = sinusoid lumen, R = RBC (bar = 2 μm).

B) This micrograph displays sinusoid dilation. The sinusoid lumen is compressed and the SoD is enlarged. The hepatocytes are atrophied and degenerating and there are RBCs in the SoD. The pale hepatocyte is dead and its nucleus has undergone karyolysis (bar = 10 μm).

C) An activated KC in a sinusoid lumen contains large vacuoles (V) full of cellular debris. An arrow points to a platelet in the SoD and the adjacent hepatocyte has endocytosed two RBCs that are contained in a vacuole (V; bar = 5 μm).

D) An area of low toxicity showing an autophagic vacuole (AV) in a hepatocyte. The sinusoid lumen contains an activated KC and two leukocytes that may be monocytes (M), one of which appears to be attached to the KC. The LSEC (EC) in the top left hand corner is swollen and has vacuoles that appear to contain P407, as do the hepatocytes (arrows; bar = 5 μm).

Ultrastructural analysis of the renal cortex and medulla did not reveal any nephrotoxicity. The glomeruli were normal and there was no tubular necrosis, however there was an unknown globular substance particularly in the distal tubules and in the collecting tubules that may have been comprised of P407 (fig 5.9). Refer to Appendix 5, A11 for micrographs of APAP control and untreated F344 kidneys.

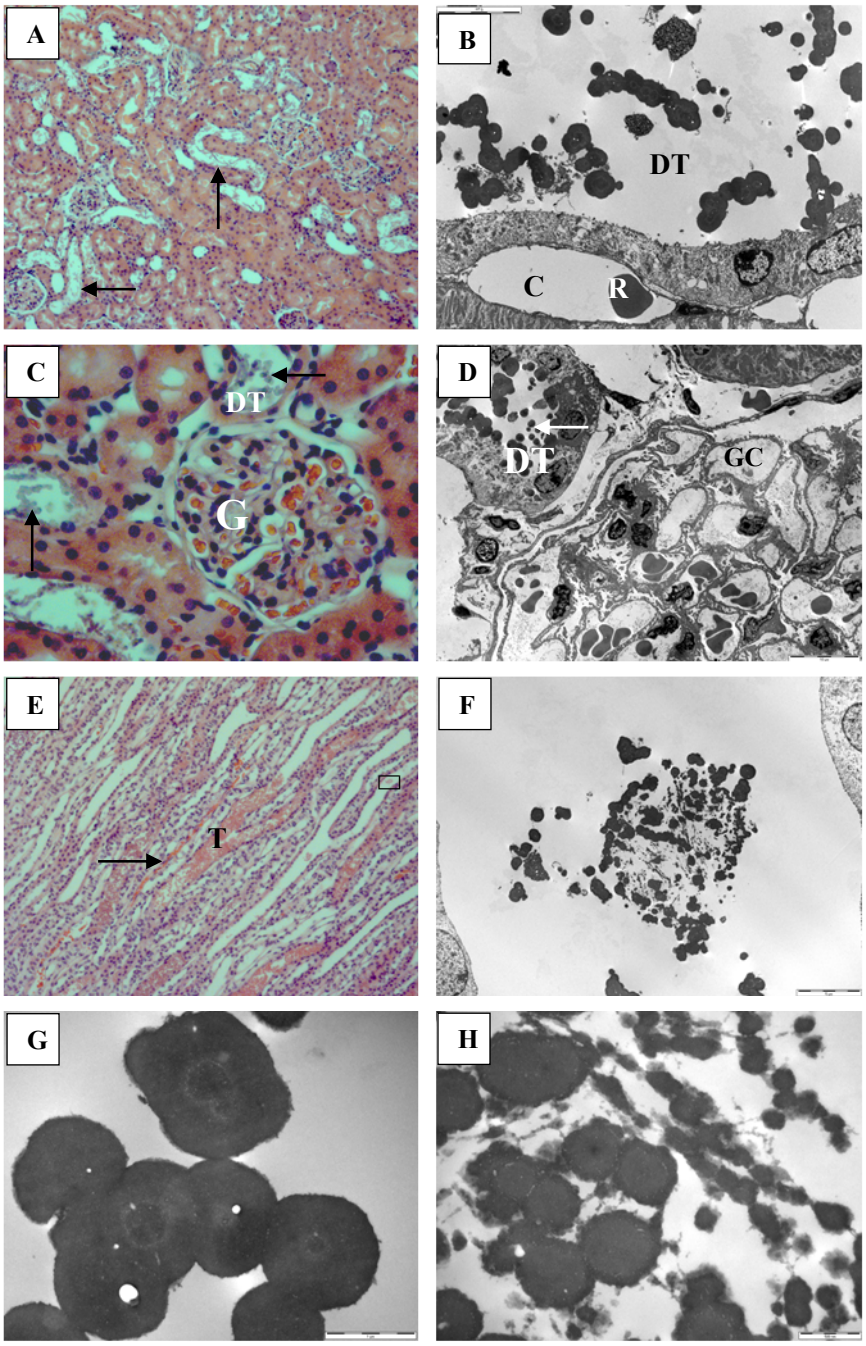

Figure 5.10 *Renal histology and electron micrographs from a fasted P407 pre-treated rat with hematuria at 24 hrs after APAP*
A) H&E stain showing renal histology is normal in the renal cortex apart from an unknown substance (arrows) present in many of the distal tubules. Bar = 100 µm.
B) Electron micrograph of a section of renal cortex showing the presence of a globular substance and some cellular debris in the distal tubules (DT). A peritubular capillary (C) contains a RBC (bar = 5 µm).
C) H&E stained section of a normal glomerulus (G) in the renal cortex. The distal tubules (DT) contain an unknown substance (arrows). Bar = 20 µm.
D) Electron micrograph of a similar section to fig (C). The distal tubule (DT) contains a globular substance (arrow), and the glomerulus appears normal (GC = glomerular capillary; bar = 10 µm). See fig G for a close view of the unknown substance.

E) H&E stained section from the renal medulla showing the same globular substance in the collecting tubules (T). An arrow points to a capillary, and an electron micrograph of the boxed area is shown in fig (F). Bar = 100 μm.
F) Electron micrograph showing the lumen of a collecting tubule in the renal medulla. A globular substance is present as well as some cellular debris (bar = 5 μm). Refer to fig (H) for a closer view.
G) Magnified view of the globular substance viewed in the tubules of the renal cortex (bar = 1 μm).
H) Magnified view of the globular substance viewed in the tubules of the renal medulla (bar = 500 nm).

5.3.5 Summary of P407 pre-treated rats

Pre-treatment with P407 did not protect the liver from APAP toxicity, and damage was exacerbated in some rats. Although there was defenestration of LSECs, it was not strikingly different to the amount of defenestration in APAP control rats, and gap formation was not inhibited. At 6 hours after APAP, livers appeared to have sustained damage similar to control APAP rats except in one rat where damage was increased. At 24 hours after APAP, fibrin clots and inflammation were increased in the P407 pre-treated groups compared to controls, and there was an increase in LSEC necrosis. The hepatotoxicity and LSEC injury was heightened in fasted rats. Refer to table 5.11, section 5.4.5 for a summary of the trends in results including electron microscopy.

5.4 Results: P407 post-treated rats

5.4.1 Macroscopic observations

At 6 and 24 hours after APAP the rats were sleepy and sedate. One rat from the fasted 24 hour P407 post-treated group had macroscopic hematuria.

5.4.2 Blood analysis

5.4.2.1 Fed P407 post-treated 24 hour group

All P407 post-treated blood samples were lipemic. ALT and AST averages were lower than controls although not significantly lower. This could have been because of variability in the APAP control group and the fact that there was no serum sample from one rat with severe hepatotoxicity. Total bilirubin was significantly lower than APAP control (table 5.6). These results suggest that there was less hepatotoxicity in the P407 post-treated rats, and that the P407 had a protective effect.

5.4.2.2 Fasted P407 post-treated 6 and 24 hour groups

At 6 and 24 hours after APAP, serum ALT, AST, and bilirubin levels were not significantly different to APAP control rats (table 5.6). Triglycerides and cholesterol were significantly increased at 24 hours after APAP, but were only mildly increased at 6 hours after APAP. Weight loss and hematocrit were significantly lower than APAP controls at 24 hours after APAP however there was no difference in average liver weight between P407 post-treated and APAP control groups (table 5.6).

Table 5.6 *Raw and mean ± S.D. data from ad libitum fed or fasted APAP treated rats culled 6 or 24 hrs after APAP and post-treated with P407 1 hr after APAP*

		Rats raw data							
P407 post-treated rats	**Group**	**1**	**2**	**3**	**4**	**5**	**6**	**Mean ± SD**	**APAP Control**
ALT (U/L)	**6 hr fast**	46	47	70	52	162		**75±49**	**45±7.2**
	24 hr fast	30	50.4	217	12420			**3179±6161**	**2143±2296**
	24 hr fed	31.2	33.6	27.6	36	46.8	38.4	**36±6.6**	**171.2±297**
AST (U/L)	**6 hr fast**	75	81	100	156	175		**117±45**	**81.4±16.4**
	24 hr fast	84	61.6	270	25479			**6474±12671**	**3008±3473**
	24 hr fed	60	62.4	70.8	130.8	61.2	62.4	**74.6±28**	**155.4±172**
Total Bilirubin (U/L)	**6 hr fast**	0	1	0	1	2		**0.8±0.8**	**1±0**
	24 hr fast	0	4.2	2	6			**3.1±2.6**	**2±0.7**
	24 hr fed	1.2	0	1.2	1.2	1.2	0	**0.8±0.6***	**3.4±1.8**
% Weight loss from time of fast	**6 hr fast**	5.1	no data	no data	5.5	6.9		**6±1**	**7.5±1.9**
	24 hr fast	10.4	no data	7.4	10.8			**9.5±2***	**13±1.7**
% Weight loss	**24 hr fed**	5.3	6.3	6.9	3.8	4.8	4.4	**5.3±1.2**	**4.6±0.5**
Total cholesterol (µmol/L)	**6 hr fast**	1.3	1.3	3.8	1.5	1.5		**2±1**	**1.3±0.1**
	24 hr fast	5.6	10.5	5	8.1			**7±2.5***	**1.1±0.2**
Triglycerides (µmol/L)	**6 hr fast**	1.1	1	19.5	1.4	1.1		**5±8**	**0.8±0.2**
	24 hr fast	26	64.8	16.7	45.4			**38±21***	**0.7±0.5**
Hematocrit (%)	**6 hr fast**	62	55	no data	58	56		**57.6±3**	**59.5±2.7**
	24 hr fast	53	48	54	50			**51±3***	**62±8**
Liver wet weight % body weight	**6 hr fast**	2.4	3.2	2.9	3.2	3.3		**3±0.3**	**3.3±0.7**
	24 hr fast	5	3.5	3.7	3.9			**4±0.7**	**4.3±0.6**

*p<0.05 compared to APAP control

5.4.3 Histology

5.4.3.1 Fed P407 post-treated 24 hour group

The fed P407 post-treated rats sustained much less histological damage than APAP controls (table 5.7). Five out of 6 rats did not show any necrosis (fig 5.11 A), with one rat displaying only a very mild amount of centrilobular necrosis accompanied by a large amount of infiltrate (fig 5.11 B). Occasionally there was vacuolisation of centrilobular hepatocytes. There was also a striking difference to APAP controls in the distribution of glycogen (table 5.7). The majority of glycogen in the livers was in the centrilobular and midzonal hepatocytes (fig 5.11 C), in comparison to APAP

control rats where glycogen was mostly depleted or found in the periportal hepatocytes. Glycogen in the P407 post-treated group was depleted only in the rat that sustained a low degree of histological damage. In 3 rats, sinusoidal collagen was mildly increased (fig 5.11 D, table 5.7) in comparison to control APAP rats where only 2 out of 6 rats had mildly increased collagen.

Table 5.7 *Graded necrosis and sinusoidal collagen, glycogen distribution, and serum ALT value for comparison in the P407 post-treated fed APAP rats 24 hrs after APAP*

Rat	ALT (U/L)	Necrosis	Collagen	Glycogen
1	31.2	0	+	CL
2	33.6	0	0	CL
3	27.6	0	0	CL
4	36	0	0	CL
5	46.8	0	+	Diffuse
6	38.4	+	+	Deplete

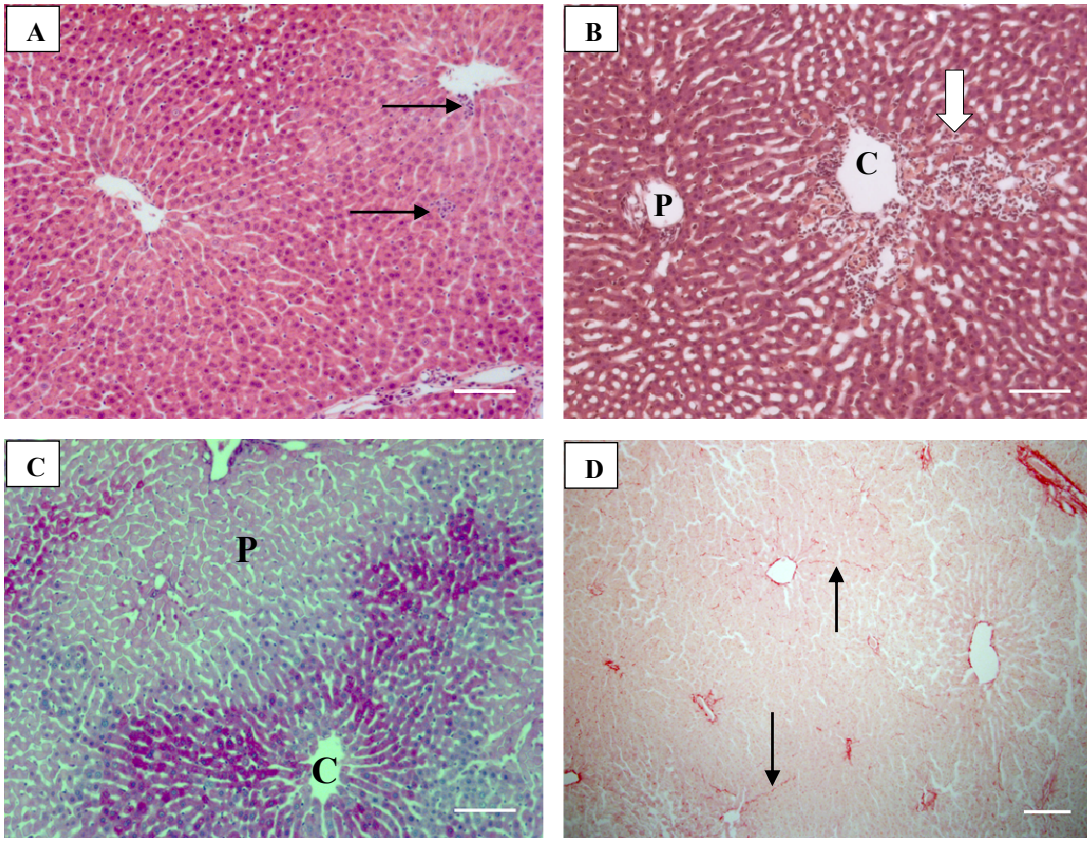

Figure 5.11 *Histology of P407 post-treated fed rats: H&E, PAS, and Sirius Red*
A) H&E. Normal histology, apart from some mild patchy inflammation (arrows) and mild vacuolisation of hepatocytes. Bar = 100 µm.
B) H&E. An example of the most severe CL toxicity in a fed P407 post-treated APAP rat, mild necrosis accompanied by infiltrate (arrow). P = portal, C = central. Bar = 100 µm.
C) PAS. There is a distinct pattern of CL glycogen staining with PP hepatocytes depleted. Bar = 100 µm.
D) Sirius Red. There is a mild increase of sinusoidal collagen in this micrograph, mainly in CL zones. Arrows point to examples of thick collagen fibres. Bar = 200 µm.

5.4.3.2 Fasted P407 post-treated 6 hour group

At 6 hours after APAP, 4 out of 5 livers were histologically normal (fig 5.12 A). The fifth rat sustained damage to two lobes (left lateral lobe and right lobe) including mild necrosis, sinusoid dilation, and congestion in some centrilobular zones (fig 5.12 B, table 6.5). There was increased glycogen in the P407 post-treated rats compared to the APAP control rats, and the zonal distribution of glycogen in the group was variable (fig 5.12 C-E, table 5.8). Sinusoidal collagen was increased (fig 5.12 F) although not quite as much on average as in APAP control rats (table 5.8).

Table 5.8 *Graded necrosis and sinusoidal collagen, glycogen distribution, and serum ALT value for comparison in the P407 post-treated fasted rats 6 hrs after APAP*

Rat	ALT (U/L)	Necrosis	Collagen	Glycogen
1	46	0	++	Diffuse
2	47	0	++	Mild/diffuse
3	70	0	+	CL
4	52	0	++	Diffuse
5	162	+	+	PP

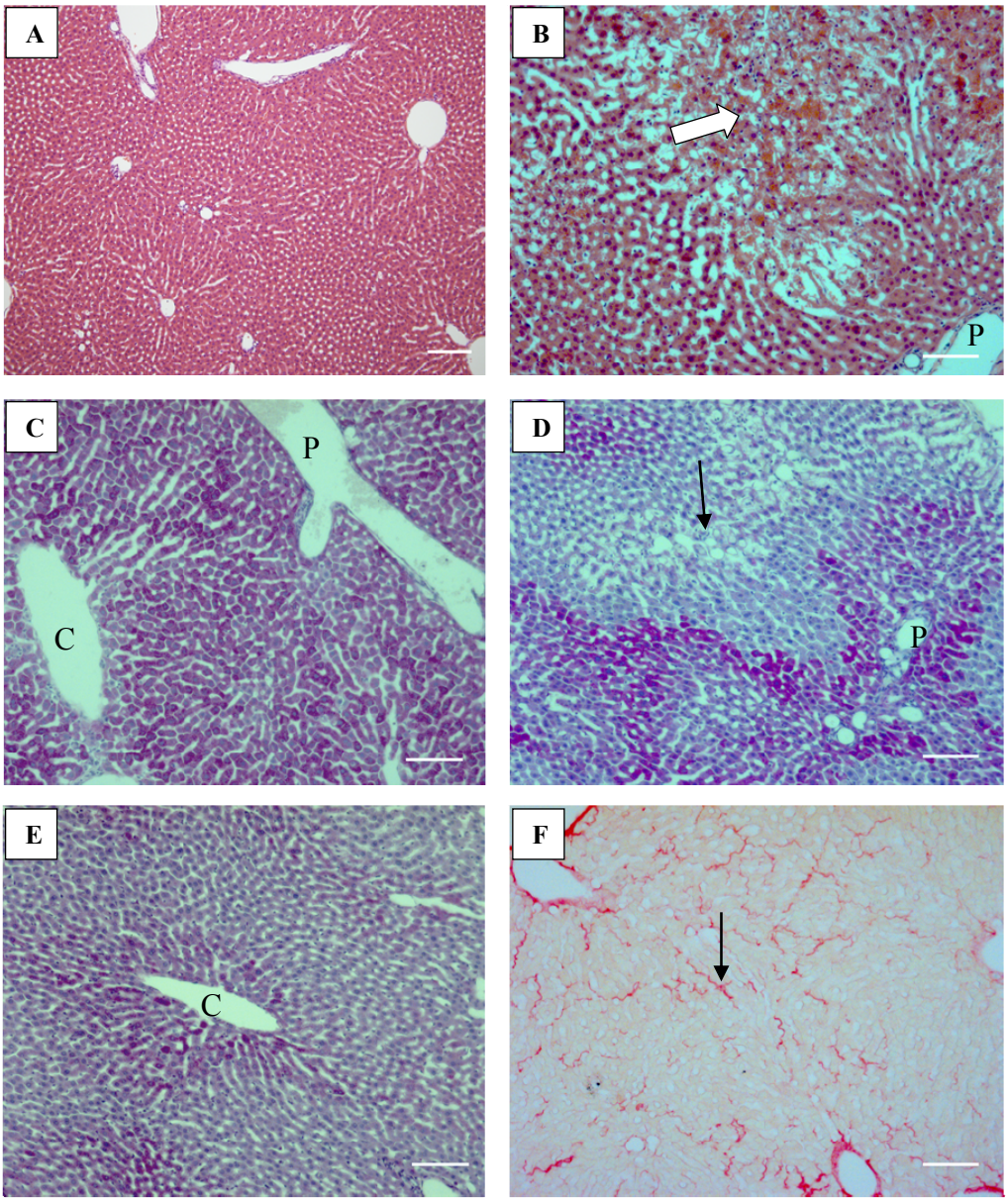

Figure 5.12 *Histology of 6 hr fasted P407 post-treated APAP rats- H&E, PAS, and Sirius Red*
A) H&E. An example of normal histology representative of most rats in this group. Bar = 200 µm.
B) H&E. A micrograph from the rat with mild toxicity consisting of congestion, sinusoid dilation, and CL necrosis (arrow). P = portal venule. Bar = 100 µm.
C) PAS. A micrograph showing diffuse glycogen distribution. C = central venule. Bar = 100 µm.
D) PAS. A micrograph from the rat with mild toxicity showing a CL zone with sinusoid dilation (arrow). There is glycogen in the PP hepatocytes. Bar = 100 µm.
E) PAS. A micrograph showing a pattern of CL glycogen and PP glycogen depletion. Bar = 100 µm.
F) Sirius Red stain showing increased sinusoidal collagen (arrow) compared to a normal rat (graded ++). Bar = 100 µm.

5.4.3.3 Fasted P407 post-treated 24 hour group

At 24 hours after APAP, 3 rats displayed a mild to moderate level of damage including variable amounts of vacuolisation of centrilobular hepatocytes, infiltrate around central veins (fig 5.13 A), and some centrilobular sinusoidal dilation and mild amounts of necrosis (fig 5.13 E). Swollen LSECs and large KCs full of clear vacuoles were visible in the sinusoids (fig 5.13 D) due to the endocytosis of P407.

The remaining rat displayed severe centrilobular hemorrhagic necrosis in two lobes reflective of the extremely high ALT and AST level (fig 5.14 A) and mild to moderate damage in the other two. Overall, it appears that there was less hepatotoxicity than in the APAP control rats however it is difficult to determine because there was a wide range of hepatotoxicity from mild to severe in both control and treatment groups.

It appears that there was a significant effect of P407 (or a combined effect of P407 and APAP) on glycogen metabolism. There was increased glycogen in the P407 post-treated rats (fig 5.13 B, table 5.9) compared to the APAP control rats. The zonal distribution of glycogen was variable (figs 5.13 B-C and 5.14 B, table 5.9).

Sinusoidal collagen was increased from normal (figs 5.13 F and 5.14 C-D, table 5.9), and on average, mildly increased compared to APAP controls. There was also intra and inter lobular variability of collagen deposition, reflective of the variability of toxicity in each lobule.

Table 5.9 *P407 post-treated fasted 24 hr group: individual graded centrilobular necrosis in four liver lobes, graded sinusoidal collagen, glycogen distribution, and ALT values for comparison in each rat*

Rat	ALT (U/L)	Graded necrosis per lobe				Collagen	Glycogen
		Median	Right	Left lateral	Caudate		
1	30	+	0	0	0	+	diffuse
2	50.4	0	+	0	+	+	CL or ML
3	217	+	+	+	0	++	PP
4	12420	+++	+++	+	0	++	depleted

Renal histology was normal in all P407 post-treated rats except for one. The rat with severe hepatotoxicity in the 24 hour group had an unknown substance in the collecting tubules of the medulla that appeared identical to that described in figure 5.10 in the pre-treated rats (fig 5.14 E and F). There was no sign of tubular necrosis. See Appendix 5, A11 for a micrograph of an APAP control kidney.

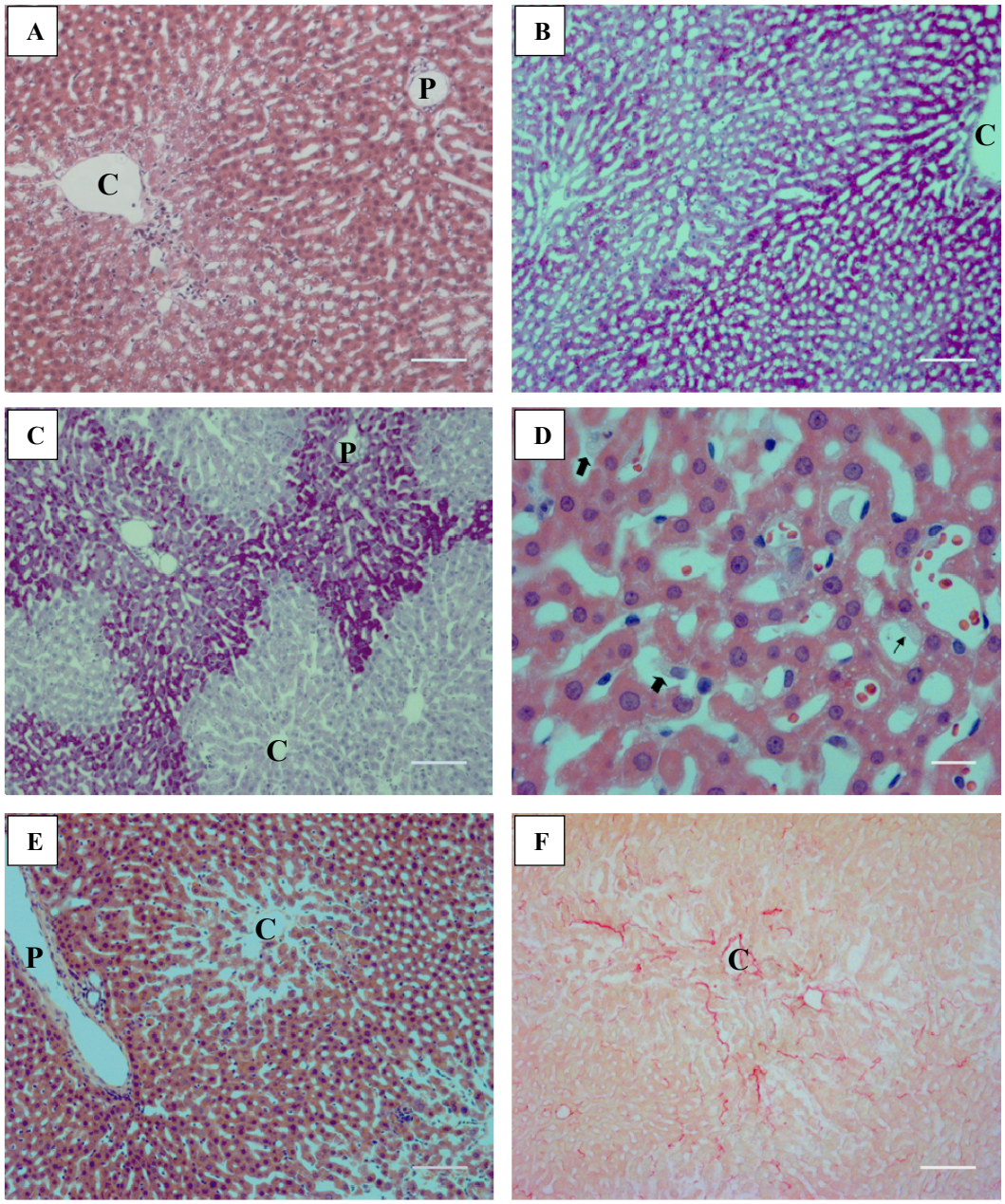

Figure 5.13 *Histology of P407 post-treated fasted rats 1, 2, and 3 (with mild toxicity) 24 hrs after APAP: H&E, PAS, and Sirius Red*
A) H&E. Mild CL damage, hepatocyte vacuolisation and infiltrate. C = central, P = portal. Bar = 100 µm.
B) PAS. A micrograph from the rat with diffuse glycogen staining. Bar = 100 µm.
C) PAS. A micrograph from the rat with PP glycogen. Bar = 100 µm.
D) H&E. Bold arrows point to possible KCs swollen with vacuoles and a swollen vacuolated LSEC is marked with a regular arrow. Hepatocytes are showing endocytosis of P407 and lipid throughout the sinusoids. Bar = 20 µm.
E) H&E. An example from a rat with mild toxicity showing sinusoid dilation in a CL zone. Bar = 100 µm.
F) Sirius red. There is increased collagen in a CL zone where there is mild toxicity and sinusoid dilation. Bar = 100 µm.

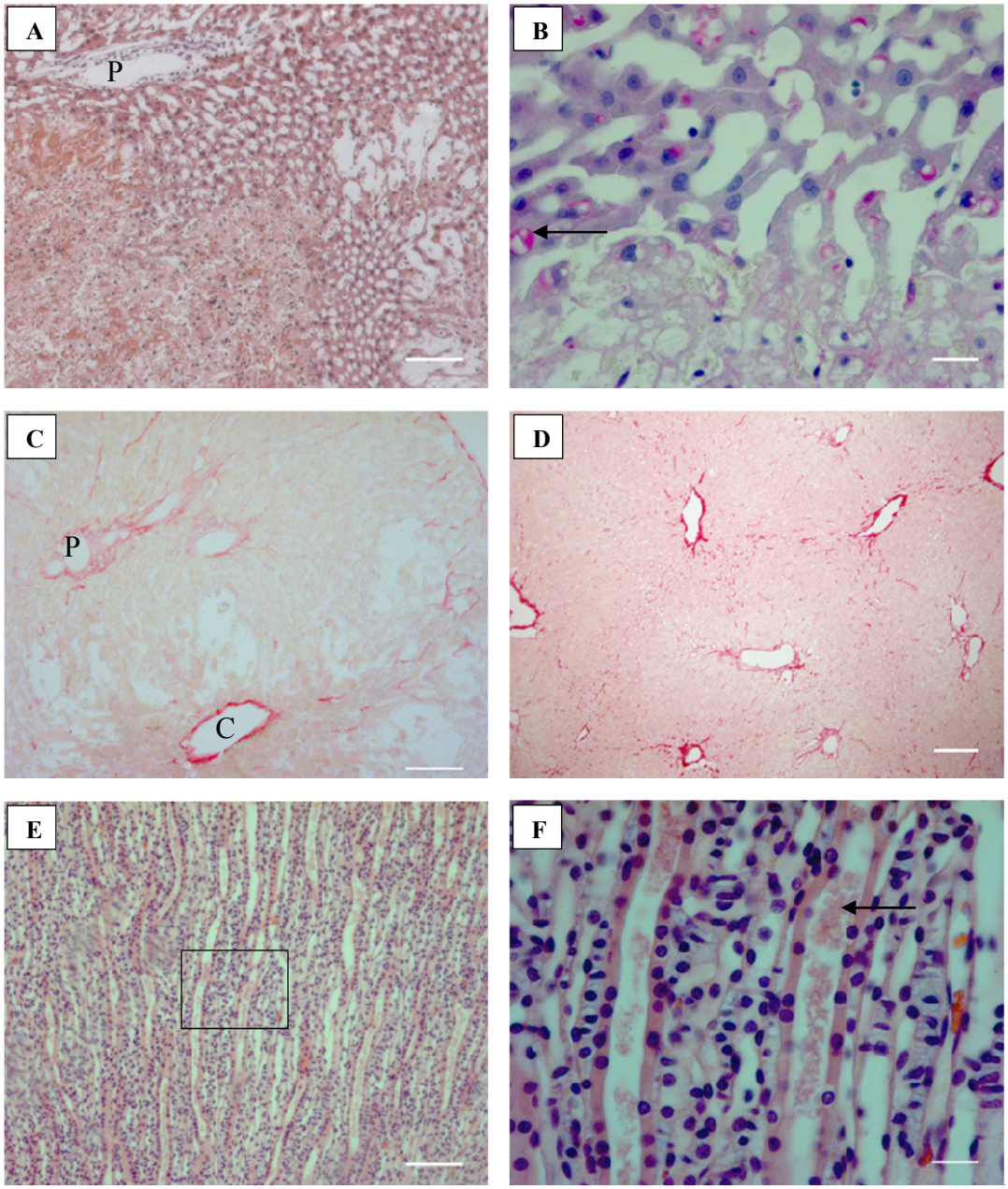

Figure 5.14 *Liver and kidney histology of the fasted 24 hr post-treated APAP rat with extreme hepatotoxicity: H&E, PAS, and Sirius Red*
A) H&E. Severe CL hemorrhagic necrosis and sinusoid dilation. P = portal venule. Bar = 100 µm.
B) PAS. The border of a necrotic area is glycogen deplete, however there are magenta stained vacuoles (arrow) in hepatocytes of unknown origin. Bar = 20 µm.
C) Sirius Red. A necrotic area showing long thick collagen bundles stretching from the central venule and portal tracts. P = portal and C = central venule. Bar = 100 µm.
D) Sirius Red. Increased collagen deposition in a non-necrotic area with collagen bundles appearing to radiate from one venule to another. Bar = 200 µm.
E) H&E. The renal collecting tubules contain a substance that could be a mixture of P407, and/or remnants of RBCs and other cellular debris. Bar = 100 µm.
F) H&E. A magnified view of the boxed area in fig (E). An arrow points to the unknown substance in the tubules. Bar = 20 µm.

Table 5.10 is a summary of the histological results for centrilobular necrosis, collagen, and glycogen in each post-treated group. At 6 hours after APAP, P407 post-treatment mildly increased sinusoidal collagen compared to APAP control, whilst decreasing level of histological necrosis. There was glycogen deposition at 6 hours after APAP whereas control APAP rats were depleted of glycogen. At 24 hours after APAP, P407 post-treatment decreased centrilobular necrosis in the fasted and fed rats. Sinusoidal collagen slightly increased compared to APAP controls in the fasted and fed rats. Glycogen deposition was affected by P407 pre-treatment in both fed and fasted groups at 24 hours after APAP. In fed P407 post-treated rats, glycogen deposition was found in centrilobular regions as well as periportal, and in the fed P407 post-treated rats, glycogen distribution was primarily in centrilobular regions whereas the APAP control rats expressed glycogen in periportal zones only.

Table 5.10 *Histology summary and comparison table of necrosis, sinusoidal collagen deposition, and glycogen deposition in P407 post-treated rats from fed and fasted groups*

		Rat raw data							
P407 post-treated rats	**Group**	**1**	**2**	**3**	**4**	**5**	**6**	**Score**	**APAP control score**
Centrilobular Necrosis	**6 hr fast**	0	0	0	0	+		1/5 = **0.2**	0/6 = **0**
	24 hr fast	0	+	+	+++			13/20 = **0.65**	32/25 = **1.28**
	24 hr fed	0	0	0	0	0	+	1/6 = **0.16**	5/6 = **0.83**
Sinusoidal Collagen	**6 hr fast**	++	++	+	++	+		8/5 = **1.6**	10/5 = **2**
	24 hr fast	+	+	++	++			6/4 = **1.5**	7/5 = **1.4**
	24 hr fed	+	0	0	0	+	+	3/6 = **0.5**	2/6 = **0.33**
Glycogen Deposition	**6 hr fast**	Diffuse	Mild/ diffuse	CL	Diffuse	PP		**CL - PP**	**0**
	24 hr fast	Diffuse	CL or ML	PP	0			**CL - PP**	**PP**
	24 hr fed	CL	CL	CL	CL	Diffuse	0	**CL**	**PP**

Note: The score from the 24 hr fasted group is the sum of all '+'s from each lobe (table 5.9) divided by the number of lobes analysed. The data shown for rats 1 - 4 in the 24 hr fasted group is an average estimate (from the four lobes) of the degree of necrosis overall in each rat.

5.4.4 Electron microscopy

5.4.4.1 Fed P407 post-treated 24 hour group

There was some defenestration of LSEC in all of the fed post-treated rats 24 hours after APAP. The defenestration was variable across the liver lobes such that some LSECs were almost completely defenestrated (fig 5.15 B) however other LSECs were normally fenestrated (fig 5.15 D). Overall there was more defenestration than found in APAP controls and defenestration was also apparent in viable areas of the liver lobe. Only occasionally there were gaps. Some LSEC cytoplasms contained vacuoles that included P407 micelles (fig 5.15 A and C) as did KCs (fig 5.15 E) as seen in histology. The P407 micelles were also present throughout the SoD in many of the sinusoids analysed (fig 5.15 A). Occasionally there were neutrophils in sinusoid lumens. In the one rat with histological damage, areas of centrilobular necrosis were few and thus none were sampled in the randomly cut blocks processed for electron microscopy. Therefore, blocks were reprocessed from paraformaldehyde-fixed tissue in paraffin for transmission electron microscopy analysis. Large amounts of leukocytes were found in and around the central venules (fig 5.16 A), greater than seen in an area of mild centrilobular necrosis any APAP control. Extravasation of infiltrate through gaps in LSEC cytoplasms was visible (fig 5.16 B). Close to the central venule, hepatocytes appeared to be absent. This may have been due to efficient clearing of necrotic hepatocytes by the infiltrate, or due extraction of loose necrotic cellular debris during reprocessing from paraffin. The LSECs appeared to be viable, although fixation was not as clear as glutaraldehyde was not used in the fixation process and intricate analysis of LSEC ultrastructure was not possible. Midlobular and periportal hepatocytes and LSECs were viable, with some mild vacuolisation of hepatocytes close to the necrotic zones (fig 5.16 C).

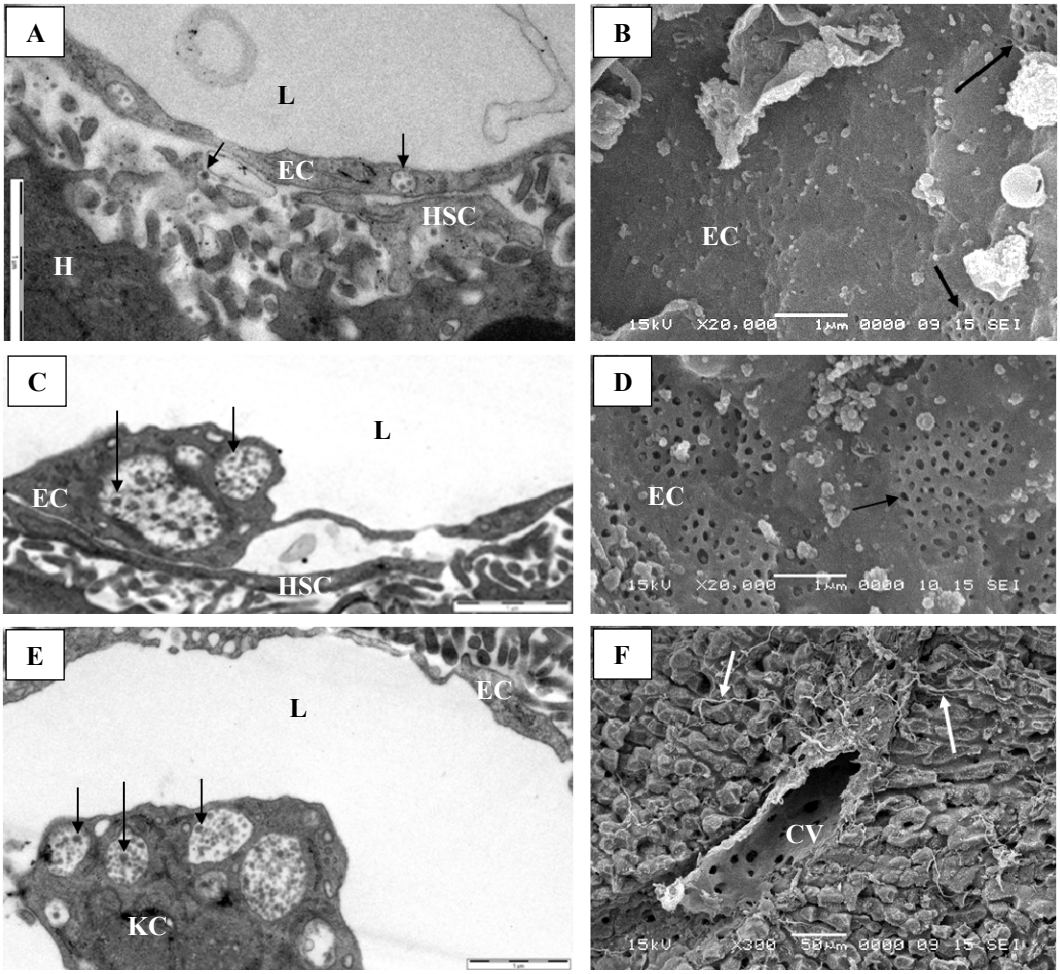

Figure 5.15 *Electron micrographs from fed P407 post-treated rats 24 hrs after APAP*
A) TEM. A defenestrated LSEC (EC) contains vacuoles that include P407 micelles (arrow). There are also P407 micelles in the SoD (arrow). L = lumen, H = hepatocyte. Bar = 1 µm.
B) A representative SEM of (A). Arrows point to two remaining sieve plates in a severely defenestrated LSEC (bar = 1 µm).
C) TEM. Part of the LSEC (EC) cytoplasm is very swollen with vacuoles containing what appear to be P407 micelles (arrows). Bar = 1 µm.
D) SEM. A normally fenestrated LSEC from a P407 post-treated rat. An arrow points to a sieve plate. Bar = 1 µm.
E) TEM. A KC in a sinusoid lumen with vacuoles that appear to include P407 (arrows). Above the KC are obliquely cut fenestrations in an LSEC cytoplasm. Bar = 1 µm.
F) SEM. A CL area from a P407 post-treated fed rat showing a typical CL zone where the hepatocytes and sinusoids look undamaged and viable. There is a central vein (CV) with emanating collagen fibres (arrows). Bar = 50 µm.

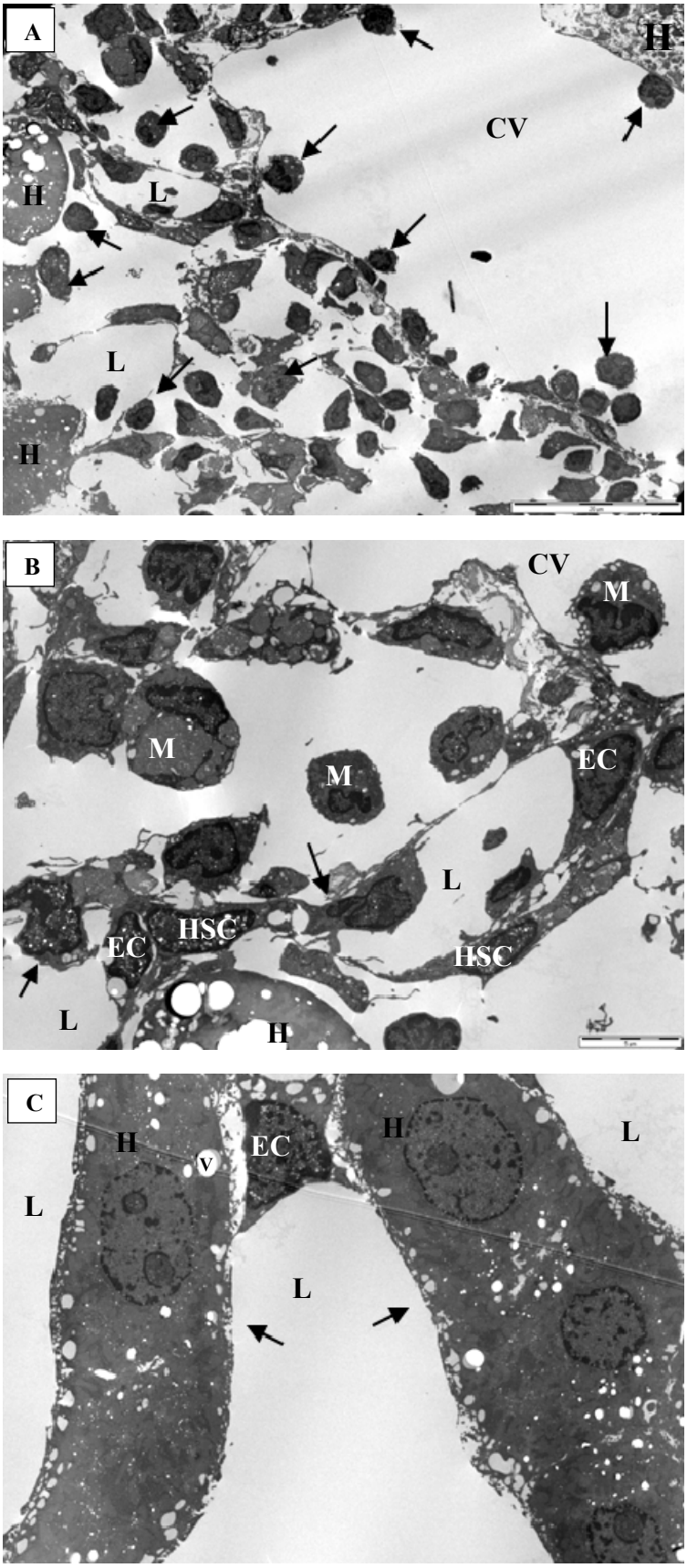

Figure 5.16 *Transmission electron micrographs from reprocessed tissue from the fed P407 post-treated rat with mild toxicity showing areas of CL necrosis*

A) An area of CL hepatocyte necrosis. A mass of infiltrate (arrows) is entering the liver sinusoids via the central venule (CV). Hepatocytes (H) appear to be missing from some areas directly around the CV. L = sinusoid lumen, bar = 20 µm.
B) A magnified view of the area adjacent to the CV. LSECs (EC) and HSCs appear viable. The parenchymal area contains infiltrate appearing to mainly consist of monocytes (M), two of which are undergoing extravasation (arrows) and open interstitial space where hepatocytes formerly resided. The process of reprocessing from paraffin may have extracted the most severely necrotic hepatocyte tissue, leaving empty space. Bar = 5 µm.
C) An adjacent midzonal area to that in micrographs (A) and (B) with intact sinusoids and viable hepatocytes with some vacuolisation (V) from where fat appears to have been extracted in the dehydration process, lined by fenestrated (arrows) LSECs (EC). L = sinusoid lumen, bar = 5 µm.

5.4.4.2 Fasted P407 post-treated 6 hour group

In 4 out of 5 rats in this group there was mild toxicity. Many LSEC sieve plates were replaced by gaps (approx 0.3 - 3 µm; fig 6.8 A and B), and some parts of the LSEC cytoplasm were mildly swollen and contained vacuoles and dense bodies. There generally appeared to be more platelets in the sinusoids than found in APAP control electron micrographs suggestive of increased endothelial injury. Some neutrophils and lymphocytes were present in the sinusoid lumens, and occasionally there was vacuolisation of centrilobular hepatocytes.

In the remaining rat with elevated ALT (rat 5) there was evidence of centrilobular congestion and hemorrhage, hepatocyte necrosis and sinusoid dilation (consisting of RBCs and platelets in the enlarged SoD, atrophy of hepatocytes, and narrowing of the sinusoid lumen; fig 5.17 C). There were also platelet aggregates and fibrin clots (fig 5.17 D) in areas devoid of LSECs (suggestive of LSEC necrosis), and infiltrate in amongst necrotic hepatocytes in damaged central zones. This degree of hepatotoxicity was greater than found in any APAP control 6 hour rat.

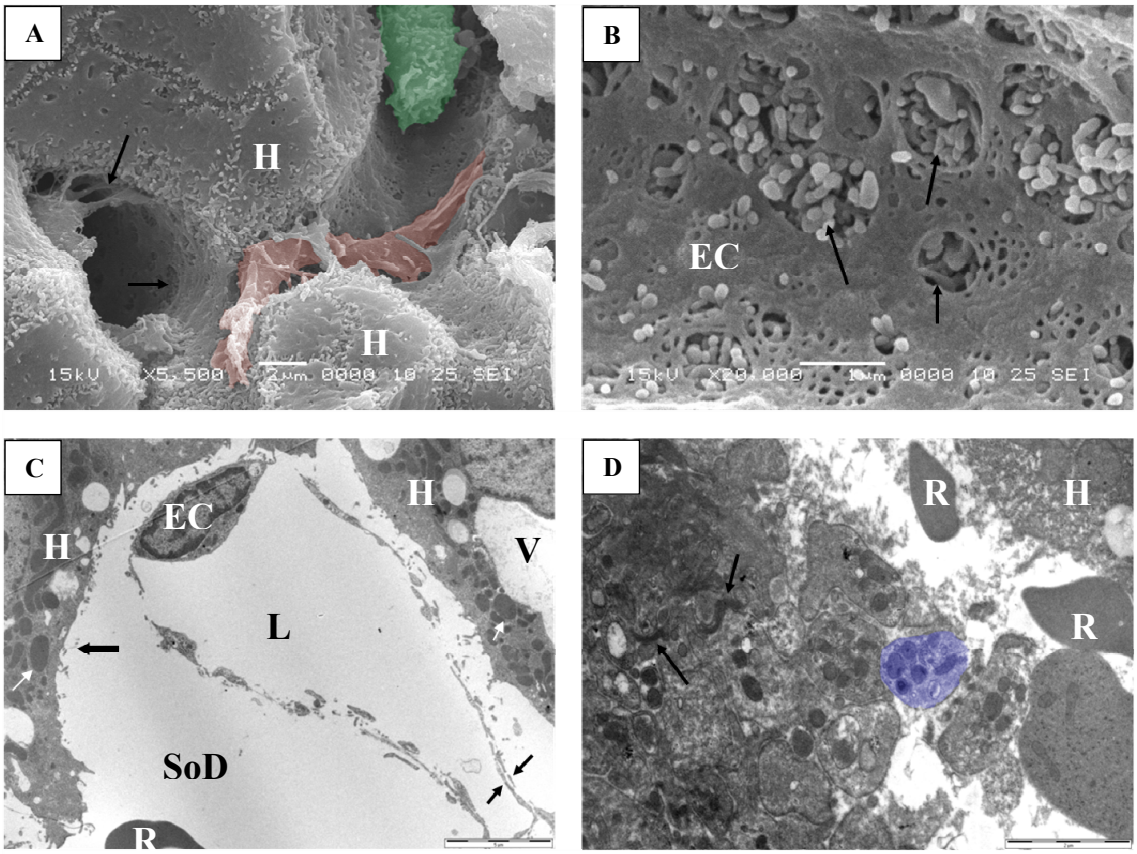

Figure 5.17 *Electron micrographs from P407 post-treated fasted rats 6 hrs after APAP*
A) SEM. A leukocyte (green, possibly a lymphocyte) and KC (red) are in the sinusoid lumen. In the furthest left sinusoid of the micrograph, the underside of an LSEC is visible with gaps (arrows) in its cytoplasm. H = hepatocytes, bar = 2 µm.
B) SEM. An LSEC (EC) cytoplasm contains gaps (arrows) replacing many of the sieve plates. Hepatocyte microvilli can clearly be seen through the gaps (bar = 1 µm).
C) TEM. This micrograph displays a CL area of moderate toxicity with a dilated sinusoid. LSEC and HSC cytoplasmic processes are tightly associated (arrows), hepatocytes are atrophied, losing microvilli (bold arrow), and degenerating with large vacuoles (V) and some swollen mitochondria (white arrows). The SoD is enlarged, and the sinusoid lumen (L) is collapsing. In the bottom right hand corner a RBC (R) is in the SoD (bar = 5 µm).
D) TEM. This micrograph displays an area of high toxicity. A mass of fibrin (arrows point to fibrin strands) and a platelet aggregate (plug/clot) are beside a degenerating hepatocyte and RBCs (R). This probably developed in place of a severely damaged sinusoid where LSECs became necrotic. A single platelet in the clot is coloured blue (bar = 2 µm).

5.4.4.3 Fasted P407 post-treated 24 hour group

In the areas of centrilobular necrosis and hemorrhage in the rat with severely elevated ALT, LSECs were dead with condensed chromatin in their nuclei (pyknosis; fig 5.18 A and C), and the remaining LSEC cytoskeletons surrounded by fibrin maintained the sinusoid lumen shape and prevented further hemorrhage (fig 5.18 A-D). There could have been viable LSECs in some necrotic areas however none were observed in the specimens analysed.

Severe defenestration of LSECs was not observed in our specimens, although there was mild defenestration (similar to APAP controls). LSEC cytoplasms contained some swollen areas, but these were only mildly swollen (up to 1 – 2 μm), and occasionally gaps were present. Vacuoles containing P407 were seen in hepatocytes, LSEC, and KCs (fig 5.18 F), and also in neutrophils in necrotic zones (fig 5.18 E). In contrast to the fed P407 post-treated rats, no P407 micelles were seen in the SoD on the TEM specimens analysed.

Examination of reprocessed kidney tissue on electron microscopy revealed that the substance found in the tubules of the rat with severe hepatotoxicity was very similar to that described for the P407 pre-treated rats in figure 5.10 with the most severe toxicity. In the specimens analysed there was no hemorrhage, although there was occasionally some cellular debris suggesting that some tubular cells had degenerated or become necrotic. Ultrastructural renal analysis did not provide an explanation for the hematuria.

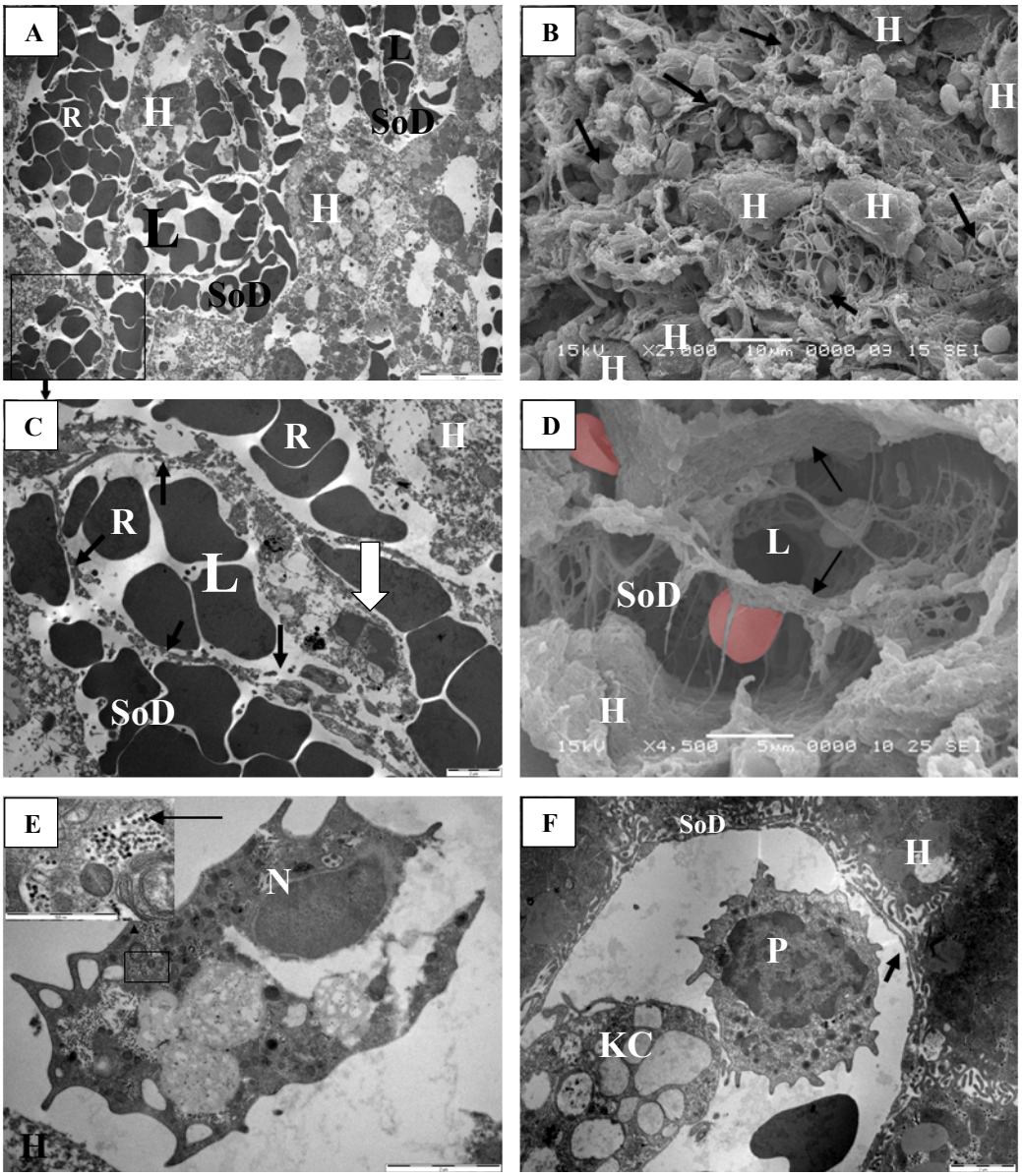

Figure 5.18 *Electron micrographs of a fasted P407 post-treated rat with severe toxicity 24 hrs after APAP*

A) TEM: An area of CL hemorrhagic necrosis where RBCs (R) are infiltrating the SoD and congested in the sinusoid lumens (L). The lumen shape is maintained although mostly by the remnants of dead LSECs associated with fibrin. Examples of RBC in the SoD and lumens (L) are marked R. The hepatocytes (H) are necrotic. Bar = 10 µm.

B) SEM: A three dimensional representation of figure A, a region of CL hemorrhagic necrosis. It is difficult to see the LSECs in this micrograph, however fibrin clots (arrows) clearly fill the sinusoids between degenerate hepatocytes (H) enhancing congestion, vascular stasis, and hypoxia whilst preventing further hemorrhage. Bar = 10 µm.

C) TEM: A magnified view of the boxed area in "A" showing hemorrhage, necrotic hepatocytes (H), and a necrotic LSEC with a pyknotic nucleus (bold arrow). The remnants of the dead LSECs (pointed out by arrows) appear to be associated with fibrin, maintaining the sinusoid lumen shape. Bar = 2 µm.

D) SEM: A magnified region similar to that in figure B. Surrounding the lumen (L) appears to be the cytoskeleton of a dead LSEC entangled with fibrin (arrow). RBCs are in the SoD (coloured red) and a dead hepatocyte is marked H. Bar = 5 μm.
E) TEM. A phagocytic cell (possibly a neutrophil) in a necrotic area that appears to have endocytosed P407 micelles (bar = 2 μm). Inset is an enlarged version of the boxed area showing the particles (arrow) are approximately 20 nm in diameter, similar to the size of P407 micelles (bar = 500 nm). Part of a necrotic hepatocyte (H) lies in the bottom corner.
F) TEM. A sinusoid from a PP zone displaying a striking contrast in toxicity from the severe damage of the CL zones. The LSEC is thin and fenestrated (arrow), the hepatocytes contain microvilli, and the SoD is of a normal size. A pit cell (P) and an activated vacuolated KC are in the sinusoid lumen. Bar = 2 μm.

5.4.5 Summary of P407 post-treated rats

Post-treatment of rats with P407 one hour after an overdose of APAP appears to have ameliorated toxicity in the fed group, and also defenestrated LSECs. Serum aminotransferase levels in all fed rats either fell within the normal range or very close to normal and only one rat out of the six displayed a very mild amount of necrosis. Whereas in the fasted groups, it is unclear whether P407 post-treatment had any protective effect because of the small sample size and extreme ranges of toxicity within the group. All fed and fasted P407 post-treated groups displayed different patterns of glycogen distribution to APAP controls and thus P407 may have affected glycogen metabolism.

5.4.6 Table summary of P407 pre- and post-treated rat data trends

Table 5.11 *Summary and trends in the blood, histological, and EM data comparing APAP controls to P407 treatment groups. ↓ = decreased compared to control, ↑ = increased compared to control, ↓* = statistically significant decrease, ↑* = statistically significant increase, nc = no change detected*

BLOOD & WEIGHT	**6hr fasted P407 pre-treated**	**6hr fasted P407 post-treated**	**24 hr fasted P407 pre-treated**	**24 hr fasted P407 post-treated**	**24hr fed P407 pre-treated**	**24hr fed P407post-treated**
ALT	↓*	↑	↑	↑	↑	↓
AST	↓	↑	↑	↑	↑	↓
TBil	↓*	↓	nc	↑	↓*	↓*
Triglycerides	↑*	↑	↑*	↑	↑	↑
Cholesterol	↑*	↑	↑*	↑	↑	↑
Hematocrit	↓*	nc	↓*	↓*	-	-
Liver wt	nc	nc	nc	nc	-	-
Body wt loss	↑*	↓	↓	↓*	↓	nc
HISTOLOGY						
CL necrosis	↑	↑	↑	↓	nc	↓
Congestion	↑	nc	↑	↓	nc	↓
Infiltrate	↑	nc	↑	nc	↑	↓
Collagen	nc	↓	↓	↑	↑	↑
Glycogen	↑	↑	nc	nc	nc	↑
Glycogen distribution	CL-PP (ctrls were depleted)	CL-PP (ctrls were depleted)	PP (same as ctrl)	diffuse (ctrls had PP)	PP (same as ctrl)	CL (ctrls had PP)
Renal	nc	nc	unknown substance in tubules	unknown substance in tubules	nc	nc
EM						
LSEC gaps	nc	nc	nc	nc	nc	↓
LSEC swelling	↑	nc	nc	nc	nc	↑
Defenestration	nc	nc	nc	nc	nc	↑
LSEC necrosis	nc	↑	↑	↑	↑	↓
Fibrin	nc	↑	↑	↑	↑	↓

* = $p<0.05$ compared to APAP controls

Refer to Appendix 4, table 1 for a table of F344 untreated, APAP treated, and P407 pre- and post-treated means ± S.D.

5.5 Discussion

Post-treatment with P407 protected against the development of APAP hepatotoxicity in ad libitum fed rats. At 24 hours after an overdose of APAP, liver histology was normal in 5 out of 6 rats. Only one rat displayed very mild amounts of centrilobular necrosis without any sign of hemorrhage, congestion, or sinusoid dilation, and thus P407 may have had a protective effect on the microvasculature. In addition, sinusoidal collagen was decreased in this group indicative of reduced oxidative stress and endothelial injury (Toklu, 2006). Electron microscopy of the fed post-treated P407 rats showed that the amount of LSEC gap formation induced by APAP toxicity was decreased correlating with the histological findings of decreased microvasculature injury. It also revealed that the LSECs had noticeably less fenestrations per cell and increased LSEC swelling. These are normal side-effects of P407 at about 24 hours after administration (Cogger, 2006, Warren, 2011) and not a result of APAP injury. LSEC swelling is primarily a result of increased endocytosis in order to remove excess serum lipids induced by P407, and P407 particles (Johnston, 2004, Warren, 2011) although the mechanism for defenestration by P407 is not yet understood (see section 5.1).

By defenestrating LSECs, P407 has been shown to reduce the availability of hepatocytes to APAP in fed rats (Mitchell, 2010) and may have slowed or reduced the production of NAPQI in this group. Micelles of P407 were clearly present in some of the sinusoids in contact with LSECs and hepatocyte microvilli in the SoD and may have played a protective role. Poloxamers are able to adsorb to cell membranes and have restorative effects on damaged areas of the membrane (Frey, 2007), therefore the

P407 may have ameliorated damaged cell membranes and protected hepatocytes and LSECs from exposure to toxins in the blood.

There was no sign of inflammation in the 5 out of 6 fed P407 post-treated rats with normal histology. However there was more infiltrate in the remaining rat in areas of centrilobular necrosis than in control APAP rats with more severe necrosis. This could be explained by a P407-mediated stimulation of immune response to injury as P407 promotes increases in both cell-mediated and humoral immune response (Dumortier, 2006, Johnston, 2009). As the areas of necrosis in this P407 post-treated rat were not wide-spread and were mild in severity, the increased infiltrate could have had an ameliorative effect on hepatotoxicity and did not appear to exacerbate it.

Glycogen was present in the centrilobular hepatocytes of 5 out of 6 rats in this group with normal histology. APAP toxicity is not associated with centrilobular glycogen deposition, and it was not observed in any of the APAP control rats. During APAP toxicity, glycogen is initially depleted, and then replenished in periportal hepatocytes just prior to the onset of centrilobular necrosis (Corcoran, 1988, Jepson, 1987). APAP depletes GSH and glycogen by similar percentages at each dose, and if NAC (a GSH precursor) is administered with APAP it prevents both the early APAP-induced glycogen depletion and toxicity (Hinson, 1983). Thus it is likely that glycogen depletion and subsequent replenishment in periportal zones is related to the formation of NAPQI. The fact that fed P407 post-treated rats had normal histology and expressed centrilobular glycogen suggests that there was decreased NAPQI formation in this group. Centrilobular glycogen is the last to be depleted during a fast due to a higher expression of glycogen storing enzymes in centrilobular hepatocytes (see

Chapter 1 section 1.3). Thus the depletion of periportal glycogen and remaining centrilobular glycogen in the post-treated rats could have been a normal metabolic adaption in the rats due to fasting from the time of APAP overdose. The presence of glycogen in centrilobular hepatocytes may have also played a minor role in protection from APAP toxicity by increasing uridine 5'-diphospho-glucuronic acid (UDPGA) levels within hepatocytes and increasing glucuronidation of APAP (Hinson, 1983).

In contrast, pre-treatment with P407 in fed rats did not protect against the development of hepatotoxicity 24 hours after APAP overdose. Aminotransferase levels were raised compared to controls (although not significantly) and exacerbated histological injury was apparent in some rats. P407 is able to occlude blood vessels (Raymond, 2004), and was observed on histology plugging and occluding some of the portal venules of fed P407 pre-treated rats. It is unclear whether this had any effect on the microvasculature by exacerbating congestion and ischemia. Ultrastructural analysis revealed that centrilobular LSECs from fed P407 pre-treated rats had more severe injury than APAP controls, and were often dead in areas of hepatocyte necrosis whereas they survived in such areas of APAP control livers. In addition, more frequent fibrin clots were observed in comparison to control APAP rats which may have in turn intensified congestion and ischemic necrosis. The hemostatic (coagulative) system augments hepatotoxicity in APAP overdose and sinusoidal fibrin deposition can disrupt blood flow, resulting in localized hypoxia and hepatocellular necrosis (Ganey, 2007). P407 has been shown to enhance the rate of assembly of fibrin, and inhibit fibrinolysis *in vitro* (Carr, 1996) which could further exacerbate hemostasis and liver injury in APAP toxicity. Periportal LSEC injury was not exacerbated, and periportal LSEC morphology at 24 hours in P407 pre-treated rats

was normal apart from some increased endocytosis and swelling of the LSEC cytoplasm secondary to the continuing clearance of P407 and excess serum lipid (Johnston, 2004, Warren, 2011). It is likely that periportal LSECs were spared from necrosis due to an increased antioxidant capacity (GSH availability) in the periportal zone (Smith, 1979) and less NAPQI production as CYP450 enzymes are not as highly expressed in the periportal zone (Gooding, 1978).

The fed P407 pre-treated group also showed a significant increase in sinusoidal collagen compared to control APAP fed rats, associated with increased oxidative stress (Toklu, 2006). P407 is able to induce oxidative stress *in vivo* by an indirect mechanism that increases the oxidation of LDL and other serum lipids resulting in malondialdehyde production (Johnston, 2007), and could have increased oxidative stress in this group via this mechanism.

Inflammatory cells were increased in fed P407 pre-treated rats, particularly in areas of hepatocyte necrosis. P407 has been reported to promote increases in both cell-mediated and humoral immune response (Dumortier, 2006). A single intraperitoneal injection of P407 can increase cell adhesion molecules (CAMs) including endothelial-leukocyte adhesion molecule (E-selectin), vascular CAM, and intercellular CAM (Johnston, 2009). These molecules expressed on endothelial cells are involved in leukocyte recruitment and adhesion, and their upregulation may have contributed to the increased amount of infiltrate present in the P407 pre-treated rats. Whether inflammatory cells have any detrimental effect in APAP toxicity remains controversial, although it is possible that an increased amount of infiltrate could exacerbate toxicity through excessive release of inflammatory mediators leading to

heightened induction of iNOS and enhancement of peroxynitrite formation (Jaeschke, 2005). Exacerbated oxidative stress would in turn increase collagen formation and LSEC injury, and could explain the increased sinusoidal collagen and LSEC damage in the fed P407 pre-treated group.

The reason why post-treatment with P407 after APAP was protective and pre-treatment before APAP was not protective is unclear. When the P407-induced changes in LSEC morphology such as defenestration and swelling occurred at the time of APAP overdose (in the pre-treated group where rats were given P407 18 hours before APAP overdose) they were not protective. However when these same P407-induced changes in LSEC morphology occurred later in APAP toxicity (when rats were post-treated with P407 1 hour after APAP) they could have had a protective effect by promoting amelioration of earlier APAP microvascular injury and decreasing gap formation.

Two time points were investigated in fasted rats treated with P407 and APAP. Analysis showed that P407 pre- or post-treatment did not protect the liver from early microvasculature injury at 6 hours after APAP, and that P407 pre- or post-treatment did not protect the liver from centrilobular hemorrhagic necrosis 24 hours after APAP. Fasting increases the hepatotoxicity of APAP overdose primarily because GSH stores, crucial to the detoxification of NAPQI, are depleted to about 50 % of their original amount by fasting (see Chapter 1, section 1.3.1). LSECs (and hepatocytes) are more vulnerable to injury in an environment with a lowered antioxidant capacity.

At 6 hours after APAP in fasted rats, P407 pre-treated liver function tests revealed a significant decrease in aminotransferase levels, suggestive of a hepatoprotective effect, however the decrease was small. In addition, there was significantly less weight loss in the pre-treated group at 6 hours compared to APAP controls, which again points to a protective effect. In contrast, P407 post-treated aminotransferase levels were raised (although not significantly) indicative of increased hepatocyte injury. In both 6 hour groups, histology was mostly normal apart from some mild centrilobular vacuolisation and focal necrosis. One rat from each group sustained a greater degree of injury than was observed in the APAP control group with centrilobular sinusoid dilation and hemorrhage, and some mild necrosis in the post-treated rat. In both pre- and post-treated groups, glycogen was present in centrilobular hepatocytes of the rats without histological damage. Centrilobular glycogen is not normally observed during APAP toxicity and was not found in any of the APAP controls. P407 does not have any influence on blood glucose or insulin levels (which could stimulate glycogen production) (Johnston, 2008), however, the effects of P407 on glycogen synthase and phosphorylation of glucose to glucose-6-phosphate have not been studied. Poloxamers have the ability to form tiny pores in membranes that can enable the flux of various cations such as calcium and potassium (Krylova, 2004, Sutachan, 2006), and it is therefore possible that in this way P407 may indirectly inhibit or stimulate enzymes that participate in glycolysis and gluconeogenesis as they are sensitive to cytoplasmic concentrations of different ions. As glycogen depletion and periportal replenishment is a sign of the progression of APAP toxicity, it is also possible that the hepatocytes of these rats were protected by P407 and that the centrilobular glycogen expression was a normal result of the initial periportal glycogen depletion in fasting.

Pre-treatment with P407 did not reduce the expression of sinusoidal collagen at 6 hours after APAP, and post-treatment only reduced sinusoidal collagen in one rat thus P407 did not reduce oxidative stress. Electron microscopy revealed that P407 also did not prevent APAP-induced LSEC gap formation injury in either group. In the post-treated group there was an increased amount of platelets in the sinusoids at 6 hours after APAP. Platelets are recruited in response to endothelial injury and could have been increased as a result of exacerbated LSEC injury. One P407 post-treated rat displayed severe congestion with fibrin clots, hemorrhage, and LSEC necrosis, a level of damage greater than found in any APAP control rat at 6 hours after APAP, suggesting that LSEC injury was increased by P407 in this group, correlating with the LFT data. This degree of injury was not apparent in the pre-treated groups. Interestingly, P407 pre-treated rats did not display LSEC defenestration as was expected at 24 hours after P407 administration. This could have been due to an unknown effect of APAP toxicity inhibiting the mechanism of P407 defenestration. Also in the pre-treated group there was P407-induced LSEC swelling secondary to the uptake of excess lipid in response to the hyperlipidemia induced by P407 (Warren, 2011) and LSECs were more swollen and vacuolated than in the control group. Hematocrit was significantly decreased secondary to the severe hyperlipidemia induced by P407 that increased the plasma fraction of the blood samples. Overall, these results at 6 hours after APAP show that pre- or post-treatment with P407 did not protect the liver from early APAP-induced microvasculature injury in fasted rats and did not coat and protect LSECs from gap formation injury.

At the second time-point, 24 hours after APAP, livers of fasted rats were also not protected by P407 pre- or post-treatment. Hematocrit was significantly decreased in

both these P407 groups secondary to the severe hyperlipidemia induced by P407 that increased the plasma fraction of the blood samples. In the fasted P407 pre-treated group, average aminotransferase levels were increased (although not significantly) compared to APAP controls correlating with histological findings of exacerbated injury in some P407 rats with more severe necrosis than controls. Sinusoidal collagen was decreased which was in this case reflective of the greater amount of hemorrhagic necrosis in the group as collagen was not upregulated in severely necrotic areas in any APAP or P407 groups. The presence of inflammatory cells was also increased in fasted P407 pre-treated rats at 24 hours after APAP particularly in areas of hepatocyte necrosis, which could have been a direct effect of P407 (Dumortier, 2006, Johnston, 2009). A higher amount of infiltrate could have added to the APAP toxicity by increasing the release of inflammatory mediators leading to heightened induction of iNOS and enhancement of peroxynitrite formation (Jaeschke, 2005). Electron microscopy revealed LSECs from the fasted pre-treated group at 24 hours after APAP were dead in centrilobular zones where hepatocytes were only mildly injured and not necrotic. This level of LSEC injury was not observed in the fasted APAP controls suggesting that pre-treatment with P407 made the LSECs more susceptible to injury. In addition, fibrin clots were more frequently observed in the fasted pre-treated rats compared to APAP controls, a sign that there was increased hemorrhage due to exacerbated endothelial injury.

In the fasted P407 post-treated rats at 24 hours after APAP overdose, there was extreme variability in the toxicity making it harder to define whether P407 protected from or exacerbated APAP toxicity. Overall, histological necrosis was decreased in comparison to controls with low toxicity in 3 out of 4 rats, however average

aminotransferase levels in the group were increased (although not significantly) as the fourth rat sustained severe injury in the form of centrilobular hemorrhagic necrosis, dead LSECs in areas of hepatocyte necrosis, and macroscopic hematuria. In contrast, 2 rats in the group sustained less damage than the APAP controls with normal range serum aminotransferase levels and glycogen in centrilobular hepatocytes, and a third displayed low range APAP toxicity. In comparison to the fed post-treated rats, the fasted P407 post-treated rats were not as defenestrated at 24 hours after APAP. Fasting opens fenestrations wider than in the fed state (see results of Chapter 3) possibly to maximise the availability of nutrients in the blood to hepatocytes. The difference in fenestration size between fed and fasted rats may be due to alterations in the levels of serum proteins in the fasted state such as endothelin, VEGF, calcium, serotonin, and noradrenaline, however the exact mechanism is unknown. It is possible that the mechanism that dilates fenestrations in fasting may somehow override the defenestrating effect of P407 allowing more APAP (and any other toxins in circulation) to reach the hepatocytes resulting in an increased production of NAPQI. This effect of fenestration dilation could potentially override the protective mechanism of P407 post-treatment found in the fed state.

The cause of hematuria in the three P407 pre- and post-treated fasted rats with severe hepatotoxicity was investigated by renal histological and ultrastructural analysis as APAP nephrotoxicity is well recognized in addition to its hepatotoxicity (McMurtry, 1978). Analysis did not reveal any tubular necrosis or hemorrhage. It is possible the bleeding that caused the hematuria occurred in the bladder instead of the kidneys, or that there was some glomerular bleeding in other areas of the kidney that were not sampled for analysis. The P407/APAP combination could have caused some minor

tubular degeneration or necrosis as cellular debris was occasionally found in some of the tubules. There was also a globular substance discovered in the tubules of the renal cortex and medulla that was not present in the other rats with lower hepatotoxicity or in any of the APAP controls. This substance may have been comprised of P407 as its structure resembled that of micelles. Whether this substance had effect on renal function or promoting the hematuria is unknown. It has previously been shown that P407 can cause alterations of the murine glomerular filtration rate in a time-dependent manner (Li, 1996, Pec, 1992), and could contribute to increasing the toxicity of APAP by decreasing its rate of elimination. One suggested mechanism of action is that at some point during its elimination, P407 may accumulate in the glomeruli and thus plug fenestrations in glomerular endothelial cells (Li, 1996). Although this was not observed in our analysis it may have occurred at other time-points, and a decrease in the filtration rate could have subsequently exacerbated the hepatotoxicity, particularly in fed and fasted P407 pre-treated groups.

In summary, P407 post-treatment one hour after APAP had a protective effect in rats ad libitum fed prior to APAP overdose, reducing hepatocyte necrosis, hemorrhage, and LSEC injury compared to APAP controls. P407's defenestrating mechanism could have helped to ameliorate microvascular dysfunction by reducing the number of gaps and fenestrations, thereby reducing the amount of APAP and other toxins from reaching the hepatocytes. By accumulating in the SoD it could have also formed a physical protective barrier and helped to prevent and restore membrane damage. However P407 post-treatment in the fasted state did not protect LSECs from early injury, and results later in the course of toxicity were inconclusive with one of the rats in the group developing very severe hepatotoxicity and others appearing to be

protected at 24 hours after APAP. Some animals are more vulnerable to APAP toxicity than others because of genetic polymorphisms in metabolic and drug-transporter enzymes (Au, 2011, Heinloth, 2004) and idiosyncratic adverse drug reactions are not uncommon (Boelsterli, 2007, Fontana, 2008). Thus it is possible that the dose of P407 administered was enough to protect some of the rats in the group from toxicity but not others. Pre-treatment with P407 did not protect the LSECs from the toxic effects of APAP in the fed or fasted state early or late in the course of toxicity. At 6 hours after APAP, pre-treatment with P407 may have had a mild hepatocyte protective effect, as aminotransferase levels were reduced, however it did not appear to protect LSECs from injury. It appears that by 24 hours after APAP overdose, pre-treatment with P407 aggravated hepatotoxicity and LSEC injury caused by APAP overdose in some of the rats in both the fed and fasted groups. Reasons for this may include a P407-induced inflammatory recruitment, exacerbated oxidative stress via P407-induced lipid oxidation, promotion of hemostasis by P407 inhibition of fibrinolysis and enhanced fibrin assembly rate, occlusion of the microvasculature and venules by P407 micelles increasing ischemia, and alteration of renal function by P407 which could have indirectly increased APAP hepatotoxicity.

Chapter 6:

The Ultrastructure of Isolated Liver Sinusoidal Endothelial Cells from Young and Old F344 Rats

6.1 Introduction

Recently old age in many species, including humans, has been found to be associated with marked ultrastructural changes of the LSEC called pseudocapillarisation (Ito, 2007, Le Couteur, 2001, Stacchiotti, 2008, Warren, 2005). These changes include defenestration with a reduction of porosity of approximately 50 % associated with increased thickness of the endothelium and altered expression of various antigens including von Willebrand factor, caveolin-1 and ICAM-1 (Le Couteur, 2008). Age-related defenestration of the LSEC is secondary both to a reduction in frequency and diameter of fenestrations (Le Couteur, 2008) and has been shown to impede the transfer of lipoproteins from blood to hepatocytes (Hilmer, 2005). This provides a novel risk factor for age-related vascular disease (Le Couteur, 2007, Le Couteur, 2002). Pseudocapillarisation has also been implicated in increasing susceptibility to drug reactions in ageing and altering the rate of drug metabolism (Le Couteur, 1998, McLean, 2003). There is evidence to suggest that thickening and defenestration of the LSEC, in addition to increased collagen deposition in the SoD, impedes drug delivery to hepatocytes (Mitchell, 2011), and reduces the rate of oxygen diffusion from the blood crucial for oxidative metabolism (Le Couteur, 1998) thereby slowing drug elimination in the elderly.

Therefore it is important that an effective method to study the ageing LSEC be discovered in order to test new substances that might modulate and reverse LSEC defenestration and thickening. The study of LSECs from old animals *in vitro* would be an ideal method to test the effects of potential therapeutic substances directly on LSECs without the influence of other biological factors and without having to

administer the substance to an animal. This would allow preliminary data to be obtained on how the substance modulates old LSEC morphology before *in vivo* studies are carried out.

Whether the pseudocapillarisation is maintained in LSECs that have been isolated and cultured from old livers is unknown. If pseudocapillarisation is maintained in isolated LSECs it would suggest that this aging change is either irreversible and/or a primary endothelial change. Furthermore, it would indicate that isolated LSECs are suitable for the study of aging.

6.2 Materials and methods

6.2.1 Animals and general information

Young mature adult (aged 6 - 10 months, weight 380 - 440 g) and old adult (aged 24 - 26 months, weight 390 - 490 g) male Fisher 344 rats were imported from the National Institute of Aging (Bethesda, MD), maintained on a 12 hour light / dark cycle and given free access to water and standard rat chow. The study was approved by the Sydney South West Area Health Service Animal Welfare Committee. Sterility was kept when weighing out materials for cell culture by using a cell culture fume hood and filtering solutions through a 2 μm filter to exclude bacteria.

6.2.2 Surgery and LSEC isolation method using a 2-step Percoll gradient

Rats (n = 4 young, n = 4 old) were anesthetised via an intraperitoneal injection of 0.2 ml/100 g rat ketamine/xylazil (as described in Chapter 2). LSECs were isolated as described (Cogger, 2006, Cogger, 2004). After laparotomy, the portal vein was cannulated with an 18 G cannula and held in place with a suture. 100 μl of heparin was injected into the IVC to prevent any clots during perfusion. Following this the IVC was severed to allow adequate drainage of perfusate during perfusion (preventing any build up of pressure). Approximately 50 ml of Hank's balanced salt solution (HBSS) without calcium at 37 ºC was perfused through the liver at a flow rate of approximately 10 ml per minute to remove the blood from the sinusoids (the liver turned from a dark reddish brown to a consistent tan colour). Immediately following this, livers were perfused with 50 - 100 ml collagenase A (0.05 % collagenase in HBSS with calcium, and 5 % fetal calf serum to neutralise non-specific proteases) at approximately 5 ml per minute (until the liver became soft). The liver was then

carefully removed using the portal vein as an anchor, rinsed with saline, and placed in a sterile petri dish. Glisson's capsule and major vessels were removed using sterile forceps, eventually leaving a paste-like substance (containing the liver cells). Collagenase B (0.05 % collagenase in HBSS with calcium, 5 % fetal calf serum and 0.001 % DNase) was added to the petri dish and mixed around to further break up the liver, then placed in an incubator (5 % CO_2 at 37 ºC) for 10 min. The remaining cell suspension was filtered through nylon gauze (100 µm mesh) to remove any undigested tissue then centrifuged in a falcon tube at 100 *g* for 5 min at 20 ºC forcing most of the hepatocytes into a pellet at the bottom of the tube. The supernatant (containing a mixture of sinusoidal liver cells) was removed and centrifuged at 350 *g* for 10 min, forcing LSECs into a pellet. The pellet was then resuspended in 50 ml PBS and centrifuged for 10 min at 350 *g*. The resulting pellet was resuspended in 20 ml PBS. Two 2-step Percoll (Stock Percoll = 90 % Percoll in PBS) gradients were made with 15 ml 50 % stock Percoll (in PBS) on the bottom layer, and 20 ml 25 % stock Percoll (in PBS) on the layer above. 10 ml of the cell suspension was carefully added on top of each of the Percoll gradients and centrifuged for 20 min at 900 *g*. The resulting intermediate zone enriched in LSECs was carefully removed and diluted with an equal volume of PBS, then centrifuged again at 900 *g* for 10 min. The pellet was resuspended in 10 ml complete Roswell Park Memorial Institute (complete RPMI-1640) medium (0.02 g/100 ml L-glutamine, 2 % heat inactivated fetal calf serum, 1 ml/100 ml of 100 U/ml penicillin, and 100 µg/ml streptomycin, in RPMI-1640 medium). The cell suspension was then pipetted into uncoated sterile dishes and incubated for 10 min (37 ºC, 5 % CO_2) to allow the selective attachment of Kupffer cells to plastic wells, enhancing LSEC purity. LSECs were then collected by firmly washing the dishes with complete RPMI-1640 to maximize the yield.

After a Trypan blue stain (450 µL Trypan blue, 50 µL cell suspension) allowing subsequent counting of the cells using a hemocytometer, LSECs were cultivated at 0.8 $\times 10^6$ LSEC per ml in 24-multiwell plates on collagen-coated Thermanox coverslips for scanning electron microscopy. Specifically, 13 mm diameter Thermanox coverslips were coated with 10 µL calf type 1 collagen. LSECs were cultured for 18 hours (37 ºC / 5 % CO_2) in 1 ml complete RPMI-1640 per well. The media did not contain vascular endothelial growth factor. Cells were rinsed in warm PBS and given fresh medium after 2 hours in culture.

6.2.3 Specimen preparation for scanning EM

Scanning electron microscopy on the cultured LSECs was performed as described (Cogger, 2006, Cogger, 2004). After 18 hours in culture, LSECs were fixed for scanning electron microscopy in 2.5 % glutaraldehyde in 0.1 M Cac (0.1 M sodium cacodylate buffer with 1 % sucrose pH 7.4) buffer for 1 hour then washed in 0.1 M Cac buffer. Filtered 1 % Tannic acid in 0.1 M Cac buffer (pH 7.4) was then added to cells on coverslips for 1 hour and rinsed thoroughly in 0.1 M Cac buffer. Cells on coverslips were then osmicated (1 % OsO_4 / 0.1 M Cac buffer pH 7.4 for 1 hour), washed in 0.1 M Cac buffer and dehydrated in an ethanol gradient from 50 to 100 % EtOH (5 min each), and incubated for 2 min in hexamethyldisilazane. After the hexamethyldisilazane was removed from the wells, coverslips were left to air-dry in a fume hood. Coverslips were then mounted on stubs using double-sided tape, coated with platinum in a sputter coater (as described in Chapter 2), and examined using a Jeol 6380 Scanning Electron Microscope.

6.2.4 Analysis

At least 30 images per animal from at least 10 cells were taken of the LSEC cytoplasm at a magnification of 15000 × for measurement of fenestration diameter and LSEC porosity. Measurements of fenestration size, number and density were carried out using Image J (as described in Chapter 2, section 2.4.5.4). Fenestrations were defined as open pores with diameters < 300 nm. Gaps were defined as pores with diameters > 300 nm, and large gaps were defined as diameters > 500 nm. Diameter was defined as the major length of each fenestration or gap. Porosity was defined as the sum area of fenestrations / total area of the cell in the micrograph. The results are expressed as mean ± S.E.M. and comparison of the two age groups was performed using the Student's *t*-test. The frequency distribution of the fenestration diameters was compared using χ^2. Differences were considered significant when $p < 0.05$.

6.3 Results

The average diameter of the fenestrations was decreased in old age from 194 ± 1 nm (n = 13467 fenestrations, 4 rats) to 185 ± 1 nm (n = 21,521 fenestrations, n = 4 rats, $p < 0.0001$). The graph of the distribution frequency of the diameters of fenestrations (fig 6.1) showed a slight shift to the left in old age ($p < 0.001$). However there was no change in the overall porosity between young and old (8.5 ± 0.4 % versus 8.6 ± 0.3 %, respectively).

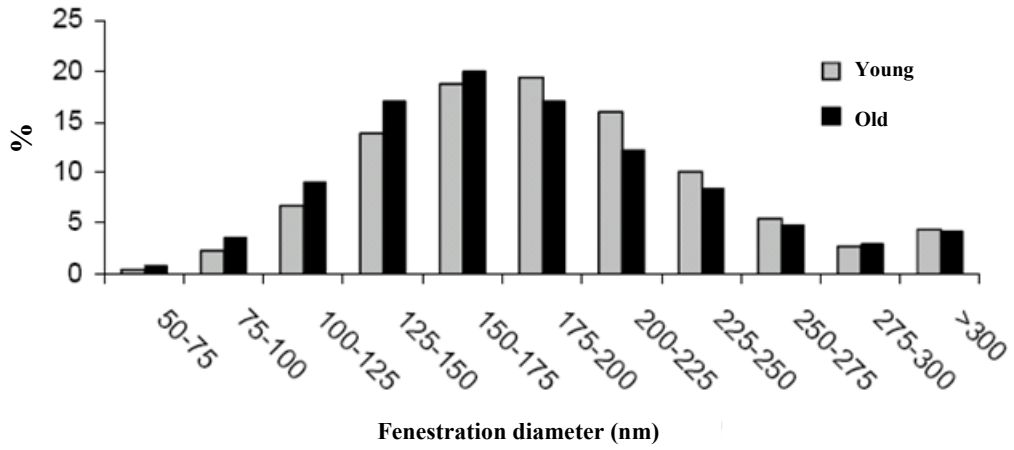

Figure 6.1 *Frequency distribution graph of the fenestration diameter in LSECs isolated from young and old rats. There is a slight shift to the left in old age concomitant with a significant reduction in average diameter.*

Figure 6.2 shows examples of isolated cells from young and old rats and highly magnified areas used for analysis. An increase in fused fenestrations, that is adjacent fenestrations that appear to have lost some of the intervening cytoplasm (fig 6.3), was increased from 0.4 ± 0.05 per μm^2 in young LSECs to 0.8 ± 0.01 per μm^2 in old age ($p < 0.0001$). In addition, mesh-like structures reminiscent of vesiculo-vacuolar organelles (Dvorak, 2001), pored domes (Koriyama, 1992, Ohata, 1984), and trabecular meshworks (Taira, 1994) were noted frequently in both young and old LSEC cytoplasm and sometimes on the LSEC nucleus (fig 6.3), and gaps in the cytoplasm were common, suggesting that the ultrastructure of LSECs is influenced by their isolation and culture. The presence of gaps greater than 500 nm in diameter was mildly increased in old age (11 ± 2 large gaps per cell in the old versus 8 ± 1.5 large gaps per cell in the young). In addition, structures that have previously been described as fenestration forming centres (Braet, 1998), and more recently described in detail using three dimensional structured illumination microscopy (Svistounov, 2012), were occasionally observed (fig 6.3).

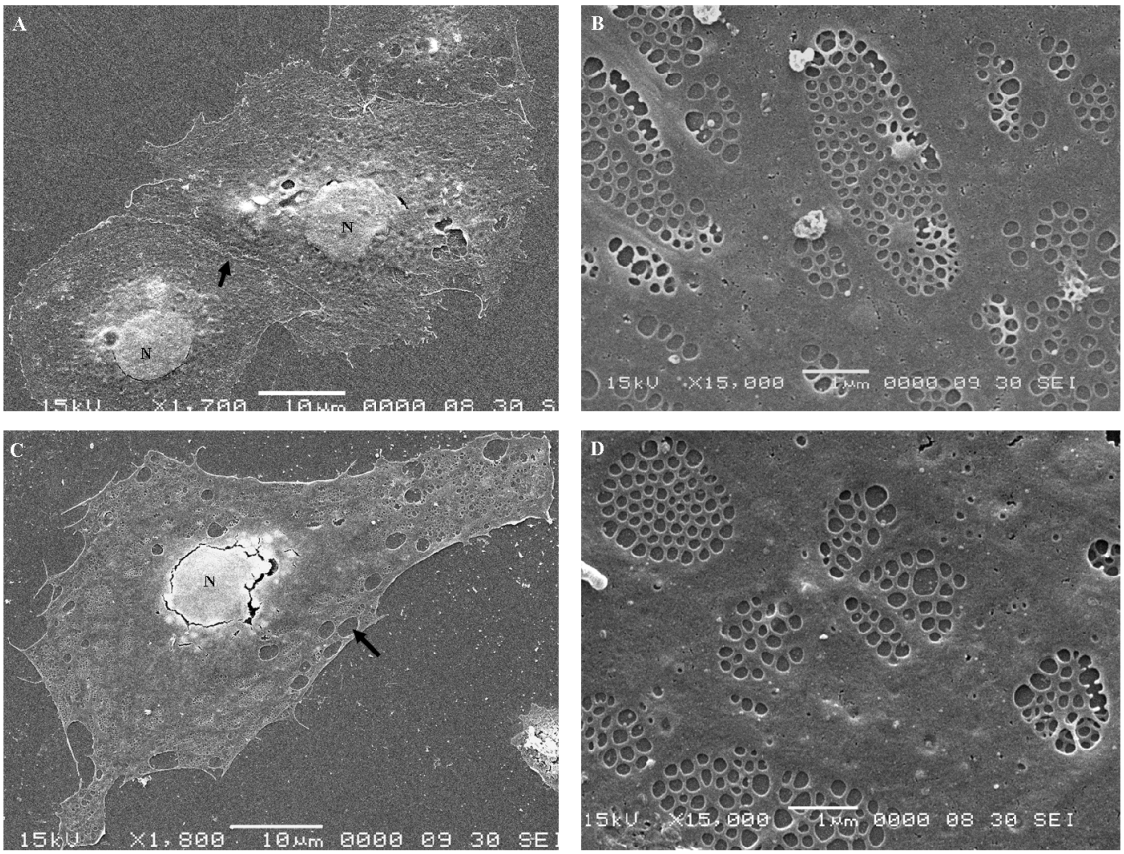

Figure 6.2 *Electron micrographs of isolated young and old LSECs*
A) LSECs from a young rat in culture. There are intercellular junctions between the LSECs (arrow) and the nuclei (N) are distinguishable from the cytoplasms (bar = 10 µm).
B) Higher magnification of the LSEC cytoplasm from a young rat showing numerous fenestrations clustered into sieve plates (bar = 1 µm).
C) An LSEC from an old rat showing the nucleus (N) and gaps in the cytoplasm (arrow; bar = 10 µm).
D) Higher magnification of the LSEC cytoplasm from an old rat. Similar to the young rat, there are numerous fenestrations clustered into sieve plates (bar = 1 µm).

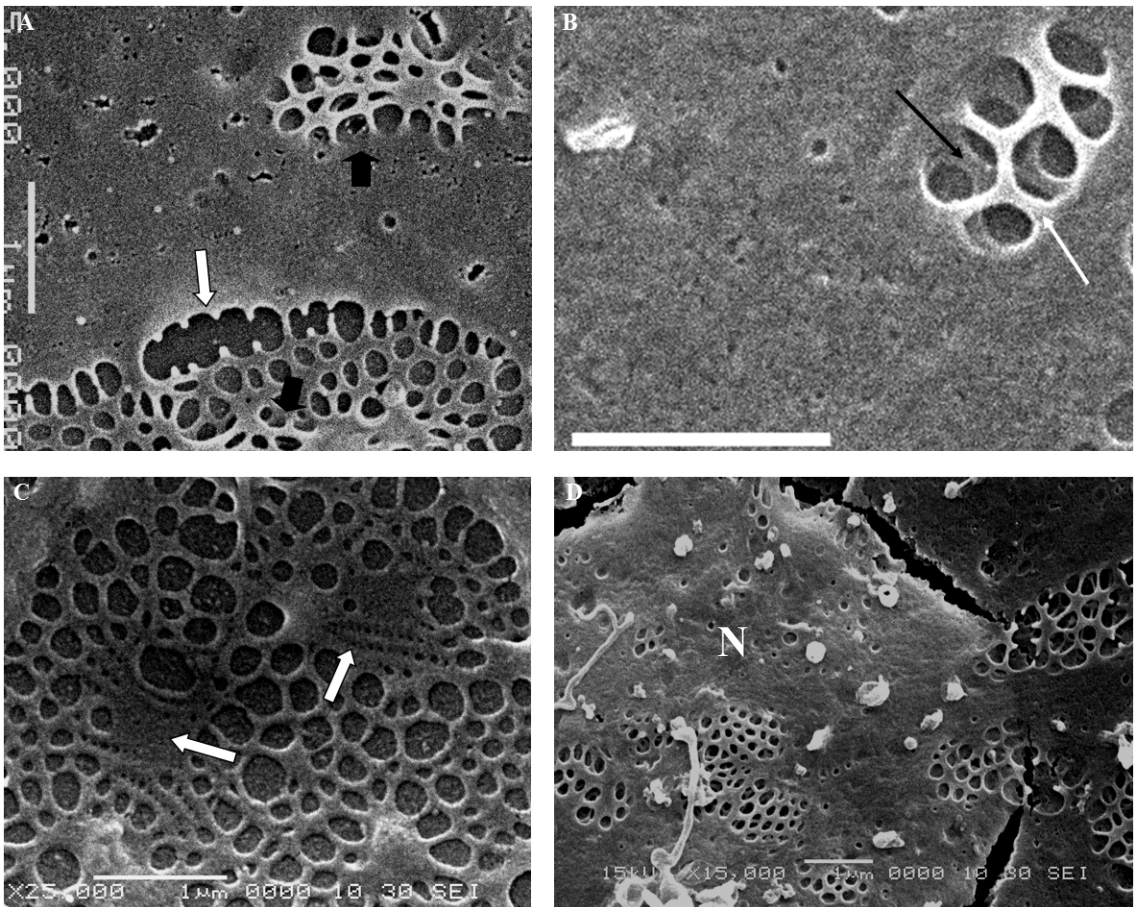

Figure 6.3 *Scanning electron micrographs of unusual fenestration structures*
A) Fused fenestrations (white arrow) and mesh-like sieve plates (black arrows) were observed in both young and old cells (bar = 1 µm).
B) Higher magnification of a mesh-like sieve plate showing what appears to be two layers of fenestrations (white and black arrows) in the LSEC cytoplasm in a sieve plate formation. Bar = 1 µm.
C) A micrograph showing examples of "fenestration forming centres" (white arrows; bar = 1 µm).
D) An LSEC nuclear region (N) containing structures resembling pored domes, vesiculo-vacuolar organelles, or trabecular meshworks (bar = 1 µm).

6.4 Discussion

LSECs occupy a critical and strategic position in the hepatic sinusoid because they facilitate the perm-selective and bi-directional transfer of substrates between blood and hepatocytes (Fraser, 1995, Le Couteur, 2005, Oda, 2003). The extreme vascularity of the liver generates a huge surface area for LSEC interactions with blood cells and particulate substrates for endocytosis. These features underpin many important physiological roles for the LSEC including their sieve, scavenger and immunological functions (Elvevold, 2008).

Old age has been reported to be associated with reduced porosity in mice (Ito, 2007, Stacchiotti, 2008, Warren, 2005), rats (Jamieson, 2007, Le Couteur, 2001), baboons (Cogger, 2003), and humans (McLean, 2003). Overall, these studies performed in intact liver tissue have shown a reduction in porosity, however results for fenestration diameter were inconsistent, with different trends in fenestration diameter in old age reported in different species (Le Couteur, 2008). In the F344 rat, two *in vivo* studies have shown a trend towards reduction in fenestration diameter with age (Jamieson, 2007, Le Couteur, 2001) however a more recent study (completed after our experiments) using the hybrid F344/BN F1 rat reported no difference in fenestration diameter of young and old rats (Simon-Santamaria, 2010). The hybrid rat type is considered to be a healthier model of ageing with less disease and greater longevity, and thus could explain the different result, particularly as rats in the "old" groups were of the same age (from 24 – 26 months old) in all three studies.

In isolated and cultured LSECs we found a reduction in fenestration diameter of about 5 %, which is consistent with the *in vivo* reports in F344 rats. However, we could not detect any reduction in overall porosity in isolated LSECs from old livers. There are several plausible reasons for this inconsistency. First, the isolation and culture method might select only the most viable cells, so that defenestrated old cells are lost during isolation and culture. Second, it is possible that the actin disruption that occurs with cell isolation might cause an artefactual hyperfenestration (Cogger, 2009), thus diminishing the capacity to detect any aging changes. Finally, it is possible that some of the age-related changes in LSEC ultrastructure are maintained by *in vivo* factors such as cytokines derived from other hepatic cells or blood. On the other hand, LSECs derived from thioacetamide-induced cirrhotic livers were defenestrated both in intact livers and isolated LSECs. This result suggests that these thioacetamide-induced changes are intrinsic to LSECs and not related to the *in vivo* microenvironment (Mori, 1993).

Consistent with our results, the study by Simon-Santamaria et al found no significant difference in the porosity of LSECs isolated from old and young rats however in contrast they found no difference in fenestration diameter (Simon-Santamaria, 2010). This study used hybrid rats and cultured the LSECs for 2 hours with fetal calf serum-free medium, however our study used inbred F344 rats and LSECs were cultured for 18 hours with fetal calf serum in the medium. These differences in methodologies could explain the inconsistent results, demonstrating that minor differences in methodology produce different conclusions.

The diameter of fenestrations from normal LSECs has a Gaussian distribution, skewed to the right by the presence of some larger pores (Wisse, 1983, Wisse, 1985). Larger pores (greater than 300 nm diameter) are known as gaps (Wisse, 1985). Gaps represent large deficits in the liver endothelium probably caused by loss of, or fusion of all the fenestrations in the liver sieve plates (Montesano, 1978, Shin, 1997, Wisse, 1985). Gaps seem to occur as a result of cellular injury, technical issues related to high pressure perfusion (Fraser, 1980, Wisse, 1983, Wisse, 1985), hypoxia (Frenzel, 1977), fixation or pathological states (Wright, 1983). The absence of large chylomicrons in the space of Disse has been proposed as evidence that gaps do not normally occur *in vivo* (Wisse, 1985). We found numerous gaps in isolated LSECs suggesting that gaps may be an artefact of the isolation process and cell culture method. Old age was associated with a shift to the left of the frequency distribution graph for fenestration diameter up to 300 nm, together with no change in gap formation between 300 – 500 nm, and a slight increase in very large gaps greater than 500 nm. Consistent with this finding, a more recent study observed gaps with a diameter greater than 300 nm in LSECs isolated from young and old rats and no significant difference in gap formation between the groups (Simon-Santamaria, 2010), although they did not analyse data for gaps greater than 500 nm. The age-related increase in large gaps observed in our study suggests that old age is associated with some reduction in the resilience of old LSECs to withstand the isolation process.

Factors innate to the isolation and culture process appear to influence the morphology of LSECs, including the extracellular matrix components used in the culture. Type 1 collagen was used in these experiments and although collagen remains the most important factor in LSEC culture (March, 2009), the use of different extracellular

components could influence the results (McGuire, 1992). However, it should be noted that recent studies show that fenestrations are better preserved when collagen is used compared to either Matrigel (Yokomori, 2009) or fibronectin (Martinez, 2008). Unusual fenestration structures were observed in both young and old LSECs. We noted fused fenestrations, which were more frequent in old LSECs. Fenestrations with irregular shaped margins or fusing fenestrations have previously been described in rat liver tissue (Young-Chul, 1997) but their significance and pathogenesis are unknown. Certainly they have the appearance of an artefact where part of the intervening cytoplasm has been lost during the fixation process however it is uncertain whether or not these structures are artefactual. We also noted the appearance of complex, multilayered sieve plates in both old and young isolated LSECs similar in structure to vesiculo-vacuolar organelles seen in capillaries of other tissues (Dvorak, 2001), and pored domes (Ohata, 1984), fenestrations in labyrinths (Braet, 2009), or trabecular meshworks (Taira, 1994) previously described in the liver *in vivo* (and consistent with the mesh-like sieve plates described by Simon-Santamaria et al in isolated LSECs).

In conclusion, old age is associated with marked ultrastructural changes in the liver sinusoidal endothelium that have been called pseudocapillarisation. Whether such changes are maintained in LSECs that have been isolated and cultured was unknown. In this study, it was found that LSECs isolated from old livers retain some but not all of the ultrastructural changes that have been documented *in vivo* and in intact liver samples. Specifically there was a reduction in fenestration diameter with old age, yet fenestration porosity was the same in LSECs isolated from young and old livers. The result suggests that reduced fenestration diameter in old age is either irreversible or intrinsic to the LSEC.

Chapter 7:

General Discussion

The majority of liver studies focus on the hepatocyte however the cells of the hepatic sinusoid are also crucial to liver function. The work of this thesis supports the vital role of the LSEC in the liver during health, toxicity, and ageing, and its important influence on hepatocyte function.

The LSEC forms a protective barrier between the blood and the hepatocytes that is modulated by changes in the size and number of fenestrations. In Chapter 3 I found that fasting significantly increased the size of fenestrations by approximately 10 % without a change in porosity. When the dietary nutrient supply is ceased, the liver plays a crucial role in maintaining homeostasis of energy metabolism and blood nutrient levels. Dilation of LSEC fenestrations could increase the exchange of nutrients between the hepatocytes and blood. For example it could enhance the delivery of hepatocyte-produced VLDL and glucose to other organs, and improve delivery of substrates from the blood to hepatocytes for the production and storage of glucose and other nutrients. Further study could investigate the correlation of fenestration dilation with changes in serum levels of various cytokines and hormones in the fasted state that are known to influence fenestrations (such as VEGF, endothelin 1, noradrenaline, and serotonin). It would also be of interest to investigate whether uptake of larger sized lipoproteins occurs with fasting by injecting radio-labelled lipoproteins into the portal vein and measuring the proportion that are trapped (hence passed into the SoD) in the fed and fasted liver. In addition, an investigation of whether the rate of hormone (such as insulin and glucagon) and drug delivery to hepatocytes is altered in the fasted state could be done by performing a multiple indicator dilution test. If drug delivery is increased in fasting it could have significant implications for drug metabolism and clearance, and could be related to the increase

in toxicity associated with fasting in some drugs (in particular the exacerbation of APAP-induced toxicity in Chapter 4 by fasting). It would also be of interest to determine whether fenestrations are dilated more in the periportal than the centrilobular zone as has been reported in the fed state. This could be done by measuring fenestration size and porosity in zones 1 and 3 of the liver to show whether the LSEC maintains a phenotype zonation in both the fed and fasted state similar to hepatocyte metabolic zonation.

In Chapter 4 I found evidence, in support of findings of previous studies, that ultrastructural changes in LSECs influence hepatocyte pathology and repair during drug toxicity. In APAP overdose, LSEC injury can have crucial implications for the degree of hepatocyte damage. Gap formation in the LSEC cytoplasm can exacerbate hepatocyte damage (already initiated by NAPQI) by facilitating direct hepatocyte contact with harmful substances in the blood. The congestion that occurs as a result of microvascular dysfunction can cause ischemic hepatocyte necrosis. LSECs are able to recover from their initial APAP injury and enable liver repair and hepatocyte rejuvenation. In the current study I found that at 24 hours after APAP overdose, LSECs and HSCs formed a tight complex with basement membrane formation and reduction of sinusoid lumen size in areas of severe hepatocyte necrosis. Fenestrations were still present in LSECs supportive of their viability. The survival of LSECs and the maintenance of basic microvasculature structure in areas of hepatocyte necrosis could be crucial to giving hepatocytes a scaffold and nutrient supply by which to regenerate after severe injury. Further investigation of how the sinusoids regenerate from their initial APAP injury could be done by ultrastructural analysis at more time points of APAP toxicity, from the earliest signs of LSEC injury to the time of liver

regeneration and recovery from centrilobular hemorrhagic necrosis up to 3 - 4 days after APAP. A serum analysis of APAP and LSEC-related hormone (such as VEGF and hepatocyte growth factor) concentration could be performed at each time point to help elucidate the physiological basis for the ultrastructural changes.

As was expected, more hepatotoxicity was observed in rats fasted before APAP overdose along with decreased resilience of LSECs in hepatocyte necrotic zones. Certainly fenestration dilation would increase the speed of delivery of APAP to hepatocytes which could result in more NAPQI formation. A multiple indicator dilution test could be performed to observe any differences in APAP uptake between fed and fasted rats that could have been caused by fasting-induced fenestration dilation. Serum analysis of APAP levels could also be performed to examine whether there is a difference in drug clearance of APAP in fasting that could be due to changes in LSEC phenotype. To date studies have only focused on the fasting-related changes in hepatocytes that influence the hepatotoxicity of APAP.

In Chapter 5 I tested the therapeutic value of P407, a substance known to modulate LSEC morphology, in APAP toxicity. P407 was protective to hepatocyte injury and prevented hemorrhage in rats that were fed prior to APAP and given P407 1 hour after APAP overdose. Further study could be performed to investigate the mechanism of P407 protection. Initially this could be done *in vitro* by administering APAP to isolated LSECs and treating them with P407 to observe the direct effect of P407 on LSECs after APAP exposure and injury. P407 post-treatment was not effective at preventing necrosis and hemorrhage in the rats fasted before APAP overdose. This could have been due to a fasting-related morphological or hormonal change that

prevented the protective effect of P407. Alternatively the dose of P407 may not have been high enough to protect liver cells that were more vulnerable in fasting. Exacerbated hepatotoxicity in rats treated with P407 18 hours before APAP was associated with increased LSEC necrosis in areas where hepatocytes were viable. Investigation of whether P407 is toxic to LSECs when administered before a dose of APAP could also be performed *in vitro*.

Age-related changes to the sinusoids, known as pseudocapillarisation, have a significant effect on drug and lipid metabolism. LSEC defenestration reduces the clearance of drugs and lipoproteins from the blood, making people of old age more vulnerable to adverse drug effects and dyslipidemia (that can lead to atherosclerotic plaque formation). *In vitro* analysis of old LSECs could be an effective method of testing substances that may reverse age-related changes in LSEC morphology. In Chapter 6 I found that *in vitro*, the old LSEC retained some but not all of its age-related changes. There was a decrease in fenestration size however porosity was not decreased as it is *in vivo*. Further studies could be performed to observe whether alterations to the cell culture medium, or changes in the time from LSEC isolation to fixation, would enable LSECs to retain all of the age-related changes needed for the study of the ageing LSEC *in vitro*.

In summary, the LSEC is crucial to the maintenance of many important liver functions. Modulation of the LSEC phenotype during fasting appears to be crucial to nutrient exchange in the liver and homeostasis. Injury to the LSEC during drug toxicity and its altered phenotype in ageing has a significant impact on the function and health of the liver. Survival of the LSEC during severe hepatocyte toxicity is vital

for the regeneration of the liver. Therefore therapeutic substances that directly target the LSEC have the potential to improve liver function and viability during disease and hepatotoxicity, and enhance drug and lipid clearance in ageing.

Reference List

Alipour, A, Elte, JW, van Zaanen, HC, Rietveld, AP and Cabezas, MC, (2007), Postprandial inflammation and endothelial dysfuction, *Biochem Soc Trans*, 35 (Pt 3) 466-9

Ankoma-Sey, V, Wang, Y and Dai, Z, (2000), Hypoxic stimulation of vascular endothelial growth factor expression in activated rat hepatic stellate cells, *Hepatology*, 31 (1) 141-8

Antoine, DJ, Williams, DP, Kipar, A, Laverty, H and Park, BK, (2010), Diet restriction inhibits apoptosis and HMGB1 oxidation and promotes inflammatory cell recruitment during acetaminophen hepatotoxicity, *Mol Med*, 16 (11-12) 479-90

Arias, IM, (1990), The biology of hepatic endothelial cell fenestrae, *Prog Liver Dis*, 9 11-26

Arthur, MJ, (1995), Role of Ito cells in the degradation of matrix in liver, *J Gastroenterol Hepatol*, 10 Suppl 1 S57-62

Au, JS, Navarro, VJ and Rossi, S, (2011), Review article: Drug-induced liver injury--its pathophysiology and evolving diagnostic tools, *Aliment Pharmacol Ther*, 34 (1) 11-20

Bacon, BR, Adams, PC, Kowdley, KV, Powell, LW and Tavill, AS, (2011), Diagnosis and management of hemochromatosis: 2011 practice guideline by the American Association for the Study of Liver Diseases, *Hepatology*, 54 (1) 328-43

Baker, RW, (2004), Membrane Transport Theory, (15–87), *Membrane Technology and Applications*, John Wiley & Sons Ltd

Bancroft, JD and Gamble, M, (2008), Theory and practice of histological techniques, Churchill Livingstone

Bardadin, KA and Scheuer, PJ, (1984), Endothelial cell changes in acute hepatitis. A light and electron microscopic study, *J Pathol*, 144 (3) 213-220

Bataller, R and Brenner, A, (2009), 29: Hepatic fibrosis, (433-452), *The Liver: Biology and Pathobiology*, I. M. Arias, John Wiley & Sons Ltd

Bedossa, P, Lemaigre, G, Paraf, F and Martin, E, (1990), Deposition and remodelling of elastic fibres in chronic hepatitis, *Virchows Arch A Pathol Anat Histopathol*, 417 (2) 159-62

Benyon, RC and Arthur, MJ, (1998), Mechanisms of hepatic fibrosis, *J Pediatr Gastroenterol Nutr*, 27 (1) 75-85

Bhunchet, E and Wake, K, (1998), The portal lobule in rat liver fibrosis: a re-evaluation of the liver unit, *Hepatology*, 27 (2) 481-7

Bilzer, M, Roggel, F and Gerbes, AL, (2006), Role of kupffer cells in host defence and liver disease, *Liver Int*, 26 1175-1186

Blouin, A, Bolender, RP and Weibel, ER, (1977), Distribution of organelles and membranes between hepatocytes and nonhepatocytes in the rat liver parenchyma. A stereological study, *J Cell Biol*, 72 (2) 441-455

Blum, I, Vered, Y, Graff, E, Grosskopf, Y, Don, R, Harsat, A and Raz, O, (1992), The influence of meal composition on plasma serotonin and norepinephrine concentrations, *Metabolism*, 41 (2) 137-40

Boelsterli, UA and Lim, PL, (2007), Mitochondrial abnormalities--a link to idiosyncratic drug hepatotoxicity?, *Toxicol Appl Pharmacol*, 220 (1) 92-107

Bosch, J, (2007), Vascular deterioration in cirrhosis: the big picture, *J Clin Gastroenterol*, 41 Suppl 3 S247-53

Bouwens, L, Bleser, PD, Vanderkerken, K, Geerts, B and Wisse, E, (1992), Liver cell heterogeneity: functions of non-parenchymal cells, *Enzyme*, 46 (1-3) 155-168

Boyer, TD, Manns, MP and Sanyal, AJ, (2012), Zakim and Boyer's Hepatology: A Textbook of Liver Disease, Elsevier Inc.

Braet, F, De Zanger, R, Sasaoki, T, Baekeland, M, Janssens, P, Smedsrod, B and Wisse, E, (1994), Assessment of a method of isolation, purification, and cultivation of rat liver sinusoidal endothelial cells, *Lab Invest*, 70 (6) 944-52.

Braet, F, Riches, J, Geerts, W, Jahn, KA, Wisse, E and Frederik, P, (2009), Three-dimensional organization of fenestrae labyrinths in liver sinusoidal endothelial cells, *Liver Int*, 29 (4) 603-13

Braet, F, Shleper, M, Paizi, M, Brodsky, S, Kopeiko, N, Resnick, N and Spira, G, (2004), Liver sinusoidal endothelial cell modulation upon resection and shear stress in vitro, *Comp Hepatol*, 3 (1) 7

Braet, F, Spector, I, De Zanger, R and Wisse, E, (1998), A novel structure involved in the formation of liver endothelial cell fenestrae revealed by using the actin inhibitor misakinolide, *Proc. Natl. Acad. Sci. USA*, 95 (23) 13635-13640

Braet, F and Wisse, E, (2002), Structural and functional aspects of liver sinusoidal endothelial cell fenestrae: a review, *Comp Hepatol*, 1 (1) 1

Braet, F, Wisse, E, Bomans, P, Frederik, P, Geerts, W, Koster, A, Soon, L and Ringer, S, (2007), Contribution of high-resolution correlative imaging techniques in the study of the liver sieve in three-dimensions, *Microsc Res Tech*, 70 (3) 230-42

Braet, F, Zanger, RD, Jans, D, Spector, I and Wisse, E, (1996), Microfilament-disrupting agent latrunculin A induces and increased number of fenestrae in rat

liver sinusoidal endothelial cells: comparison with cytochalasin B, *Hepatology*, 24 (3) 627-635

Brouwer, A, Barelds, RJ and Knook, DL, (1985), Age-related changes in the endocytic capacity of rat liver Kupffer and endothelial cells, *Hepatology*, 5 (3) 362-6

Brouwer, A, Horan, MA, Barelds, RJ and Knook, DL, (1986), Cellular aging of the reticuloendothelial system, *Arch Gerontol Geriatr*, 5 (4) 317-24

Burt, AD, (1993), Cellular and molecular aspects of hepatic fibrosis, *J Pathol*, 1970 105-114

Cacciatore, I, Cornacchia, C, Pinnen, F, Mollica, A and Di Stefano, A, (2010), Prodrug approach for increasing cellular glutathione levels, *Molecules*, 15 (3) 1242-64

Carr, ME, Jr., Carr, SL and High, AA, (1996), Effects of poloxamer 407 on the assembly, structure and dissolution of fibrin clots, *Blood Coagul Fibrinolysis*, 7 (2) 109-13

Cattley, RC and Popp, JA, (2002), 31: Liver, (187-225), *Handbook of Toxicologic Pathology*, W. M. Haschek, C. G. Rousseaux and M. A. Wallig, Academic Press

Cederbaum, AI, (2006), Cytochrome P450 2E1-dependent oxidant stress and upregulation of anti-oxidant defense in liver cells, *J Gastroenterol Hepatol*, 21 Suppl 3 S22-5

Chen, J, Reheman, A, Gushiken, FC, Nolasco, L, Fu, X, Moake, JL, Ni, H and Lopez, JA, (2011), N-acetylcysteine reduces the size and activity of von Willebrand factor in human plasma and mice, *J Clin Invest*, 121 (2) 593-603

Cherkasov, AN, (1990), Selective Ultrafiltration, *J Membr Sci*, 50 109-130

Chichili, GR and Rodgers, W, (2009), Cytoskeleton-membrane interactions in membrane raft structure, *Cell Mol Life Sci*, 66 (14) 2319-28

Cho, ES, Sahyoun, N and Stegink, LD, (1981), Tissue glutathione as a cyst(e)ine reservoir during fasting and refeeding of rats, *J Nutr*, 111 (5) 914-22

Clark, SA, Angus, HB, Cook, HB, George, PM, Oxner, RB and Fraser, R, (1988), Defenestration of hepatic sinusoids as a cause of hyperlipoproteinaemia in alcoholics, *Lancet*, 2 (8622) 1225-7

Clemens, MG, (1999), Nitric oxide in liver injury, *Hepatology*, 30 (1) 1-5

Cogger, VC, Hilmer, SN, Sullivan, D, Muller, M, Fraser, R and Le Couteur, DG, (2006), Hyperlipidemia and surfactants: the liver sieve is a link, *Atherosclerosis*, 189 (2) 273-81

Cogger, VC and Le Couteur, DG, (2009), 27: Fenestrations in the liver sinusoidal endothelial cell, (387-404), *The Liver: Biology and Pathobiology* Arias I. M., John Wiley & Sons Ltd

Cogger, VC, McNerney, GP, Nyunt, T, DeLeve, LD, McCourt, P, Smedsrod, B, Le Couteur, DG and Huser, TR, (2010), Three-dimensional structured illumination microscopy of liver sinusoidal endothelial cell fenestrations, *J Struct Biol*, 171 (3) 382-8

Cogger, VC, Muller, M, Fraser, R, McLean, AJ, Khan, J and Le Couteur, DG, (2004), The effects of oxidative stress on the liver sieve, *J Hepatol*, 41 (3) 370-376

Cogger, VC, Warren, A, Fraser, R, Ngu, M, McLean, AJ and Le Couteur, DG, (2003), Hepatic sinusoidal pseudocapillarization with aging in the non-human primate, *Exp Gerontol*, 38 (10) 1101-7

Corcoran, GB, Bauer, JA and Lau, TW, (1988), Immediate rise in intracellular calcium and glycogen phosphorylase a activities upon acetaminophen covalent binding leading to hepatotoxicity in mice, *Toxicology*, 50 (2) 157-67

Crispe, IN, (2011), Liver antigen-presenting cells, *J Hepatol*, 54 (2) 357-65

Crispe, IN, (2009), The liver as a lymphoid organ, *Annu Rev Immunol*, 27 147-63

Dandona, P, Aljada, A, Mohanty, P, Ghanim, H, Bandyopadhyay, A and Chaudhuri, A, (2003), Insulin suppresses plasma concentration of vascular endothelial growth factor and matrix metalloproteinase-9, *Diabetes Care*, 26 (12) 3310-4

Dariush Fahimi, H, (1967), Perfusion and immersion fixation of rat liver with glutaraldehyde, *Lab Invest*, 16 (5) 736-750

Dasarathy, S and McCullough, AJ, (2007), 32: Alcoholic Liver Disease, *Schiff's diseases of the liver.*, E. R. Schiff, F. Sorrell and W.C. Maddrey, Lippincott Williams & Williams

Davis, M, Ideo, G, Harrison, NG and Williams, R, (1975), Early inhibition of hepatic bilirubin conjugation after paracetamol (acetaminophen) administration in the rat, *Digestion*, 13 (1-2) 42-8

De Leeuw, A, Brouwer, A and Knook, D, (1990), Sinusoidal endothelial cells of the liver: fine structure and function in relation to age., *J Electron Microsc Tech*, 14 (3) 218-236

Deaciuc, IV, D'Souza, NB, Sarphie, TG, Schmidt, J, Hill, DB and McClain, CJ, (1999), Effects of exogenous superoxide anion and nitric oxide on the scavenging function and electron microscopic appearance of the sinusoidal endothelium in the isolated, perfused rat liver, *J Hepatol*, 30 213-221

DeLeve, LD, (1998), Glutathione defence in non-parenchymal cells, *Semin Liver Dis*, 18 (4) 403-13

DeLeve, LD, (2007a), Hepatic microvasculature in liver injury, *Semin Liver Dis*, 27 (4) 390-400

DeLeve, LD, (2007b), 133: The hepatic sinusoidal endothelial cell, (1226-1238), *Endothelial biomedicine: a comprehensive reference*, W. C. Aird, Cambridge University Press

DeLeve, LD, (2009), 26: The hepatic sinusoidal endothelial cell: morphology, function, and pathobiology, (371-388), *The Liver: Biology and Pathobiology*, I M Arias, John Wiley & Sons Ltd

DeLeve, LD, (2011), 2: Vascular liver disease and the liver sinusoidal endothelial cell, *Vascular liver disease: mechanisms and management*, L. D. DeLeve and G. Garcia-Tsao, Springer

DeLeve, LD, Ito, Y, Bethea, NW, McCuskey, MK, Wang, X and McCuskey, RS, (2003a), Embolization by sinusoidal lining cells obstructs the microcirculation in rat sinusoidal obstruction syndrome, *Am J Physiol Gastrointest Liver Physiol*, 284 (6) G1045-52

DeLeve, LD, McCuskey, RS, Wang, X, Hu, L, McCuskey, MK, Epstein, RB and Kanel, GC, (1999), Characterization of a reproducible rat model of hepatic veno-occlusive disease, *Hepatology*, 29 (6) 1779-91

DeLeve, LD, Shulman, HM and McDonald, GB, (2002), Toxic injury to hepatic sinusoids: sinusoidal obstruction syndrome (veno-occlusive disease), *Semin Liver Dis*, 22 (1) 27-42

DeLeve, LD, Wang, X and Guo, Y, (2008), Sinusoidal endothelial cells prevent rat stellate cell activation and promote reversion to quiescence, *Hepatology*, 48 (3) 920-30

DeLeve, LD, Wang, X, Hu, L, McCuskey, MK and McCuskey, RS, (2004), Rat liver sinusoidal endothelial cell phenotype is maintained by paracrine and autocrine regulation, *Am J Physiol Gastrointest Liver Physiol*, 287 (4) G757–G763

DeLeve, LD, Wang, X, Kaplowitz, N, Shulman, HM, Bart, JA and van der Hoek, A, (1997), Sinusoidal endothelial cells as a target for acetaminophen toxicity: direct action versus requirement for hepatocyte activation in different mouse strains, *Biochem Pharmacol*, 53 1339-1345

DeLeve, LD, Wang, X, McCuskey, MK and McCuskey, RS, (2006), Rat liver endothelial cells isolated by anti-CD31 immunomagnetic separation lack fenestrae and sieve plates, *Am J Physiol Gastrointest Liver Physiol*, 291 (6) G1187-9

DeLeve, LD, Wang, X, Tsai, J, Kanel, G, Strasberg, S and Tokes, ZA, (2003b), Sinusoidal obstruction syndrome (veno-occlusive disease) in the rat is prevented by matrix metalloproteinase inhibition, *Gastroenterology*, 125 882-890

Dixon, MF, Nimmo, J and Prescott, LF, (1971), Experimental paracetamol-induced hepatic necrosis: a histopathological study, *J Pathol*, 103 (4) 225-9

Donahower, B, McCullough, SS, Kurten, R, Lamps, LW, Simpson, P, Hinson, JA and James, LP, (2006), Vascular endothelial growth factor and hepatocyte regeneration in acetaminophen toxicity, *Am J Physiol Gastrointest Liver Physiol*, 291 (1) G102-9

Donahower, BC, McCullough, SS, Hennings, L, Simpson, PM, Stowe, CD, Saad, AG, Kurten, RC, Hinson, JA and James, LP, (2010), Human recombinant vascular endothelial growth factor reduces necrosis and enhances hepatocyte

regeneration in a mouse model of acetaminophen toxicity, *J Pharmacol Exp Ther*, 334 (1) 33-43

Duffy, A, Wilkerson, J and Greten, TF, (2013), Hemorrhagic events in hepatocellular carcinoma patients treated with antiangiogenic therapies, *Hepatology*, 57 (3) 1068-77

Dumortier, G, Grossiord, JL, Agnely, F and Chaumeil, JC, (2006), A review of poloxamer 407 pharmaceutical and pharmacological characteristics, *Pharm Res*, 23 (12) 2709-28

Dvorak, AM and Feng, D, (2001), The vesiculo-vacuolar organelle (VVO). A new endothelial cell permeability organelle, *J Histochem Cytochem*, 49 (4) 419-32

Dykstra, MJ and Reuss, LE, (1992), Biological electron microscopy: theory, techniques, and troubleshooting, Springer

Elvevold, K, Smedsrod, B and Martinez, I, (2008), The liver sinusoidal endothelial cell: a cell type of controversial and confusing identity, *Am J Physiol Gastrointest Liver Physiol*, 294 (2) G391-400

Esser, S, Wolburg, K, Wolburg, H, Breier, G, Kurzchalia, T and Risau, W, (1998), Vascular endothelial growth factor induces endothelial fenestrations in vitro, *J Cell Biol*, 140 (4) 947-59

Ezaki, J, Matsumoto, N, Takeda-Ezaki, M, Komatsu, M, Takahashi, K, Hiraoka, Y, Taka, H, Fujimura, T, Takehana, K, Yoshida, M, Iwata, J, Tanida, I, Furuya, N, Zheng, DM, Tada, N, Tanaka, K, Kominami, E and Ueno, T, (2011), Liver autophagy contributes to the maintenance of blood glucose and amino acid levels, *Autophagy*, 7 (7) 727-36

Fallatah, HI and Akbar, HO, (2012), Autoimmune hepatitis as a unique form of an autoimmune liver disease: immunological aspects and clinical overview, *Autoimmune Dis*, 2012 312817

Farrell, GC, Teoh, NC and McCuskey, RS, (2008), Hepatic microcirculation in fatty liver disease, *Anat Rec (Hoboken)*, 291 (6) 684-92

Fausto, N and Campbell, JS, (2003), The role of hepatocytes and oval cells in liver regeneration and repopulation, *Mech Dev*, 120 (1) 117-30

Fawcett, DW, (1955), Observations on the cytology and electron microscopy of hepatic cells, *J Natl Cancer Inst*, 15 (suppl 5) 1475-1503

Ferral, H, Behrens, G and Lopera, J, (2012), Budd-Chiari syndrome, *AJR Am J Roentgenol*, 199 (4) 737-45

Ferri, C, Pittoni, V, Piccoli, A, Laurenti, O, Cassone, MR, Bellini, C, Properzi, G, Valesini, G, De Mattia, G and Santucci, A, (1995), Insulin stimulates endothelin-1 secretion from human endothelial cells and modulates its circulating levels in vivo, *J Clin Endocrinol Metab*, 80 (3) 829-35

Fisher, PJ, Bulur, PA, Vuk-Pavlovic, S, Prendergast, FG and Dietz, AB, (2008), Dendritic cell microvilli: a novel membrane structure associated with the multifocal synapse and T-cell clustering, *Blood*, 112 (13) 5037-45

Foley, JF, Collins, JB, Umbach, DM, Grissom, S, Boorman, GA and Heinloth, AN, (2006), Optimal sampling of rat liver tissue for toxicogenomic studies, *Toxicol Pathol*, 34 (6) 795-801

Fontana, L, Zhao, E, Amir, M, Dong, H, Tanaka, K and Czaja, MJ, (2013), Aging promotes the development of diet-induced murine steatohepatitis but not steatosis, *Hepatology*, 57 (3) 995-1004

Fontana, RJ, (2008), Acute liver failure due to drugs, *Semin Liver Dis*, 28 175-187

Fraser, JW and Fraser, EH, (1895), Preliminary note on intra and intercellular passages in the liver of the frog, *J Anat Physiol*, 29 240

Fraser, R, Bosanquet, AG and Day, WA, (1978), Filtration of chylomicrons by the liver may influence cholesterol metabolism and atherosclerosis, *Atherosclerosis*, 29 (2) 113-23

Fraser, R, Bowler, LM, Day, WA, Dobbs, B, Johnson, HD and Lee, D, (1980), High perfusion pressure damages the sieving ability of sinusoidal endothelium in rat livers, *Br J Exp Pathol*, 61 (2) 222-228

Fraser, R, Dobbs, BR and Rogers, GWT, (1995), Lipoproteins and the liver sieve: the role of the fenestrated sinusoidal endothelium in lipoprotein metabolism, atherosclerosis, and cirrhosis, *Hepatology*, 21 863-874

Frenzel, H, Kremer, B and Hucker, H, (1977), The liver sinusoids under various pathological conditions. A TEM and SEM study of rat liver after respiratory hypoxia, telecobalt irradiation and endotoxin application, (213-222), *Kupffer Cells and Other Liver Sinusoidal Cells*, E. Wisse and D. L. Knook, Elsevier North Holland Biomedical Press

Frey, SL, Zhang, D, Carignano, MA, Szleifer, I and Lee, KY, (2007), Effects of block copolymer's architecture on its association with lipid membranes: experiments and simulations, *J Chem Phys*, 127 (11) 114904

Friedman, SL, (2008), Hepatic stellate cells: protean, multifunctional, and enigmatic cells of the liver, *Physiol Rev*, 88 (1) 125-72

Funyu, J, Mochida, S, Inao, M, Matsui, A and Fujiwara, K, (2001), VEGF can act as vascular permeability factor in the hepatic sinusoids through upregulation of porosity of endothelial cells, *Biochem Biophys Res Commun*, 280 (2) 481-5.

Furrer, K, Rickenbacher, A, Tian, Y, Jochum, W, Bittermann, AG, Kach, A, Humar, B, Graf, R, Moritz, W and Clavien, PA, (2011), Serotonin reverts age-related capillarization and failure of regeneration in the liver through a VEGF-dependent pathway, *Proc Natl Acad Sci U S A*,

Ganey, PE, Luyendyk, JP, Newport, SW, Eagle, TM, Maddox, JF, Mackman, N and Roth, RA, (2007), Role of the coagulation system in acetaminophen-induced hepatotoxicity in mice, *Hepatology*, 46 (4) 1177-86

Gatmaitan, Z, Varticovski, L, Ling, L, Mikkelsen, R, Steffan, AM and Arias, IM, (1996), Studies on fenestral contraction in rat liver endothelial cells in culture, *Am J Pathol*, 148 (6) 2027-41

Geerts, A, Schuppan, D, Lazeroms, S, De Zanger, R and Wisse, E, (1990), Collagen type I and III occur together in hybrid fibrils in the space of Disse of normal rat liver, *Hepatology*, 12 (2) 233-41

Giffin, BF, Drake, RL, Morris, RE and Cardell, RR, (1993), Hepatic lobular patterns of phosphoenolpyruvate carboxykinase, glycogen synthase, and glycogen phosphorylase in fasted and fed rats, *J Histochem Cytochem*, 41 (12) 1849-62

Gomaa, AI, Khan, SA, Toledano, MB, Waked, I and Taylor-Robinson, SD, (2008), Hepatocellular carcinoma: epidemiology, risk factors and pathogenesis, *World J Gastroenterol*, 14 (27) 4300-8

Gonzalez, FJ and Tukey, RH, (2006), 3: Drug metabolism, (71-91), *Goodman & Gilman's The Pharmacological Basis of Therapeutics*, L. L. Brunton, J. S. Lazo and K. L. Parker, McGraw Hill

Gooding, PE, Chayen, J, Sawyer, B and Slater, TF, (1978), Cytochrome P-450 distribution in rat liver and the effect of sodium phenobarbitone administration, *Chem Biol Interact*, 20 (3) 299-310

Gotthardt, D, Riediger, C, Weiss, KH, Encke, J, Schemmer, P, Schmidt, J and Sauer, P, (2007), Fulminant hepatic failure: etiology and indications for liver transplantation, *Nephrol Dial Transplant*, 22 Suppl 8 viii5-viii8

Govindarajan, S and Bonacini, M, (2009), Liver biopsy and histopathological diagnosis, *Textbook of Gastroenterology*, T. Yamada, Blackwell Publishing

Griffith, WP, (1974), Osmium tetroxide and its applications, *Platinum Metals Rev*, 18 (3) 94-96

Gujral, JS, Knight, TR, Farhood, A, Bajt, ML and Jaeschke, H, (2002), Mode of cell death after acetaminophen overdose in mice: apoptosis or oncotic necrosis?, *Toxicol Sci*, 67 (2) 322-8

Gulubova, MV, (1996), Ultrastructural sinusoidal changes in extrahepatic cholestasis. Light and electron microscopic immunohistochemical localization of collagen type III and type IV, *Acta Histochemica*, 98 (3) 271-83

Harrison, SA, Brunt, EM, Goodman, ZD and Di Bisceglie, AM, (2006), Diabetic hepatosclerosis: diabetic microangiopathy of the liver, *Arch Pathol Lab Med*, 130 (1) 27-32

Hayat, MA, (1981), Fixation for electron microscopy, Academic Press

Hayat, MA, (2000), Principles and techniques of electron microscopy: biological applications, University Press

Hayat, MA, (1993), Stains and cytochemical methods, Springer

Heath, T and Lowden, S, (1998), Pathways of interstitial fluid and lymph flow in the liver acinus of the sheep and mouse, *J Anat*, 192 (Pt 3) 351-8

Heinloth, AN, Irwin, RD, Boorman, GA, Nettesheim, P, Fannin, RD, Sieber, SO, Snell, ML, Tucker, CJ, Li, L, Travlos, GS, Vansant, G, Blackshear, PE, Tennant, RW, Cunningham, ML and Paules, RS, (2004), Gene expression

profiling of rat livers reveals indicators of potential adverse effects, *Toxicol Sci*, 80 193-202

Hessel, G, De-Santi-Neto, D and Collares, EF, (1996), Correlation between the severity of acute hepatic necrosis induced by acetaminophen and serum aminotransferase levels in fasted and sucrose-fed rats, *Braz J Med Biol Res*, 29 (6) 793-6

Hilmer, SN, Cogger, VC, Fraser, R, McLean, AJ, Sullivan, D and Le Couteur, DG, (2005), Age-related changes in the hepatic sinusoidal endothelium impede lipoprotein transfer in the rat, *Hepatology*, 42 1349-1354

Hinson, JA, Mays, JB and Cameron, AM, (1983), Acetaminophen-induced hepatic glycogen depletion and hyperglycemia in mice, *Biochem Pharmacol*, 32 (13) 1979-88

Hinson, JA, Reid, AB, McCullough, SS and James, LP, (2004), Acetaminophen-induced hepatotoxicity: role of metabolic activation, reactive oxygen/nitrogen species, and mitochondrial permeability transition, *Drug Metab Rev*, 36 (3-4) 805-22

Hinson, JA, Roberts, DW and James, LP, (2010), Mechanisms of acetaminophen-induced liver necrosis, *Handb Exp Pharmacol*, (196) 369-405

Holt, MP, Yin, H and Ju, C, (2010), Exacerbation of acetaminophen-induced disturbances of liver sinusoidal endothelial cells in the absence of Kupffer cells in mice, *Toxicol Lett*, 194 (1-2) 34-41

Hopwood, D, (1969), Fixatives and fixation: a review, *Histochem J*, 1 323-360

Horn, T, Christoffersen, P and Henriksen, JH, (1987), Alcoholic liver injury: defenestration in noncirrhotic livers-a scanning electron microscopic study, *Hepatology*, 7 (1) 77-82

Hudacko, RM, Sciancalepore, JP and Fyfe, BS, (2009), Diabetic microangiopathy in the liver: an autopsy study of incidence and association with other diabetic complications, *Am J Clin Pathol*, 132 (4) 494-9

Igusa, Y, Yamashina, S, Izumi, K, Inami, Y, Fukada, H, Komatsu, M, Tanaka, K, Ikejima, K and Watanabe, S, (2012), Loss of autophagy promotes murine acetaminophen hepatotoxicity, *J Gastroenterol*, 47 (4) 433-443

Ingelmo-Torres, M, Gaus, K, Herms, A, Gonzalez-Moreno, E, Kassan, A, Bosch, M, Grewal, T, Tebar, F, Enrich, C and Pol, A, (2009), Triton X-100 promotes a cholesterol-dependent condensation of the plasma membrane, *Biochem J*, 420 (3) 373-81

Irwin, RD, Parker, JS, Lobenhofer, EK, Burka, LT, Blackshear, PE, Vallant, MK, Lebetkin, EH, Gerken, DF and Boorman, GA, (2005), Transcriptional profiling of the left and median liver lobes of male F344/N rats following exposure to acetaminophen, *Toxicol Pathol*, 33 111-117

Ishida, Y, Kondo, T, Kimura, A, Tsuneyama, K, Takayasu, T and Mukaida, N, (2006), Opposite roles of neutrophils and macrophages in the pathogenesis of acetaminophen-induced acute liver injury, *Eur J Immunol*, 36 (4) 1028-38

Ito, K, Bethea, NW, Abril, ER and McCuskey, RS, (2003), Early hepatic microvascular injury in response to acetaminophen toxicity, *Microcirculation*, 10 391-400

Ito, Y, Abril, ER, Bethea, NW, McCuskey, MK, Cover, C, Jaeschke, H and McCuskey, RS, (2006), Mechanisms and pathophysiological implications of sinusoidal endothelial cell gap formation following treatment with galactosamine/endotoxin in mice, *Am J Physiol Gastrointest Liver Physiol*, 291 (2) G211-8

Ito, Y, Abril, ER, Bethea, NW and McCuskey, RS, (2005), Inhibition of matrix metalloproteinases minimizes hepatic microvascular injury in response to acetaminophen in mice, *Toxicol Sci*, 83 190-196

Ito, Y, Sorensen, KK, Bethea, NW, Svistounov, D, McCuskey, MK, Smedsrod, BH and McCuskey, RS, (2007), Age-related changes in the hepatic microcirculation of mice, *Exp Gerontol*, 48 789-797

Iwakiri, Y, (2012), Endothelial dysfunction in the regulation of cirrhosis and portal hypertension, *Liver Int*, 32 (2) 199-213

Iwakiri, Y and Groszmann, RJ, (2007), Vascular endothelial dysfunction in cirrhosis, *J Hepatol*, 46 (5) 927-34

Jaeschke, H, (2005), Role of inflammation in the mechanism of acetaminophen-induced hepatotoxicity, *Expert Op in Drug Metab Toxicol*, 1 (3) 389-397

Jaeschke, H, Gores, GJ, Cederbaum, AI, Hinson, JA, Pessayre, D and Lemasters, JJ, (2002), Mechanisms of hepatotoxicity, *Toxicol Sci*, 65 (2) 166-76

Jaeschke, H and Hasegawa, T, (2006), Role of neutrophils in acute inflammatory liver injury, *Liver Int*, 26 (8) 912-9

Jaeschke, H, McGill, MR and Ramachandran, A, (2012a), Oxidant stress, mitochondria, and cell death mechanisms in drug-induced liver injury: Lessons learned from acetaminophen hepatotoxicity, *Drug Metab Rev*, 44 (1) 88-106

Jaeschke, H, Williams, CD, Ramachandran, A and Bajt, ML, (2012b), Acetaminophen hepatotoxicity and repair: the role of sterile inflammation and innate immunity, *Liver Int*, 32 (1) 8-20

Jamieson, HA, Hilmer, SN, Cogger, VC, Warren, A, Cheluvappa, R, Abernethy, DR, Everitt, AV, Fraser, R, de Cabo, R and Le Couteur, DG, (2007), Caloric

restriction reduces age-related pseudocapillarization of the hepatic sinusoid, *Exp Gerontol*, 42 (4) 374-8

Jancova, P, Anzenbacher, P and Anzenbacherova, E, (2010), Phase II drug metabolizing enzymes, *Biomed Pap Med Fac Univ Palacky Olomouc Czech Repub*, 154 (2) 103-16

Jansen, PL, (2002), Liver disease in the elderly, *Best Practice & Research Clinical Gastroenterology*, 16 (1) 149-58

Jepson, MA, Davis, MJ, Horton, AA and Walker, DG, (1987), Histochemical and biochemical observations on the cytotoxicity of paracetamol and its effects on glycogen metabolism in rat liver, *Toxicology*, 47 (3) 325-37

Johnston, TP, (2004), The P-407-induced murine model of dose-controlled hyperlipidemia and atherosclerosis: a review of findings to date, *J Cardiovasc Pharmacol*, 43 (4) 595-606

Johnston, TP, (2009), Poloxamer 407 increases soluble adhesion molecules, ICAM-1, VCAM-1 and E-selectin, in C57BL/6 mice, *J Pharm Pharmacol*, 61 (12) 1681-8

Johnston, TP and Waxman, DJ, (2008), Circulating free fatty acids are increased independently of PPARgamma activity after administration of poloxamer 407 to mice, *Can J Physiol Pharmacol*, 86 (9) 643-9

Johnston, TP and Zhou, X, (2007), Oxidation of low-density lipoprotein cholesterol following administration of poloxamer 407 to mice results from an indirect effect, *J Cardiovasc Pharmacol*, 49 (4) 246-52

Jonges, GN, Van Noorden, CJ and Lamers, WH, (1992), In situ kinetic parameters of glucose-6-phosphatase in the rat liver lobulus, *J Biol Chem*, 267 (7) 4878-81

Junaidi, O and Di Bisceglie, AM, (2007), Aging liver and hepatitis, *Clin Geriatr Med*, 23 (4) 889-903, viii

Jungermann, K, Heilbronn, R, Katz, N and Sasse, D, (1982), The glucose/glucose-6-phosphate cycle in the periportal and perivenous zone of rat liver, *Eur J Biochem*, 123 (2) 429-36

Jungermann, K and Kietzmann, T, (2000), Oxygen: modulator of metabolic zonation and disease of the liver, *Hepatology*, 31 (2) 255-60

Kahn, E, Baarine, M, Dauphin, A, Ragot, K, Tissot, N, Seguin, A, Menetrier, F, Kattan, Z, Bachelet, CM, Frouin, F and Lizard, G, (2011), Impact of 7-ketocholesterol and very long chain fatty acids on oligodendrocyte lipid membrane organization: evaluation via LAURDAN and FAMIS spectral image analysis, *Cytometry A*, 79 (4) 293-305

Kalderon, B, Mayorek, N, Berry, E, Zevit, N and Bar-Tana, J, (2000), Fatty acid cycling in the fasting rat, *Am J Physiol Endocrinol Metab*, 279 (1) E221-7

Kamegaya, Y, Oda, M, Yokomori, H and Ishii, H, (2002), Role of endothelin receptors in endothelin-1-induced morphological changes of hepatic sinusoidal endothelial fenestrae: morphometric evaluation with scanning electron microscopy, *Hepatol Res*, 22 (2) 89-101

Karkkainen, MU, Wiersma, JW and Lamberg-Allardt, CJ, (1997), Postprandial parathyroid hormone response to four calcium-rich foodstuffs, *Am J Clin Nutr*, 65 (6) 1726-30

Karsan, HA and Parekh, S, (2012), Management of alcoholic hepatitis: Current concepts, *World J Hepatol*, 4 (12) 335-41

Kato, T, Ito, Y, Hosono, K, Suzuki, T, Tamaki, H, Minamino, T, Kato, S, Sakagami, H, Shibuya, M and Majima, M, (2011), Vascular endothelial growth factor

receptor-1 signaling promotes liver repair through restoration of liver microvasculature after acetaminophen hepatotoxicity, *Toxicol Sci*, 120 (1) 218-29

Kawada, N, Tran-Thi, TA, Klein, H and Decker, K, (1993), The contraction of hepatic stellate (Ito) cells stimulated with vasoactive substances. Possible involvement of endothelin 1 and nitric oxide in the regulation of the sinusoidal tonus, *Eur J Biochem*, 213 (2) 815-23

Kersten, S, Seydoux, J, Peters, JM, Gonzalez, FJ, Desvergne, B and Wahli, W, (1999), Peroxisome proliferator-activated receptor alpha mediates the adaptive response to fasting, *J Clin Invest*, 103 (11) 1489-98

Kiernan, F, (1833), The anatomy and physiology of the liver, *Philos Trans R Soc Lond B Biol Sci, Biol* 123 711-770

Kim, JS, He, L and Lemasters, JJ, (2003), Mitochondrial permeability transition: a common pathway to necrosis and apoptosis, *Biochem Biophys Res Commun*, 304 (3) 463-70

Kmiec, Z, (2001), Cooperation of liver cells in health and disease, *Adv Anat Embryol Cell Biol*, 161 III-XIII, 1-151

Knight, TR and Jaeschke, H, (2004), Peroxynitrite formation and sinusoidal endothelial cell injury during acetaminophen-induced hepatotoxicity in mice, *Comp Hepatol*, 3 Suppl 1 S46

Knook, DL, (1982), Aging of cells: accident or programme?, *Endeavour*, 6 (4) 162-7

Knook, DL and Sleyster, EC, (1980), Isolated parenchymal, Kupffer and endothelial rat liver cells characterized by their lysosomal enzyme content, *Biochem Biophys Res Commun*, 96 (1) 250-7

Koriyama, Y, Yamada, E and Watanabe, I, (1992), "Pored-domes" of the fenestrated endotheliocyte of the glomerular and peritubular capillaries in the rodent kidney, *J Electron Microsc (Tokyo)*, 41 (1) 30-6

Kostrubsky, VE, Lewis, LD, Wood, SG, Sinclair, PR, Wrighton, SA and Sinclair, JF, (1997), Effect of Taxol on cytochrome P450 3A and acetaminophen toxicity in cultured rat hepatocytes: comparison to dexamethasone, *Toxicol Appl Pharmacol*, 142 (1) 79-86

Krasinski, SD, Cohn, JS, Schaefer, EJ and Russell, RM, (1990), Postprandial plasma retinyl ester response is greater in older subjects compared with younger subjects. Evidence for delayed plasma clearance of intestinal lipoproteins, *J Clin Invest*, 85 (3) 883-92

Krause, P, Markus, PM, Schwartz, P, Unthan-Fechner, K, Pestel, S, Fandrey, J and Probst, I, (2000), Hepatocyte-supported serum-free culture of rat liver sinusoidal endothelial cells, *J Hepatol*, 32 (5) 718-26

Krylova, OO and Pohl, P, (2004), Ionophoric activity of pluronic block copolymers, *Biochemistry*, 43 (12) 3696-703

Kumar, V, Abbas, AK, Fausto, N and Aster, JC, (2009), Mechanisms of cell injury: Robbins and Cotran Pathologic Basis of Disease, Saunders

Kuntz, E and Kuntz, H, (2008), Hepatology: textbook and atlas, Springer

Lalor, PF, Shields, P, Grant, A and Adams, DH, (2002), Recruitment of lymphocytes to the human liver, *Immunol Cell Biol*, 80 (1) 52-64

Latry, P, Bioulac-Sage, P, Echinard, E, Gin, H, Boussarie, L, Grimaud, JA and Balabaud, C, (1987), Perisinusoidal fibrosis and basement membrane-like material in the livers of diabetic patients, *Hum Pathol*, 18 (8) 775-80

Lauterburg, BH, (2002), Analgesics and glutathione, *Am J Ther*, 9 225-233

Le Bail, B, Bioulac-Sage, P, Senuita, R, Quinton, A, Saric, J and Balabaud, C, (1990), Fine structure of hepatic sinusoids and sinusoidal cells in disease, *J Electron Microsc Tech*, 14 (3) 257-82

Le Couteur, D, Rivory, LP, Roberts, MS and Pond, SM, (1992), Aging and the response of the isolated perfused rat liver to vasoactive drugs, *Biochemical Pharmacology*, 43 913-915

Le Couteur, DG, Cogger, VC, Markus, AM, Harvey, PJ, Yin, ZL, Ansselin, AD and McLean, AJ, (2001), Pseudocapillarization and associated energy limitation in the aged rat liver, *Hepatology*, 33 (3) 537-43

Le Couteur, DG, Cogger, VC, McCuskey, RS, R, DEC, Smedsrod, B, Sorensen, KK, Warren, A and Fraser, R, (2007), Age-related changes in the liver sinusoidal endothelium: a mechanism for dyslipidemia, *Ann N Y Acad Sci*, 1114 79-87

Le Couteur, DG, Fraser, R, Cogger, VC and McLean, AJ, (2002), Hepatic pseudocapillarisation and atherosclerosis in ageing, *Lancet*, 359 (9317) 1612-5

Le Couteur, DG, Fraser, R, Hilmer, S, Rivory, LP and McLean, AJ, (2005), The hepatic sinusoid in aging and cirrhosis - Effects on hepatic substrate disposition and drug clearance, *Clin Pharmacokinet*, 44 (2) 187-200

Le Couteur, DG and McLean, AJ, (1998), The aging liver. Drug clearance and an oxygen diffusion barrier hypothesis, *Clin Pharmacokinet*, 34 (5) 359-73

Le Couteur, DG, Warren, A, Cogger, VC, Smedsrod, B, Sorensen, KK, De Cabo, R, Fraser, R and McCuskey, RS, (2008), Old age and the hepatic sinusoid, *Anat Rec (Hoboken)*, 291 (6) 672-83

LeCouter, J, Moritz, DR, Li, B, Phillips, GL, Liang, XH, Gerber, H-P, Hillan, KJ and Ferrara, N, (2003), Angiogenesis-independent endothelial protection of liver: role of VEGFR-1, *Science*, 299 890-893

Lee, KP, (1983), Peliosis hepatis-like lesion in aging rats, *Vet Pathol*, 20 (4) 410-23

Lee, YS, Kim, YW, Kim, SG, Lee, I, Lee, MG and Kang, HE, (2011), Effects of poloxamer 407-induced hyperlipidemia on the pharmacokinetics of carbamazepine and its 10,11-epoxide metabolite in rats: Impact of decreased expression of both CYP3A1/2 and microsomal epoxide hydrolase, *Eur Neuropsychopharmacol*, 22 (6) 431-40

Lee, YS, Yoon, JN, Yoon, IS, Lee, MG and Kang, HE, (2012), Pharmacokinetics of verapamil and its metabolite norverapamil in rats with hyperlipidaemia induced by poloxamer 407, *Xenobiotica*, 42 (8) 766-74

Li, C, Palmer, WK and Johnston, TP, (1996), Disposition of poloxamer 407 in rats following a single intraperitoneal injection assessed using a simplified colorimetric assay, *J Pharm Biomed Anal*, 14 (5) 659-65

Licastro, F, Candore, G, Lio, D, Porcellini, E, Colonna-Romano, G, Franceschi, C and Caruso, C, (2005), Innate immunity and inflammation in ageing: a key for understanding age-related diseases, *Immun Ageing*, 2 8

Lighezan, R, Baderca, F, Alexa, A, Iacovliev, M, Bonte, D, Murarescu, ED and Nebunu, A, (2009), The value of the reprocessing method of paraffin-embedded biopsies for transmission electron microscopy, *Rom J Morphol Embryol*, 50 (4) 613-7

Lim, SP, Andrews, FJ and O'Brien, PE, (1995), Acetaminophen-induced microvascular injury in the rat liver: protection with misoprostol, *Hepatology*, 22 (6) 1776-81

Luo, DZ, Vermijlen, D, Ahishali, B, Triantis, V, Plakoutsi, G, Braet, F, Vanderkerken, K and Wisse, E, (2000), On the cell biology of pit cells, the liver-specific NK cells, *World J Gastroenterol*, 6 (1) 1-11

MacSween, RNM, Desmet, VJ, Roskams, T and Scothorne, RJ, (2002), Developmental anatomy and normal structure, (1–66), *Pathology of the Liver*, R. N. M. MacSween, A. D. Burt, B. C. Portmann, K. G. Ishak, P. J. Scheuer and P. P. Anthony, Churchill Livingstone

Malarkey, DE, Johnson, K, Ryan, L, Boorman, G and Maronpot, RR, (2005), New insights into functional aspects of liver morphology, *Toxicol Pathol*, 33 27-34

March, S, Hui, EE, Underhill, GH, Khetani, S and Bhatia, SN, (2009), Microenvironmental regulation of the sinusoidal endothelial cell phenotype in vitro, *Hepatology*, 50 (3) 920-8

Martinez, I, Nedredal, GI, Oie, CI, Warren, A, Johansen, O, Le Couteur, DG and Smedsrod, B, (2008), The influence of oxygen tension on the structure and function of isolated liver sinusoidal endothelial cells, *Comp Hepatol*, 7 4

Martins, IJ, Tran, JM and Redgrave, TG, (2002), Food restriction normalizes chylomicron remnant metabolism in murine models of obesity as assessed by a novel stable isotope breath test, *J Nutr*, 132 (2) 176-81

Massip, L, Garand, C, Paquet, ER, Cogger, VC, O'Reilly, JN, Tworek, L, Hatherell, A, Taylor, CG, Thorin, E, Zahradka, P, Le Couteur, DG and Lebel, M, (2010), Vitamin C restores healthy aging in a mouse model for Werner syndrome, *Faseb J*, 24 (1) 158-72

Matsumoto, T, Komori, R and Hamadeh, HK, (1979), A study on the normal structure of human liver, with special reference to its angioarchitecture., *Jikeikai Med J*, 26 1-40

Matsuno, K and Ezaki, T, (2000), Dendritic cell dynamics in the liver and hepatic lymph, *Int Rev Cytol*, 197 83-136

Mazer, M and Perrone, J, (2008), Acetaminophen-induced nephrotoxicity: pathophysiology, clinical manifestations, and management, *J Med Toxicol*, 4 (1) 2-6

McCuskey, RS, (2008), The hepatic microvascular system in health and its response to toxicants, *Anat Rec (Hoboken)*, 291 661-671

McCuskey, RS, (2006), Sinusoidal endothelial cells as an early target for hepatic toxicants, *Clin Hemorheol Microcirc*, 34 (1-2) 5-10

McCuskey, RS, Ito, Y, Robertson, GR, McCuskey, MK, Perry, M and Farrell, GC, (2004), Hepatic microvascular dysfunction during evolution of dietary steatohepatitis in mice, *Hepatology*, 40 (2) 386-93

McCuskey, RS and McCuskey, PA, (1990), Fine structure and function of Kupffer cells, *J Electron Microsc Tech*, 14 (3) 237-46

McCuskey, RS, Reilly, FD, McCuskey, PA and Dimlich, RV, (1979), In vivo microscopy of the hepatic microvascular system, *Bibl anat*, (18) 73-6

McGuire, RF, Bissell, DM, Boyles, J and Roll, FJ, (1992), Role of extracellular matrix in regulating fenestrations of sinusoidal endothelial cells isolated from normal rat liver, *Hepatology*, 15 989-997

McLean, AE and Day, PA, (1975), The effect of diet on the toxicity of paracetamol and the safety of paracetamol-methionine mixtures, *Biochem Pharmacol*, 24 (1) 37-42

McLean, AJ, Cogger, VC, Chong, GC, Warren, A, Markus, AM, Dahlstrom, JE and Le Couteur, DG, (2003), Age-related pseudocapillarization of the human liver, *J Pathol*, 200 (1) 112-7

McMurtry, RJ, Snodgrass, WR and Mitchell, JR, (1978), Renal necrosis, glutathione depletion, and covalent binding after acetaminophen, *Toxicol Appl Pharmacol*, 46 (1) 87-100

Millar, JS, Cromley, DA, McCoy, MG, Rader, DJ and Billheimer, JT, (2005), Determining hepatic triglyceride production in mice: comparison of poloxamer 407 with Triton WR-1339, *J Lipid Res*, 46 (9) 2023-8

Minassian, C, Ajzannay, A, Riou, JP and Mithieux, G, (1994), Investigation of the mechanism of glycogen rebound in the liver of 72-hour fasted rats, *J Biol Chem*, 269 (24) 16585-8

Mitchell, SJ, Huizer-Pajkos, A, Cogger, VC, McLachlan, AJ, Le Couteur, DG and Hilmer, SN, (2010), Poloxamer 407 increases the recovery of paracetamol in the isolated perfused rat liver, *J Pharm Sci*, 100 (1) 334-40

Mitchell, SJ, Huizer-Pajkos, A, Cogger, VC, McLachlan, AJ, Le Couteur, DG, Jones, B, de Cabo, R and Hilmer, SN, (2011), Age-related pseudocapillarization of the liver sinusoidal endothelium impairs the hepatic clearance of acetaminophen in rats, *J Gerontol A Biol Sci Med Sci*, 66 (4) 400-8

Moller, L, Stodkilde-Jorgensen, H, Jensen, FT and Jorgensen, JO, (2008), Fasting in healthy subjects is associated with intrahepatic accumulation of lipids as assessed by 1H-magnetic resonance spectroscopy, *Clin Sci (Lond)*, 114 (8) 547-52

Montesano, R and Nicolescu, P, (1978), Fenestrations in endothelium of rat liver sinusoids revisited by freeze-fracture, *Anat Rec*, 190 (4) 861-870

Mori, T, Okanoue, T, Sawa, Y, Hori, N, Ohta, M and Kagawa, K, (1993), Defenestration of the sinusoidal endothelial cell in a rat model of cirrhosis, *Hepatology*, 17 (5) 891-7.

Moriyama, T, Tsujioka, S, Ohira, T, Nonaka, S, Ikeda, H, Sugiura, H, Tomohiro, M, Samura, K and Nishikibe, M, (2008), Effects of reduced food intake on toxicity study parameters in rats, *J Toxicol Sci*, 33 (5) 537-47

Morsy, MA, Ibrahim, SA, Abdelwahab, SA, Zedan, MZ and Elbitar, HI, (2010), Curative effects of hydrogen sulfide against acetaminophen-induced hepatotoxicity in mice, *Life Sci*, 87 (23-26) 692-8

Murata, K and Nakashima, H, (1985), Clinical and metabolic studies on Werner's syndrome: with special reference to disorders of lipid and liver function, *Adv Exp Med Biol*, 190 285-304

Musso, O, Rehn, M, Saarela, J, Theret, N, Lietard, J, Hintikka, Lotrian, D, Campion, JP, Pihlajaniemi, T and Clement, B, (1998), Collagen XVIII is localized in sinusoids and basement membrane zones and expressed by hepatocytes and activated stellate cells in fibrotic human liver, *Hepatology*, 28 (1) 98-107

Nagai, T, Yokomori, H, Yoshimura, K, Fujimaki, K, Nomura, M, Hibi, T and Oda, M, (2004), Actin filaments around endothelial fenestrae in rat hepatic sinusoidal endothelial cells, *Med Electron Microsc*, 37 (4) 252-5

Naito, M, Hasegawa, G, Ebe, Y and Yamamoto, T, (2004), Differentiation and function of kupffer cells, *Med Electron Microsc*, 37 16-28

Nakatani, K, Kaneda, K, Seki, S and Nakajima, Y, (2004), Pit cells as liver-associated natural killer cells: morphology and function, *Med Electron Microsc*, 37 29-36

Nasr, SH, Markowitz, GS, Valeri, AM, Yu, Z, Chen, L and D'Agati, VD, (2007), Thin basement membrane nephropathy cannot be diagnosed reliably in deparaffinized, formalin-fixed tissue, *Nephrol Dial Transplant*, 22 (4) 1228-32

Neal, MJ, (1992), Pathways of Drug metabolism, (5-7), *Medical pharmacology at a glance*, Blackwell Science

Neubauer, K, Saile, B and Ramadori, G, (2001), Liver fibrosis and altered matrix synthesis, *Can J Gastroenterol*, 15 (3) 187-93

Newton, JF, Kuo, CH, Gemborys, MW, Mudge, GH and Hook, JB, (1982), Nephrotoxicity of p-aminophenol, a metabolite of acetaminophen, in the fischer 344 rat, *Toxicol Appl Pharmacol*, 65 (2) 336-44

Ni, HM, Bockus, A, Boggess, N, Jaeschke, H and Ding, WX, (2012), Activation of autophagy protects against acetaminophen-induced hepatotoxicity, *Hepatology*, 55 (1) 222-32

Oda, M, Kamegaya, K, Yokomori, H, Han, JY, Akiba, Y, Nakamura, M, Ishii, H and Tsuchiya, M, (1997), Roles of plasma membrane Ca2+-ATPase in the relaxation and contraction of hepatic sinusoidal endothelial fenestrae- effects of prostaglandin E1 and endothelin 1, (313-317), *Cells of the hepatic sinusoid*, E. Wisse, D. L. Knook and C. Balabaud, Kupffer Cell Foundation

Oda, M, Yokomori, H and Han, JY, (2003), Regulatory mechanisms of hepatic microcirculation, *Clin Hemorheol Microcirc*, 29 (3-4) 167-82

Oda, M, Yokomori, H and Han, JY, (2006), Regulatory mechanisms of hepatic microcirculatory hemodynamics: hepatic arterial system, *Clin Hemorheol Microcirc*, 34 11-26

Ohata, M, Tanuma, Y and Ito, T, (1984), A transmission electron microscopic study on sinusoidal cells of guinea pig liver, with special reference to the occurrence of a canalicular system and pored domes in the endothelium, *Arch Histol Jap*, 47 359-376

Ohtani, O and Ohtani, Y, (2008), Lymph circulation in the liver, *Anat Rec (Hoboken)*, 291 (6) 643-52

Ohtani, Y, Wang, BJ, Poonkhum, R and Ohtani, O, (2003), Pathways for movement of fluid and cells from hepatic sinusoids to the portal lymphatic vessels and subcapsular region in rat livers, *Arch Histol Cytol*, 66 (3) 239-52

Palmer, WK, Emeson, EE and Johnston, TP, (1997), The poloxamer 407-induced hyperlipidemic atherogenic animal model, *Med Sci Sports Exerc*, 29 (11) 1416-21

Papastefanou, VP, Bozas, E, Mykoniatis, MG, Grypioti, A, Garyfallidis, S, Bartsocas, CS and Nicolopoulou-Stamati, P, (2007), VEGF isoforms and receptors expression throughout acute acetaminophen-induced liver injury and regeneration, *Arch Toxicol*, 81 (10) 729-41

Parker, GA and Picut, CA, (2005), Liver immunobiology, *Toxicol Pathol*, 33 (1) 52-62

Pec, EA, Wout, ZG and Johnston, TP, (1992), Biological activity of urease formulated in poloxamer 407 after intraperitoneal injection in the rat, *J Pharm Sci*, 81 (7) 626-30

Pessayre, D, Dolder, A, Artigou, J-Y, Wandscheer, J-C, Descatoire, V, Degott, C and Benhamou, J-P, (1979), Effect of fasting on metabolite-mediated hepatotoxicity in the rat, *Gastroenterology*, 77 264-271

Pessayre, D, Wandscheer, JC, Cobert, B, Level, R, Degott, C, Batt, AM, Martin, N and Benhamou, JP, (1980), Additive effects of inducers and fasting on acetaminophen hepatotoxicity, *Biochem Pharmacol*, 29 (16) 2219-23

Popper, H, (1986), Aging and the liver, *Progress in Liver Diseases*, 8 659-683

Price, VF and Jollow, DJ, (1988), Mechanism of decreased acetaminophen glucuronidation in the fasted rat, *Biochem Pharmacol*, 37 (6) 1067-75

Price, VF, Miller, MG and Jollow, DJ, (1987), Mechanisms of fasting-induced potentiation of acetaminophen hepatotoxicity in the rat, *Biochem Pharmacol*, 36 (4) 427-33

Protzer, U, Maini, MK and Knolle, PA, (2012), Living in the liver: hepatic infections, *Nat Rev Immunol*, 12 (3) 201-13

Racanelli, V and Rehermann, B, (2006), The liver as an immunological organ, *Hepatology*, 43 (2 Suppl 1) S54-62

Ramachandran, R and Kakar, S, (2009), Histological patterns in drug-induced liver disease, *J Clin Pathol*, 62 (6) 481-92

Rappaport, AM, Borowy, ZJ, Loughheed, WM and Lotto, WN, (1954), Subdivision of hexagonal liver lobules into a structural and functional unit, *Anat Rec*, 119 11-33

Raymond, J, Metcalfe, A, Salazkin, I and Schwarz, A, (2004), Temporary vascular occlusion with poloxamer 407, *Biomaterials*, 25 (18) 3983-9

Reeves, HL and Friedman, SL, (2002), Activation of hepatic stellate cells--a key issue in liver fibrosis, *Front Biosci*, 7 d808-26

Rehm, J, Taylor, B, Mohapatra, S, Irving, H, Baliunas, D, Patra, J and Roerecke, M, (2010), Alcohol as a risk factor for liver cirrhosis: a systematic review and meta-analysis, *Drug Alcohol Rev*, 29 (4) 437-45

Reid, LM, Fiorino, AS, Sigal, SH, Brill, S and Holst, PA, (1992), Extracellular matrix gradients in the space of Disse: relevance to liver biology, *Hepatology*, 15 (6) 1198-203

Reynaert, H, Thompson, MG, Thomas, T and Geerts, A, (2002), Hepatic stellate cells: role in microcirculation and pathophysiology of portal hypertension, *Gut*, 50 (4) 571-81

Robbins, SJ, (2007), 1: Robbins basic pathology (1-30), Kumar, Abbas, Fausto and Mitchell, Saunders/Elsevier

Roth, RA and Ganey, PE, (2009), 47: Inflammation and drug-induced liver injury, (773-781), *The Liver: Biology and Pathobiology*, I. M. Arias, John Wiley & Sons Ltd

Rothacker, DL, Kanerva, RL, Wyder, WE, Alden, CL and Maurer, JK, (1988), Effects of variation of necropsy time and fasting on liver weights and liver components in rats, *Toxicol Pathol*, 16 (1) 22-6

Rowden, AK, Norvell, J, Eldridge, DL and Kirk, MA, (2005), Updates on acetaminophen toxicity, *Med Clin North Am*, 89 (6) 1145-59

Russmann, S, Kullak-Ublick, GA and Grattagliano, I, (2009), Current concepts of mechanisms in drug-induced hepatotoxicity, *Curr Med Chem*, 16 (23) 3041-53

Sanchez-Valle, V, Chavez-Tapia, NC, Uribe, M and Mendez-Sanchez, N, (2012), Role of oxidative stress and molecular changes in liver fibrosis: a review, *Curr Med Chem*, 19 (28) 4850-60

Sankary, HN, Chong, A, Foster, P, Brown, E, Shen, J, Kimura, R, Rayudu, G and Williams, J, (1995), Inactivation of Kupffer cells after prolonged donor fasting improves viability of transplanted hepatic allografts, *Hepatology*, 22 (4 Pt 1) 1236-42

Sarsik, B, Sen, S, Kirdok, FS, Akarca, US, Toz, H and Yilmaz, F, (2012), Hepatic amyloidosis: morphologic spectrum of histopathological changes in AA and non AA amyloidosis, *Pathol Res Pract*, 208 (12) 713-8

Saville, JG, Davidson, CP, D'Adrea, GH, Born, CK and Hamrick, ME, (1988), Inhibition of acetaminophen hepatotoxicity by chlorpromazine in fed and fasted mice, *Biochem Pharmacol*, 37 (12) 2467-71

Saxena, R and Theise, N, (2004), Canals of Hering: recent insights and current knowledge, *Semin Liver Dis*, 24 (1) 43-8

Saxena, R, Theise, ND and Crawford, JM, (1999), Microanatomy of the human liver-exploring the hidden interfaces, *Hepatology*, 30 (6) 1339-46

Schmucker, DL, (2005), Age-related changes in liver structure and function: Implications for disease?, *Exp Gerontol*, 40 (8-9) 650-9

Schmucker, DL, (1998), Aging and the liver: an update, *Journals of Gerontology. Series A, Biological Sciences & Medical Sciences*, 53 (5) B315-20

Schmucker, DL, Mooney, JS and Jones, AL, (1978), Stereological analysis of hepatic fine structure in the Fischer 344 rat Influence of sublobular location and animal age, *Journal of Cellular Biology*, 78 (2) 319-337

Schroeder, B and McNiven, M, (2009), 7: Endocytosis as an essential process in liver function and pathology, (107-123), *The Liver: Biology and Pathobiology*, I M Arias, John Wiley & Sons Ltd

Sellaro, TL, Ravindra, AK, Stolz, DB and Badylak, SF, (2007), Maintenance of hepatic sinusoidal endothelial cell phenotype in vitro using organ-specific extracellular matrix scaffolds, *Tissue Eng*, 13 (9) 2301-10

Sener, G, Sehirli, O, Cetinel, S, Yegen, BG, Gedik, N and Ayanoglu-Dulger, G, (2005), Protective effects of MESNA (2-mercaptoethane sulphonate) against acetaminophen-induced hepatorenal oxidative damage in mice, *J Appl Toxicol*, 25 (1) 20-9

Senoo, H, (2004), Structure and function of hepatic stellate cells, *Med Electron Microsc*, 37 3-15

Senoo, H, Kojima, N and Sato, M, (2007), Vitamin A-storing cells (stellate cells), *Vitam Horm*, 75 131-59

Setum, CM, Serie, JR and Hegre, OD, (1993), Dendritic cell/lymphocyte clustering: morphologic analysis by transmission electron microscopy and distribution of gold-labeled MHC class II antigens by high-resolution scanning electron microscopy, *Anat Rec*, 235 (2) 285-95

Shayeganpour, A, Korashy, H, Patel, JP, El-Kadi, AO and Brocks, DR, (2008), The impact of experimental hyperlipidemia on the distribution and metabolism of amiodarone in rat, *Int J Pharm*, 361 (1-2) 78-86

Shin, YC, (1997), Revaluation on the types and pattern of distribution of sinusoidal fenestrations in the lobule of normal rat liver, *Anatomical Record*, 247 (2) 206-213

Simon-Santamaria, J, Malovic, I, Warren, A, Oteiza, A, Le Couteur, D, Smedsrod, B, McCourt, P and Sorensen, KK, (2010), Age-related changes in scavenger receptor-mediated endocytosis in rat liver sinusoidal endothelial cells, *J Gerontol A Biol Sci Med Sci*, 65 (9) 951-60

Slayter, EM and Slayter, HS, (1992), Light and electron microscopy, Cambridge University Press

Smedsrod, B, Bleser, PJD, Braet, F, Lovisetti, P, Vanderkerken, K, Wisse, E and Geerts, A, (1994), Cell biology of liver endothelial and Kupffer cells., *Gut*, 35 (11) 1509-1516

Smedsrod, B, Melkko, J, Araki, N, Sano, H and Horiuchi, S, (1997), Advanced glycation end products are eliminated by scavenger-receptor-mediated endocytosis in hepatic sinusoidal Kupffer and endothelial cells, *Biochem J*, 322 (Pt 2) 567-73

Smedsrod, B and Pertoft, H, (1985), Preparation of pure hepatocytes and reticuloendothelial cells in high yield from a single rat liver by means of Percoll centrifugation and selective adherence, *J Leukoc Biol*, 38 (2) 213-30

Smedsrod, B, Pertoft, H, Gustafson, S and Laurent, TC, (1990), Scavenger functions of the liver endothelial cell, *Biochem J*, 266 (2) 313-27

Smith, MT, Loveridge, N, Wills, ED and Chayen, J, (1979), The distribution of glutathione in the rat liver lobule, *Biochem J*, 182 (1) 103-8

Sokolovic, M, Sokolovic, A, van Roomen, CP, Gruber, A, Ottenhoff, R, Scheij, S, Hakvoort, TB, Lamers, WH and Groen, AK, (2010), Unexpected effects of fasting on murine lipid homeostasis--transcriptomic and lipid profiling, *J Hepatol*, 52 (5) 737-44

Sokolovic, M, Sokolovic, A, Wehkamp, D, Ver Loren van Themaat, E, de Waart, DR, Gilhuijs-Pederson, LA, Nikolsky, Y, van Kampen, AH, Hakvoort, TB and Lamers, WH, (2008), The transcriptomic signature of fasting murine liver, *BMC Genomics*, 9 528

Sorensen, KK, McCourt, P, Berg, T, Crossley, C, Le Couteur, D, Wake, K and Smedsrod, B, (2012), The scavenger endothelial cell: a new player in homeostasis and immunity, *Am J Physiol Regul Integr Comp Physiol*, 303 (12) R1217-30

Sowa, G, Pypaert, M and Sessa, WC, (2001), Distinction between signaling mechanisms in lipid rafts vs. caveolae, *Proc Natl Acad Sci U S A*, 98 (24) 14072-7

Stacchiotti, A, Lavazza, A, Ferroni, M, Sberveglieri, G, Bianchi, R, Rezzani, R and Rodella, LF, (2008), Effects of aluminium sulphate in the mouse liver: similarities to the aging process, *Exp Gerontol*, 43 (4) 330-8

Steinberg, P, Lafranconi, WM, Wolf, CR, Waxman, DJ, Oesch, F and Friedberg, T, (1987), Xenobiotic metabolizing enzymes are not restricted to parenchymal cells in rat liver, *Mol Pharmacol*, 32 (4) 463-70

Strazzabosco, M and Fabris, L, (2008), Functional anatomy of normal bile ducts, *Anat Rec (Hoboken)*, 291 (6) 653-60

Strubelt, O, Dost-Kempf, E, Siegers, CP, Younes, M, Volpel, M, Preuss, U and Dreckmann, JG, (1981), The influence of fasting on the susceptibility of mice to hepatotoxic injury, *Toxicol Appl Pharmacol*, 60 (1) 66-77

Summerfield, JA, Vergalla, J and Jones, EA, (1982), Modulation of a glycoprotein recognition system on rat hepatic endothelial cells by glucose and diabetes mellitus, *J Clin Invest*, 69 (6) 1337-47

Sutachan, JJ, Montoya, GJ, Xu, F, Chen, D, Blanck, TJ and Recio-Pinto, E, (2006), Pluronic F-127 affects the regulation of cytoplasmic Ca2+ in neuronal cells, *Brain Res*, 1068 (1) 131-7

Svegliati Baroni, G, D'Ambrosio, L, Ferretti, G, Casini, A, Di Sario, A, Salzano, R, Ridolfi, F, Saccomanno, S, Jezequel, AM and Benedetti, A, (1998), Fibrogenic effect of oxidative stress on rat hepatic stellate cells, *Hepatology*, 27 (3) 720-6

Svistounov, D, Warren, A, McNerney, GP, Owen, DM, Zencak, D, Zykova, SN, Crane, H, Huser, T, Quinn, RJ, Smedsrod, B, Le Couteur, DG and Cogger, VC, (2012), The Relationship between fenestrations, sieve plates and rafts in liver sinusoidal endothelial cells, *PLoS One*, 7 (9) e46134

Taira, K, (1994), Trabecular meshworks in the sinusoidal endothelial cells of the golden hamster liver: a freeze-fracture study, *J Submicrosc Cytol Pathol*, 26 (2) 271-7

Tanabe, M and Goto, M, (2001), Elevation of serum hyaluronan level in Werner's syndrome, *Gerontology*, 47 (2) 77-81

Tateishi, N, Higashi, T, Naruse, A, Nakashima, K and Shiozaki, H, (1977), Rat liver glutathione: possible role as a reservoir of cysteine, *J Nutr*, 107 (1) 51-60

Teschke, R, Glass, X and Schulze, J, (2011), Herbal hepatotoxicity by Greater Celandine (Chelidonium majus): causality assessment of 22 spontaneous reports, *Regul Toxicol Pharmacol*, 61 (3) 282-91

Teutsch, HF, (1988), Regionality of glucose-6-phosphate hydrolysis in the liver lobule of the rat: metabolic heterogeneity of "portal" and "septal" sinusoids, *Hepatology*, 8 (2) 311-7

Teutsch, HF, Altemus, J, Gerlach-Arbeiter, S and Kyander-Teutsch, TL, (1992), Distribution of 3-hydroxybutyrate dehydrogenase in primary lobules of rat liver, *J Histochem Cytochem*, 40 (2) 213-9

Teutsch, HF, Schuerfeld, D and Groezinger, E, (1999), Three-dimensional reconstruction of parenchymal units in the liver of the rat, *Hepatology*, 29 (2) 494-505

Thimgan, MS and Yee, HF, Jr., (1999), Quantitation of rat hepatic stellate cell contraction: stellate cells' contribution to sinusoidal resistance, *Am J Physiol*, 277 (1 Pt 1) G137-43

Thummel, KE, Lee, CA, Kunze, KL, Nelson, SD and Slattery, JT, (1993), Oxidation of acetaminophen to N-acetyl-p-aminobenzoquinone imine by human CYP3A4, *Biochem Pharmacol*, 45 (8) 1563-9

Toklu, HZ, Sehirli, AO, Velioglu-Ogunc, A, Cetinel, S and Sener, G, (2006), Acetaminophen-induced toxicity is prevented by beta-D-glucan treatment in mice, *Eur J Pharmacol*, 543 (1-3) 133-40

Tooke, JE, (1995), Microvascular function in human diabetes. A physiological perspective, *Diabetes*, 44 (7) 721-6

Trigueiro de Araujo, MS, Gerard, F, Chossegros, P, Guerret, S, Barlet, P, Adeleine, P and Grimaud, JA, (1993), Cellular and matrix changes in drug abuser liver sinusoids: a semiquantitative and morphometric ultrastructural study, *Virchows Arch A Pathol Anat Histopathol*, 422 (2) 145-52

Trotter, NL, (1967), Electron-opaque bodies and fat droplets in mouse liver after fasting or glucose injection, *J Cell Biol*, 34 (3) 703-11

Tsokos, M and Erbersdobler, A, (2005), Pathology of peliosis, *Forensic Sci Int*, 149 (1) 25-33

Tsuchiya, K and Accili, D, (2013), Liver sinusoidal endothelial cells link hyperinsulinemia to hepatic insulin resistance, *Diabetes*, 62 (5) 1478-89

Viola, A and Gupta, N, (2007), Tether and trap: regulation of membrane-raft dynamics by actin-binding proteins, *Nat Rev Immunol*, 7 (11) 889-96

Vollmar, B and Menger, MD, (2009), The hepatic microcirculation: mechanistic contributions and therapeutic targets in liver injury and repair, *Physiol Rev*, 89 (4) 1269-339

Wake, K, (1999), Cell-cell organization and functions of 'sinusoids' in liver microcirculation system, *J Electron Microsc (Tokyo)*, 48 (2) 89-98

Wake, K, (1989), Three-dimensional structure of the sinusoidal wall in the liver: a Golgi study, *Prog Clin Biol Res*, 295 257-62

Wake, K, Motomatsu, K, Dan, C and Kaneda, K, (1988), Three-dimensional structure of endothelial cells in hepatic sinusoids of the rat as revealed by the Golgi method, *Cell Tissue Res*, 253 (3) 563-71

Walker, RM, Massey, TE, McElligott, TF and Racz, WJ, (1982), Acetaminophen toxicity in fed and fasted mice, *Can J Physiol Pharmacol*, 60 399-404

Walker, RM, Racz, WJ and McElligott, TF, (1985), Acetaminophen-induced hepatotoxic congestion in mice, *Hepatology*, 5 (2) 233-40

Walker, RM, Racz, WJ and McElligott, TF, (1980), Acetaminophen-induced hepatotoxicity in mice, *Lab Invest*, 42 (2) 181-9

Walker, RM, Racz, WJ and McElligott, TF, (1983), Scanning electron microscopic examination of acetaminophen-induced hepatotoxicity and congestion in mice, *Am J Pathol*, 113 321-330

Wang, NS and Minassian, H, (1987), The formaldehyde-fixed and paraffin-embedded tissues for diagnostic transmission electron microscopy: a retrospective and prospective study, *Hum Pathol*, 18 (7) 715-27

Wang, X, Chowdhury, JR and Chowdhury, NR, (2006), Bilirubin metabolism: Applied physiology., *Curr Paediatr*, 16 (1) 70-74

Wang, X, McCormick, K and Mick, G, (2003), Nutritional regulation of white adipocyte vascular endothelial growth factor (VEGF), *Horm Metab Res*, 35 (4) 211-6

Wanless, IR, Belgiorno, J and Huet, PM, (1996), Hepatic sinusoidal fibrosis induced by cholesterol and stilbestrol in the rabbit: 1. Morphology and inhibition of fibrogenesis by dipyridamole, *Hepatology*, 24 (4) 855-64

Warren, A, Benseler, V, Cogger, VC, Bertolino, P and Le Couteur, DG, (2011), The impact of poloxamer 407 on the ultrastructure of the liver and evidence for clearance by extensive endothelial and kupffer cell endocytosis, *Toxicol Pathol*, 39 (2) 390-7

Warren, A, Bertolino, P, Benseler, V, Fraser, R, McCaughan, GW and Le Couteur, DG, (2007), Marked changes of the hepatic sinusoid in a transgenic mouse model of acute immune-mediated hepatitis, *J Hepatol*, 46 239-246

Warren, A, Bertolino, P, Cogger, VC, McLean, AJ, Fraser, R and Le Couteur, DG, (2005), Hepatic pseudocapillarization in aged mice, *Exp Gerontol*, 40 (10) 807-12

Warren, A, Cogger, VC, Arias, IM, McCuskey, RS and Le Couteur, DG, (2010), Liver sinusoidal endothelial fenestrations in caveolin-1 knockout mice, *Microcirculation*, 17 (1) 32-8

Warren, A, Le Couteur, DG, Fraser, R, Bowen, DG, McCaughan, GW and Bertolino, P, (2006), T lymphocytes interact with hepatocytes through fenestrations in murine liver sinusoidal endothelial cells, *Hepatology*, 44 (5) 1182-90

Wasan, KM, Subramanian, R, Kwong, M, Goldberg, IJ, Wright, T and Johnston, TP, (2003), Poloxamer 407-mediated alterations in the activities of enzymes regulating lipid metabolism in rats, *J Pharm Pharm Sci*, 6 (2) 189-197

Wendel, A, Feuerstein, S and Konz, KH, (1979), Acute paracetamol intoxication of starved mice leads to lipid peroxidation in vivo, *Biochem Pharmacol*, 28 (13) 2051-5

Whitcomb, DC and Block, GD, (1994), Association of acetaminophen hepatotoxicity with fasting and ethanol use, *Jama*, 272 (23) 1845-50

Williams, AM, Langley, PG, Osei-Hwediah, J, Wendon, JA and Hughes, RD, (2003), Hyaluronic acid and endothelial damage due to paracetamol-induced hepatotoxicity, *Liver Int*, 23 (2) 110-5

Winau, F, Hegasy, G, Weiskirchen, R, Weber, S, Cassan, C, Sieling, PA, Modlin, RL, Liblau, RS, Gressner, AM and Kaufmann, SH, (2007), Ito cells are liver-

resident antigen-presenting cells for activating T cell responses, *Immunity*, 26 (1) 117-29

Wisse, E, (1970), An electron microscopic study of the fenestrated endothelial lining of rat liver sinusoids, *J Ultrastruct Res*, 31 (1) 125-150

Wisse, E, (1972), An ultrastructural characterization of the endothelial cell in the rat liver sinusoid under normal and various experimental conditions, as a contribution to the distinction between endothelial and Kupffer cells, *J Ultrastruct Res*, 38 (5) 528-562

Wisse, E, Braet, F, Duimel, H, Vreuls, C, Koek, G, Olde Damink, SW, van den Broek, MA, De Geest, B, Dejong, CH, Tateno, C and Frederik, P, (2010), Fixation methods for electron microscopy of human and other liver, *World J Gastroenterol*, 16 (23) 2851-66

Wisse, E, Braet, F, Luo, DZ, Dezanger, R, Jans, D, Crabbe, E and Vermoesen, A, (1996), Structure and function of sinusoidal lining cells in the liver, *Toxicol Pathol*, 24 100-111

Wisse, E, De Zanger, RB, Jacobs, R and McCuskey, RS, (1983), Scanning electron microscope observations on the structure of portal veins, sinusoids and central veins in rat liver, *Scan Electron Microsc*, (Pt 3) 1441-52

Wisse, E, Luo, D, Vermijlen, D, Kanellopoulou, C, De Zanger, R and Braet, F, (1997), On the function of pit cells, the liver-specific natural killer cells, *Semin Liver Dis*, 17 (4) 265-86

Wisse, E, van't Noordende, JM, van der Meulen, J and Daems, WT, (1976), The pit cell: description of a new type of cell occurring in rat liver sinusoids and peripheral blood, *Cell Tissue Res*, 173 (4) 423-35

Wisse, E, Van Dierendonck, JH, de zanger, RB, Fraser, R and McCuskey, RS, (1980), On the role of the liver endothelial filter in the transport of particulate fat (chylomicrons and their remnants) to parenchymal cells and the influence of certain hormones on endothelial fenestrae, (195-200), *Communication of Liver Cells*, H. Popper, L. Bianchi, F. Gudat and W. Reutter, MTP Press Ltd

Wisse, E, Zanger, RBD, Charels, K, Smissen, PVD and McCuskey, RS, (1985), The liver sieve: considerations concerning the structure and function of endothelial fenestrae, the sinusoidal wall and the space of Disse, *Hepatology*, 5 (4) 683-692

Woodhouse, K, (1992), Drugs and the liver. Part III: Ageing of the liver and the metabolism of drugs, *Biopharmaceutics & drug disposition*, 13 (5) 311-320

Woodhouse, KW and James, OF, (1990), Hepatic drug metabolism and ageing, *British Medical Bulletin*, 46 (1) 22-35

Woodhouse, KW, Mutch, E, Williams, FM, Rawlins, MD and James, OF, (1984), The effect of age on pathways of drug metabolism in human liver, *Age & Ageing*, 13 (6) 328-334

Woodhouse, KW and Wynne, HA, (1988), Age-related changes in liver size and hepatic blood flow. The influence on drug metabolism in the elderly, *Clinical Pharmacokinetics*, 15 (5) 287-294

Wout, ZG, Pec, EA, Maggiore, JA, Williams, RH, Palicharla, P and Johnston, TP, (1992), Poloxamer 407-mediated changes in plasma cholesterol and triglycerides following intraperitoneal injection to rats, *J Parenter Sci Technol*, 46 (6) 192-200

Wright, PL, Smith, KF, Day, WA and Fraser, R, (1983), Hepatic sinusoidal endothelium in sheep: an ultrastructural reinvestigation, *Anat Rec*, 206 (4) 385-90

Wynne, HA, Goudevenos, J, Rawlins, MD, James, OF, Adams, PC and Woodhouse, KW, (1990), Hepatic drug clearance: the effect of age using indocyanine green as a model compound, *British Journal of Clinical Pharmacology*, 30 (4) 634-637

Xie, G, Wang, X, Wang, L, Wang, L, Atkinson, RD, Kanel, GC, Gaarde, WA and Deleve, LD, (2012), Role of differentiation of liver sinusoidal endothelial cells in progression and regression of hepatic fibrosis in rats, *Gastroenterology*, 142 (4) 918-927 e6

Yang, C, Zeisberg, M, Mosterman, B, Sudhakar, A, Yerramalla, U, Holthaus, K, Xu, L, Eng, F, Afdhal, N and Kalluri, R, (2003), Liver fibrosis: insights into migration of hepatic stellate cells in response to extracellular matrix and growth factors, *Gastroenterology*, 124 (1) 147-59

Yang, ZF and Poon, RT, (2008), Vascular changes in hepatocellular carcinoma, *Anat Rec (Hoboken)*, 291 (6) 721-34

Yannariello-Brown, J, Chapman, SH, Ward, WF, Pappas, TC and Weigel, PH, (1995), Circulating hyaluronan levels in the rodent: effects of age and diet, *Am J Physiol*, 268 (4 Pt 1) C952-7

Yokomori, H, Oda, M, Ogi, M, Kamegaya, Y, Tsukada, N and Ishii, H, (2001), Endothelial nitric oxide synthase and caveolin-1 are co-localized in sinusoidal endothelial fenestrae, *Liver*, 21 (3) 198-206

Yokomori, H, Oda, M, Ogi, M, Yoshimura, K, Nomura, M, Fujimaki, K, Kamegaya, Y, Tsukada, N and Ishii, H, (2003a), Endothelin-1 suppresses plasma

membrane Ca++-ATPase, concomitant with contraction of hepatic sinusoidal endothelial fenestrae, *Am J Pathol*, 162 (2) 557-66

Yokomori, H, Oda, M, Yoshimura, K and Hibi, T, (2012), Recent advances in liver sinusoidal endothelial ultrastructure and fine structure immunocytochemistry, *Micron*, 43 (2-3) 129-34

Yokomori, H, Oda, M, Yoshimura, K, Nagai, T, Fujimaki, K, Watanabe, S and Hibi, T, (2009), Caveolin-1 and Rac regulate endothelial capillary-like tubular formation and fenestral contraction in sinusoidal endothelial cells, *Liver Int*, 29 (2) 266-76

Yokomori, H, Oda, M, Yoshimura, K, Nagai, T, Ogi, M, Nomura, M and Ishii, H, (2003b), Vascular endothelial growth factor increases fenestral permeability in hepatic sinusoidal endothelial cells, *Liver Int*, 23 (6) 467-75

Yokomori, H, Yoshimura, K, Funakoshi, S, Nagai, T, Fujimaki, K, Nomura, M, Ishii, H and Oda, M, (2004a), Rho modulates hepatic sinusoidal endothelial fenestrae via regulation of the actin cytoskeleton in rat endothelial cells, *Lab Invest*, 84 857-864

Yokomori, H, Yoshimura, K, Ohshima, S, Nagai, T, Fujimaki, K, Nomura, M, Oda, M and Hibi, T, (2006), The endothelin-1 receptor-mediated pathway is not involved in the endothelin-1-induced defenestration of liver sinusoidal endothelial cells, *Liver Int*, 26 (10) 1268-76

Yokomori, H, Yoshimura, K, Toshihiro, N, Fujimaki, K, Nomura, M, Hibi, T, Ishii, H and Oda, M, (2004b), Sinusoidal endothelial fenestrae organization regulated by myosin light chain kinase and Rho-kinase in cultured rat sinusoidal endothelial cells, *Hepatol Res*, 30 169-174

Young-Chul, S, (1997), Revaluation on the types and pattern of distribution of sinusoidal fenestrations in the lobule of normal rat liver, *Anat Rec*, 247 206-213

Young, JB and Landsberg, L, (1977), Suppression of sympathetic nervous system during fasting, *Science*, 196 (4297) 1473-5

Yu, KC and Cooper, AD, (2001), Postprandial lipoproteins and atherosclerosis, *Frontiers Biosci*, 6 332-354

Zafrani, ES, Bernuau, D and Feldmann, G, (1984a), Peliosis-like ultrastructural changes of the hepatic sinusoids in human chronic hypervitaminosis A: report of three cases, *Hum Pathol*, 15 (12) 1166-70

Zafrani, ES, Cazier, A, Baudelot, AM and Feldmann, G, (1984b), Ultrastructural lesions of the liver in human peliosis: A report of 12 cases, *Am J Pathol*, 114 (3) 349-59

Zarbock, A, Polanowska-Grabowska, RK and Ley, K, (2007), Platelet-neutrophil-interactions: linking hemostasis and inflammation, *Blood Rev*, 21 (2) 99-111

Zhang, L, Parsons, DL, Navarre, C and Kompella, UB, (2002), Development and in-vitro evaluation of sustained release poloxamer 407 (P407) gel formulations of ceftiofur, *J Control Release*, 85 (1-3) 73-81

Zhao, Y, Wang, Y, Wang, Q, Liu, Z, Liu, Q and Deng, X, (2012), Hepatic stellate cells produce vascular endothelial growth factor via phospho-p44/42 mitogen-activated protein kinase/cyclooxygenase-2 pathway, *Mol Cell Biochem*, 359 (1-2) 217-23

Zimmermann, A, Zimmermann, H, Fellay, M and Reichen, J, (1999), Cells with morphological and immunohistochemical features of hepatic stellate cells (Ito

cells) form an extralittoral (extrasinusoidal) compartment in the cirrhotic rat liver, *Histol Histopathol*, 14 (3) 719-27

Appendices

Appendix 1: Embedding protocols

A) Spurr's resin embedding protocol for TEM specimens

1. After primary fixation in EM fixative, wash specimens in fixative buffer for 5 min

2. Incubate in 2 % Osmium tetroxide in 0.1 M Na Cacodylate for 30 min, and wash in 0.1 M Na Cacodylate (pH 7.4) for 5 min, then distilled water for 2 × 5 min

3. For an *en bloc* uranyl acetate stain, incubate specimens in 2 % aqueous uranyl acetate for 20 min and wash in distilled water for 5 min, otherwise proceed straight to step 4

4. Dehydrate the specimens in a series of ethanols - 50 %, 70 %, 90 %, 95 %, 100 % EtOH for at least 5 to 10 min each, then another 2 × 100 % in EtOH for 10 min each

5. Incubate in acetone 2 × 10 min

6. Incubate in 50 % acetone 50 % Spurr's resin for 30 min

7. Incubate in Spurr's resin 2 × 30 mins and 1 × 60 min before placing specimens into BEEM® capsules filled with Spurr's resin

8. Set the Resin in an oven at 75 - 80 ºC overnight (until hard). Specimens are now ready for sectioning on an ultratome

B) Paraffin embedding protocol for histological specimens

1. Following primary fixation in formaldehyde, washing in fixative buffer, and placing of specimens in cassettes, dehydrate the specimens in a series of ethanols (70 %, 95 % × 2, 100 % × 3) for at least 1 hour each wash

2. Incubate specimens in xylene, 3 × 1 hour

3. Incubate specimens in hot paraffin wax - first incubation in paraffin wax for 2 hours, second in fresh paraffin wax for at least 1 hour

4. Pour fresh hot paraffin wax onto the specimens, and set them on a cold plate until the paraffin becomes hard, ready for sectioning

Appendix 2: Staining protocols for histology

A) Hematoxylin and Eosin: stains RBCs red, cytoplasm pink, nuclei blue

1. Firmly stick 4 μm thick paraffin-embedded sections on slides at 60 ºC
2. Incubate sections in xylene for 2 × 1 min
3. Dehydrate sections in 100 % ethanol, 2 × 1 min, and wash in water for 1 min
4. Incubate sections in Harris Haematoxylin for 4 to 5 min then wash in water 1 min
5. Dip sections into acid alcohol for approx 15 sec, then wash in water for 30 sec
6. Incubate sections in Scott's Blue for 1 min then wash in water for 30 sec
7. Incubate sections in Eosin for 1 min
8. Dehydrate sections in 100 % EtOH for 3 × 1 min
9. Incubate in xylene for 2 × 1 min
10. Coverslip sections with coverglass and mountant and view under the microscope

B) Periodic Acid Schiff: stains glycogen and reticular fibres pink/magenta

1. Firmly stick 4 μm thick paraffin-embedded sections on slides at 60 ºC
2. Incubate sections in xylene for 2 × 1 min, then 100 % EtOH for 2 × 1 min
3. Hydrate sections in water for 1 min before incubation in Periodic acid for 10 min
4. Wash in water for 30 sec before incubation in Schiff's reagent for 10 min
5. Wash in water for 30 sec before incubation in Harris Hematoxylin for 2 min
6. Wash in water 30 sec, incubate in Scott's Blue 30 sec, wash in water 30 sec
7. Dehydrate in 100 % EtOH 2 × 1 min, incubate in xylene 2 × 1 min
8. Coverslip sections with mountant and coverglass before viewing on the microscope

C) Sirius Red: stains collagen (I, II, III, and V) red, Fast Green FCF counterstain stains cells green

1. Firmly stick 4 µm thick paraffin-embedded sections on slides at 60 ºC

2. Incubate sections in xylene 2 × 1 min, before rehydrating in 100 % EtOH 2 × 1 min, 95 % EtOH 1 min, 70 % EtOH 1 min, then water 2 × 1 min

3. Incubate in 0.1 % Sirius Red for 1 hour

4. Rinse sections in running water for 10 min

5. To counterstain, incubate sections in 0.1 % Fast Green FCF for 5 min, and rinse briefly in water (up to 1 min), otherwise go straight to step 6. The dehydration steps after counterstaining must be very brief, only 1 - 2 dunks per section, as the dye will run out of the specimens very easily

6. Dehydrate in 100 % EtOH 2 × 1 min (or 1 - 2 dunks if counterstained), and incubate in xylene 2 × 1 min (or 1 - 2 dunks if counterstained)

7. Coverslip sections with mountant and coverglass before viewing on the microscope

Appendix 3: Staining protocols for TEM

A) Toluidine blue stain

Toluidine blue is made with 200 ml dH_2O, 2 g Toluidine Blue powder, and 2 g borax, stirred on heat (simmered just under boiling) for 1 hour, poured through Whatman's filter paper no.1 whilst warm into a fresh bottle. Filter the solution twice to remove all traces of precipitates.

1. Place 0.5 µm thick sections on a drop of water on a glass slide
2. Place slide on a heat pad (at 80 - 100 ºC) to evaporate the water in order to firmly stick sections to the slide
3. Add a drop of toluidine blue onto the sections, and heat on the heat pad until a shiny film appears around the drop (approximately 2 - 5 sec)
4. Rinse with dH_2O and dry on the heat pad before viewing the sections on a microscope

B) Ultrathin sections for transmission EM were stained as follows

1. 80 nm sections on grids were placed in a drop of uranyl acetate (taken from the top of the solution in the bottle to avoid precipitate) for 3 min
2. Rinsed in dH_2O for 5 sec and dried briefly on filter paper
3. Grids were placed in a drop of lead citrate for 3 min, exposure to oxygen and CO_2 were minimised by placing a lid over the Petri dish containing the grids, and not breathing directly onto the grids
4. Rinsed in dH_2O for 5 sec and dried briefly on filter paper
5. Specimens are ready for viewing on the TEM

Appendix 4: Summary of the data from Chapters 4 and 5

Table 1 *Means ± S.D. of untreated control ad libitum fed and 48 hour fasted rats, fed and fasted APAP treated rats, and fed and fasted P407 pre and post treated rats. 6 hr = rats culled 6 hours after APAP, 24 hr = rats culled 24 hours after APAP.*

	Group	Untreated control rats fed & fasted	Treatment Group	APAP treated	P407 pre treated	P407 post treated
ALT (U/L)			**6hr fast**	45±7.2	29±6*	75±49
	fast	40±3.6	**24hr fast**	2143±2296	5729±6903	3179±6161
	fed	36.8±3	**24hr fed**	171.2±297	402±643	36±6.6
AST (U/L)			**6hr fast**	81.4±16.4	68±10	117±45
	fast	70.7±9.1	**24hr fast**	3008±3473	9512±11612	6474±12671
	fed	52.4±4	**24hr fed**	155.4±172	782±1453	74.6±28
Total Bilirubin (U/L)			**6hr fast**	1±0	0.3±0.6*	0.8±0.8
	fast	1±0	**24hr fast**	2±0.7*†	2±2.3	3.1±2.6
	fed	1±0	**24hr fed**	3.4±1.8*	0*	0.8±0.6*
% Weight loss from time of fast			**6hr fast**	7.5±1.9	6.6±1	6±1
	fast	7±1.6	**24hr fast**	13±1.7*†	10±0.5	9.5±2*
% Weight loss	**fed**	0	**24hr fed**	4.6±0.5	6.7±1.5*	5.3±1.2
Total cholesterol (µmol/L)			**6hr fast**	1.3±0.1	10.7±1.8*	2±1
	fast	1.5±0.1	**24hr fast**	1.1±0.2*†	10.3±4.5*	7±2.5*
Triglycerides (µmol/L)			**6hr fast**	0.8±0.2	53±14.3*	5±8
	fast	0.4±0.1	**24hr fast**	0.7±0.5	40±25.3*	38±21*
Urea			**6hr fast**	4.2±2.1	no data	no data
	fast	4.6±0.3	**24hr fast**	7.7±2.1*†	no data	no data
Creatinine			**6hr fast**	21±7.5	no data	no data
	fast	24.3±1.5	**24hr fast**	36.8±11.6*†	no data	no data
Hematocrit (%)			**6hr fast**	59.5±2.7	46±1*	57.6±3
	fast	52.7±2.1	**24hr fast**	62±8†	43±5*	51±3*
Liver wet weight % body weight			**6hr fast**	3.3±0.7	3.4±0.3	3±0.3
	fast	2.5±0.2	**24hr fast**	4.3±0.6*†	4.4±0.8	4±0.7
Centrilobular Necrosis			**6hr fast**	0/5 = 0	1/5 = 0.2	1/5 = 0.2
	fast	0	**24hr fast**	32/25 = 1.28	37/25 = 1.4	13/20 = 0.65
	fed	0	**24hr fed**	5/6 = 0.83	5/6 = 0.83	1/6 = 0.16
Sinusoidal Collagen			**6hr fast**	10/5 = 2	10/5 = 2	8/5 = 1.6
	fast	0	**24hr fast**	7/5 = 1.4	6/5 = 1.2	6/4 = 1.5
	fed	0	**24hr fed**	2/6 = 0.33	6/6 = 1	3/6 = 0.5
Glycogen Deposition			**6hr fast**	0	CL	no trend
	fast	CL	**24hr fast**	PP	PP	no trend
	fed	Diffuse	**24hr fed**	PP	PP	CL

APAP treated group: *p<0.05 compared to 6 hour rats, †p<0.05 compared to untreated control rats.
P407 pre and post treated groups: *p<0.05 compared to APAP control.
Data for centrilobular necrosis and sinusoidal collagen are scores from the sum of '+'s in each group divided by the number of rats per group, or lobes analysed for necrosis in the 24 hour fasted groups.

Appendix 5: Micrographs not included in thesis chapters

All micrographs are from F344 rats used in experiments for this thesis (unless otherwise specified)

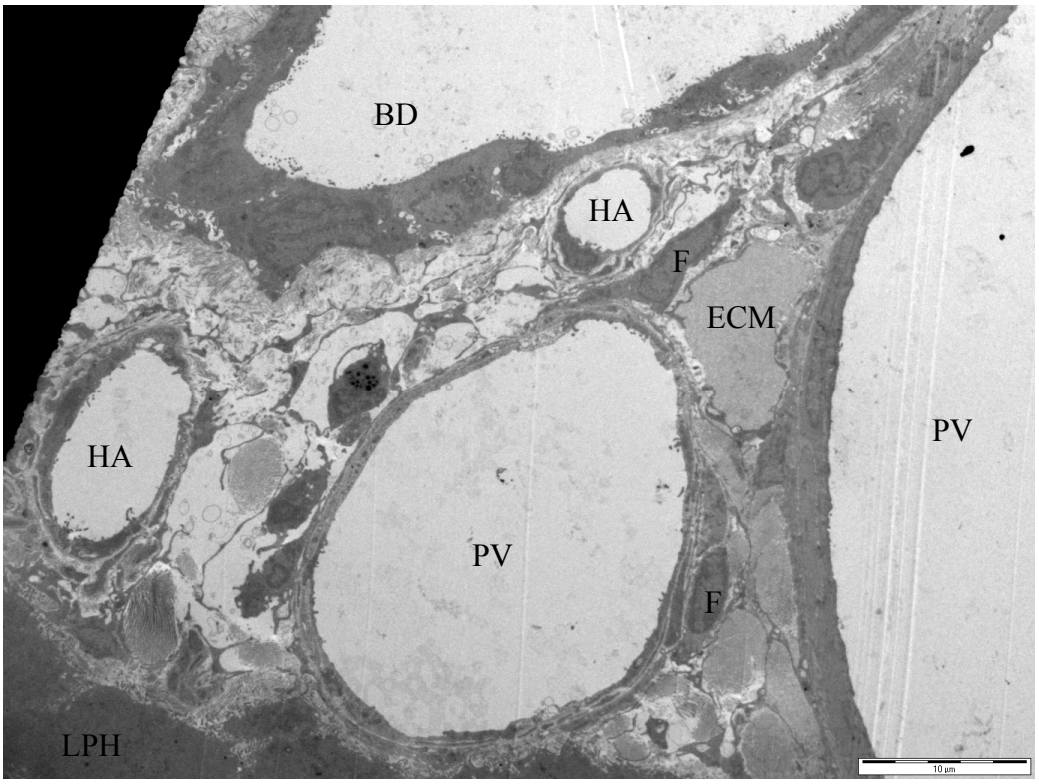

A1: Portal tract (TEM)
HA = hepatic arterioles, PV = portal venules, BD = bile duct, ECM = extra cellular matrix (portal interstitium), F = fibroblasts, LPH = limiting plate of hepatocytes. Bar = 10 µm

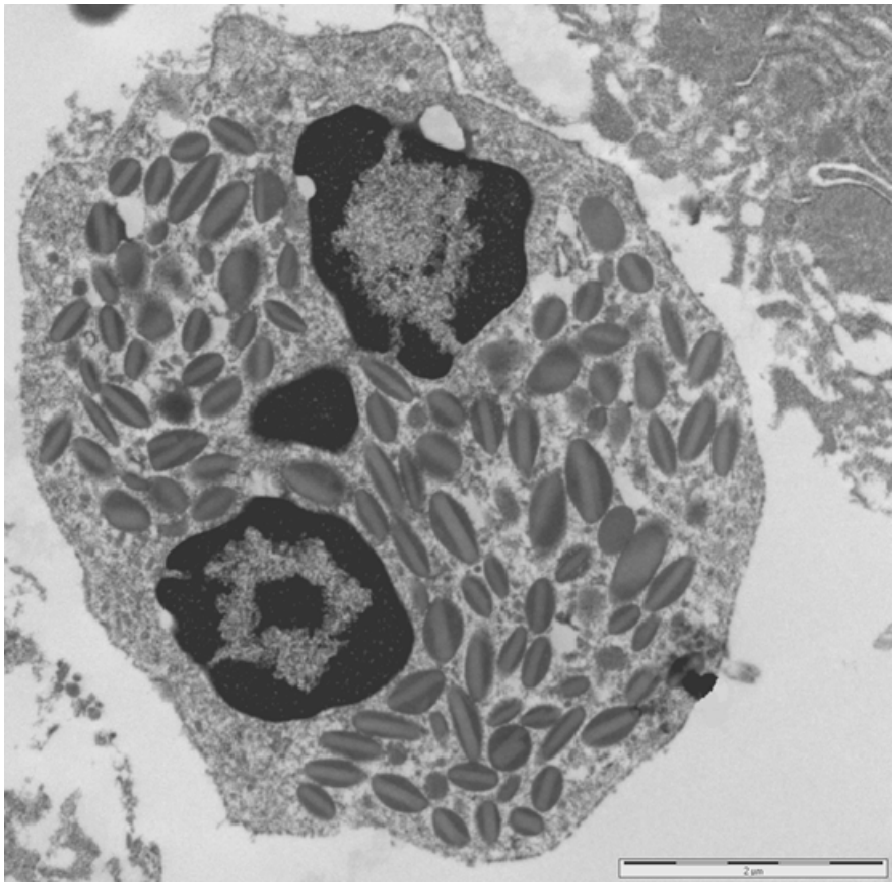

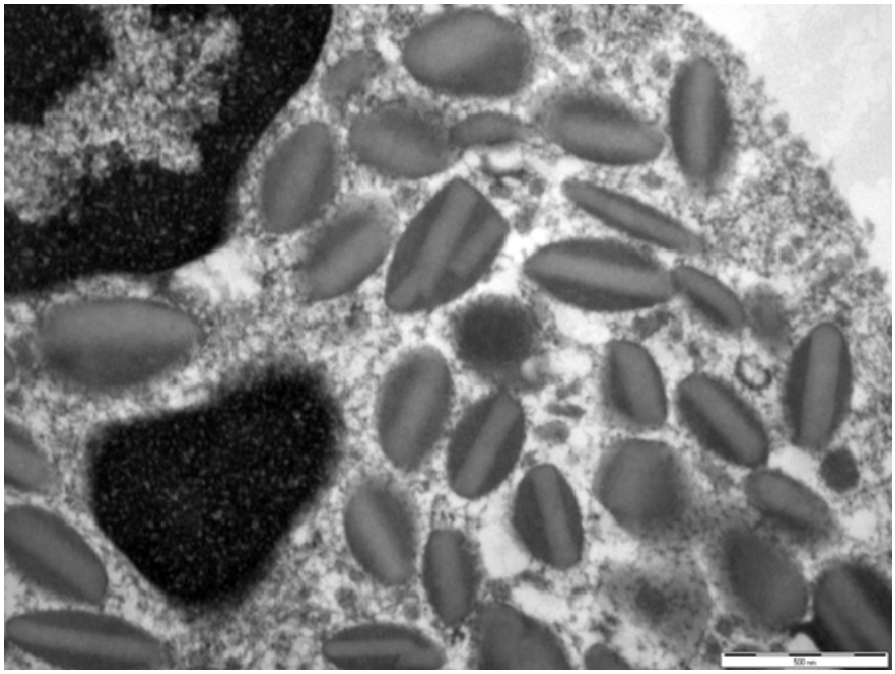

A2: Eosinophil (TEM from a reprocessed specimen) showing typical rod shaped granules (from a P407 pre-treated liver in Chapter 5). Top picture bar = 2 μm, bottom bar = 500 nm.

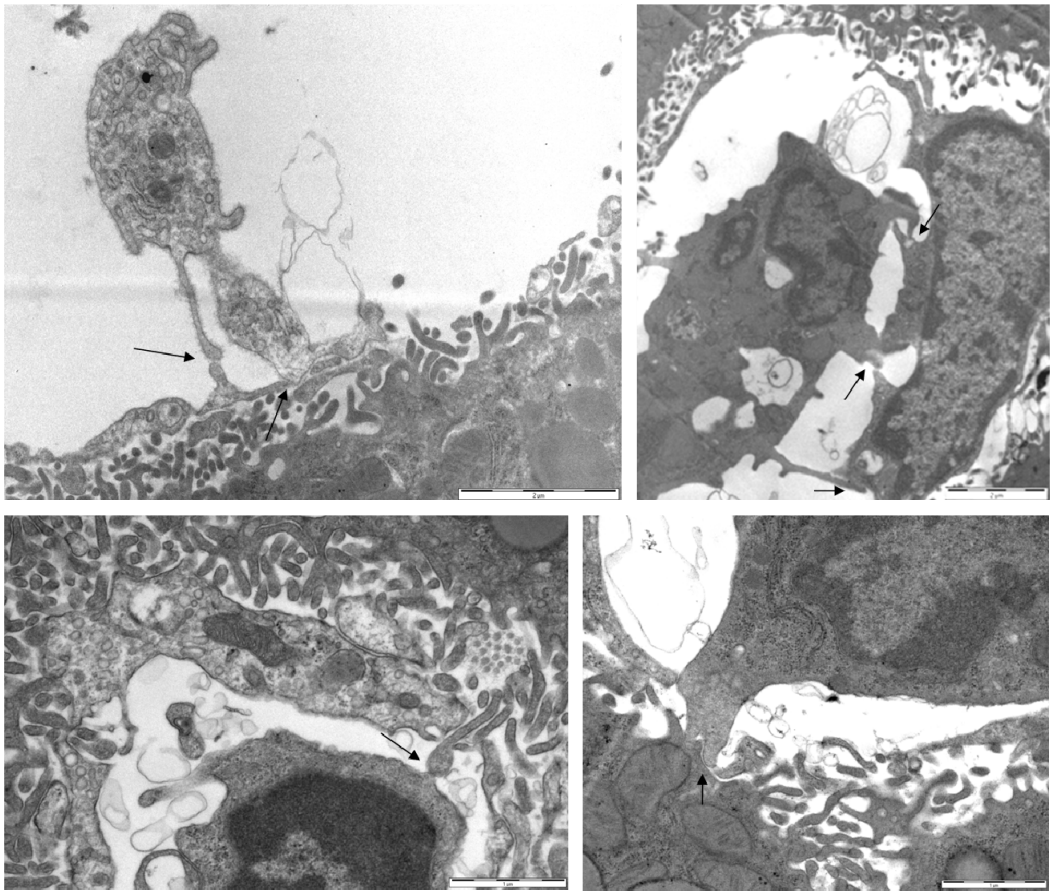

A3: Direct communication between cells of the hepatic sinusoids (arrows). Top picture bars = 2 μm, bottom picture bars = 1 μm.

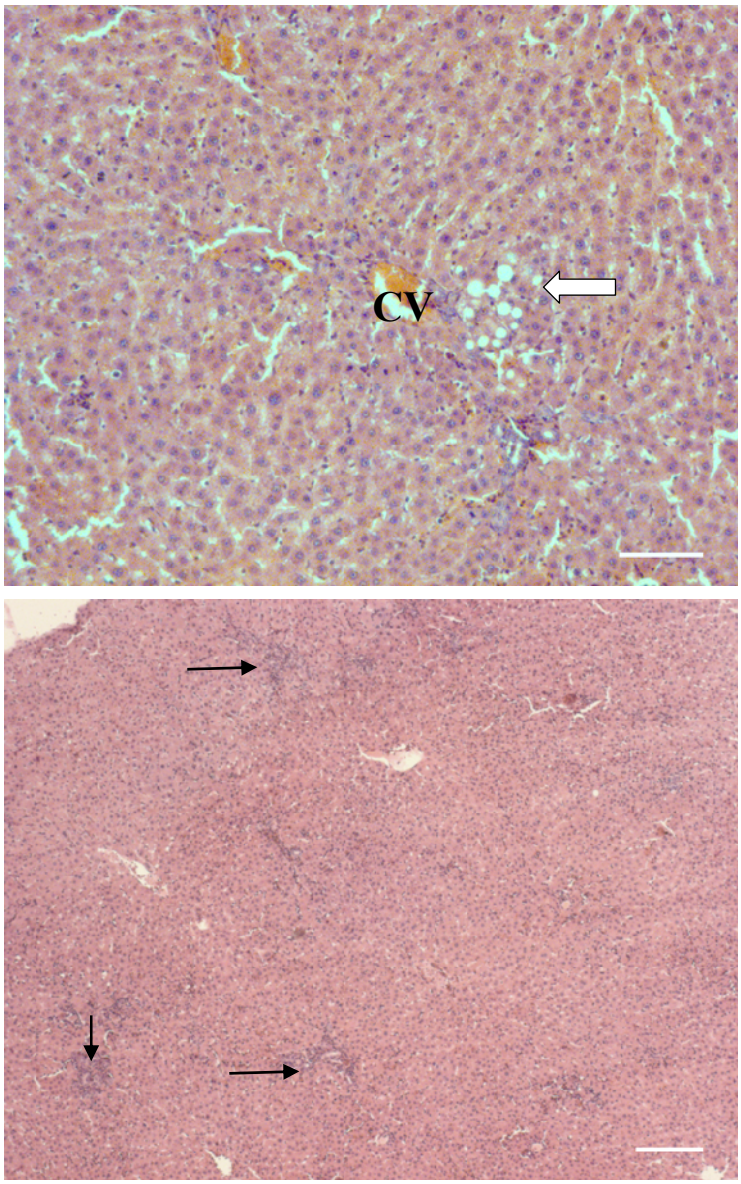

A4: H & E stained sections from old rats (24 - 26 months old, Chapter 6). The top picture shows what looks to be lipid engorged HSCs, typical of ageing (bar = 100 µm). The bottom picture shows patchy inflammation in an ageing rat (bar = 200 µm).

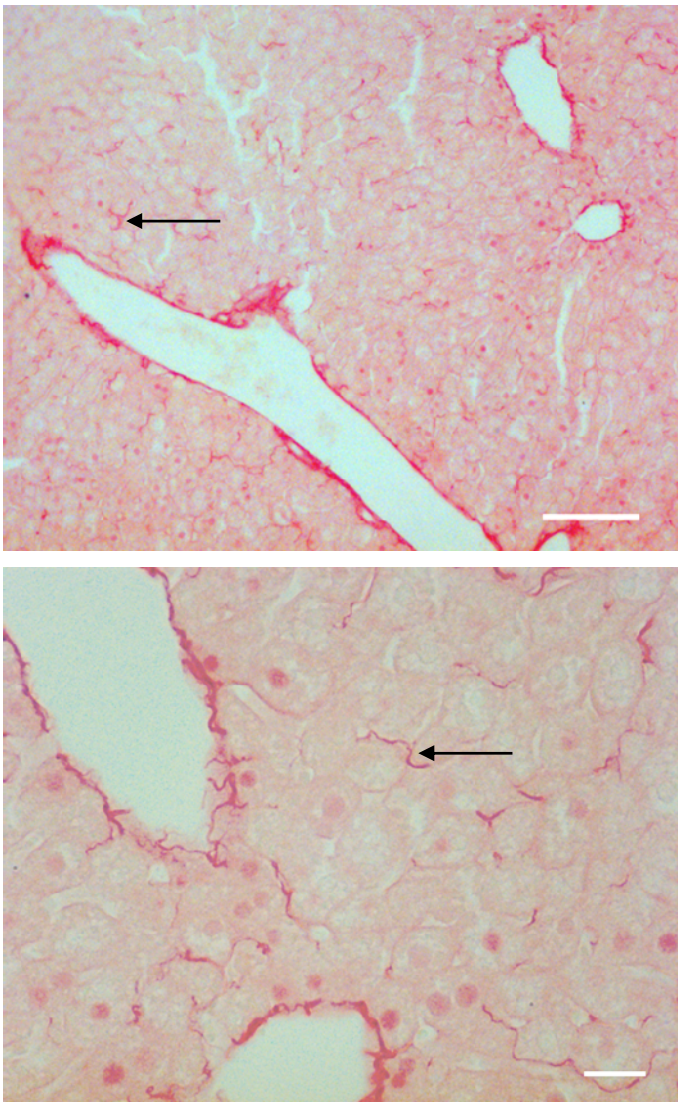

A5: Sirius red stained section of a male 9 month old mouse with Werner's syndrome. There is mildly increased collagen, associated with age-related pseudocapillarisation. The bottom picture (bar = 20 µm) displays an enlarged area from the top right hand corner of the top picture (bar = 100 µm). Refer to (Massip, 2010) for mice used.

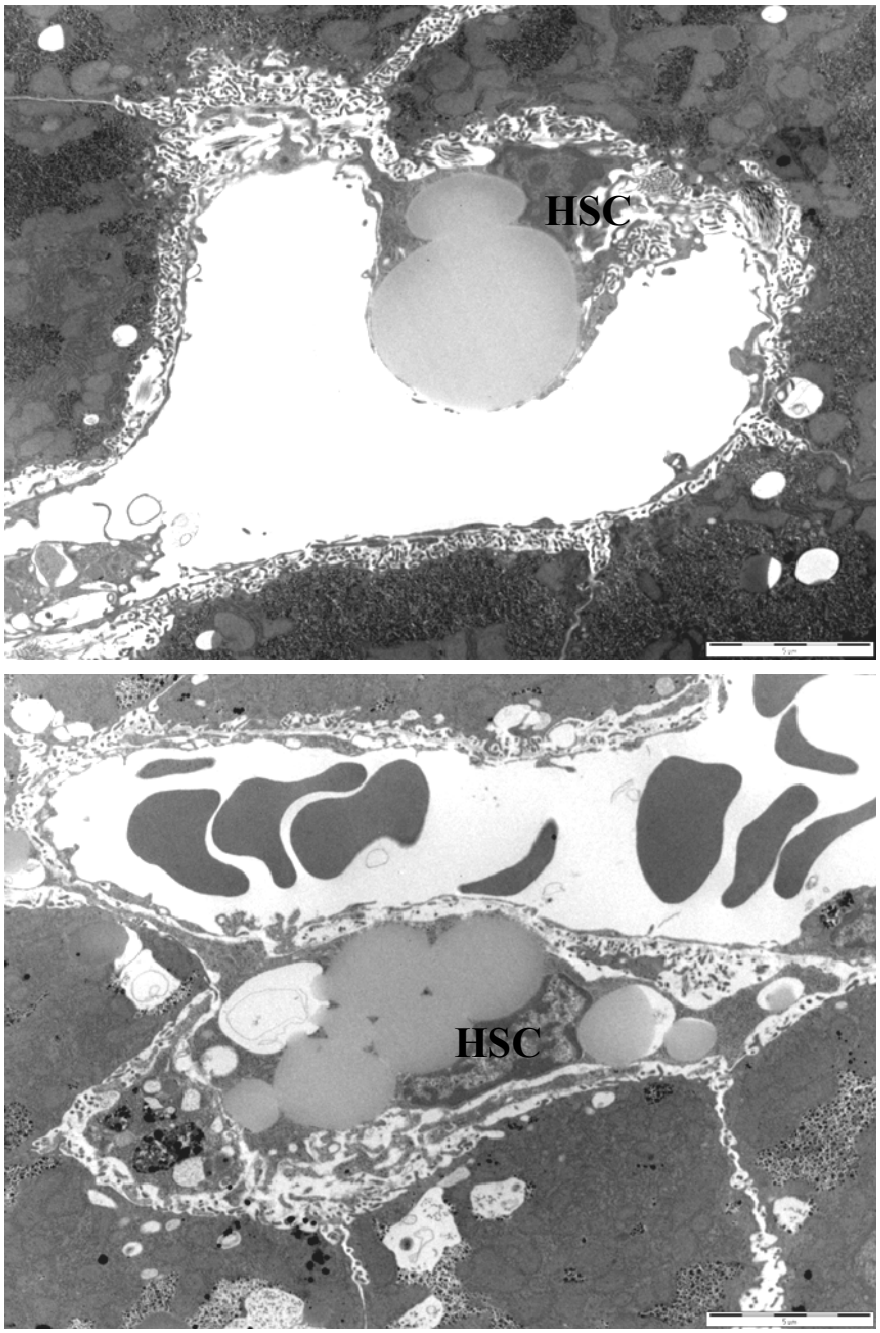

A6: Sinusoids from mice with Werner's syndrome aged 7-9 months showing an age-related increase in numbers of fat engorged HSCs associated with mild pseudocapillarisation. Refer to (Massip, 2010) for mice used. Bars = 5 µm.

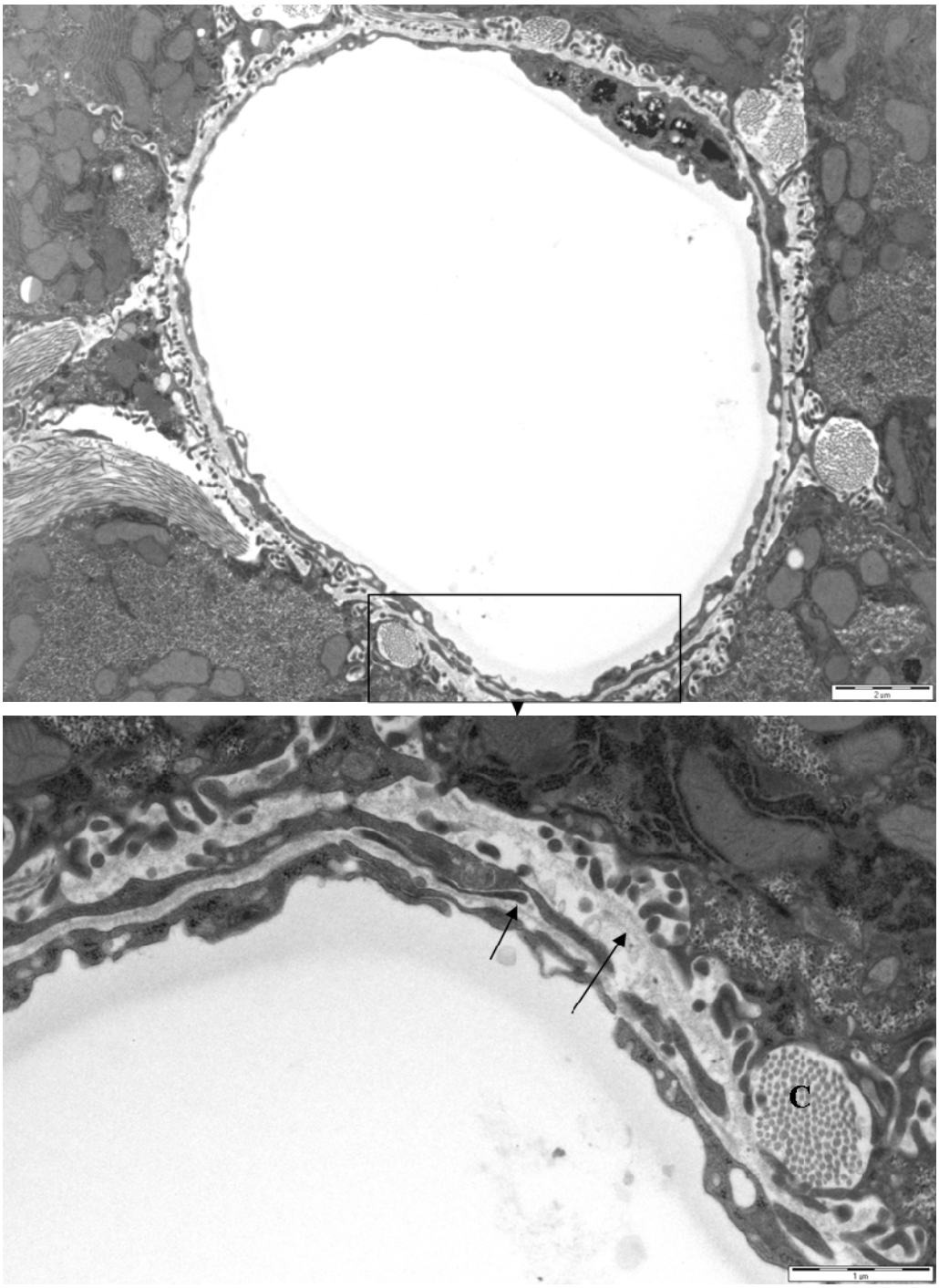

A7: A sinusoid with age-related pseudocapillarisation from a male mouse with Werner's syndrome aged 7 months. There is mild LSEC swelling and defenestration, some basement membrane formation (arrows) and increased collagen fibrils (C). There appears to be accumulation of lipofuscin and/or ferritin-like electron dense particles in the LSEC cytoplasm. Bottom micrograph is an enlarged version of the boxed area in the top micrograph. Refer to (Massip, 2010) for mice used. Top picture bar = 2 μm, bottom bar = 1 μm.

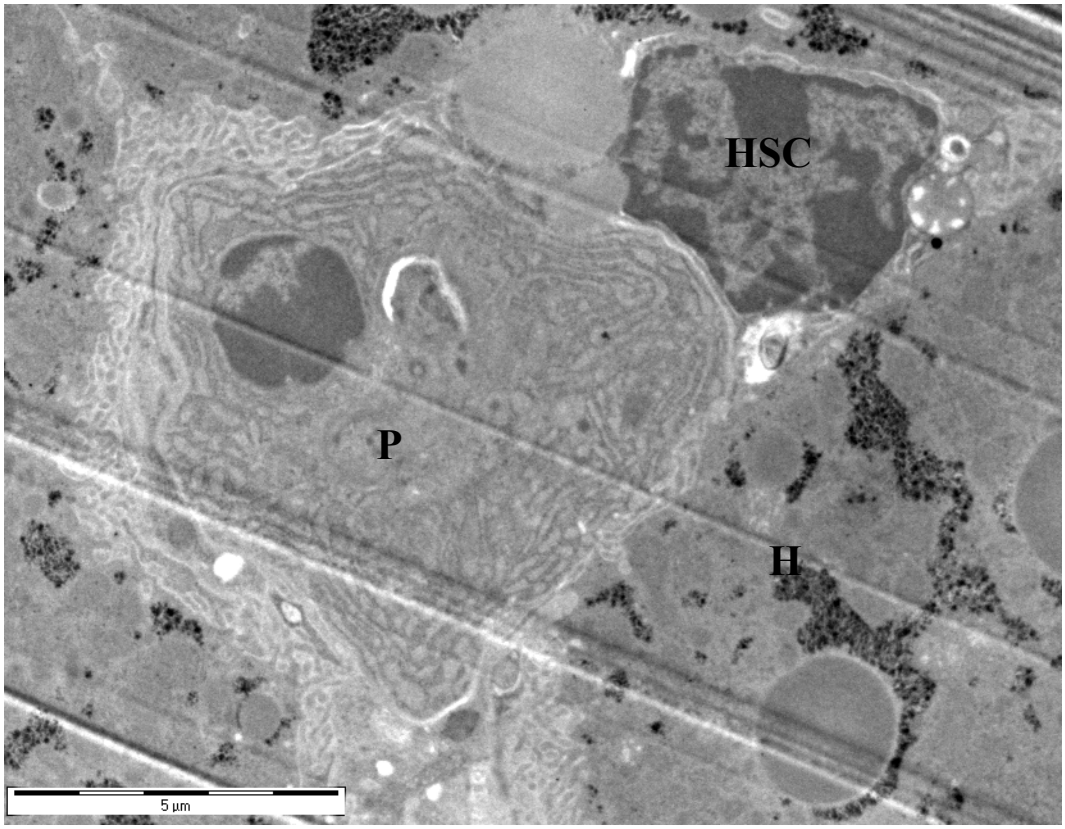

A8: A plasma cell ((P), effector B-cell) in a sinusoid lumen of a Werner Syndrome mouse showing abundant ER. There are large knife marks through the section however it is rare to spot a plasma cell so I have included this micrograph. H = hepatocyte, HSC = hepatic stellate cell. Refer to (Massip, 2010) for mice used. Bar = 5 µm.

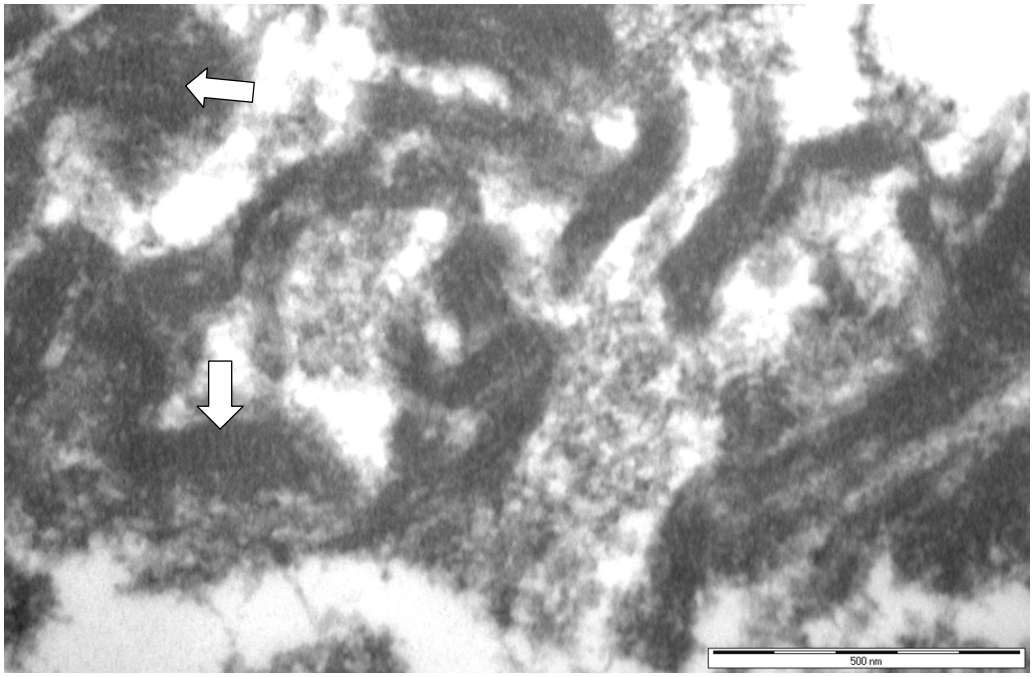

A9: Fibrin (TEM, from a reprocessed specimen from Chapter 4). The white arrows point to fibrin tactoids with typical periodicity observed by tilting the transmission electron microscope stage to an appropriate angle. This micrograph was taken from a rat liver severely affected by APAP toxicity. Bar = 500 nm.

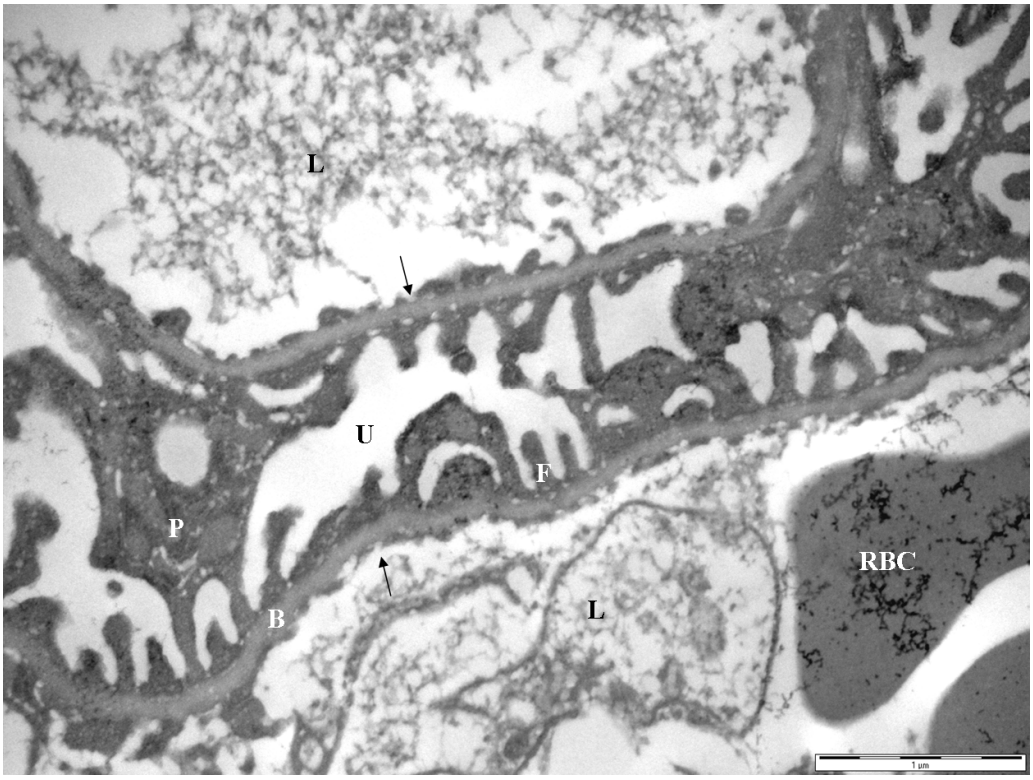

A10: Glomerular endothelial cells (a reprocessed TEM specimen from Chapter 5). Close view of a glomerulus. The glomerular endothelial cells contain fenestrations (arrows) without diaphragms however have an underlying basement membrane (B) separating them from podocyte foot processes (F). The podocyte cell body (P) and foot processes (F) reside along the underside of the basement membrane in the urinary space (U).

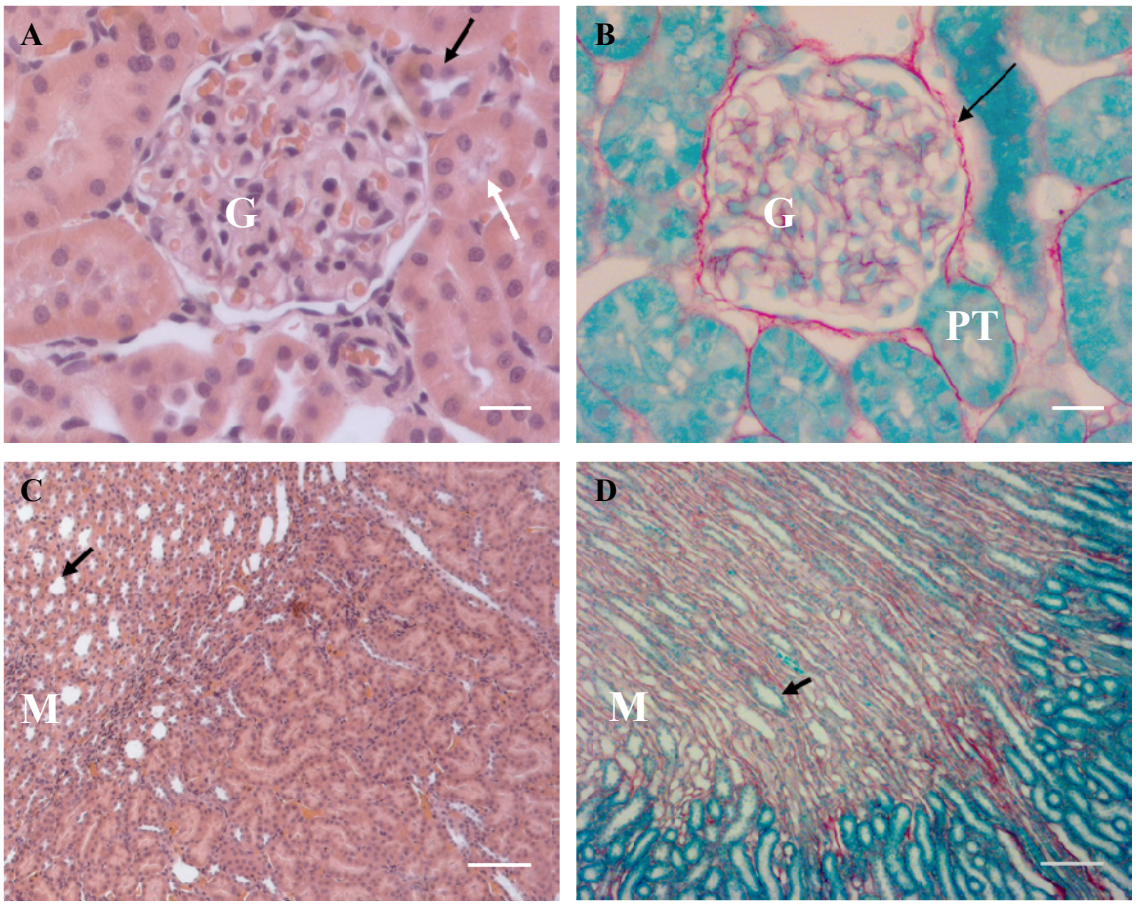

A11: Control untreated and APAP-treated rat renal histology
A) Renal cortex from a normal untreated F344 rat. Black arrow points to a distal convoluted tubule and the white arrow indicates a proximal convoluted tubule. H & E stain. G = glomerulus. Bar = 20 µm.
B) Renal cortex from an F344 APAP treated rat 24 hours after APAP overdose. The glomerulus and surrounding tubules are histologically normal. The arrow points to Bowman's capsule stained red by a Sirius Red stain. Fast Green was used as a counter stain to stain the cells green. PT = the start of the proximal tubule. Bar = 20 µm.
C) Renal medulla from an untreated normal F344 rat. The thin loops of Henle and collecting ducts are clear and histologically normal. H & E stain. Bar = 100 µm.
D) The renal medulla from an APAP-treated rat is histologically normal. The collecting tubules and thin loops of Henle of the medulla (M) are open and clear and do not contain any substances. No tubular necrosis was observed. Sirius Red/Fast Green FCF stain. Bar = 100 µm.